Université catholique de Louvain

Institute of Condensed Matter and Nanosciences

Bio- and Soft Matter

Polymer microcarriers with tunable properties for stem cell culture

Eleana Somville

Thesis submitted in partial fulfillment of the requirements for the Ph.D. Degree in Engineering Sciences

Supervisor	Pr. Karine Glinel	*Université catholique de Louvain*
Supervisor	Pr. Alain Jonas	*Université catholique de Louvain*
Reviewer	Dr. Karine Anselme	*Université Haute Alsace*
Reviewer	Pr. Sylvain Gabriele	*Université de Mons*
Reviewer	Pr. Jérome Guicheux	*Université de Nantes*
Reviewer	Pr. Anne des Rieux	*Université catholique de Louvain*
Chair	Pr. Arnaud Delcorte	*Université catholique de Louvain*

Louvain-la-Neuve

November 2020

Acknowledgement

J'aimerais tout d'abord remercier mes promoteurs, les professeurs Karine Glinel et Alain Jonas de m'avoir donné l'opportunité de mener à bien cette thèse. Leur encadrement m'a permis d'évoluer et de résoudre de nombreux problèmes. En particulier, j'aimerais remercier Karine pour sa disponibilité sans faille et sa proactivité dans la résolution des problèmes quotidiens, ses corrections méticuleuses et ses conseils. Je remercie également Alain pour ses conseils avisés et ses explications toujours très claires ainsi que pour son aide dans l'analyse des données de porosité de surface.

Je remercie ensuite les membres de mon jury, les professeurs Arnaud Delcorte, Anne des Rieux, Jérôme Guicheux, Sylvain Gabriele ainsi que Dr. Karine Anselme d'avoir accepté de juger ce travail. J'apprécie grandement le temps qu'ils auront dédié à la lecture et à la correction de ce manuscrit.

Merci également aux professeurs Sophie Demoustier-Champagne et Anne des Rieux, membres de mon comité d'accompagnement pour leur implication dans le projet FEDER PROSTEM et leurs conseils. Merci également à Anne qui m'a ouvert les portes de son laboratoire afin de pouvoir me former et débuter les premières expériences de culture cellulaire. Les discussions scientifiques à ce sujet me furent d'une grande aide. Ainsi, je remercie également les membres de son équipe, Audrey Smith, Loïc Germain, Ariane Mwema, Viridiane Grattepain, Yasmine Labrack, Bernard Ucakar, Kevin Vanvarenberg, *etc*. qui ont toujours été d'une grande aide que ce soit au niveau logistique ou pour répondre à mes questions. Je remercie vivement Jérôme Guicheux et Boris Halgand pour leur aide lors de la mise en place de la culture de cellules souches.

I would like to thank Anitha Ajith Kumar with whom I worked for the past two years. Our collaboration was enjoyable and the various discussions about your culture were really instructive and enlightening. I also improved my English thanks to you as you forced me to step out of my comfort zone by talking English

everyday. Thank you also to Mirasbek Kuterbekov for his valuable help at the beginning of the thesis.

Merci à Luc Coquillart, Claire Umutoni et Colette Douchamps pour la gestion des commandes, pas toujours évidente dans le cadre d'un projet FEDER. Je remercie Anne Bouchat et Aurore Becquevort pour la gestion des aspects administratifs ainsi que Pascal van Velthem pour son aide relative aux soucis informatiques. Je remercie également les personnes qui m'ont apporté leur aide pour l'utilisation de différentes techniques de charactérisation : Pascale Lipnik, Marie-Christine Eloy, Tristan da Câmara Santa Clara Gomes. Merci aussi à Sabine Bebelman avec qui j'ai, un moment, partagé la tâche de gestion des déchets et à qui j'ai toujours pu demander de l'aide pour celle-ci.

Je remercie l'ensemble de la TMT : Cécile D'Haese, Delphine Magnin, Naïma Sallem et Pascal Van Velthem pour leur aide pratique dans la vie du labo et l'organisation des différents drinks qui ont jalonné ces dernières années.

Je salue également l'ensemble des doctorants et post-docs qui furent mes collègues pendant ces quatre ans : Catherine, Amir, Jeremy, Vivien, Flavio, Hamid, Vincent, Prakash, Ronggang, Jie, Qian, Imane, Quentin, Wanlin, Sashi, Varvara, Elena, Diana, Tristan, Waël, Bruno, Anthony. Merci en particulier à Catherine Phillipart qui m'a encadrée durant mon mémoire et m'a donné le goût pour la recherche.

Colette, je te remercie pour ta gentillesse et ton dévouement. Ce fut un plaisir de discuter avec toi durant ces nombreuses années.

Cécile et Delphine, outre votre aide technique tout au long de la thèse (SEM, ellipsométrie, résolution de problèmes divers), merci pour votre gentillesse et votre écoute. Je me suis toujours sentie la bienvenue dans votre bureau.

Un tout grand merci à ceux qui ont partagé mon bureau tout au long de la thèse. Vous avez largement contribué à une chouette ambiance de travail : Florian Jurin, Guillaume Staelens, Claire Chattaway, Paul Rouster et Damien Lefevre. Plus particulièrement, j'aimerais adresser toute ma gratitude à Paul et Damien avec qui j'ai passé ces deux dernières années. Votre soutien, vos nombreux conseils et la bonne humeur qui régnait dans le bureau ont sans aucun doute contribué à l'aboutissement de cette thèse. Paul, merci pour ta motivation sans faille et ta présence indéfectible, c'était toujours agréable de travailler à tes côtés. Les discussions plus personnelles ainsi que les échanges

de conseils variés ont été également très appréciés. Damien, tu fus présent de mes débuts jusqu'à la (presque) fin de cette thèse, j'ai donc eu de nombreuses années pour apprendre à te connaître. Outre tes qualités professionnelles telles que ta rigueur et tes nombreuses connaissances, j'ai pu découvrir d'autres facettes comme ton humour, tantôt scabreux tantôt piquant, ou bien ton côté plus littéraire. Merci donc pour ta présence et tes conseils toutes ces années. Petite pensée à Loïc, bien que nous n'étions pas dans le même bureau, tes visites au Boltzmann étaient toujours très chouettes.

Je remercie également mes amis, en thèse ou non, qui ont toujours été là pour me soutenir, m'écouter et me rebooster : Céline, Guillaume, Sarah, Thomas, Méric et Simon.

Finalement, je conclurai en remerciant ma famille au sens large mais surtout Maman et Michel qui ont toujours cru en moi et m'ont permis, via leur soutien aussi bien logistique que moral, d'arriver au bout de ce projet. Merci également à Piet de me suivre dans tous mes projets et d'en créer de nouveaux...

Abstract

Cell-based therapies are promising for tissue engineering and for treating various diseases. However, their development is impaired by the large cell doses required per patient, since the common method to expand cells is not well-suited for large-scale production. Therefore, cell culture on microcarriers (MCs) emerges as an alternative, providing a larger surface-to-volume ratio. However, most commercially available MCs are not designed for stem cell expansion as they are frequently coated with animal-proteins and/or produced using toxic organic solvents. In this context, the aim of the thesis was to develop novel polymeric MCs produced by a green solvent-free process and free of animal protein. We also aim to obtain MC with tunable characteristics (size, porosity, *etc*.) in order to deal with the multiparameter nature of dynamic cell culture. The MC core is obtained thanks to a versatile and green fabrication process meeting the requirements described above. A polyelectrolyte film composed of poly(L-ornithine) and hyaluronic acid is deposited on MCs using the Layer-by-Layer technique, followed by a crosslinking step and the grafting of a bioadhesive peptide to ensure optimal cell adhesion. The ability of these new MCs to expand human adipose-derived mesenchymal stem cells in both static and dynamic conditions is demonstrated. More precisely, a range of parameters such as growth medium, cell seeding density, MC morphology and composition of coating are optimized in semi-static condition. We also show in semi-static condition that these new MCs offer similar performance in term of cell expansion compared to a widely used commercial MC while being superior in terms of detachment efficiency. Finally, the possibility of using these new MCs in dynamic condition as well as performing bead-to-bead transfer to improve cell yield is proven.

Contents

List of Acronyms **xv**

List of Figures **xix**

List of Tables **xxvii**

1 Context of research **1**

1.1 Stem cells and cell-based therapies 1

1.1.1 Stem cells 1

1.1.1.1 Definition 1

1.1.1.2 Classification 1

1.1.1.3 Adipose-derived stem cells 3

1.1.2 Cell-based therapies 6

1.1.2.1 Introduction and definition 6

1.1.2.2 Types of therapies 6

1.1.2.3 Regulative aspects of cell-based therapies . . 9

1.2 Cell expansion systems 14

1.2.1 Classical monolayer culture 14

1.2.2 Small-scale dynamic culture 16

1.2.3 Large-scale dynamic systems 18

1.2.4 Summary of cell expansion systems 20

1.3 Microcarriers 22

1.3.1 Concept 22

1.3.2 Microcarrier properties 22

1.3.3 Important considerations for cell culture on microcarriers 24

1.3.3.1 Inoculation protocol 24

1.3.3.2 Culture parameters 25

1.3.3.3 Detachment procedure 27

1.3.4 Commercial microcarriers 27

1.3.5 Microcarriers in development 29
1.3.6 Microcarrier fabrication 31
1.3.7 Advantages and drawbacks 32
1.4 Mammalian cell behaviour on surfaces 33
1.4.1 Cell adhesion on surfaces 33
1.4.1.1 Cell adhesion receptors: the integrin family . . 33
1.4.1.2 Dynamics of cell adhesion 35
1.4.1.3 Production of extracellular matrix 35
1.4.2 Surface properties influencing cell behaviour 39
1.4.2.1 Chemical properties 39
1.4.2.2 Physical properties 41
1.5 Biofunctionalization techniques to improve cell adhesion 49
1.5.1 Biomolecules of interest for bioadhesion 49
1.5.1.1 Animal Proteins 49
1.5.1.2 Recombinant proteins 51
1.5.1.3 Synthetic cell adhesion peptides 52
1.5.1.4 Comparison of bioadhesive derivatives 54
1.5.2 Protein and peptide immobilization techniques 54
1.5.2.1 Physical adsorption 55
1.5.2.2 Covalent immobilization 56
1.5.2.3 Bioaffinity immobilization 59
1.5.2.4 Comparison of protein and peptide surface immobilization approaches 60
1.5.3 Methods to introduce surface functionalities 61
1.5.3.1 Self-assembled monolayer 61
1.5.3.2 Polymer brush 65
1.5.3.3 Layer-by-layer assembly 68
1.5.3.4 Comparison 74

2 Aim of the thesis **77**

3 Microcarrier production, characterization and optimization **81**
3.1 Introduction 81
3.2 Strategy 82
3.3 Experimental section 86
3.3.1 Materials 86
3.3.2 Preparation of PLLA microcarriers 87

3.3.2.1 Preparation of polyethylene glycol powder containing magnetic nanoparticles 87
3.3.2.2 Isothermal crystallization of PLLA spherulites . 87
3.3.3 Characterization of PLLA microcarriers 88
3.3.3.1 Characterization of microcarrier morphology . 88
3.3.3.2 Characterization of microcarrier size 88
3.3.3.3 Evidence for the presence of magnetic nanoparticles in microcarriers 88
3.3.3.4 Characterization of magnetic nanoparticle spatial distribution at the nanoscale 88
3.3.3.5 Determination of magnetic nanoparticle content in microcarriers 89
3.3.3.6 Study of magnetic nanoparticle release over time 89
3.3.3.7 Characterization of microcarrier magnetic properties 89
3.3.3.8 Measurement of microcarrier sedimentation rate 90
3.3.3.9 Estimation of the surface area of microcarriers 90
3.3.3.10 Qualitative observation of microcarrier mechanical resistance under stirring 90
3.3.3.11 Surface roughness evaluation 91
3.4 Results and discussion 91
3.4.1 Characterization of PLLA spherulites according to processing parameters 91
3.4.1.1 Influence of the PLLA/PEG ratio 91
3.4.1.2 Influence of the crystallization temperature . . 93
3.4.1.3 Influence of PLLA molar mass 94
3.4.2 Production and characterization of magnetic microcarriers 95
3.4.2.1 Evidence for the presence of magnetic nanoparticles in microcarriers 96
3.4.2.2 Characterization of magnetic nanoparticle spatial distribution at the nanoscale 97
3.4.2.3 Determination of the amount of magnetic nanoparticles incorporated in microcarriers 98
3.4.2.4 Measurement of magnetic nanoparticle release in solution 99
3.4.2.5 Characterization of the magnetic properties of microcarriers entrapping magnetic nanoparticles 100

3.4.3 Optimization of spherulite properties for use in dynamic condition . . . 101
3.4.4 Summary of the characteristics of microcarriers selected for cell culture . . . 104
3.4.4.1 Microcarriers for semi-static cell culture assays 104
3.4.4.2 Microcarriers for dynamic cell culture assays . 106
3.5 Conclusion . . . 107
3.6 Appendix . . . 108
3.6.1 Influence of PLLA molar mass . . . 108
3.6.2 Characterization of PEG containing magnetic nanoparticles . . . 108

4 Surface biofunctionalization of microcarriers 109
4.1 Introduction . . . 109
4.2 Strategy . . . 110
4.3 Experimental section . . . 112
4.3.1 Materials . . . 112
4.3.2 Deposition and crosslinking of PLO/HA films . . . 113
4.3.3 Grafting of bioadhesive peptide on crosslinked LbL film 114
4.3.4 Characterization of biofunctional films . . . 114
4.3.4.1 Characterization of LbL film deposited on flat model surfaces . . . 114
4.3.4.2 Characterization of LbL film deposition on microcarriers . . . 115
4.3.4.3 Evidence for the peptide grafting . . . 115
4.4 Results and discussion . . . 116
4.4.1 Characterization of PLO/HA films . . . 116
4.4.2 Evidence for the peptide grafting . . . 120
4.5 Conclusion . . . 122
4.6 Appendix . . . 123
4.6.1 Fluorescence intensity quantification . . . 123

5 Stem cell culture on microcarriers in semi-static condition 125
5.1 Introduction . . . 125
5.2 Experimental section . . . 126
5.2.1 Materials . . . 126
5.2.2 Selection of growth medium and characterization of cells grown in monolayer culture . . . 127

5.2.3 Routine culture of hASCs 127
5.2.4 Microcarrier preparation and conditioning 128
5.2.5 Culture on microcarriers in semi-static condition 128
5.2.5.1 General procedure 128
5.2.5.2 Cell seeding density optimization 129
5.2.5.3 Influence of coating and microcarrier morphology on cell behaviour 129
5.2.5.4 Comparison of performance of MC50-RGD-1 with a commercial microcarrier 131
5.2.5.5 Influence of magnetic nanoparticles on cell adhesion and proliferation 133
5.2.6 Cell characterization 133
5.2.6.1 Metabolic activity 133
5.2.6.2 DNA quantification 134
5.2.6.3 Cell viability 134
5.2.6.4 Cell nucleus and cytoskeleton staining 134
5.2.6.5 Oil red O staining 134
5.2.6.6 Alizarin red staining 135
5.2.7 Statistical analysis 135
5.3 Results and discussion 136
5.3.1 Selection of growth medium and characterization of cell proliferation in monolayer culture 136
5.3.2 Cell seeding density optimization 138
5.3.3 Influence of coating and microcarrier morphology . . . 141
5.3.3.1 Cell adhesion and proliferation 141
5.3.3.2 Cell morphology 146
5.3.4 Comparison of MC50-RGD-1 with a commercial microcarrier 148
5.3.4.1 Proliferation assays 148
5.3.4.2 Preliminary differentiation assays 152
5.3.5 Comparison of cell adhesion and proliferation on magnetic and non-magnetic microcarriers 153
5.4 Conclusion 155
5.5 Appendix 156
5.5.1 Feasibility of DNA quantification of cells in presence of microcarriers 156

6 Stem cell culture on microcarriers in dynamic condition 157

6.1 Introduction . . . 157
6.2 Experimental section . . . 159
6.2.1 Materials . . . 159
6.2.2 Microcarrier preparation and conditioning . . . 160
6.2.3 Cell culture on microcarriers in dynamic conditions . . . 160
6.2.3.1 General procedure . . . 160
6.2.3.2 Bead-to-bead cell transfer assays . . . 161
6.2.4 Cell characterization . . . 163
6.2.4.1 Metabolic activity . . . 163
6.2.4.2 Cell viability . . . 163
6.2.4.3 Cell nucleus and cytoskeleton staining . . . 163
6.2.4.4 SEM observation . . . 163
6.2.5 Statistical analysis . . . 163
6.3 Results and discussion . . . 164
6.3.1 Cell proliferation . . . 164
6.3.2 Bead-to-bead transfer . . . 167
6.4 Conclusion . . . 168

7 Conclusion and perspectives **169**
7.1 Conclusion . . . 169
7.2 Future work . . . 171
7.3 Alternative uses of microcarriers . . . 172

Bibliography **175**

A Appendix **213**
A.1 Accepted paper: Green and Tunable Animal Protein-Free Microcarriers for Cell Expansion. . . . 213

List of Acronyms

αMEM Minimum Essential Medium Eagle alpha.

AGM alternating gradient magnetometry.

ALG alginate.

ASC adipose-derived stromal/stem cell.

AT adipose tissue.

ATMPs advanced therapy medicinal products.

ATRP atom transfer radical polymerization.

BDNF brain-derived neurotrophic factors.

BMSC bone-marrow mesenchymal stem cell.

BSA bovine serum albumin.

CAP cell adhesion peptide.

CHI chitosan.

CLSM confocal laser scanner microscopy.

COL collagen.

CSA chondroitin sulfate A.

DAPI 4',6-Diamidine-2'-phenylindole dihydrochloride.

DMEM Dulbecco's modified Eagle medium.

DNA deoxyribonucleic acid.

ECM extracellular matrix.

EDC 1-ethyl-3-(3-dimethylaminopropyl) carbodiimide.

ELRs elastin-like recombinamers.

EMA European Medicines Agency.

ESC embryonic stem cell.

FA focal adhesion.

FBS fetal bovine serum.

FDA Food and Drug Administration.

FN fibronectin.

GAG glycosaminoglycan.

GCP good clinical practice.

GEM global eukariotic microcarrier.

GMP good manufacturing practice.

GTMP gene therapy medicinal product.

HA hyaluronic acid.

hASC human adipose-derived stromal/stem cell.

HEMA 2-hydroxyethylmethacrylate.

HEP heparin.

HFR hollow-fiber reactor.

hPL human platelet lysate.

HSC hematopoietic stem cell.

HUVEC human umbilical vein endothelial cell.

ICP-AES inductively coupled plasma atomic emission spectrometry.

iPSC induced pluripotent stem cell.

LbL layer-by-layer.

LCST lower critical solution temperature.

LN laminin.

MA marketing authorization.

MC microcarrier.

MNP superparamagnetic nanoparticle.

MRI magnetic resonance imaging.

MRN magnetic resonance navigation.

MSC mesenchymal stromal/stem cell.

NHS N-hydroxysuccinimide.

NIPAM N-isopropylacrylamide.

NMRP nitroxide-mediated radical polymerization.

NP nanoparticle.

NSC neural mesenchymal stem cell.

PAA poly(acrylic acid).

PAH poly(allylamine hydrochloride).

PBR packed bed reactor.

PBS phosphate buffer saline.

PCL polycaprolactone.

PDMS poly(dimethylsiloxane).

PE polyelectrolyte.

PEG poly(ethylene glycol).

PEM polyelectrolyte multilayer.

PEST penicillin/streptomycin.

PFA paraformaldehyde.

PGA poly(L-glutamic) acid.

pI isolectric point.

PLA poly(lactide).

PLGA poly(lactic-co-glycolic acid).

PLL poly-L-lysine.

PLLA poly-(L-lactide).

PLO poly-L-ornithine.

PNIPAM poly(N-isopropyl acrylamide).

PS polystyrene.

PSS poly(styrenesulfonate).

RAFTP reversible addition-fragmentation chain transfer polymerization.

RGD arginine-glycine-aspartic acid.

rhBMP2 human recombinant bone morphogenetic protein 2.

ROP ring opening polymerization.

SAM self-assembled monolayer.

SCTMP somatic-cell therapy medicinal product.

SEM scanning electron microscope.

SPION superparamagnetic iron oxide nanoparticle.

ST stirred tank.

Sulfo-NHS N-hydroxysulfo-succinimide.

SVF stromal vascular fraction.

TCPS tissue culture-treated poly(styrene).

TEM transmission electron microscope.

TEP tissue-engineered product.

UMSC umbilical cord mesenchymal stem cell.

VN vitronectin.

List of Figures

1.1 Schematic view of AT components.[6]. 4
1.2 (a) Number of clinical trials using MSCs according to MSC source and clinical trial phase (BM : bone-marrow, UC : umbilical cord). (b) Number of clinical trials per type of condition and clinical trial phase. Clinical trials data gathered from 2004 to 2018.[32]. . . . 8
1.3 Current therapeutic strategies using stem cells. Adapted from reference [33]. 9
1.4 Schematic view of EU legal texts relevant to cell-based medicine.[34]. 10
1.5 Classical monolayer culture vessels: (a) well-plate, (b) flask, (c) multilayer flask, (d) roller bottle.[51]. 15
1.6 Small-scale dynamic culture systems: (a) spinner flask, (b) shaker flask.[51]. 16
1.7 Schematic view of different spinner flask types : (A) Traditional (B) paddle impeller (C) rod-stirred (D) plough impeller.[55]. 17
1.8 Schematic representation of large-scale dynamic systems and their working principle: (A) stirred tanks, (B) wave bioreactor, (C) hollow-fiber reactor, (D) packed-bed reactor.[56]. 18
1.9 Schematic representation of integrins in their active and inactive conformation.[144]. 34
1.10 The different stages of the cell adhesion process.[146]. 35
1.11 An overview of the macromolecular organization of the ECM.[161]. 37
1.12 Tissue elasticity widely varies depending on its function.[155]. . . 38
1.13 Positive charge density in HEMA hydrogels supports better cell attachment and spreading that neutral and negative charge densities.[169]. 40
1.14 Cell adhesion as a function of surface wettability.[170]. 41
1.15 Differentiation of naive hMSCs as a function of the value of the Young modulus (E) of polyacrylamide gel substrates. Scale bar is 20 µm.[178]. 43

1.16 A) Osteoblast cultures mineralize significantly less on grooved surfaces as compared with rough surfaces, as demonstrated by Alizarin Red S staining. Non-mineralizing "UI" cells were used as a negative control. Surface morphology of grooved and rough surfaces are shown in images (B) and (C), respectively. Adapted from reference [195]. 45
1.17 Cell adhesion on surfaces with roughness gradient. A) Representative images of actin filaments of MSCs cultured 24 h on a surface showing roughness gradient. B) Cell spreading area versus different roughness gradients. C) Circularity and D) filopodia length of the adhered MSCs on different surface gradients. E) Representative SEM images of adhered cells on roughness gradient surfaces. Scale bar indicates 15 µm, inset bar indicates 5 µm.[189]. 47
1.18 Schematic representation of the cytoskeletal forces acting on the nucleus. Cytoskeletal tension creates a push force on convex and flat surfaces leading to compression and deformation of the nucleus. A cytoskeletal pull force on concave surfaces results in a rounded nucleus shape.[200] 49
1.19 Arginylglycylaspartic acid (RGD) sequence.[141]. 53
1.20 Overview of protein immobilization techniques. 55
1.21 Coupling reactions using (a) amine chemistry on (1) NHS-derivatized and (2) aldehyde-derivatized surfaces; (b) carboxyl chemistry using carbodiimide activation; (c) thiol chemistry on (1) maleimide-derivatized, (2) disulfide-derivatized, and (3) vinyl sulfone-derivatized surfaces.[256] 58
1.22 Schematic illustration of the interaction between avidin/streptavidin and biotin. 60
1.23 Schematic illustration of SAM. Adapted from [272]. 62
1.24 Formation of (a) silane monoloayer on hydroxylated surface and (b) thiol monolayer on gold surface. Adapted from [275]. 63
1.25 Schematic illustration of different methods to synthesize polymer brushes on material surface: physisorption, “grafting-to” and “grafting-from”.[288]. 67
1.26 Principle of cell harvesting on MCs that are surface-modified with a thermoresponsive PNIPAM polymer brush. Adapted from reference [136]. 68

1.27 Illustration of the first two steps of LbL technique based on the alternate deposition of oppositely charged polymer chains.[291]. 69
1.28 Schematic illustration of the dipping process used to produce LbL assemblies.[291]. 70
1.29 Modulation of PLL/HA film stiffness following crosslinking improves chondrosarcoma cell adhesion and spreading.[315]. 74

3.1 (a) L-lactic acid monomer; (b) D-lactic acid monomer. 83
3.2 (a) Poly(L-lactide) structure, (b) Poly(ethylene glycol) structure. . 84
3.3 Description of the fabrication process of magnetic MCs via spherulitic crystallization of PLLA. 86
3.4 SEM images illustrating the influence of PLLA20 content in the blend (indicated in sample name) on MC morphology. The MCs were obtained at a crystallisation temperature of 110° C. The scale bars are identical in the six panels. 93
3.5 (A) SEM images of MC20 prepared with PLLA20 at different crystallization temperatures. The scale bars are identical in all panels. (B) Boxplot showing the variation of MC20 size versus crystallization temperature (N=50)."+" signs indicate outliers. 94
3.6 SEM images (A) and Boxplot (N=50) of size (B) of MC50 prepared at a crystallization temperature of 110°C, using the same PLLA/PEG ratio (50/50) but different PLLA molar masses (*i.e.*, PLLA20 and PLLA40). The scale bars are identical in the two panels. "+" signs indicate outliers. 95
3.7 Epifluorescence microscopy images showing MC20 (prepared with PLLA20 and crystallized at 130 °C) containing different concentrations of fluorescent MNPs: (A) 3; (B) 1; (C) 0.1 and (D) 0.01 mg Fe/g PLLA20. The scale bars are identical in all panels. 97
3.8 TEM images showing MNPs distribution in MC20 (prepared with PLLA20 and crystallized at 110 °C) and loaded with 3 mg Fe /g PLLA20 at two magnifications. 98
3.9 Amount of iron (measured by ICP-AES) released from MC20 prepared from PLLA20 and crystallised at 110 °C as a function of the incubation time in PBS buffer at room temperature and under agitation. 100
3.10 AGM hysteresis curves measured for MC20 prepared from PLLA20 and crystallised at 110 °C with 1 mg Fe/g PLLA20 and 3 mg Fe/g PLLA20 incorporated in the blend. 101

3.11 (Left) optical microscopy images of MC50 crystallized at 110°C, using PLLA20 (A) and PLLA40 (C), after two days and seven days of stirring at 40 rpm in a spinner flask, respectively. The scale bars are identical in both panels. (Right, B) Variation of the sedimentation rate of PLLA40 MCs measured in water as a function of the processing parameters used for their fabrication, *i.e.*, crystallization temperature and PLLA40/PEG ratio. 103
3.12 SEM images of MCs crystallized at 110 °C using different PLLA40 content: (A) MC30, (B) MC50 and (C) MC70 for semi-static cell assays. (D) Size distribution of MCs prepared at 110 °C before and after sieving, (N=50). The scale bars are identical in all panels. . 104
3.13 Magnetic MC50 can be immobilized in solution by using a magnet and quickly released after magnet removal. 106
3.14 A) SEM images of MC50 used for dynamic culture assays. B) Size distribution of M50 prepared at 103 °C before and after sieving, (N=50). "+" signs indicate outliers. 106
3.15 Size of MC20 prepared at a crystallization temperature of 103 °C, using the same PLLA/PEG ratio (20/80) but different PLLA molar masses (*i.e.*, PLLA20 and PLLA40), (N=50). "+" signs indicate outliers. 108
3.16 A) PEG powder containing fluorescent NPs after freeze-drying. B) PEG containing fluorescent NPs molten at 230 °C confirms that NPs remain fluorescent even after exposure to a high temperature. The control consists of an area without any molten PEG-MNP. The scale bars are identical in both images. 108

4.1 Chemical structure of (a) HA and (b) PLO used for LbL deposition onto PLLA MCs. 111
4.2 Surface biofunctionalization of PLLA MC by LbL assembly of PLO and HA followed by post-crosslinking and grafting of a bioadhesive RGD peptide. 112
4.3 Deposition of LbL film composed of PLO and HA on MCs. 113

4.4 (a) EDC/Sulfo-NHS coupling scheme: (1) EDC reacts with a carboxylic group and activates it to give a O-acylisourea intermediate; (2) The activated complex is converted into an active ester with sulfo-NHS; (3) The active ester reacts with primary amine to form an amide bond; (4) The unreacted sites are hydrolyzed to give a regeneration of the carboxylic groups. Scheme adapted from [308]. (b) Crosslinking of PLO/HA film by formation of amide bonds following the reaction of activated carboxylic sites coming from HA with primary amine groups coming from PLO. 117
4.5 (A) Variation of the dry thickness of crosslinked PLO/HA films grown on silicon substrate, as a function of the number of deposited bilayers n (ellipsometry measurements); confocal laser scanner microscopy (CLSM) images of $(PLO/HA)_8$-coated (B) and bare (C) MC50 dipped in rhodamine solution. Fluorescence intensity quantification is provided in Figure 4.8 in appendix 4.6.1. 119
4.6 RGD peptide grafting on crosslinked PLO/HA films is performed through the formation of amide bonds between the activated carboxylic sites coming from HA with amine groups in the peptide sequence following the action of EDC and sulfo-NHS. 120
4.7 (Top) Fluorescence microscopy images of crosslinked $(PLO/HA)_8$ films deposited on flat model surfaces (A) activated by sulfo-NHS/EDC and incubated in 1 mM or (B) 0.1 mM RGD-FITC solution; (C) control consisting of crosslinked $(PLO/HA)_8$ film incubated in 0.1 mM RGD-FITC solution without any prior activation. Deliberate scratches (see white arrows) were made on the films to visualize the fluorescence background. (Bottom) Fluorescence microscopy images of MC50 coated with crosslinked $(PLO/HA)_8$ (D) activated and incubated in 1 mM or (E) 0.1 mM RGD-FITC peptide solution; (F) control without any prior activation then incubated in 0.1 mM RGD-FITC solution. The scale bars are identical in each line. Fluorescence intensity quantification is provided in Figures 4.9 and 4.10 in appendix 4.6.1. 121
4.8 Fluorescence intensity of $(PLO/HA)_8$-coated and bare MC50 dipped in rhodamine solution. Bars topped with different letters indicate significant difference (p-value < 0.05). 123

4.9 Fluorescence intensity of crosslinked $(PLO/HA)_8$ films deposited on flat model surfaces either adsorbed with 0.1 mM RGD-FITC (no activation through sulfo-NHS/EDC) or grafted with 0.1 mM or 1 mM RGD-FITC solution following sulfo-NHS/EDC activation. Bars topped with different letters indicate significant difference (p-value < 0.05). 123
4.10 Fluorescence intensity of crosslinked $(PLO/HA)_8$ films deposited on MC50 either adsorbed with 0.1 mM RGD-FITC (no activation through sulfo-NHS/EDC) or grafted with 0.1 mM or 1 mM RGD-FITC solution following sulfo-NHS/EDC activation. Bars topped with different letters indicate significant difference (p-value < 0.05) .124

5.1 General procedure for hASC culture on MCs in semi-static condition.129
5.2 Methodology used to assess hASC differentiation potential. . . . 133
5.3 Phase contrast images of cell grown in (A) Mesenchymal Stem Cell Growth Medium 2 from PromoCell and (B) DMEM from Thermo Fisher Scientific supplemented with 10 % FBS bought from Sigma-Aldrich. Scale bars are identical in all panels. 137
5.4 Proliferation of hASCs grown in monolayer culture in Mesenchymal Stem Cell Growth Medium 2 (Promocell) as measured via the metabolic activity change relative to D0. (N=2, n=3). 137
5.5 Live/Dead images of MC50-RGD-1 inoculated with hASCs at densities of 2 500, 3 500, 5 000 and 7 500 cells/mg of MC on day 1, 3 and 5. White arrows indicate floating cells. Scale bars are identical in all panels. Magnified images can be visualized in the electronic version. 140
5.6 hASC proliferation performed in semi-static condition on MCs with different surface morphologies and coatings. Bars represent the mean $\pm$ standard deviation. Bars topped with different letters indicate significant difference (p-value < 0.05). Horizontal dashed lines indicate the limit of detection. (N=2, n=3). 141
5.7 Live/Dead images of cells on MCs with different surface morphologies and coatings on D0. Scale bars are identical in all panels. Magnified images can be visualized in the electronic version. . . 144
5.8 Live/Dead images of cells on MCs with different surface morphologies and coatings on D2. Scale bars are identical in all panels. Magnified images can be visualized in the electronic version. . . 145

5.9 Live/Dead images of cells on MCs with different surface morphologies and coatings on D5. Scale bars are identical in all panels. Magnified images can be visualized in the electronic version. . . 146
5.10 CLSM images of cytoskeletal organization and spreading of hASCs grown on MC50 with different coatings on day 0 (left) and day 4 (right). Phalloidin stains actin filaments (green) and DAPI stains cell nuclei (blue). White arrows indicates spreading cells on day 0. Scale bars are identical in all panels. Magnified images can be visualized in the electronic version. 147
5.11 Cell proliferation on MC50-RGD-1 and Cytodex® 3: (A) relative fluorescence intensity (RFU); (B) metabolic activity change. Bars topped with different letters indicate significant difference (p-value < 0.05). (N=2, n=3) 150
5.12 Live/Dead images of cell grown on MC50-RGD-1 and Cytodex® 3 on day 0, day 2 and day 5, as well as a qualitative evaluation of the detachment efficiency. Scale bars are identical in all panels. Magnified images can be visualized in the electronic version. . . 151
5.13 Osteogenic and adipogenic differentiation of hASCs grown in 2D and on MC50-RGD-1 and Cytodex® 3. (A) Visualization of the matrix mineralization by Alizarin Red staining after 21 days of osteogenic induction. (B) Visualization of the lipid droplets by Oil red O staining after 21 days of adipogenic induction. Scale bars in whole-well images represent 2 mm. 153
5.14 Cell proliferation of hASCs on magnetic and non magnetic MC50-RGD-1 as measured by metabolic activity. Bars topped with different letters indicate significant difference (p-value < 0.05). (N=2, n=3) 154
5.15 Displacement of cell-laden magnetic MCs when submitted to a 1.4 T magnet. The arrow indicates the direction of the field. Each picture is taken approximately every three seconds. 154
5.16 DNA quantification of cells alone and cells in presence of MC50-RGD-1 and Cytodex® 3 using 3000 and 30000 cells. (N=2, n=3). 156

6.1 Magna-Flex™ spinner flask used for dynamic cell culture. 159
6.2 Methodology used for hASC culture on MCs in dynamic condition. 161

6.3 Methodology used for bead-to-bead cell transfer assays performed with hASCs cultured on MC50-RGD-1. 50% of fresh MC50-RGD-1 (stained in red) were added to the existing culture after four days of cell expansion. 162
6.4 Viability and proliferation of hASCs grown on MC50-RGD-1 in dynamic condition. (A) Quantification of cellular metabolic activity. (N=3, n=3). (B) Analysis of hASC viability by Live/Dead staining. 165
6.5 Cytoskeletal organization and spreading of hASCs grown on MC50-RGD-1 surface: (A) CLSM micrographs of stained hASCs. Phalloidin stains actin filaments (green) and DAPI stains cell nuclei (blue). (B) SEM images of hASCs grown on MC50-RGD-1. . . . 166
6.6 Bead-to-bead cell transfer assay performed with hASCs cultured on MC50-RGD-1. 50% of fresh MC50-RGD-1 (stained in red) were added to the existing culture after four days of cell expansion. Images were taken after 12 h of intermittent agitation. Cells were stained with Calcein AM. 168

List of Tables

1.1 Surface antigen expression for MSCs. 3
1.2 List of ATMPs with MA in the European Union until 2018. Adapted from reference [45]. 13
1.3 Overview of the advantages and drawbacks of various cell expansion technologies. 21
1.4 Overview of the most known commercial MCs and their characteristics. DEAE stands for diethylaminoethyl. Macroporous MCs are in bold.[56, 78]. 28
1.5 Overview of the advantages and drawbacks of natural proteins, synthetic peptides and recombinant proteins for the biofunctionalization of surfaces. 54
1.6 Commonly available functional groups in proteins, associated amino acid and required functionality of the surface. Adapted from reference [256]. 56
1.7 Overview of the advantages and drawbacks of the different surface immobilization techniques. 61
1.8 Overview of the advantages and drawbacks of methods allowing to introduce surface functionalities. 75

3.1 Amount of MNPs incorporated in MCs prepared from different PLLA20/PEG ratios at 110 °C as measured by ICP-AES. 99
3.2 Number of MCs per mg as counted by optical microscopy and estimated surface area per mg of MC. 105
3.3 Surface roughness of MC30, MC50 and MC70 crystallized at 110 °C from PLLA40 and used for semi-static cell assays. 105

5.1 Summary of the samples used to assess the influence of the coating and MC morphology on cell adhesion and proliferation. The percentage of PLLA40 used to prepare each sample is clearly indicated in the name of the samples. Uncoated MCs are referred to as MC-bare, MCs coated with crosslinked $(PLO/HA)_8$ are referred to as MC-LbL, and MCs coated with crosslinked $(PLO/HA)_8$ then grafted using 0.1 and 1 mM RGD peptide are referred to as MC-RGD-0.1 and MC-RGD-1, respectively. 131
5.2 Overview of the characteristics of MC50-RGD-1 and Cytodex® 3. 132
5.3 Overview of the different seeding densities tested in semi-static condition. 138

1 Context of research

1.1 Stem cells and cell-based therapies

1.1.1 Stem cells

1.1.1.1. Definition

Stem cells differ from other cell types by two important properties. The first one is the ability of self-renewal which means the capacity to go through numerous cycles of cell division while maintaining the undifferentiated state. The second key property of stem cells is their potential to develop, under the right conditions, or given the right signals, into mature cells with characteristic shapes and specialized functions. This ability is a process called differentiation.[1] However, not all stem cells possess the same differentiation propensity. Totipotent or omnipotent cells are able to differentiate into both embryonic and extra-embryonic tissues, thereby forming the embryo and the placenta. Pluripotent stem cells can differentiate into any of the three germ layers (ectoderm, endoderm, and mesoderm) from which all tissues and organs develop. Multipotent stem cells are found in most tissues and differentiate into cells from a single germ layer. Oligopotent stem cells are able to self-renew and form two or more lineages within a specific tissue. Finally, unipotent stem cells can self-renew and differentiate into only one specific cell type and form a single lineage.[2]

1.1.1.2. Classification

Stem cells can be classified based on their origin:

- **Embryonic stem cells (ESCs)**: ESCs are derived from embryos. More precisely, these cells are isolated from the inner cellular mass of a blastocyst. They are pluripotent cells, which means they have the potential to

generate cells derived from the three germ layers: ectoderm, mesoderm and endoderm. However, since harvesting those cells necessitates destroying the embryo, the use of ESCs raises ethical concerns related to the moral status of the embryo.[1, 3]

- **Induced pluripotent stem cells (iPSCs)**: IPSCs are adult cells that have been genetically reprogrammed into cells that behave like embryonic stem cells. iPSCs are derived from differentiated cells such as skin fibroblasts following the introduction of four specific genes encoding transcription factors. They appear to have the same potential and properties as ESCs but do not require a source of embryos.[4] In addition, they could potentially constitute an unlimited supplies of autologous cells. However, clinical applications are still limited as the genetic stability of iPSCs remains to be elucidated. Indeed, the vectors used to introduce transcription factors to adult cells could cause cancers.[5]
- **Adult stem cells**: Adult stem cells also known as resident stem cells are undifferentiated cells found in stem cell niches located throughout the body that divide to replenish dying cells and regenerate damaged tissues.[1, 2] Those cells thus contribute to the continuous regeneration of our body, with specific cycles for each type of tissue. For example, human epidermis is renewed every three to four weeks while it takes only a few days to regenerate the gastrointestinal epithelium.[2] While adult stem cells have a lower ability to differentiate than ESCs and iPSCs, they still offer several advantages. Unlike ESCs, they do not raise issues of rejection or ethical controversies. Compared to iPSCs, the production cost is lower and there is no issue regarding potential risks associated with the transcription factors mentioned above.[5, 6]

  The first adult stem cells to be described were the hematopoietic stem cells (HSCs) discovered by Becker and co-workers in 1963.[6] These cells are non-adherent cells found in the bone marrow that are in charge of blood cell production in a process called hematopoiesis.[7]

  Mesenchymal stromal/stem cells (MSCs) belong to another subcategory of adult stem cells precisely defined by the International Society for Cellular Therapy [8] based on the following three criteria:

  1. **Plastic adherence** on tissue culture-treated poly(styrene) (TCPS);

2. **Specific surface antigen expression** described in Table 1.1;

Positive (>95%)	Negative (<2%)
CD105	CD45
CD73	CD34
CD90	CD14 or CD11b
	CD19 or CD79α
	HLα-DR

Table 1.1.: Surface antigen expression for MSCs.

3. **Multipotent differentiation potential** to osteogenic, adipogenic and chondrogenic lineages under standard in vitro differentiating conditions.

Bone-marrow mesenchymal stem cells (BMSCs) were the first type of MSCs to be identified, following a pioneering study of Friedenstein and coworkers in 1966.[9] Following their identification almost 60 years ago, BMSCs have been widely studied and considered as the reference in the field of adult stem cell biology and regenerative medicine. Since then, other types of MSCs have been located in many tissues (umbilical cord blood, adipose tissue, brain, liver, lungs, spleen and placenta).[10, 11] The therapeutic potential of MSCs is now well described and three mechanisms of action have been associated with their therapeutic effects [11] : tissue replacement via multipotent differentiation,[12] immunomodulation [13] and paracrine effect via the secretion of molecules that instigate or assist in tissue repair.[14] It is now believed that immunomodulatory properties and paracrine activity play a more predominant role in the beneficial effect of MSCs than differentiation itself.[11, 14]

1.1.1.3. Adipose-derived stem cells

Adipose tissue. While adipose tissue (AT) has long been considered as a simple energy storage, it is now clear that it serves as an important endocrine

organ that controls metabolism, immunity and satiety with systemic as well as local effects through the release of various molecules. For example, secretion of adipokines such as adiponectin, leptin, resistin, *etc.*, modulate homeostasis, blood pressure, and lipid and glucose metabolism.[15, 16] Since 2001, AT is also recognized as an important source of MSCs.[17] The AT is thus a complex tissue consisting of mature adipocytes and a stromal vascular fraction (SVF) which includes preadipocytes, endothelial cells, fibroblasts, vascular smooth muscle cells, resident monocytes/macrophages, lymphocytes, and adipose-derived stromal/stem cells (ASCs) [18–20], as illustrated in Figure 1.1. In culture, ASCs typically display a fibroblast-like spindle-shaped morphology.[21]

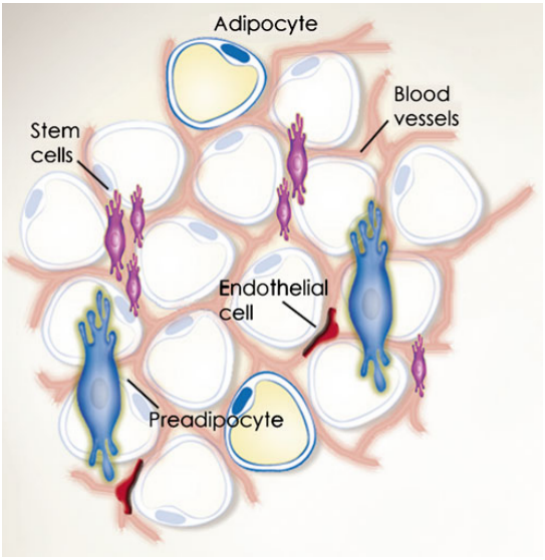

Figure 1.1.: Schematic view of AT components.[6].

Isolation. Current methods for isolating ASCs from AT consist of several steps. The adipose tissue is firstly minced into small fragments then digested using collagenase. The cellular components are then separated by centrifugation, allowing to isolate the SVF from primary adipocytes. Indeed, the supernatant contains the mature adipocytes, which float due to their high lipid content, and the pellet contains the SVF components. The final separation step allows to isolate ASCs from other SVF components by taking advantage of the adhesion properties of ASCs. The SVF cells are thus plated and incubated overnight followed by washing to remove non-adherent cells.[6, 18, 22, 23] The number of

ASCs isolated from 1 g of AT is highly variable, ranging from 5×10^3 to 2×10^5 cells. These differences arise from donor characteristics, such as gender, age, ethnicity, body mass index, disease history, type of AT (yellow/brown), location (subcutaneous/ visceral fat) and the tissue collection method or culture conditions.[18]

ASCs versus BMSCs. ASCs offer several advantages over BMSCs and are now considered as an interesting alternative source of MSCs for regenerative medicine.[10, 18] Unlike bone-marrow, subcutaneous AT is easily accessible and abundant and thus ASCs can be harvested in large quantities with minimal risk and pain. As obesity becomes an increasing problem, wastes coming from plastic surgery such as liposuction aspirates constitute a promising source of ASCs. Indeed, about 400 000 liposuction surgeries are performed in the US each year and these procedures yield from 100 mL to 3 L of lipoaspirate.[18] AT also yields a greater number of cells compared to bone-marrow. While the average frequency of ASCs in processed fat tissue is 2 % of nucleated cells, this number drops to 0.001–0.01 % in the case of BMSCs.[6, 10, 18] Then, even if ASCs and BMSCs can both differentiate into chondrocytes, osteoblasts, adipocytes, hepatocytes, neuron-like cells, and myocytes, their differentiation potential is not always identical.[24] Controversial results have been obtained for both the osteogenic and chondrogenic differentiation capacity. For example, earlier studies show that there is no difference between ASCs and BMSCs regarding the chondrogenic differentiation potential, while some recent articles claim that the BMSCs show a higher chondrogenic differentiation potential.[24] However, these results should be considered with caution as ASCs may require different chemical stimuli for differentiation, considering the different niches of the two cell populations. Indeed, most studies used the same culturing conditions for both ASCs and BMSCs.[24] Finally, when the neovascularization potential of BMSCs and ASCs was compared in mice, a better neovascularization was observed with ASCs.[25]

1.1.2 Cell-based therapies

1.1.2.1. Introduction and definition

The use of live cell-based therapies in medicine is not a new concept. The first successful human HSC transplant took place in 1956. The patient, who had leukemia, was given radiotherapy and then treated with healthy bone marrow from an identical twin.[26] Several years of research on histocompatibility were necessary for the first successful HSC transplant where donor and recipient were not twins to happen.[27] In the following years, this procedure was widely adopted for bone marrow cancers and extended to treat a variety of other clinical indications such as inherited immunodeficiency.[27, 28] Since then, a wide variety of cell types have been assessed for various therapeutic applications. It is worth noting that cell-based therapies are not restricted to stem cells, as other cell types such as fibroblasts, lymphocytes, endothelial cells, pancreatic islets, *etc.*, have been considered as well.[29]

1.1.2.2. Types of therapies

Cell-based therapies can be classified according to various criteria. A first important distinction arises from the cell source : a therapy based on the patient's own cells is referred to as autologous as opposed to allogeneic therapies for which the cells come from a donor. While autologous therapies avoid concerns about immune rejection, it also presents several drawbacks such as variability of source material, difficulty to generate large numbers of cells, inability to deal with emergencies and difficulties to address large numbers of patients at reasonable costs due to minimal potential for economies of scale. On the other hand, allogeneic therapies are associated with risks of immune rejection or cell abnormalities due to large *in vitro* replication but obtaining a large population of homogeneous cells is easier and less expensive and cells are always available. Autologous therapies are thus more suitable for hospital-centered personalized patient services while allogeneic therapies are more commercial product-oriented.[30]

Cell therapies can also be classified by the therapeutic indication they aim to address such as cardiovascular, musculoskeletal , neurological, ophthalmological pathologies, *etc.* as well as the cell source. For example, focusing only on

MSCs, the first and most widely used cell type in clinical trials is still BMSCs, followed by umbilical cord mesenchymal stem cells (UMSCs) and ASCs, with these three sources accounting for the vast majority of clinical trials, as seen in Figure 1.2a.[31, 32] From Figure 1.2b, it is clear that MSCs-based therapies aiming to address neurological (*e.g.*, spinal cord injury, multiple sclerosis, amyotrophic lateral sclerosis, stroke Alzheimer's disease and Parkinson's disease), joint (*e.g.*, osteoarthritis, disc disease, rheumatoid arthritis) and cardiovascular (*e.g*., myocardial infarction, coronary artery disease) pathologies are the most predominant, with these three categories accounting for 42% of all trials.[32] Interestingly, these two Figures also indicate the phase of investigation of those clinical trials, which is an important parameter used to describe the status of a clinical trial. Indeed, phase I trial includes safety studies that elucidate the safety, side effects and best dose related to drug administration; phase II trial is performed on larger groups and allows to gather preliminary data on effectiveness in human patients; phase III trial aims at comparing the safety and effectiveness of the new treatment against the current standard treatment; and phase IV trial is a study of approved drugs involving thousands of participants for several years to gather additional information including medication long-term safety, effectiveness and any other benefits.[31] As of now, it is clear from Figure 1.2 that most clinical trials based on MSCs are still in an early phase (phase I, I/II, or II), demonstrating that the therapeutic effectiveness of MSCs still needs to be investigated.

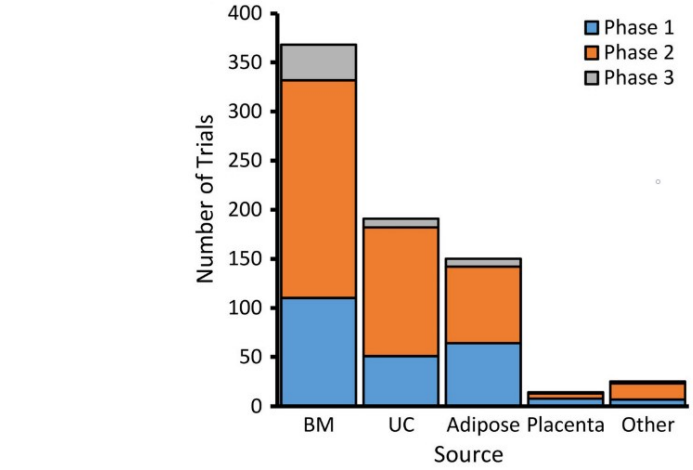

(a)

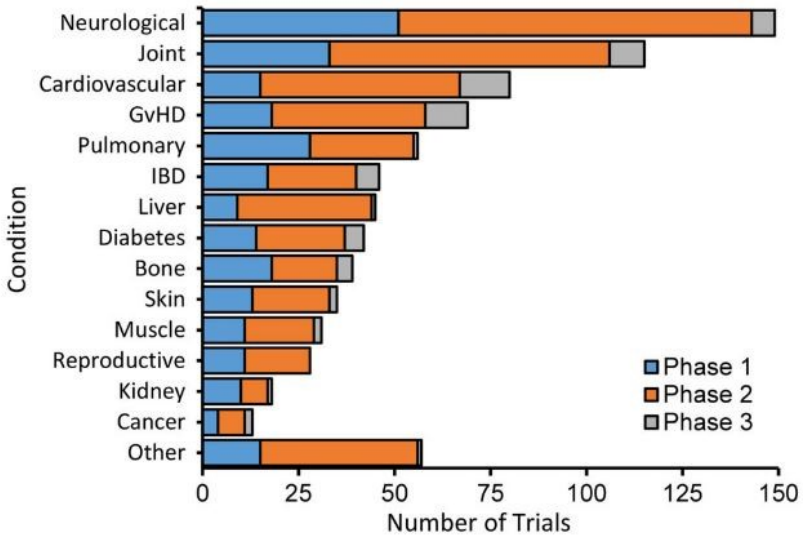

(b)

Figure 1.2.: (a) Number of clinical trials using MSCs according to MSC source and clinical trial phase (BM : bone-marrow, UC : umbilical cord). (b) Number of clinical trials per type of condition and clinical trial phase. Clinical trials data gathered from 2004 to 2018.[32].

A final classification relies on the therapeutic strategy, as illustrated in Figure 1.3. Stem cells can be directly transplanted in the host recipient tissue following *ex vivo* expansion. They can also be transduced with a viral-vector carrying a therapeutic gene and then implanted in the host recipient tissues. Finally, they can be expanded *ex vivo* and combined with biomaterials to be implanted in the recipient host to regenerate damaged tissues.[33]

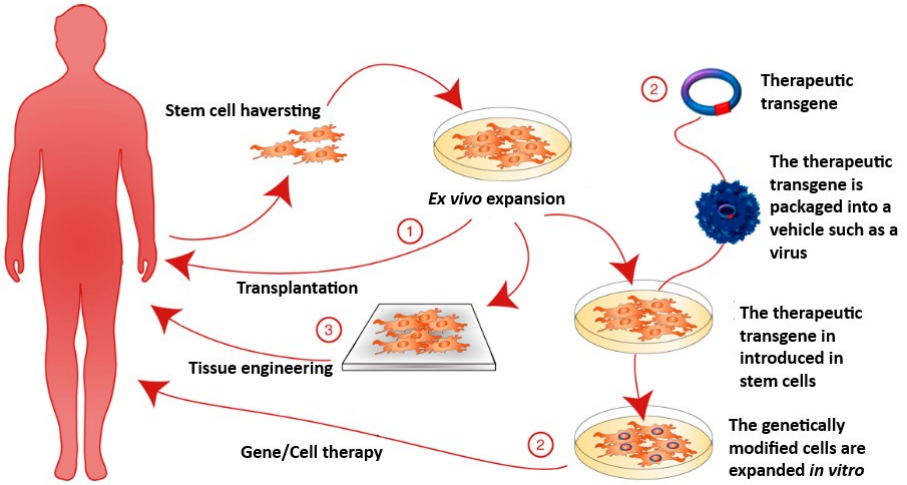

Figure 1.3.: Current therapeutic strategies using stem cells. Adapted from reference [33].

One critical aspect of those cell-based therapies is the need of a high number of cells. Indeed, several studies suggest a minimal effective dose between 100 and 150 million cells per patient.[33] Such a dose requires extensive cell expansion prior to their therapeutic use, highlighting the need for safe, efficient and cost-effective expansion technologies.

1.1.2.3. Regulative aspects of cell-based therapies

The translation of cell-based therapies from basic research to commercialization is covered by a variety of legal instruments regulating each step of the process. For Europe, these legal texts, summarized in Figure 1.4, include directives, guidelines and regulations regarding cell and tissue procurement, good manu-

facturing practice (GMP), good clinical practice (GCP), marketing authorization (MA) and pharmacovigilance.[34]

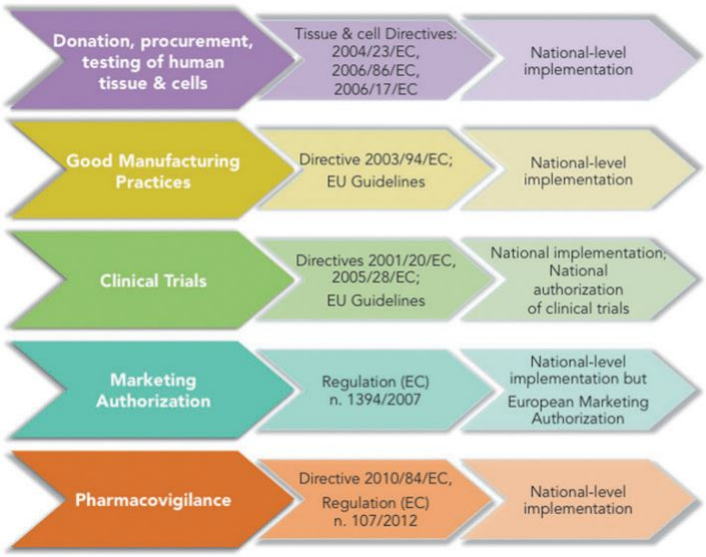

Figure 1.4.: Schematic view of EU legal texts relevant to cell-based medicine.[34].

Concerning the GMP, a critical consideration is the use of chemically-defined xeno-free cell culture media for the safe expansion of stem cells. Indeed, culture medium formulations are generally composed of a basal medium (*e.g.*, Dulbecco's modified Eagle medium (DMEM), Minimum Essential Medium Eagle alpha (αMEM)) containing nutrients such as glucose and glutamine and also a protein-rich supplement that contains growth and adhesion factors essential for the adhesion and expansion of MSCs.[35] Currently, this supplement usually consists of fetal bovine serum (FBS) which raises several issues such as ill-defined composition, batch-to-batch variability and most importantly, the risk of contamination with virus and prions. As a result, FBS has been critically rated by the European Medicines Agency (EMA) (Directive EMA/CHMP/BWP/457920/2012).[36] Moreover, it was reported that proteins derived from FBS were internalized by MSCs during culture, which increased their immunogenicity.[37] This highlights the need to find alternative culture medium formulations for the safe, reproducible and efficient large-scale production of clinical-grade cells. Several humanized culture medium formulations

were considered as an alternative, including those supplemented with platelet-rich plasma, human platelet lysate (hPL) and autologous or allogeneic human serum (auto-HS and allo-HS, respectively).[35, 38] Auto-HS has been shown to improve the expansion of MSCs from different sources but its availability is limited and contradicting results have been reported for the other alternatives.[35, 38]

Regarding the MA, it is the EMA, as the responsible body for the protection of public and animal health in EU Member States through the scientific evaluation, supervision, and safety monitoring of medicines, that is in charged of reviewing MA application for all medicinal products in EU.[39, 40] More specifically for cell-based therapies, a first important distinction arises from the concepts of "minimal manipulation" and "homologous use" of cells.[39–41] Broadly speaking, minimal manipulation involves processing that does not alter the relevant biological, physiological, or structural properties of cells or tissues such as cutting, grinding, separation, centrifugation, cryopreservation and freezing, sterilization, *etc.* More specifically, the activities considered as minimal manipulations are precisely defined by the primary regulatory body. Examples of substantial manipulation include cell culture, *in vitro* differentiation, genetic modifications, cell seeding on a medical device or enzymatic dissociation of tissue.[39] Homologous use of cells refers to "*cells or tissues that are intended to be used for the same essential function(s) in the recipient and the donor*".[40] Based on those criteria, minimally manipulated cell therapies for homologous use are governed by the same regulations that apply to any cell or tissue taken from a patient such as transfusions or transplants.[28] On the other hand, products that are either substantially manipulated or not intended for homologous use are referred to as advanced therapy medicinal products (ATMPs) by the EMA and regulated as medicines with more stringent rules.[28, 39, 40, 42] More specifically, these ATMPs are further subdivided into 3 categories:

- **Gene therapy medicinal product (GTMP)**: this category contains genes that lead to a therapeutic, prophylactic or diagnostic effect. These genes work by inserting 'recombinant' genes into the cells of the body, usually to treat a variety of diseases, including genetic disorders, cancers or long-term diseases. A recombinant gene is a stretch of DNA that is created in the laboratory, bringing together DNA from different sources;
- **Somatic-cell therapy medicinal product (SCTMP)**: these contain cells or tissues that have been manipulated *in-vitro* to change their biological

characteristics or cells or tissues not intended to be used for the same essential functions in the body. They can be used to cure, diagnose or prevent diseases;

- **Tissue-engineered product (TEP)**: these contain cells or tissues that have been modified so that they can be used to repair, regenerate or replace human tissue;

In addition, some ATMPs may contain one or more medical devices as an integral part of the medicine, which are referred to as combined ATMPs. An example of this are cells embedded in a biodegradable matrix or scaffold.

As an illustration, Table 1.2 shows the current status of ATMPs having received MA from the EMA. ChondroCelet (Tigenix, Belgium) was the first ATMP to receive MA on October 2009. It is a one-to-one treatment for cartilage lesions consisting of a suspension of cartilage cells to be implanted.[43] Since then, several ATMPs adressing various pathologies were accepted. However, several MAs were subsequently suspended for various reasons such as bankruptcy, lack of demand or commercial reasons, illustrating the difficulties faced when developing ATMPs.[44]

Name (MA holder)	ATMP type	Indication	Cell type	MA date	Status
Kymriah (Novartis)	GTP	Blood cancer	Autologous lymphocyte T	August 2018	Approved
Yescarta (Kite Pharma)	GTP	Blood cancer	Autologous lymphocyte T	August 2018	Approved
Alofisel (Takeda Pharma)	SCTMP	Perianal fistulas in Crohn's disease	Allogeneic ASCs	March 2018	Approved
Spherox (CO.DON)	TEP	Cartilage defect in the knee	Autologous chondrocytes	May 2017	Approved
Zalmoxis (MolMed)	SCTMP	Stem cell transplantation in high risk blood cancer	Genetically modified allogeneic lymphocyte T	June 2016	Approved
Strimvelis (GSK)	GTMP	Severe combined immunodeficiency	Genetically modified autologous CD34+ cells	April 2016	Approved
Imlygic (Amgen)	GTMP	Melanoma	Genetically modified herpex simplex virus	October 2015	Approved
Holoclar (Chiesi Farmaceutici)	TEP	Severe limbal stem cell deficiency in the eye	Autologous human corneal epithelial cells	March 2015	Approved
Provenge (Dendreon)	SCTPM	Metastatic prostate cancer	Autologous peripheral-blood mononuclear cells activated	October 2013	Withdrawn in 2015 (bankruptcy)
MACI (Vericel)	TEP	Cartilage defect in the knee	Autologuous chondrocytes	July 2013	Withdrawn in 2014
Glybera (uniQure)	GTMP	Lipoprotein lipase defiency	Viral vector	November 2012	Withdrawn in 2017 (lack of demand)
Chondroselect (Tigenix)	TEP	Cartilage defect	Autologous cartilage cells	November 2009	Withdrawn in 2016 (commercial reason)

Table 1.2.: List of ATMPs with MA in the European Union until 2018. Adapted from reference [45].

1.2 Cell expansion systems

As highlighted in the previous section, the industrial development of cell-based therapies relies on an efficient and cost-effective solution to expand cells up to a required number. Here, the various cell expansion techniques are reviewed from the smaller scale to the larger scale. The advantages and drawbacks of each technique are emphasized.

Animal cell lines can be cultivated *in vitro* in two basically different modes: as anchorage-independent cells by growing in suspension or as anchorage-dependent cells which require attachment to a solid substrate to spread and further proliferate.[46] Naturally, a majority of mammalian cells (with the exception of hematopoeitic cell lines and a few others) require a solid substrate for spreading and further proliferation like it occurs *in vivo*. This section thus focuses on systems used to expand anchorage-dependent cells.

1.2.1 Classical monolayer culture

The expansion of anchorage-dependent cells usually involves the culture of cells as a monolayer inside plastic well-plates (Figure 1.5a) or flasks (Figure 1.5b) in static conditions.[47–50] When large numbers of cells are not required, this technique offers the advantages of simplicity and easy-handling. Surface area ranging from 0.32 cm^2 to 9.5 cm^2 can be found in well-plates while conventional flasks offer a surface area ranging from 25 cm^2 to 225 cm^2 per flask.[51]

To increase the expansion potential, multi-layered flasks (Figure 1.5c) have been developed in an effort to provide both a space and labor-saving solution (*e.g.*, Corning® CellSTACK®, Nunc™ Cell Factory™[49]). With a number of layers ranging from 1 to 40, these multi-layered flasks offer surface areas between 636 and more than 25 000 cm^2 per vessel.[52] However, as those culture vessels grow in size and weight, they become more difficult and time consuming to handle and may even require reinforced incubators and often mechanical assist devices to support medium changes.[53] The limited possibility to monitor cell growth in line also constitutes a drawback.[49, 51]

The systems based on flasks show several other disadvantages. First, gas exchange occurs only at the medium/gas interface and the static nature of

the culture leads to concentration gradients (pH, dissolved oxygen, nutrients, metabolites, *etc.*). They also offer limited scalability as only scaling-out is possible, by increasing the number of culture units.[48] Finally, such systems also generate a significant amount of pastic waste.

An alternative to flasks are roller bottles (Figure 1.5d) which consists of revolving cylindrical containers made of glass (reusable) or plastic (disposable). Cells grow as a monolayer on the inner surface of the bottle, which is only partially filled with medium. Thanks to the movement of the roller bottle, the cells are alternately exposed to medium in the lower part and to oxygen in the upper part. The gentle agitation prevents concentration gradients in the medium while the direct contact with air provides superior gas exchange compared to flasks. Roller bottles are available typically with surface areas between 490 and 1750 cm^2 per bottle.[51] However, the absence of precise pH and pO_2 control limits the possibility for real process optimization.[48] This type of vessels also requires more incubator space compared to flasks and an automated roller bottle platform is needed, making this system more expensive than flasks.[51, 52]

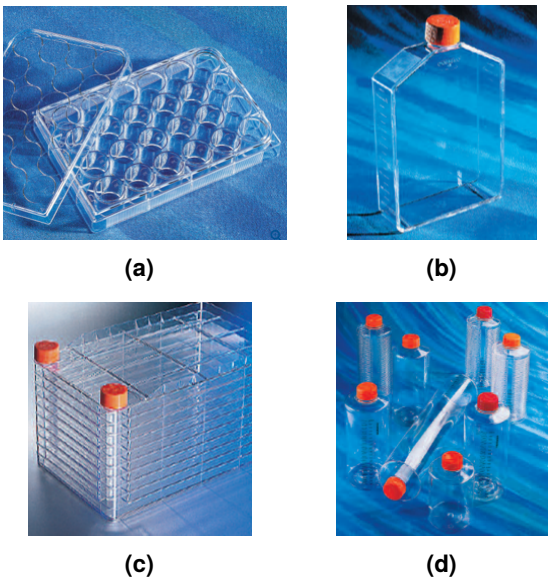

Figure 1.5.: Classical monolayer culture vessels: (a) well-plate, (b) flask, (c) multilayer flask, (d) roller bottle.[51].

1.2.2 Small-scale dynamic culture

The limitations of the aforementioned systems could finally be alleviated by the introduction of microcarrier (MC) technology by Van Wezel in 1967 (section 1.3 for detailed explanation), which relies on cell growth on the surface of small solid particles suspended in the growth medium by slow agitation.[54] This dynamic approach ensures efficient mass transfer, avoids nutrient gradients and, interestingly, allows direct bead-to-bead transfer.[48] It was indeed demonstrated that cells could colonize freshly added MCs following MC bridging and cell migration. The addition of fresh MCs leads to an increase of the available culture surface, providing an attractive solution for scale-up.[48]

(a) **(b)**

Figure 1.6.: Small-scale dynamic culture systems: (a) spinner flask, (b) shaker flask.[51].

Spinner flasks (Figure 1.6a), consisting of a vessel equipped with a stirring rod or impeller driven by a magnetic base unit, have been widely used for the suspension culture of anchorage-independent cells. Thanks to MCs, spinner flasks can also be used to grow anchorage-dependent cells. This vessel, which can either be disposable (plastic) or reusable (glass), is the most common and efficient way to expand cells using suspended MCs. It offers culture volumes ranging from approximately 100 mL to 3-5 L (plastic) or up to 36 L (glass).[49, 51, 55] The system can be found in various configurations with different impeller geometries or ball-shaped rotating agitator (Figure 1.7).

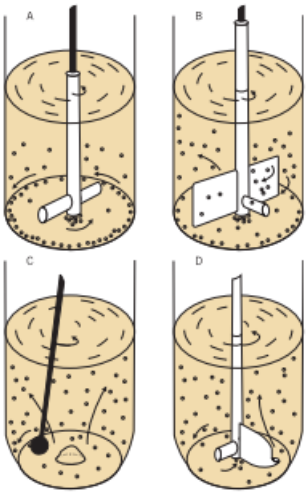

Figure 1.7.: Schematic view of different spinner flask types : (A) Traditional (B) paddle impeller (C) rod-stirred (D) plough impeller.[55].

An altervative way of using MCs includes shaker flasks (Figure 1.6b) for which MCs are kept in suspension by using a rocking platform.[55] Volumes range from 50 mL up to 6 L.[51]

MCs can also be added to roller bottles using different methods. Using the standard roller bottle technique, MCs adhere to the vessel wall thus increasing the surface area available for the cells. MCs can also be added to confluent roller bottles. Cells coming from the vessel wall migrate to MCs and continue to expand, allowing to accomplish two subcultures in the same vessel. Finally, thanks to siliconizing reagent which prevents MC and cell adhesion on the bottle surface, siliconized roller bottles can also be used for regular suspension culture, similarly to shaker flasks. [55]

Spinner flasks, shaker flasks and roller bottles all require external equipments which take space in the incubator and lead to extra costs.[51]

1.2.3 Large-scale dynamic systems

Overall, the small-scale culture systems described above are characterized by a simple design and a low level of instrumentation and control. External equipments such as incubators and shakers are thus needed to ensure the appropriate culture conditions.[52] When switching to even larger production volumes (36 L up to 2000 L), specific equipments are required to precisely monitor and control culture parameters and the dynamic approach is critical to ensure culture homogeneity in such large volumes.[55] Dynamic systems can be subdivided into two categories based on whether they are mechanically driven such as stirred and waved-mixed bioreactors or hydraulically driven such as hollow-fiber and packed-bed reactors (Figure 1.8).[56]

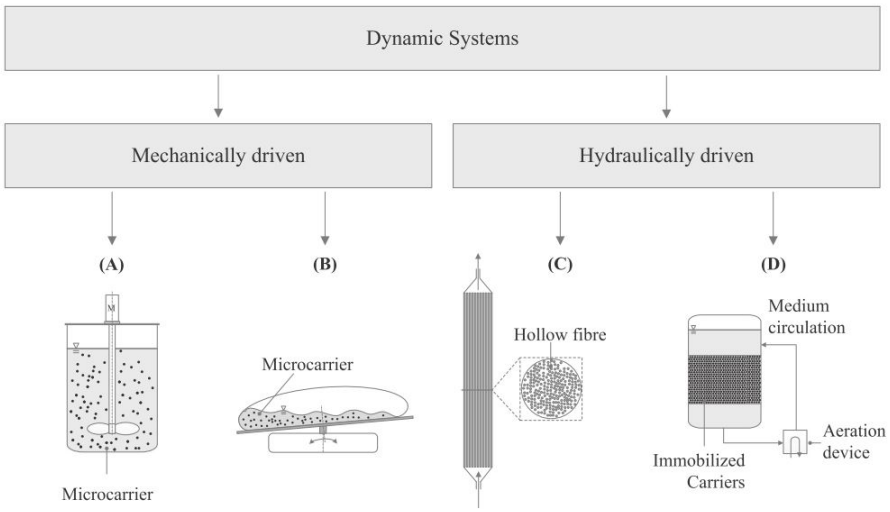

Figure 1.8.: Schematic representation of large-scale dynamic systems and their working principle: (A) stirred tanks, (B) wave bioreactor, (C) hollow-fiber reactor, (D) packed-bed reactor.[56].

Stirred tanks (STs) (Figure 1.8A) are by far the commonest method for the industrial-scale production of animal cells.[52, 56] This type of bioreactor relies on impellers to promote mixing, resulting in an homogeneous culture systems. Among the advantages of this technique are the ease of monitoring and control of culture parameters and the possibility for constant collection of samples

during the culture, allowing real time monitoring of cell growth.[57] However, beside the possibility of cell damage due to shear stress resulting from the agitation, one other downside of STs is the possible formation of MC agglomerates that restricts the transfer of nutrients to cells and impairs cell harvesting. Nevertheless, STs are more applicable for GMP production compared to other types of bioreactors due to their simplicity and scale up feasibility.[58] As a result, most commercial FDA-approved biopharmaceuticals are produced using this type of bioreactor.[57] For the wave bioreactor system (Figure 1.8B), mass transfer is based on a gentle wave motion whose intensity can be regulated by the bioreactor rocking angle, rocking rate, and filling level.[59] This type of agitation system provides good nutrient distribution and excellent oxygen transfer with moderate shear stress, resulting in an optimal culture environment for cell growth.[57] It was reported to provide a higher oxygen transfer than in spinner flask, and has been shown to perform comparably with stirred-tank bioreactors for working volumes between 1 and 100 L.[60]

Adherent cells can also be cultured on immobilized substrates, with mass transfers relying on perfusion rather than mixing. These substrates are available in various forms such as beads, fibers and scaffolds and are usually made of glass, plastic (polystyrene (PS) or polyester) or ceramics.[61, 62] This kind of system provides a low shear stress environment compared to stirred culture systems, provided that a low-flow velocity (typically not more than 3×10^{-4} m/s) is used to minimize the shear stress experienced by cells; but this can result in reduced oxygen delivery to the cells.[61] These substrates also allow the 3D culture of cells which imitates the cell natural environment with more fidelity.[63] Among these systems, hollow-fiber reactors (HFRs) (Figure 1.8C) consist of fiber-based two-compartment systems composed of intracapillary and extracapillary spaces. Cells can either grow in the intra-capillary space while the medium is perfused on the outside of fibres or into the extracellular space with intra-capillary perfusion.[64] The use of HFRs to expand cells for a clinical application was first described in 1990 by Knazek *et al.* using tumor infiltrating lymphocytes expected to treat melanoma.[65] Since then, several authors reported its use to expand stem cells such as UMSCs [66, 67], BMSCs [67, 68], iPSCs [69], neural mesenchymal stem cells (NSCs) [70], ASCs [71], *etc*. However, while HFRs provide an increased surface area for cell culture, they present difficulties in culture monitoring and scale-up.[72] Packed bed reactors (PBRs) (Figure 1.8D) are another type of perfusion-based systems.[73] The cell substrate is typically composed of immobilized carriers that are perfused with

cell culture medium. While PBRs can provide extremely high productivity within a compact size, harvesting efficiency is typically low (18%) [74] limiting the final yield. Another limitation comes from the potential concentration gradients across the packed bed through which nutrients and oxygen must diffuse which could affect cell potency and performance.[61]

From a general point of view, the majority of cell cultivation systems described in this section are single-use versions, for which the cultivation unit is only used once and then discarded. This renders cleaning and sterilization procedures unnecessary while complex qualification and validation procedures can be made easier, leading to significant cost reductions.[75] Single-use bioreactors also reduce the risk of cross contamination and enhance the biological and process safety.[56] However, environmental aspects regarding single-use bioreactors are important to consider due to the amount of disposable material used compared with conventional bioreactors.

1.2.4 Summary of cell expansion systems

As a conclusion on cell expansion technologies, an overview of the advantages and drawbacks of each cell expansion system detailed above is provided in Table 1.3. The optimal choice greatly depends on the intended use for the produced cells as well as the required cell quantity. Indeed, Simaria and coworkers performed an interesting cost-effectiveness analysis of the different expansion technologies.[76] According to them, considering a dose of 10^9 cells, the maximum feasibly achievable in flasks using eighty units of 500 mL flasks is 0.9 of a dose while using eighty ten-multilayer flasks allows to produce 11 doses. Finally, using eight bioreactors of 2000 L combined with MCs leads to 4708 doses. Additionally, the production cost varies also drastically between the different technologies, ranging from $49 per million cells produced in flasks and $15 per million cells produced in multilayer flasks to 70 cents per million cells produced in bioreactors with MCs.[76]

	Advantages	**Drawbacks**
Flask	- Simple and easy to handle - Low-cost - Widely used - Cell monitoring	- Labor-intensive - Inhomogeneous culture due to static conditions - Only scaling out
Multilayer flask	- Increased surface area available for cell growth compared to flask	- Bigger systems that are difficult to handle - Cell monitoring sometimes difficult - Inhomogeneous culture due to static conditions
Roller bottle	- Easy to use - Low-cost - Less concentration gradients due to rolling movement	- Only scaling out possible
Spinner flask	- Simple and easy to use - Homogeneous culture conditions - Cell sampling and monitoring of cell culture - Bead-to-bead transfer	- Shear stress may affect cells - Formation of MC aggregates
Stirred tank	- Homogeneous culture - Well-characterized - Easy cell sampling and monitoring - Bead-to-bead transfer - 3D environment	- Shear stresses towards cells - Formation of MC aggregates
Wave bioreactor	- Homogeneous culture - Limited shear stresses towards cells - 3D environment	- Higher cost - Cell sampling and monitoring not as easy as for ST - Formation of MC aggregates
Packed-bed reactor	- 3D culture - High production yields	- Concentration gradients of nutrients and oxygen - Cell monitoring impossible - Cell harvesting difficult
Hollow-fiber reactor	- 3D culture - High productivity	- Concentration gradients of nutrients and oxygen - Cell monitoring impossible - Cell harvesting difficult - Complex scale-up

Table 1.3.: Overview of the advantages and drawbacks of various cell expansion technologies.

1.3 Microcarriers

1.3.1 Concept

As mentioned above, the concept of MCs was developed by van Wezel in 1967 to overcome the limitations of classical 2D culture. This system combines features of monolayer and suspension culture. Indeed, the MC surface offers a substrate for cell growth while the mobility of MCs in the medium results in an environment similar to the one of the suspension culture. In the following section, important characteristics relative to MCs and their use for dynamic culture are reported.

1.3.2 Microcarrier properties

The characteristics of MCs such as the nature of the core material, the porosity, the surface properties, *etc*. have been reported to considerably influence cell attachment, growth rates and cell pluripotency as well as the differentiation process.[77] Thus, important MCs characteristics include:

- **Core material**: It determines several important characteristics of the MC such as its biocompatibility, morphology as well as mechanical and optical properties. Therefore, the choice of the material is of great importance. Also, the tunability of MC density, porosity and shape significantly depends on the material.[46] Various natural and synthetic polymers as well as glass have been used to produce commercial MCs, including dextran, gelatin, cellulose, polystyrene, polyester, *etc*.[56, 78] Other materials such as poly(lactic-co-glycolic acid) (PLGA) and chitosan have been also used in research labs to produce MCs.[79]
- **Surface properties and charge**: As cell behaviour is mostly influenced by the surface properties of the MC, the surface characteristics are of critical importance. Functionalization techniques are used to modify the surface properties of the MC core in order to provide good conditions for cell growth regarding adhesion, spreading, proliferation, *etc*. In order to do so, the surface of a MC can be modified or grafted with functional groups such as positively charged quaternary or primary amines or with

biopolymers such as gelatin, collagen, or other proteins and peptides known for their bioadhesive properties.[80] However, surface design can be challenging as one of the main obstacle of using MC as cell substrate is efficient cell harvesting from the MC surface at the end of the culture.[80] Indeed, a strong adhesion of cells grown on MCs induces a more difficult detachment. Thus, the ideal MC surface should be able to promote cell adhesion and growth during the expansion phase while providing easy cell detachment from the support at the end of the cultivation process.

- **Porosity**: MCs can be non-porous, *i.e.* impermeable even towards low molecular compounds, microporous, *i.e.* allowing the diffusion of macromolecules, and macroporous presenting pore size within 30-400 µm range. These microcarriers allow cell growth inside the pores, thereby increasing cell density and protecting cells against mechanical stress resulting from agitation.[46]
- **Particle shape**: Currently available MCs are mainly spherical but cylindrical and disc-shaped MCs which maximize the surface-to-volume ratio of the material are also available.[46, 49]
- **Particle size and size distribution**: For spherical microporous MCs, diameters of 100–230 µm are reported to provide the best cell growth.[46, 80] This size range results from a compromise between the maximization of the surface-to-volume ratio, the stability of the dispersion and a surface per bead which is needed to provide adhesion and spreading of several hundred cells.[46] The width of the size distribution of spherical MC is usually of about 25 µm in order to prevent uneven distribution of cells on the MCs.[46, 80] In the case of macroporous MC, which present pores of 30-400 µm, MC diameters up to several mm are obviously required.[46]
- **Core mechanical properties**: The mechanical properties of the MC core depend on both the selected material and its production process, as it controls the porosity. MCs should be rigid enough in order to support cell spreading and withstand any mechanical forces encountered during the cell culture. On the opposite, the rigidity has to be equilibrated in order to avoid cell damage during MC collisions in stirred culture. However, it is worth noting that biomechanical characterization is lacking for most MCs as the elastic modulus of MCs is hard to evaluate with conventional deformation systems due to their small size.[46, 79, 80]

- **Cytocompatibility**: Obviously, MCs are required to be non-toxic not only for cell survival and good growth but also to satisfy requirements in clinical applications.[46]
- **Optical properties**: Ideally, MCs should be transparent, allowing microscopic observation of cultured cells.[46, 81]
- **Core density**: In order to avoid MC flotation and minimize the stirring speed during culture, MC density should be slightly higher compared to that of the culture medium. Thus, the optimum density for microporous microcarriers is within the range of 1.02-1.04 $\mathrm{g/cm^3}$.[46, 55, 81]

1.3.3 Important considerations for cell culture on microcarriers

1.3.3.1. Inoculation protocol

Initial cell attachment is influenced by several factors such as cell and MC concentration, pH, temperature, medium composition, agitation protocol and seeding duration.[82] The conditions for cell attachment need to be optimal from the moment the cells are inoculated in the culture. An equilibration step of at least 30 min in culture medium is thus usually advised for MCs to reach the appropriate temperature and to allow protein adsorption on MC surface.[55] The agitation protocol during the adhesion step (from 1 to 24 h) is also of critical importance to promote MC-cell interaction, ensure homogeneous cell distribution as well as to avoid cell aggregation. A variety of protocols have been reported in the literature [83] ranging from completely static [84] to continuous agitation [85, 86] with intermittent stirring (*e.g.*, 2 min at 30 rpm followed by 30 min rest for 6 h [87], 30 min of agitation at 25 rpm followed by 10 min rest during 2 h [88], and 15 min at 25 rpm followed by 2 h rest during 24 h [89]) being the most common. Indeed, the resting period is believed to ensure successful cell anchorage onto MCs.[82] Finally, another interesting parameter is the volume of medium used during the attachment period, as cell seeding in a reduced volume (such as one-half or one-third of final operating volume) can improve cell-MC interaction thus maximizing cell adhesion.[55, 82]

1.3.3.2. Culture parameters

Agitation. Agitation during the culture is crucial to keep the MC suspension homogeneous and to ensure sufficient mass transfer of nutrients and oxygen to the cells.[35] A minimal agitation rate is required to maintain a good suspension while inducing the lowest shear stress possible to the cell. Indeed, if the agitation rate is too low, MCs settle at the bottom of the bioreactor and form aggregates limiting cell growth.[90] On the other hand, excessive agitation rate may lead to higher shear stress for the cells and can increase collisions between MCs or MCs and the impeller which result in lower viability and growth of cells.[35, 77] Continuous agitation is usually performed throughout the culture once the adhesion step is achieved. Various agitations rates are reported in the literature from 25 rpm to 140 rpm.[85–89, 91–93] Only a few studies report on culture performed with an intermittent agitation during the culture.[84]

The careful selection of the agitation rate is of particular importance as cells grown on MCs in an agitated culture system are exposed to turbulences and shear stress with potentially adverse effects on cell number and quality.[48] The most commonly addressed stress associated with agitation is the one arising from turbulence. The nature of a flow can be characterized by its Reynolds number defined as follows for a cylindrical vessel stirred by a central rotating paddle:

$$\mathrm{Re} = \frac{\mathrm{N}\mathrm{D}^2}{\nu}$$

where N is the impeller rotation rate, D the diameter of the impeller and ν the kinematic viscosity. When this number exceeds 10000, the flow is in a turbulent regime.[48, 94] In this case, Kolmogorov's theory can be applied to the flow to establish the potential for damage to cells in suspension as well as cells on MCs.[94] Several papers addressing mechanical stress issues in spinner flasks had Reynolds number just below the turbulent flow threshold,[90, 95] meaning the flow was in the transition regime and not fully turbulent. Nevertheless, the Kolmogorov's theory has always been assumed to be still applicable under these transitional flow conditions.[94] According to this theory, the size of the smallest eddies is given by the Kolmogorov eddy length

$$\mathrm{L} = (\frac{\nu^3}{\varepsilon})^{1/4}$$

where ν is the kinematic viscosity and ε is the specific energy dissipation rate which is directly proportional to the impeller diameter and rotation rate.[48, 94] No detrimental effect on cell growth and viability was observed as long as the eddy length is comparable or greater than the MC size, while cell death occurs when the eddy length falls below two-third of the MC diameter.[48, 94] Indeed, in this case, eddies directly interact with the cells, damaging them.[48] Notably, the Kolmogorov eddy length decreases with an increase of the impeller size or rotation rate, meaning more risk of detrimental effect for the cells. It is also important to notice that the energy dissipation rate is not homogeneous throughout the vessel, with the highest values reported near the impeller and the lowest values found near the surface, meaning that cells growing on MCs experience considerable variations in turbulences when moving through the culture medium.[48] Possibilities to reduce cell damages linked to turbulences thus include reducing the impeller rotation rate or size, reducing MC size or increasing the kinematic viscosity thanks to the addition of thickening agents.[48] Regardless of the nature of the flow, cells in agitated cultures are also submitted to shear stress. Specific attention should be paid to this aspect, as shear stress has been shown to influence stem cell fate. Indeed, shear stress was shown to induce osteogenic differentiation of MSC and increase expression of several osteogenic markers (osteopontin, bone sialoprotein, osteocalcin, etc.) as well as increased calcium deposition and alkaline phosphatase activity.[96–99] Similarly, shear stress was found to up-regulate the expression of endothelial cell-related markers.[96, 100]

Feeding regimen. The feeding regimen is of critical importance for a successful cell expansion. It should be optimized in order to maximize cell number while minimizing the use of culture medium and its associated cost.[82] Frequent medium exchange with removal/addition of exhausted/fresh culture medium is required to ensure the removal of toxic metabolites such as lactate and ammonia which could hinder cell growth as well as to avoid the shortage of nutrients such as glucose or glutamine.[35, 82] On the other hand, paracrine and autocrine factors produced by the cells have been shown to have a positive influence on cell expansion. Therefore, the frequent removal of those factors could be detrimental for the cells and special attention needs to be paid in order to ensure that these beneficial paracrine and autocrine factors are not completely removed or diluted to residual levels.[35] Usually, 50% medium exchange every 2-3 days is reported.[84, 88, 91, 92]

1.3.3.3. Detachment procedure

One of the main hurdles of MC-based culture is the downstream process needed to collect the cells at the end of the culture. It consists of detaching the cells from the MC surface and separating the harvested cells from MCs. Cell harvesting protocols need to be optimized to ensure efficient cell-MC separation, high cell yields while guaranteeing cellular viability, potency, and functionality.[82] Typical detachment procedures include an enzymatic treatment based on proteases such as trypsin, use of cationic chelating agents such as EDTA, increase of pH, application of mild hydrodynamic forces or some combination thereof.[49, 55] Among these techniques, proteolytic enzyme treatments are most commonly employed for detaching cells from MCs. However, such treatments have many drawbacks. First, proteolytic enzymes inevitably degrade cell membrane proteins which can impact cell viability. Secondly, enzymes are usually animal-derived proteins and bring potential risks of disease transmission when cells are used for therapeutic applications. Third, it is reported that proteolytic enzymes might have potential to alter cell phenotype. Finally, enzyme treatments are complicated and labor-intensive, because they require several steps including enzyme deactivation and cell washing. Other alternatives for cell harvesting are currently investigated including degradable or thermoresponsive microcarriers.[101] However, they are not yet applicable for a large variety of cells.

1.3.4 Commercial microcarriers

The first microcarriers developed by van Wezel were hydrophilic ion-exchange chromatographic beads, namely diethylaminoethyl (DEAE)-Sephadex® A-50 carriers based on crosslinked dextran. These MCs provide a positive net surface charge with a large surface-to-volume ratio, a spherical shape, good optical properties and a suitable density to disperse them in aqueous media. These MCs, used at a concentration of 1 mg/mL were used to demonstrate that a homogeneous MC system could be used for the large-scale culture of anchorage-dependent cells. However, they were also toxic for cells at concentrations higher than 1 mg/mL which considerably limits their use for large scale production.[46, 55] Nowadays, a wide variety of MCs are commercially available. They can be distinguished according to different criteria: rigidity, porosity,

density, charge, presence and nature of coating, particle size, material core,... However, most of these commercial MCs have been designed with the aim of propagating anchorage-dependent cell lines used in production of vaccine and biopharmaceuticals and are not optimized for cell therapeutic use.

	Commercial name	Manufacturer	Core material	Coating	Charge	Diameter (µm)
Animal protein-based	Cytodex® 3	GE Healthcare	Crosslinked dextran	Crosslinked gelatin	None	141-211
	Cultisphere® G and S	**Percell**	**Crosslinked gelatin**	**None**	**None**	**130-380 (pores 10-20)**
	Collagen	SoloHill®	Polystyrene	Gelatin	None	125-212
	GEM™	Global Cell Solution	Alginate + MNPs	Various (fibronectin, gelatin, laminin, etc.)	Cationic	75-150
Animal protein-free	Cytodex® 1	GE Healthcare	Crosslinked dextran + DEAE	None	Cationic	147-248
	Cytopore™ 1 and 2	**SoloHill®**	**Cellulose + DEAE**	**None**	**Cationic**	**200-280 (pores 30)**
	Hillex®	SoloHill®	Crosslinked dextran	Trimethyl ammonium	Cationic	160-180
	Plastic	SoloHill®	Polystyrene	None	None	125-212
	Plastic Plus	SoloHill®	Polystyrene	None	Cationic	125-212
	Synthemax™	Corning®	Polystyrene	Synthemax™ II	Unknown	125-212
	Biosilon	Nunc™	Polystyrene	None	Anionic	160-300
	Pronectin F	SoloHill®	Polystyrene	Recombinant fibronectin	Cationic	90-150

Table 1.4.: Overview of the most known commercial MCs and their characteristics. DEAE stands for diethylaminoethyl. Macroporous MCs are in bold.[56, 78].

The most common commercial MCs as well as some of their characteristics are reviewed in Table 1.4. MCs have been divided in two groups according to the presence/absence of animal proteins. A significant part of MCs are considered xeno-free as they do not contain any animal proteins. However, except for the Synthemax MC that is coated using a synthetic vitronectin-based peptide and the Pronectin F based on recombinant fibronectin, these MCs do not display any specific sequence to improve cell adhesion which thus only relies on electrostatic interactions between cells and MC surface. Interestingly, the global eukariotic microcarrier (GEM) is magnetic thanks to the incorporation of superparamagnetic nanoparticles (MNPs) in its alginate core. These magnetic properties facilitate control during medium exchange, harvesting and assay

washes but a special device (BioLevitator) is required to take advantage of their magnetic properties for medium change, washing, *etc*.[102, 103]

1.3.5 Microcarriers in development

Aside from commercial MCs, researchers continue to develop new MCs to overcome the shortcomings of existing MCs or further improve cell yield. In particular, the need for detrimental proteolytic enzymes to harvest the cultured cells and the low harvesting efficiencies sometimes encountered [104] have been considered. For example, Luck and coworkers synthesized degradable MCs obtained by reacting telechelic poly(2-oxazoline) (POx) crosslinkers with a disulfide core and (2-(methacryloyloxy)ethyl)trimethylammonium chloride (METAC) monomer by inverse emulsion polymerization in a microfluidic device. This protocol results in the formation of beads with regular and homogeneous shape and a narrow size distribution.[105] Interestingly, the addition of glutathione (GSH) at physiological concentrations (2.8 mM) led to the degradation of the MCs. The complete degradation was however achieved after only two to three days. In another study, Li *et al.* developed MCs base on alginate/PEG interpenetrating networks containing cleavable disulfide bonds allowing an efficient and quicker non-invasive harvest (70% harvesting efficiency after 60 min) of the cells following the degradation of the MCs thanks to the addition of a reductant such as L-cysteine.[106] Another type of strategy to avoid the use of proteolytic enzymes to harvest the cells relies on thermo-responsive polymers. For example, glass MCs were surface-grafted with N-isopropylacrylamide (NIPAM) and hydroxypropyl methacrylate resulting in the formation of a coating showing both good cell adhesion, proliferation d facilitating cell harvesting by varying the temperature.[107] Yang *et al.* also grafted poly(N-isopropyl acrylamide) (PNIPAM) on the surface of Cytodex® 3 MCs which allowed BMSCs to adhere, spread, and grow in the same manner as on nongrafted MCs.[108] When reducing the temperature below 32°C, more than 82.5% of BMSCs were detached from PNIPAM-grafted MCs. This harvesting efficiency was not significantly different than the one obtained following trypsin-induced detachment, but cell death was considerably reduced with the cold temperature treatment (from 16% to 8%).

Alternatively, biodegradable MCs were also produced with the aim of obtaining implantable MCs for regenerative applications. For this purpose, polycaprolactone (PCL) was widely used. Indeed, PCL is degraded by hydrolysis of

its ester linkages in physiological conditions making it suitable for biomedical applications. Lam et al. developed a biocompatible and biodegradable porous MC based on PCL that can support high MSC proliferation in stirred bioreactor while maintaining their differentiation capability and potency.[109] Cell yield on this new MC was comparable to the one obtain on Cytodex® 3. Zhou and coworkers prepared PCL MCs via the integration of the emulsion/solvent evaporation and particle leaching mechanisms.[110] These MCs were subjected to alkaline hydrolysis, followed by surface coating with hydroxyapatite. While the increase of surface hydrophilicity following hydrolysis did not significantly promote cell adhesion and proliferation, further surface coating with hydroxyapatite nanoparticles resulted in a significantly higher growth rate. Finally, the use of a microfluidic device to obtain uniform PCL MCs was also reported.[111] These MCs, either coated with vitronectin or laminin, allowed a 5–7 fold cell expansion that was comparable to a commercial MC (Plastic Plus, SoloHill®). Other groups also developed MCs based on other biodegradable polymers. For example, Hong and coworkers prepared PLA MCs covalently grafted with collagen I. Chondrocytes successfully attached and proliferated on these PLA MCs.[112] In another study by Li *et al.*, PLLA MCs physically doped with nanohydroxyapatite and/or grafted with chitosan were produced. Compared to unmodified PLLA MCs, the addition of nanohydroxyapatite alone led to the greatest proliferation-promoting effect, while the combination of nanohydroxyapatite and chitosan led to the strongest cell attachment.[113] Gabler *et al.* also produced degradable PLGA MCs. Cartilage cells grown on these MCs had a 100% survival rate after three and five days and the MCs were shown to significantly degrade after 3 months.[114]

Some studies also focused on reducing the use of toxic reagents such as organic solvents or crosslinkers to produce MCs. For example, Li *et al.* developed new MCs based on zein, a protein found in corn which is easily available and has good biocompatibility. These MCs were prepared via a novel method relying only on biocompatible glycerol.[115] Another group produced porous chitosan MCs by adapting a simple emulsion-based thermally induced phase separation process, avoiding the need for toxic reagents.[116]

1.3.6 Microcarrier fabrication

To date, various MC fabrication techniques have been reported, each with their advantages and drawbacks. Here, these techniques are detailed by distinguishing synthetic and natural polymers.

For synthetic polymers that are soluble in organic solvents (*e.g.*, PLA, PLGA, PCL, *etc*.), spherical MCs can be obtained using an emulsion-solvent evaporation technique.[112, 117] In this case, polymers are dissolved in a good solvent and emulsified with a surfactant thereby forming a polymeric emulsion. The solvent is then evaporated through the continuous aqueous phase and the polymer precipitates to yield the particles.[118] The surfactant is required to mediate the sphere formation and MC size largely depends on process conditions such as surfactant type and concentration, type of solvent and stirring speed.[119] A modified emulsion-solvent evaporation technique also allows some control over MC morphology: ammonium bicarbonate was incorporated in the droplets to generate carbon dioxide and ammonia gas bubbles during the solvent evaporation process, leading to different porosities depending on the gas foaming conditions.[120, 121] Fabrication of MCs by a emulsion solvent evaporation process can also be achieved using a microfluidic device which allows for a better control over MC size distribution.[122] Alternatively, a spray-drying technique was reported which also requires the use of organic solvents.[123] However, all these techniques suffer from one common drawback which is the use of organic solvents which requires complex setups, extensive purification processes, time-consuming drying steps and costly waste-management. This markedly hampers the large-scale development of those MCs for therapeutic applications due to safety, environmental and economical aspects. Other techniques were thus developed to circumvent the limitations of organic-solvent based techniques. Among these, a jet-milling method based on a grinding process was reported by Nykamp *et al*. [124] and a jet break-up solvent displacement was described by Levato and coworkers.[125] However, both these methods only allowed to control MC size but not their morphology.

On the opposite, natural polymers, including collagen, gelatin, alginate, and chitosan, can be formulated in water-based solutions to form MCs.[126, 127] However, these natural polymers often degrade easily and lose their structural stability. For this reason, they are usually crosslinked using chemicals such as glutaraldehyde which raises the issue of cellular toxicity [119] if an appropriate

detoxifying strategy is not performed.[128] Finally, MCs were also obtained by combining decellularized adipose tissue with an electrospraying approach.[129] This strategy allows to retain the complex biochemical and biophysical elements of the cell natural environment which have been shown to modulate cellular behaviour.

Finally, regarding the sterilization procedure of MCs, the most used technique is autoclaving with steam (121°C for at least 15 min).[106, 116, 130–133] Alternatively, MCs were also reported to be sterilized through incubation in 70% ethanol solution followed by several rinsing with PBS and culture medium [106, 109, 133, 134] or through UV light exposure[114, 135] or a combination of these two methods.[112, 136] Finally, gamma irradiation was also reported in a few cases.[133]

1.3.7 Advantages and drawbacks

MCs offer several advantages over other techniques. The main asset of this technique is to provide a substrate for cell adhesion within a limited volume, while keeping relatively homogeneous and controlled environmental culture conditions leading to more reproducible cell culture. The particularly high surface to volume ratio, which can be increased easily by changing MC concentration, leads to high cell density in long-term cultures. This technique also allows easy monitoring of culture as a representative cell sample can be collected during the culture for microscopic observation and cell characterization. Moreover, biodegradable MCs offer a more sustainable alternative to non-biodegradable ones and could be used as scaffolds for *in vivo* transplantation of cells. MC culture can be scaled up with ease in conventional stainless steel or disposable bioreactors.[46, 80] As a consequence, limited human intervention is required once the process is under way, reducing the risk of contamination.[137] Also, as most of biotechnology companies already possess bioreactor systems and their associated infrastructure, significant setup costs inherent to new technologies may not be required. Likewise, a short or no extra training is needed for operators, who are already familiar with this kind of technology.[137] Finally, the possibility of bead-to-bead transfer provides an attractive solution to the scale up process. Indeed, as cells are able to migrate on freshly added MCs, the available surface area can be progressively increased during the culture,

avoiding the need of sub-culturing the cells, thus reducing cell handling and the use of enzymatic agents.[35]

However, the dynamic nature of MC culture can lead to extra shear stress on cells and cause MC collision resulting in cell detachment and/ or impact on viability and cell growth.[49, 77] The preparation of some MCs can be labor-intensive as they sometimes need to be hydrated, sterilized, washed or even coated. Cell harvesting can be difficult, especially for macroporous MCs which also show restricted diffusion of nutrients to some cells.[46] Finally, it was found that in some cases, excessive stirring may lead to MC breakage.[138] This is of particular concern when the cells are subsequently used for *in vivo* applications because they must be free of any residual MC fragment.[48]

1.4 Mammalian cell behaviour on surfaces

1.4.1 Cell adhesion on surfaces

Cell adhesion is a key phenomenon for anchorage-dependent cells. The extent and strength of cell adhesion even play a critical role in regulating subsequent events such as proliferation, differentiation or cell death.[139] Indeed, anchorage-dependent cells do not divide in suspension and can even undergo anoikis, a specific type of apoptosis following lack of attachment.[139] It was also demonstrated that cells poorly adhered, which adopt a round shape without formation of focal contacts, usually do not survive. For an intermediate adhesion strength, the cells are most active in migration and proliferation. On the contrary, if cell spreading is very large with multiple well-developed focal adhesion sites associated with a rich cytoskeleton, the cells tend to differentiate.[140]

1.4.1.1. Cell adhesion receptors: the integrin family

Integrins are the main receptors involved in cell-extracellular matrix (ECM) interactions. They are transmembrane proteins involved not only in the anchorage of cells but also in the regulation of other processes such as embryogenesis, cell differentiation, immune response, wound healing and hemostasis.[141] They

are composed of two subunits, called α and β. Different types of α and β subunits can be combined forming 24 different integrins [142] and the particular combination of these subunits determines the ligand specificity of the integrin. Some integrins can bind to several types of ligands and, in the same manner, some ligands can bind to several types of integrins.[141] Binding events induce conformational changes in integrins which leads to integrin activation from the resting state (outside-in activation). Conversely, intracellular signals are able to regulate the affinity of integrins for their ECM ligands and modulate their activation (inside-out activation), as illustrated in Figure 1.9.[143]

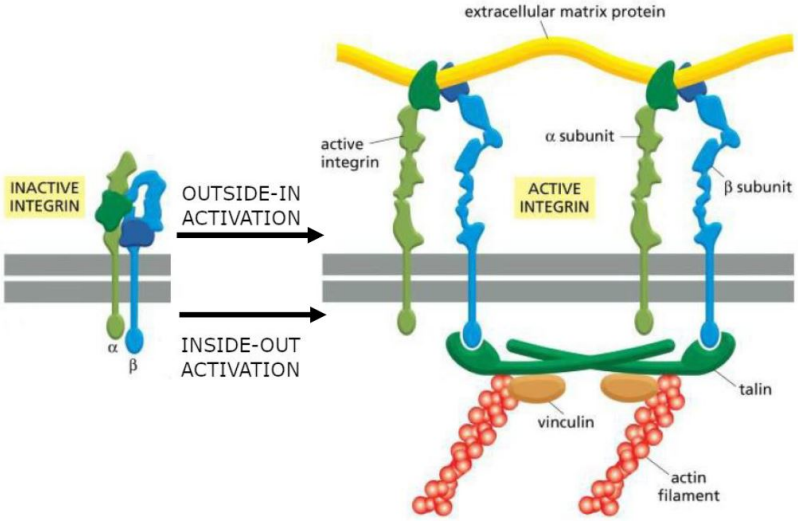

Figure 1.9.: Schematic representation of integrins in their active and inactive conformation.[144].

Following binding, integrins move laterally inside the cell membrane to form clusters which trigger the recruitment of cytosolic proteins such as vinculin, paxillin, tensin, and talin to form dynamic and multiprotein structures that provide a mechanical linkage between the ECM and cytoskeletal actin filaments.[145] These multiprotein structures are called focal adhesions (FAs). Aside from providing this mechanical link between the intracellular actin cytoskeleton and the ECM, integrin binding also provides cells with a bidirectional transmembrane signaling pathway.[141, 146] Indeed, these FAs allow the cells to sense the mechanical properties of their environment and convert this mechanical stimulus into a biochemical signal in a process called mechanotransduction.[147]

Mechanotransduction can be further divided in two types of sensing: a passive or "outside-in" sensing in which the cell responds to external forces such as shear stress, extension, compression and pressure and an active or "inside-out" sensing for which the cells generate forces to analyze features such as substrate stiffness, topography or ligand density.[148, 149]

1.4.1.2. Dynamics of cell adhesion

The cell adhesion process is characterized by three stages as depicted in Figure 1.10. The first stage is the initial attachment of cells following cell-surface contact. This stage is driven by weak interactions such as electrostatic interactions and cell morphology retains the round shape typical of cells in solution. In the following step, cells flatten and spread and adhesion becomes stronger following integrin binding. Finally, cells are fully spread and the actin cytoskeleton reorganizes following the formation of FAs described in the previous section. The adhesion strength is thus the strongest.

Cell Adhesion Phases	Phase I	Phase II	Phase III
Schematic diagram of cell adhesion	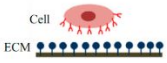	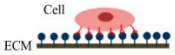	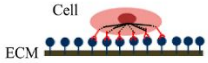
Schematic diagram of the transformation of cell shape	Initial attachment	Flattening	 Fully spreading and structural organization
Cell adhesion intervension	Electrostatic interaction	Integrin bonding	Focal adhesion
Adhesion stages	Sedimentation	Cell attachment	Cell spreading and stable adhesion

Figure 1.10.: The different stages of the cell adhesion process.[146].

1.4.1.3. Production of extracellular matrix

Following adhesion, cells secrete soluble biochemical factors for cell-cell signalling and remodel their microenvironment by depositing specific insoluble proteins usually found in their native environment, the ECM.[150–152] These deposited ECM proteins in turn influence cell behaviour. Indeed, Horton *et*

al. showed that ECM secretion into the pericellular space of hydrogels facilitates spreading and adhesion of MSCs in the absence of material-presented adhesion motifs.[153] Loebel and coworkers reached the same conclusion with MSCs grown in hydrogels but also found that secreted proteins progressively mask the presentation of signals from the engineered hydrogels.[154] In another example, it was shown by Berthod *et al.* that deposition of ECM by fibroblasts is necessary to promote capillary-like tube formation in vitro.

In the following paragraphs, native ECM characteristics are detailed, as understanding the essential parameters guiding cell fate *in vivo* can help designing efficient cell-instructive materials able to sustain basic cell processes such as adhesion and proliferation.

ECM composition and structure. The ECM is composed of over 300 molecules, [155] among which the major components can be grouped into four categories: proteins, glycoproteins, glycosaminoglycans (GAGs), and proteoglycans.[156] Each type of tissue possesses a distinct ECM composed of a specific subset of those molecules according to the structure and function of the considered tissue.[157] This compositional diversity reflects the broad range of biofunctional requirements of those different tissues.[156]

The most abundant protein and main structural component of the ECM is collagen (COL).[155, 156] Together with elastin, these proteins have a structural role as they impart mechanical properties to tissue, such as tensile strength or elasticity.

Glycoproteins are composed of a protein and covalently linked oligosaccharide(s). A variety of glycoproteins are found in the ECM including adhesive glycoproteins which include molecules such as fibronectin (FN) and laminin (LN), vitronectin (VN), thrombospondin and von Willebrand factor. Their ability to influence cell behaviour by allowing attachment and migration of cells through specific receptors called integrins (section 1.4.1.1) is clearly a major function of the adhesive glycoproteins.[156, 158] Other types of glycoproteins have been identified in skeletal tissues (osteopontin, bone sialoprotein) as well as glycoproteins associated with elastin deposition, such as fibrillin. Overall, those molecules play a role in various important functions and are implicated in a variety of developmental and pathological changes in the ECM.[158]

GAGs are linear anionic polysaccharides made of repeating disaccharides units that can be divided into sulfated (chondroitin/dermatan sulfate, heparan sulfate and keratan sulfate) and non-sulfated (hyaluronic acid (HA)) GAGs.[159] They contribute to the regulation of important biological functions such as migration and modulation of signalling pathways.[156]

Proteoglycans consist of GAG chains covalently linked to a specific protein core.[159] Diverse types of proteoglycans exist based on variation of the core protein and decorated GAGs. Small proteoglycans (<50 kDa) include decorin, biglycan, testican, fibromodulin, and lumican; large proteoglycans (>100 kDa) include versican, perlecan, aggrecan, neurocan, and brevican.[145] . Those molecules interact with numerous growth factors, cytokines and chemokines, cell surface receptors and ECM molecules either via their core proteins or, mainly, through their GAG side chains participating in several cell functional properties, such as cell signaling, proliferation, migration, differentiation, apoptosis and adhesion.[160] Thanks to their highly negative charges, both GAGs and proteoglycans attract and retain water conferring space-filling, lubrication and shock-absorbing properties to tissues.[145]

All these components form an interlocking 3D mesh as illustrated in Figure 1.11.

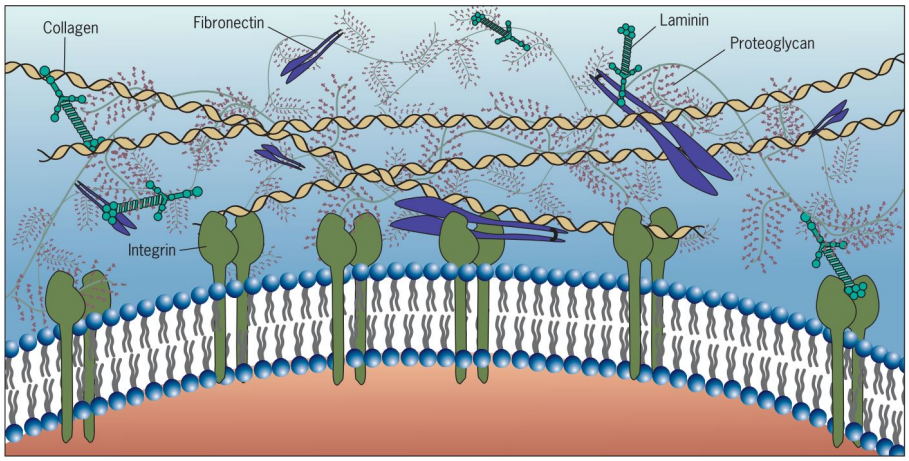

Figure 1.11.: An overview of the macromolecular organization of the ECM.[161].

ECM mechanical properties. In the body, tissues exhibit a wide range of mechanical properties that reflect their function and that are imparted by both the composition and structure of the ECM. For example, brain tissue is rather soft which reflects the abundant hydrated HA found in this tissue. By contrast, bone tissue is very rigid and this mechanical strength stems from the high amount of densely packed, mineralized collagens fibers found in bones. From the soft brain tissue (100 Pa) to the rigid bone tissue (2-4 GPa), the mechanical properties of the ECM can vary from several orders of magnitude, as illustrated in Figure 1.12. The stiffness of the ECM in specific tissues is not only critical for the structure and function of the considered tissue but also regulates the growth, survival, and motility of the cellular constituents and can even direct their lineage-specific differentiation (section 1.4.2.2).[162]

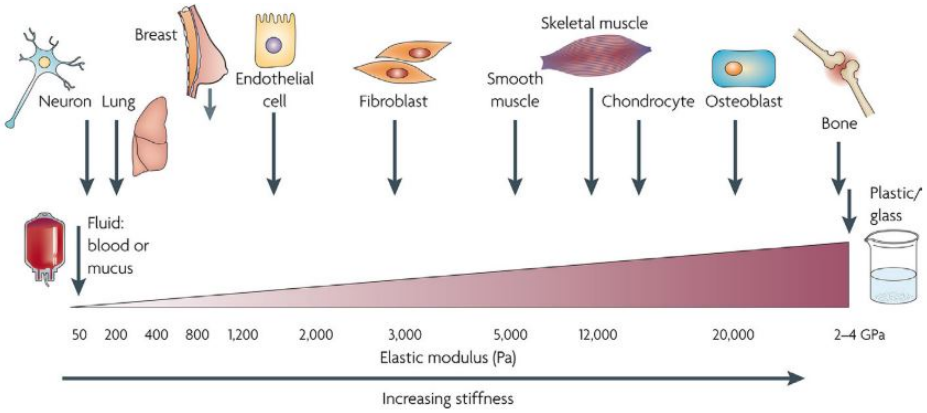

Figure 1.12.: Tissue elasticity widely varies depending on its function.[155].

Roles of the ECM. The ECM has historically been considered as a simple mechanical support for the cells in tissues, having a necessary but largely passive role consisting in maintaining tissue structure and form under mechanical loads, as well as providing a physical support for cell adhesion and migration.[155] However, it is now recognized that the ECM acts as a regulator of cell and tissue behaviour via transmembrane signaling, providing contextual informations regulating cell fate in an active and instructive way.[155] Three important characteristics of the ECM are known to influence cell fate: the physical properties such as elasticity and stiffness, the nanoscale topography and the specific chemical signals contained in a variety of ECM molecules.[157] Indeed, besides

its intrinsic components described above, the ECM has the capacity to act as a reservoir for various bioactive molecules such as growth factors, cytokines, *etc.* required for organ and tissue development.[157, 159]

Dynamic remodelling of the ECM. The ECM is a highly dynamic and adaptative structure which is constantly undergoing remodelling through matrix degradation, synthesis, assembly, and modification.[145, 156, 159] This remodelling is crucial for guiding important biological processes such as morphogenesis, angiogenesis, development, and regeneration.[145] This process is highly regulated by a complex network of enzymes and inhibitors [156] and abnormal ECM remodelling is associated with pathological conditions (*e.g.*, fibrosis).[145]

1.4.2 Surface properties influencing cell behaviour

1.4.2.1. Chemical properties

Biological molecules. The exposure of a material to a biological environment usually results in the rapid adsorption of proteins. The type, amount and conformation of these adsorbed proteins in turn regulates cell adhesion phenomena.[163, 164] Proteins adsorption itself greatly depends on the physicochemical properties of the surface such as surface charge as well as wettability, topography and roughness.[165] The effect of these parameters on cell adhesion are thus detailed in the sequel.

Surface charge. It is widely accepted that cells adhere better to positively charged surfaces than to negatively charged surfaces.[139, 166] This effect may be attributed to two mechanisms. Indirectly, surface charge impacts protein adsorption which in turn affects cell adhesion.[167] Indeed, as cell adhesion-mediating ECM molecules are negatively charged at physiological pH, they adsorb preferentially to positively charged surfaces.[139, 166, 168] More directly, electrostatic interactions between the substrate and the negatively charged cell membrane also influence cell initial attachment.[167] For example, Shelton *et al.* showed that cells flattened and adhered closely to positively charged surfaces while cell-material contact only occurred at distinct points on near-neutral and negatively charged surface.[168] Schneider *et al.* also showed that positively

charged 2-hydroxyethylmethacrylate (HEMA) and poly(ethylene glycol) (PEG) hydrogels supported the greatest osteoblast attachment, followed by negative, and neutral charge densities, respectively, as can be seen in Figure 1.13.[169]

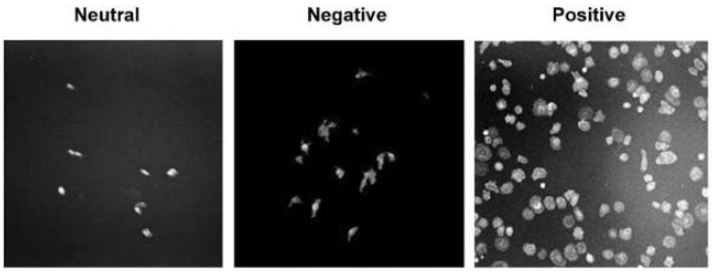

Figure 1.13.: Positive charge density in HEMA hydrogels supports better cell attachment and spreading that neutral and negative charge densities.[169].

Wettability. Wettability is also an important characteristic of the surface, as it influences the behaviour of molecules, proteins, and cells. When considering cellular adhesion, experimental results show improved attachement on weakly hydrophilic surfaces (*i.e.*, with water contact angles between 45°and 75°), while strongly hydrophilic or hydrophobic surfaces (*i.e.*, water contact angle lower than 30° or higher than 90° , respectively) are frequently used to avoid cell attachment (Figure 1.14).[166, 170] Indeed, highly hydrophilic surfaces prevent the adsorption of proteins, or these molecules are bound with relatively weak forces on the surface leading to the detachment of these molecules. On the other hand, highly hydrophobic surfaces favour the adsorption of non-adhesive proteins which restrict the access of the surface to adhesive proteins and consequently cell adhesion. Moreover, it has also been shown that proteins adsorbing on hydrophobic surfaces undergo denaturation which also restricts cell adhesion.[139]

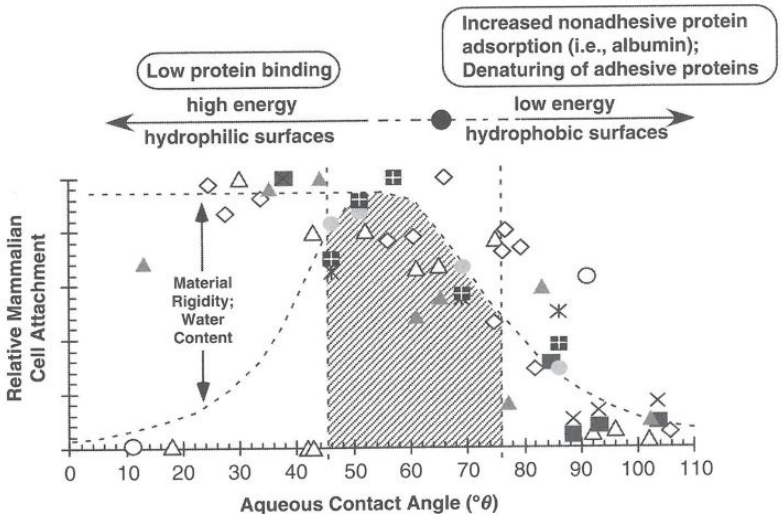

Figure 1.14.: Cell adhesion as a function of surface wettability.[170].

1.4.2.2. Physical properties

As detailed in section 1.4.1.1, biophysical cues can be sensed and transduced into intracellular biochemical and functional responses by cells in a process known as mechanotransduction.[171] As a result, physical parameters of the surface such as stiffness, roughness and curvature can influence cell behaviour. In the following sections, the effect of these three parameters on various cell functions such as adhesion, proliferation, migration and differentiation are reviewed.

Stiffness. Substrate stiffness is known to regulate a variety of cell functions such as cell adhesion and spreading, proliferation, migration and differentiation. For example, Vasquez *et al.* showed that myoblast cell adhesion and proliferation was considerably higher on crosslinked polyelectrolyte films of poly-L-lysine (PLL)/HA showing an increased rigidity compared to non-crosslinked films.[172] This effect was confirmed for several types of PEM films including (CHI/HA), PLL/poly(alginic acid), PLL/poly(galacturonic acid) and (PLL/PGA) and using a

variety of cell types (chondrosarcomas, chondrocytes, osteoblasts, neurons, smooth muscle cells).[173]

In the 2000s, several groups demonstrated that cells spontaneously migrate from a soft to a stiffer region.[174–177] This phenomenon is now known as durotaxis.[176, 177] For example, Lo *et al.* produced polyacrylamide gels displaying gradients of rigidities by changing the crosslinker concentration. They showed that cells would migrate from soft to stiffer regions but also that cells coming from the stiffer region turned around when reaching softer regions.[177] Gray *et al.* used micropatterned poly(dimethylsiloxane) (PDMS) to show that migration, and not proliferation of cells was responsible for the accumulation of cells on stiffer regions.[175]

Regarding differentiation, Engler and coworkers demonstrated that substrate stiffness could drive the lineage commitment of naive MSCs without any soluble inducer. MSCs grown on 2D polyacrylamide gels showing different Young moduli (E) mimicking brain (E = 0.1-1 kPa), muscle (E = 8-17 kPa) and collagenous bone (E = 25-40 kPa) showed both morphology and transcriptional profile similar to those of neurons, myoblasts and osteoblasts, respectively (Figure 1.15).[178]

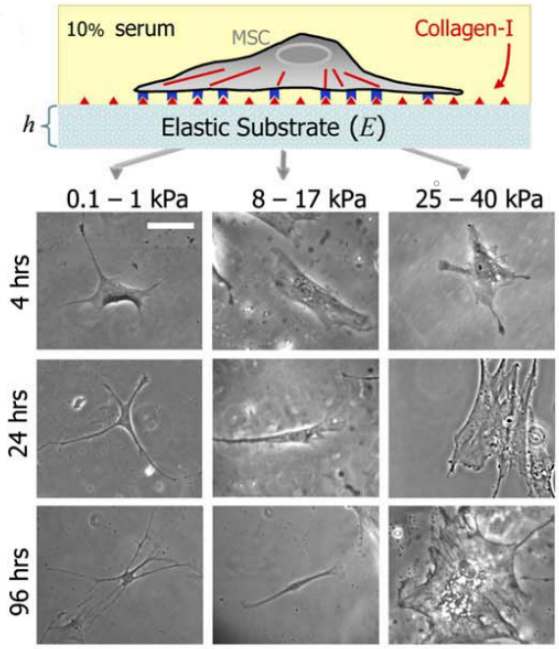

Figure 1.15.: Differentiation of naive hMSCs as a function of the value of the Young modulus (E) of polyacrylamide gel substrates. Scale bar is 20 µm.[178].

The impact of the mechanical properties of the environment on cell differentiation was also investigated in 3D structures by other groups. Huebsch *et al.* encaspulated naive mouse MSCs in 3D alginate hydrogels with tunable elastic modulus (from 2.5 to 110 kPa) functionalized with RGD peptides. They showed that cell phenotype was significantly impacted by matrix rigidity after one week, with osteogenic commitment occurring primarily at intermediate E (11–30 kPa) and adipogenic lineage predominating in softer (2.5–5 kPa) microenvironments. However, in contrast with 2D results for which cell morphology was impacted by matrix rigidity, cells remained grossly spherical regardless of the value of the Young modulus.[179] These findings were further confirmed by Pek *et al.* using human MSCs embedded in a polyethylene glycol-silica (PEG-silica) nanocomposite gel. The highest expressions of neural, myogenic and osteogenic transcription factors were observed for gels of low, intermediate and high stiffness, respectively, and cells also showed a rounded shape.[180]

The results described above were obtained using purely elastic substrates showing a time-independent elastic modulus.[181] This means that sample deformations are elastic, not plastic, so that resistance to traction forces exerted by cells is constant over time, and elastic energy is stored in the substrate. In contrast, reconstituted ECM based on collagen or fibrin as well as various tissues, such as brain, liver, adipose tissue, *etc.* all display viscoelastic properties.[182] These materials dissipate energy due to deformation and display a time-dependent mechanical response, as stress relaxation is observed when a constant strain is applied.[183] Recently, researchers thus focused on studying cell behaviour on viscoelastic materials which better mimic natural tissues than elastic ones.[181–185] For example, Chaudhuri *et al.* produced alginate hydrogels with a controlled matrix stress relaxation to investigate the effect of the rate of substrate stress relaxation on cell spreading and proliferation in 3D culture.[182] More precisely, the time for the initial stress of the material to be relaxed to half its value ($\mathrm{mathsf}\tau_{1/2}$) could be varied from one hour to one minute, while keeping alginate concentration and the initial gel elastic modulus constant. They demonstrated that both cell spreading and proliferation were suppressed within materials with long timescales for stress relaxation ($t_{1/2}$ of about 1 h). Interestingly, both spreading and proliferation were found to increase with faster stress relaxation. They also showed that osteogenic differentiation was significantly enhanced in gels with faster stress relaxation, for which the timescale of stress relaxation is similar to the one of fracture hematoma and early fracture callus. Similar results regarding cell spreading and proliferation were also obtained by Lou *et al.* using interpenetrating network hydrogels based on HA and collagen I.[185]

Roughness. It is a general consensus that surface roughness has a great influence on cell behaviour.[186–189] Several grades of surface roughness can be defined according to the scale of the surface irregularities. Surface macroroughness is characterized by irregularities from 100 µm to millimeters. Microroughness can be defined by irregularities with a size ranging from 100 µm to 100 nm, and nanoroughness is specified by irregularities less than 100 nm. Each type of surface roughness has a specific influence on the behaviour of cells.[139, 190]

Regarding macroroughness, the irregularities are too large to be felt by the cells so they usually do not restrict cell adhesion and spreading.[139, 190]

The micro-scale roughness is more controversial, as conflicting effects on cell behaviour were reported. Some authors reported lower cell numbers on microrough surfaces compared to smoother substrates.[191–193] Zhao *et al.* also showed that the number of MC63 osteoblast-like cells was lower on rough titanium disks (average peak to valley height (R_a) of 700 and 400 nm) than on smoother surfaces (R_a of 60 nm) but that osteoblastic activity was favoured on these rougher surfaces.[194] On the contrary, Balloni *et al.* reported no difference in MSCs adhesion and proliferation on smooth and rough titanium surfaces but also found evidence of an increased expression of markers of osteoblastic phenotype on the rough substrates. This enhanced differentiation towards osteoblastic lineage on microrough surfaces was also reported by other groups, as illustrated in Figure 1.16.[193, 195]

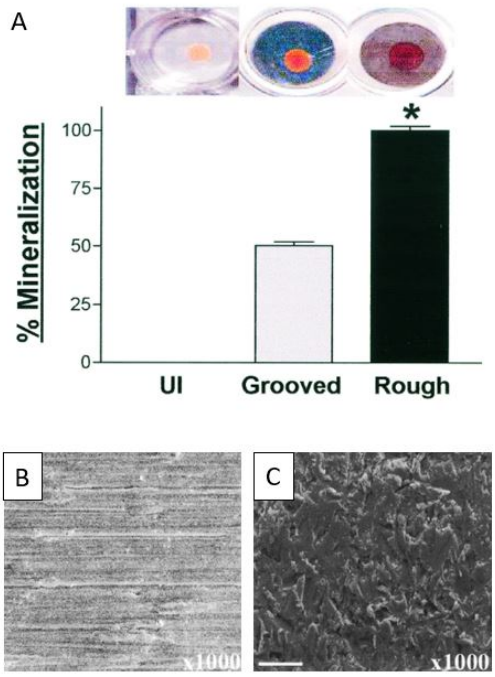

Figure 1.16.: A) Osteoblast cultures mineralize significantly less on grooved surfaces as compared with rough surfaces, as demonstrated by Alizarin Red S staining. Non-mineralizing "UI" cells were used as a negative control. Surface morphology of grooved and rough surfaces are shown in images (B) and (C), respectively. Adapted from reference [195].

These conflicting results can be explained by a lack of comparable studies as many different cell types and materials have been used and there is no consensus for roughness characterization.[142, 187] Indeed, in most cases, substrates are simply characterized using some amplitude roughness parameters such as average peak-to-valley height, while other parameters such as roughness organization, feature shape and spacing between features are not considered [139, 142, 187] even though they have been recognized important to understand roughness influence on cell behaviour.[187] These discrepancies may also arise from the lack of an appropriate strategy to simultaneously investigate the effect of a broad range of roughness.[189] Surfaces displaying roughness gradients have been used in order to screen cell behaviour on a wide range of roughness. In a study by Faia-Torres *et al.*, a PCL substrate showing a roughness gradient with R_a varying from the sub-micron to the micrometer range (0.530 µm to 4.71 µm) allowed to study cell differentiation. They reported that an optimal roughness of R_a around 2.1-3.1 µm accelerated osteogenic commitment of BMSCs and strongly accentuated their osteogenic differentiation in comparison to flat TCPS.[196] In an interesting study by Hou *et al.*, a roughness gradient (defined from 5% to 95%) was produced to investigate the influence of roughness on MSCs characteristics such as cell adhesion (*i.e.*, cell spreading, circularity, number of FAs) and differentiation as well as elucidating the underlying mechanism of how topography signals modulate cell behaviors. Specifically, the roughness gradient (RG) showed nanometer amplitude features from the position RG5% to RG50% with R_a linearly increasing from 53.86 nm for the smoother surface (referred to as RG5%) to 183.18 nm for RG50%. From RG75% to RG95%, the roughness rapidly increased in the submicrometer range with R_a varying from 353.66 to 1050.31 nm. They showed (Figure 1.17) that cell spreading area linearly decreased with increasing roughness while the formation of FAs and filopodia as well as cellular tension was optimized in the region with intermediate roughness. As a result of higher nuclear tension and transcriptional activity, osteogenic differentiation was also improved in that region. On the contrary, higher roughness was associated with maintenance of cell phenotype by reducing cell adhesion to a certain level.[189]

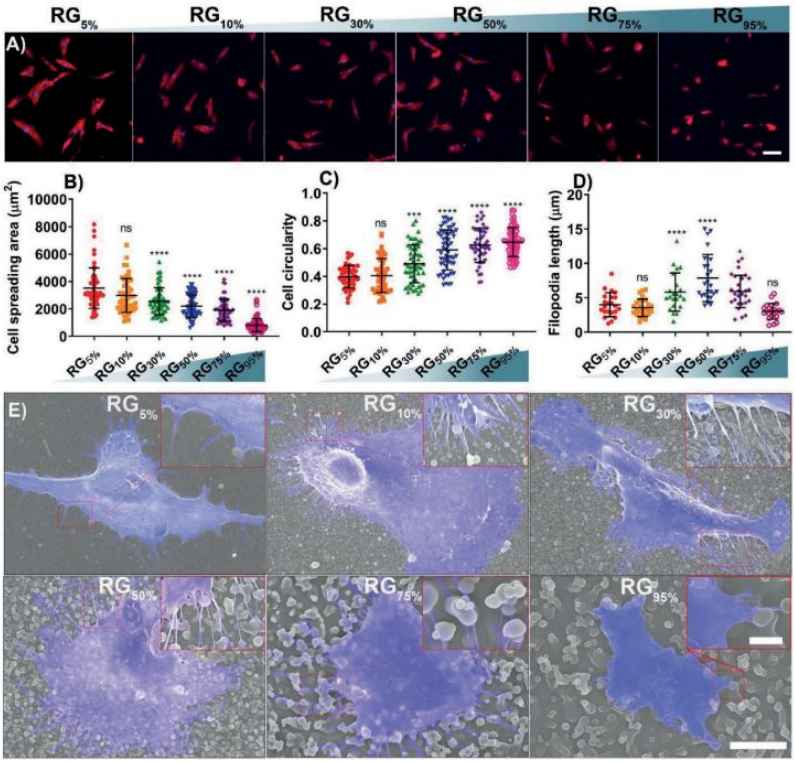

Figure 1.17.: Cell adhesion on surfaces with roughness gradient. A) Representative images of actin filaments of MSCs cultured 24 h on a surface showing roughness gradient. B) Cell spreading area versus different roughness gradients. C) Circularity and D) filopodia length of the adhered MSCs on different surface gradients. E) Representative SEM images of adhered cells on roughness gradient surfaces. Scale bar indicates 15 µm, inset bar indicates 5 µm.[189].

Finally, nanoscale roughness of a material surface is considered to have a positive influence on the adhesion, growth and maturation of cells as it resembles the nanoarchitecture of the natural ECM, thus allowing cell adhesion-mediating proteins to adsorb in an appropriate geometrical orientation.[139, 190] For example, using four cell types, Gentile *et al.* showed that the number of adhering cells and their proliferation rates exhibited a maximum on moderately rough (R_a = 10-45 nm) surfaces.[188] Webster *et al.* also demonstrated increased

osteoblasts adhesion on three metal alloys showing a nanoscale roughness compared to their smoother counterpart.[197]

Curvature Besides the effect of surface topography, which includes surface roughness but also organized topographical features such as grooves or pillars (not discussed here), it has been recently highlighted that the three dimensional shape of the environment and in particular substrate curvature can affect cell behavior such as cell alignment, migration and even differentiation, even at a scale larger than the cell size.[198, 199] For example, adherent cells such as fibroblasts, smooth muscle cells and MSCs seeded on convex cylinders align preferentially along the cylinder axis, thus avoiding curvature.[200] This phenomenon could obviously not be observed on spherical substrate because the curvature is constant in all directions.[200] In addition to static cell body alignment, substrate curvature also leads to directional cell migration. Indeed, hBMSCs cultured on convex cylindrical substrates migrate preferentially along the cylinder axis and this phenomenon increases with increasing curvature (radius of curvature going from 500 µm to 125 µm). However, the same cells seeded on concave cylinders with the same curvatures showed no preferential alignment.[201] In another study by Pieuchot et al., an isotropic substrate displaying simultaneously convex hills and concave valleys was produced to investigate the migration behavior of MSCs.[199] They showed that adherent cells such as fibroblasts and MSCs position themselves on concave valleys thus migrating towards negative curvature. Similarly to the durotaxis process for which cells migrate to stiffer regions, this tendency to preferentially migrate toward negative curvatures is now referred to as curvotaxis.[199] Interestingly, nuclei of cells positioned on flat and convex substrates show a flattened and stretched morphology while cells on concave substrates display more rounded nuclei, suggesting a mechanical relaxation of the nucleus on concave substrates, as illustrated in Figure 1.18.[198–200]

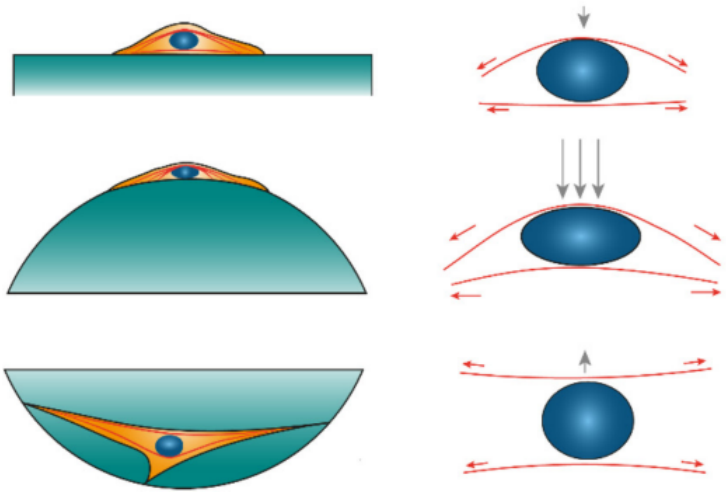

Figure 1.18.: Schematic representation of the cytoskeletal forces acting on the nucleus. Cytoskeletal tension creates a push force on convex and flat surfaces leading to compression and deformation of the nucleus. A cytoskeletal pull force on concave surfaces results in a rounded nucleus shape.[200]

1.5 Biofunctionalization techniques to improve cell adhesion

1.5.1 Biomolecules of interest for bioadhesion

1.5.1.1. Animal Proteins

FN and VN are the primary glycoproteins in serum that promote adhesion of various cell types to surfaces. FN is a large glycoprotein composed of two mostly identical polypeptide chains (220 kDa each) joined by disulfide bonds at their C-terminal ends. It can be found in soluble form as a major component of plasma (300 µg/mL) or in a less-soluble form associated with cells in the ECM.[202, 203] FN has been studied extensively and has been shown to regulate various cell processes such as cell growth, cytoskeletal organisation, differentiation, migration and survival.[204] Owing to its strong

cell adhesiveness, FN has been widely used to coat a variety of surfaces such as titanium implants,[205] membranes [206] or MCs [122, 126] in a effort to enhance their cell adhesiveness. Similarly to FN, VN can be found in plasma at a concentration similar to FN (250-450 µg/ml) and in tissues as well. While the cell attachment behaviour is similar to that of FN, both proteins are structurally and immunologically distinct.[207] Some examples of the use of VN are also reported.[208, 209]

LNs constitute the main component of basement membranes which are 25-50 nm thin sheets of a specialized ECM located at the basal side of all epithelial and endothelial cells, surrounding also neurons, myoblasts and myotubes and many tumor cells.[204] They are heterotrimeric glycoproteins (400–800 kDa) composed of α, β, and γ chains that exist, respectively, as five, three and three genetically distinct types forming 15 different combinations which are named according to chain composition (*e.g.*, LN-511 consists of $\alpha 5$, $\beta 1$ and $\gamma 1$ chains).[159, 210] They regulate various biological functions of a wide range of cells including epithelial and endothelial cells, myoblasts, neurons, hematopoietic cells and stem cells [204] and show different spatio-temporal expression patterns as well as tissue-specific locations and functions.[210] LN was used to coat MCs and showed improved cell adhesion even in dynamic conditions.[208, 211]

COLs are the most abundant proteins in mammals constituting up to 30% of total protein mass.[212] They confer mechanical stability, strength and toughness to a variety of tissues such as tendons, ligaments, skin, cornea, bone or dentin which present a wide range of mechanical properties, indicating the versatility of collagens.[213] COLs are composed of three polypeptide α chains forming a triple helical structure.[214] These chains can either be identical to form homotrimers or different to form heterotrimers resulting in as much as 28 collagen types numbered with Roman numerals in vertebrates. COLs can be classified based on their supramolecular structure into fibril-forming COLs or non-fibrillar COLs.[212] Collagen or gelatin (its denatured counterpart) has been widely used directly as a scaffold [215] or to coat a variety of substrates such as titanium implant [216], bioactive-glass scaffold [217], silk scaffold [218], *etc*. also including MCs.[112] As detailed in Table 1.4, several gelatin-based MCs are commercially available (Cytodex 3, Cultisphere G and S, Collagen, GEM).

Elastin is another structural ECM protein responsible for confering elasticity and resilience to tissues such as blood vessels, ligaments, lungs and skin which are subjected to repetitive and reversible deformations.[159, 219] Elastin is the most elastic natural protein and can reversibly stretch up to eight times its resting length.[220, 221] Elastin has been reported to have a positive influence of cell behaviour such as cell growth, migration and differentiation through the activation of a number of cell receptors such as integrins and surface glycosaminoglycan receptors.[220] However, reports of the use of elastin to coat biomaterials are rather scarce. Porous polypropylene fumarate based scaffolds were coated using elastin which showed improved cell adhesion and proliferation using two cell lines (NIH 3T3 mouse embryonic fibroblasts and human umbilical vein endothelial cells (HUVECs)).[222] Electrospun nanofibers were also coated with elastin and showed promises for application in regenerative therapies for salivary glands.[223]

1.5.1.2. Recombinant proteins

While animal proteins are widely used to improve cell-material interactions, they possess some inherent limitations such as risk of immugonenicity and high product variability. For example, Wondimu *et al.* compared several commercial human laminin preparations, and found both compositional and functional differences between batches which contained highly fragmented proteins, mixtures of isoforms, and/or contaminating fibronectin detected in variable amounts.[224] Recombinant proteins constitute an alternative to animal proteins as they offer enhanced safety, greater reproducibility and quality, and the ability to be tailored to enhance product performance.[225] These recombinant proteins are obtained following their amplification in the appropriate expression system (bacteria, yeasts, molds, mammals, plants or insects) which can greatly impacts protein quality, functionality, production speed and yield and thus need to be carefully selected.[226]

Several ECM proteins were used as the basis of recombinant proteins designed to improve cell adhesion. For example, Braam and coworkers reported that recombinant VN is a functionally defined substrate that supports hESCs adhesion and proliferation.[227] The same conclusion was reached by Rodin *et al.* using recombinant LN.[210] In another work, a recombinant FN fragment ($FNIII_{7-10}$) was immobilized onto a non-adhesive support by Cutler *et al.* They showed

that cell could adhere and spread thanks to the presence of this $FNIII_{7-10}$.[228] Punet *et al.* used elastin-like recombinamers (ELRs) incorporating an arginine-glycine-aspartic acid (RGD) motif to functionalize poly-(L-lactide) (PLLA) and they showed that those ELRs were able to elicit higher rates of rat MSCs attachment, stronger cell anchorages and faster levels of proliferation than short peptides.[229]

Commercial alternatives to natural proteins have also been developed. For example, ProNectin F is a genetically engineered protein of 980 amino acids containing a repeated sequence of GAGAGS from silk fibroin and GAAVTGRGDSPASAAGY from fibronectin.[230, 231] The structure of the protein is such that it is resistant to heat, biologically stable for several months at room temperature, highly water-soluble, and adsorbable to the hydrophobic surface of polystyrene, even in the presence of water. It can also be autoclaved at $121\,°C$ without any loss of cell adhesive activity.[230] Mammalian cells are able to adhere on ProNectin F coated on a support of polystyrene at a very low concentration of the order of 160 ng/cm^2 [232] and its capacity to fix cells is superior to that of fibronectin.[230, 232] Cellnest™ is a recombinant gelatin composed of 571 amino acids and based on human collagen I. It was originally developed for Fujifilm corporation for photography applications but was quickly used for regenerative medicine applications.[233] For example, Confalonieri *et al.* investigated the potential of a new macroporous MC fomulation based on crosslinked Cellnest™ for mouse myoblast cell line C2C12 and BMSCs proliferation. They showed that their MC supported higher cell proliferation comparing to a commercially available equivalent based on porcine gelatin (Cultispher® G) and that BMSCs retained their differentiation capacity.[234]

1.5.1.3. Synthetic cell adhesion peptides

In 1984, Pierschbacher and Ruoslahti discovered that the minimum sequence required for cells to bind fibronectin is a short sequence composed of only three amino acids : Arg-Gly-Asp (RGD) shown in Figure 1.19.[235] This sequence is recognised by integrins and is of significant importance not only for cell adhesion but also for other vital phenomena linked to adhesion such as cell differentiation and growth.[236] Since then, this RGD sequence was found in several other proteins from the ECM such as vitronectin, fibrinogen, von Willebrand factor, collagen, laminin, osteopontin, tenascin, *etc*.[141, 237] On top of that, Aota

et al. identified in 1994 a pentapeptide site, involving a Pro-His-Ser-Arg-Asn (PHRSN) sequence, that synergistically enhances the cell-adhesive activity of the fibronectin RGD sequence.[238]

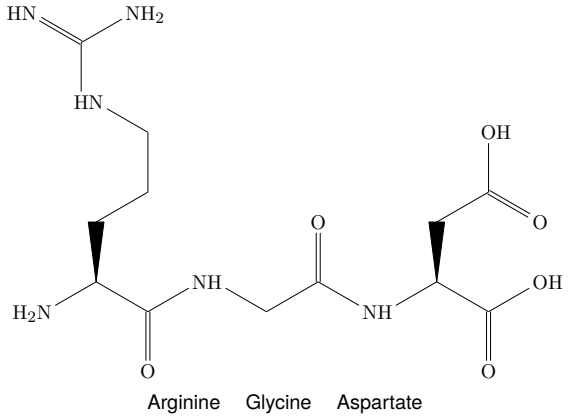

Figure 1.19.: Arginylglycylaspartic acid (RGD) sequence.[141].

The RGD sequence can be used in two different ways.[239] On one hand, RGD peptides in solution inhibit cell adhesion by competing for cellular receptors and can thus be used as an antiadhesive substance.[237, 239] On the other hand, they promote cell adhesion once immobilized on surfaces.[141, 239] For example, RGD peptides have been used to coat a wide range of materials such as titanium implants [240–243], hydrogels [244–246], hydroxyapatite scaffolds [247, 248], electrospun scaffolds [249, 250] or MCs [117, 251, 252] in order to improve cell response.

Since the indentification of the RGD sequence, a large number of other cell adhesion peptides (CAPs) were discovered in various ECM proteins including fibronectin (*e.g.*, KQAGDV, REDV, *etc.*), laminin (*e.g.*, IKLLI, LRE, LRGDN, PDGSR, IKVAV, LGTIPG, YIGSR, *etc.*), collagen (*e.g.*, DGEA, GFOGER) and elastin (*e.g.*, VAPG).[253–255] However, Huettner *et al.* reveals a scarcity in the number of CAPs used for surface biofuntionalization.[254] Based on a search on three databases (PubMed, Scopus, and Web of Science) for articles published between 1970 and early 2018 on CAPs used to functionalize scaffolds, hydrogels, implants, and fibers, the larger part (89%) of the published studies used the RGD sequence. IKVAV and YIGSR, both isolated from the laminin sequence, represented only 6% and 4% of the publications, respectively. Finally,

other marginal CAPs such as DGEA, PHRSN, and PRARI represented less than 1% of the literature.

1.5.1.4. Comparison of bioadhesive derivatives

To conclude this section, an overview of the advantages and drawbacks of each type of biomolecules detailed above is provided in Table 1.5.

	Advantages	**Drawbacks**
Natural proteins	- Strong efficiency as natural proteins have specific secondary structure allowing optimal presentation of adhesive sequences as well as synergistic sequences increasing their efficacy.[229]	- Isolation and purification of proteins result in increased cost and complexity.[141, 229] - Natural proteins may elicit immune response.[143, 229] - Protein denaturation caused by heat (sterilization), pH variation, adsorption,...[141, 203] - Batch-to-batch variability.[143]
Synthetic peptides	- Can be synthesized in large quantity at low cost.[141] - Good stability (sterilization, storage, pH, heat,...) as peptides cannot be denatured [141, 236] - No immune reaction.[143] - Reproducibility.[143]	- Fail to reproduce the biological activity and specificity of natural proteins due to oversimplification (lack of specific conformation and synergies).[143, 229]
Recombinant proteins	- The modularity of the production process of recombinant proteins allows to engineer tailored sequences for specific purposes [225, 229] - The high fidelity of the production process promises precise control over protein sequence and thus high reproducibility [225] - No immune reaction.[231]	- Increased complexity and cost compared to peptides.[229]

Table 1.5.: Overview of the advantages and drawbacks of natural proteins, synthetic peptides and recombinant proteins for the biofunctionalization of surfaces.

1.5.2 Protein and peptide immobilization techniques

For biofunctionalization purposes, adhesive biomolecules need to be immobilized on the surface of the considered material. Immobilization can be defined

as the attachment of molecules to a surface. Protein immobilization approaches rely on the following three mechanisms: physical, covalent, and bioaffinity immobilization as depicted in Figure 1.20.[256, 257] These three mechanisms are detailed in the following sections.

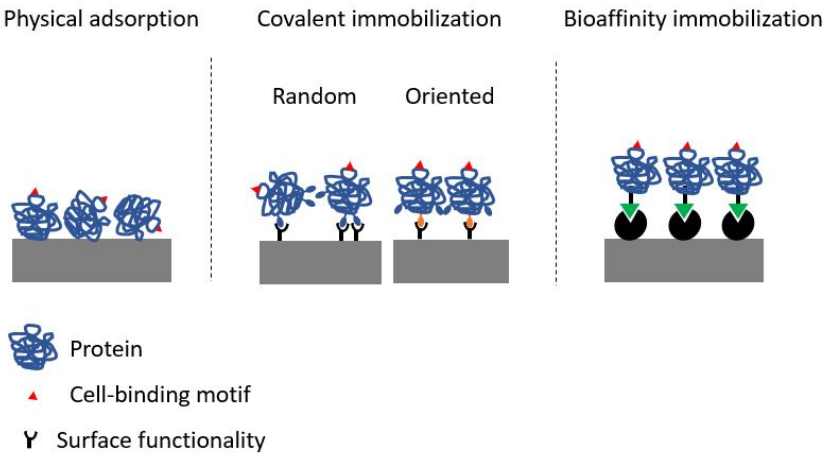

Figure 1.20.: Overview of protein immobilization techniques.

1.5.2.1. Physical adsorption

Physical adsorption is the simplest, fastest and cheapest technique for presenting proteins and peptides at the surface of a material.[258] Physical adsorption is driven by weak interactions such as hydrophobic interactions, electrostatic interactions, hydrogen bonding and van der Waals forces.[259] Protein parameters such as primary structure, size, and structural stability as well as surface properties including surface energy and chemistry influence the quantity and biological activity of the adsorbed biomacromolecules.[256, 260, 261] These weak interactions often result in low stability of the layer due to desorption of proteins or replacement over time of pre-adsorbed molecules with other proteins or peptides. Protein adsorption also typically results in a range of protein conformations on the surface such that the receptor binding domains are not always sterically available.[256, 261] This technique has been used as soon as the early 1980s, when Seitz *et al.* showed that coating bioglass with

fibronectin reduced the time needed for NIL8 M-2 cell (hamster cell line) spreading and attachment-dependent morphological changes.[262] More recently, Rivera-Chacon and coworkers found that adsorbing vitronectin and fibronectin on nanoporous titanium surface helps promoting human fetal osteoblast attachment and proliferation.[209]

1.5.2.2. Covalent immobilization

To circumvent the limitations of physical adsorption, covalent immobilization is often used to allow for a stable, long-term presentation of the biomolecule with a well-defined conformation.[261] This technique requires the presence of appropriate functional groups on both surface and target molecule. As the amino acid side chains do not participate in polypeptide bonds, they are free to react with the surface functional groups. On the other hand, if not already present, functional groups can be easily introduced on the material surface following several strategies, some of which are detailed in section 1.5.3. A summary of the functional groups potentially available in proteins for immobilization and the required functionalities of the surface is provided in Table 1.6.

Side Group	Amino acid	Surface functionality
NH_2	Lysine Hydroxyl-Lysine	Carboxylic acid Active ester (NHS) Aldehyde
COOH	Aspartic acid Glutamic acid	Amine
SH	Cysteine	Maleimide Pyridyil disulfide Vinyl sulfone

Table 1.6.: Commonly available functional groups in proteins, associated amino acid and required functionality of the surface. Adapted from reference [256].

For example, lysine residues with their amine side group are widely used as anchoring points because they are usually present on the exterior of proteins.[256, 257] N-hydroxysuccinimide (NHS) is the most commonly used agent for coupling them with acid groups, forming stable amide bonds (Figure 1.21a.(1)). However, N-hydroxysulfo-succinimide (Sulfo-NHS) is preferred over NHS because Sulfo-NHS is more water soluble while showing the same reactivity and

specificity as NHS. Alternatively, aldehyde-amino chemistry has been extensively used for protein immobilization.[256] The interaction between amine and aldehyde groups leads to the formation of an imine bond (Figure 1.21a.(2)).

Immobilization via carboxyl groups is another possibility since aspartic and glutamic acids usually constitute the major fraction of surface groups on proteins.[256] Carbodiimide is used to form amide linkage between carboxyl groups and amines. 1-ethyl-3-(3-dimethylaminopropyl) carbodiimide (EDC) is the most frequently used carbodiimide thanks to its water solubility. As described in Figure 1.21b, EDC reacts with carboxylic acid to form an o-acrylisourea intermediate, which subsequently reacts with primary amines to form amide bonds.

The covalent immobilization of proteins/peptides via amino acid side chains such as lysine, aspartic and glutamic acid is often random and attachment may occur simultaneously through many residues leading to structural deformation and potential reduction or loss of activity.[256, 263] However, well-defined immobilization procedures providing reproducible single-site oriented immobilization, thus avoiding protein denaturation, also exist.[256] One of the most common strategy for oriented immobilization relies on cysteine amino acid residue. Cysteine residue possesses a thiol group which is able to create an internal disulfide bond with another cysteine, contributing to the stability of the protein. As cysteine residue is not abundant in proteins (sometimes only one residue such as for bovine serum albumin (BSA)), site-directed immobilization is possible.[258] Incorporation of a unique cysteine residue into target proteins has also been accomplished by genetic modification to allow for oriented surface immobilization.[264] Three strategies to take advantage of cysteine residues are described in Figure 1.21c. In Figure 1.21c.(1), the maleimide double bond undergoes an addition reaction with thiol groups to form stable thioether bonds. In Figure 1.21c.(2), disulfide reagents participate in disulfide exchange reactions with another thiol leading to the formation of a new mixed disulfide. However, the reversibility of the linkage following exposure to reducing reagents can be an issue for stable immobilization.[256] Finally, in Figure 1.21c(3), vinyl sulfone reacts with thiol groups following a Michael addition, which is suitable for selective modification of cysteine residues under mild and physiological conditions.[265]

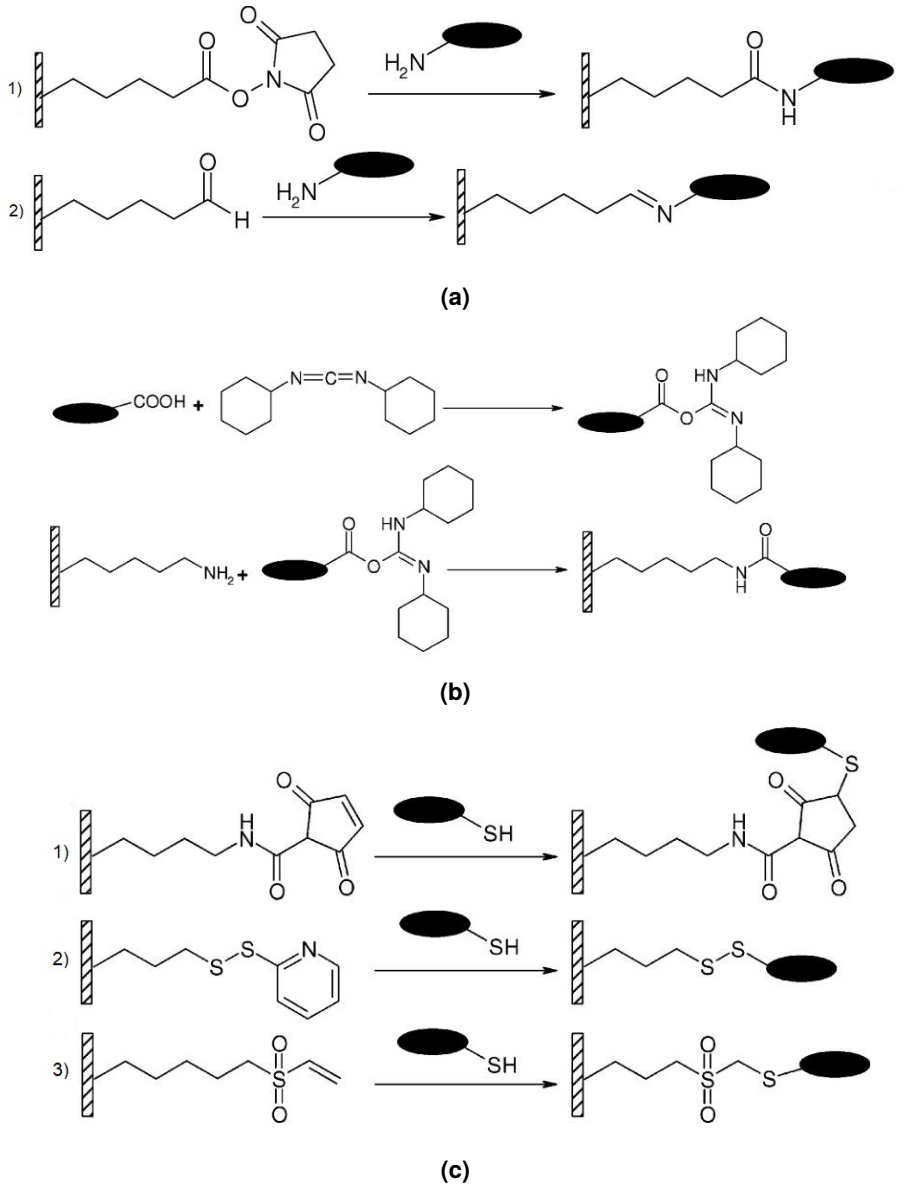

Figure 1.21.: Coupling reactions using (a) amine chemistry on (1) NHS-derivatized and (2) aldehyde-derivatized surfaces; (b) carboxyl chemistry using carbodiimide activation; (c) thiol chemistry on (1) maleimide-derivatized, (2) disulfide-derivatized, and (3) vinyl sulfone-derivatized surfaces.[256]

Linker molecules, which can react with both surface and functional groups present on the biomolecule are sometimes needed when the biomolecules cannot be directly grafted onto the surface. More specifically for biomedical applications, the choice of the linker is of critical importance as several studies have demonstrated that linker molecule characteristics influence the interaction between cells and the immobilized biomolecules.[259]

1.5.2.3. Bioaffinity immobilization

Immobilization based on biochemical affinity reactions allows for a gentle oriented immobilization. Moreover, as opposed to covalent coupling, this kind of reaction is reversible, allowing for protein detachment.[256] A widely used strategy for bioaffinity based immobilization relies on the strong interaction between avidin or streptavidin and biotin (Figure 1.22). Avidin is a tetrameric glycoprotein soluble in aqueous solutions and stable over wide pH and temperature ranges, which can bind up to four molecules of biotin. Streptavidin is a closely related tetrameric protein, with similar affinity to biotin, but differing in other aspects, such as molecular weight, amino acid composition and isolectric point (pI).[256] Streptavidin is usually preferred over avidin, as glycoamino acids occurring on avidin can potentially lead to unwanted non-specific adsorption.[263] This type of binding system is the strongest non-covalent biological interaction (affinity constant $K = 10^{15} M^{-1}$) and is unaffected by environmental stimuli such as temperature, pH, most denaturing agents, and organic solvents.[266] This immobilization strategy is attractive because of the number of biotinylated (and biotinylating) reagents available [267] but also for the specificity of this interaction which allows to obtain oriented immobilization.[256] Moreover, since biotin is a small molecule, its conjugation to biomolecules does not affect their conformation, size, or functionality. Both biotin and avidin/streptavidin may be attached to a variety of substrates.[256] However, this strategy involves multiple steps, including synthetic modification of the surface, immobilization of streptavidin/avidin, and blocking, each step increasing the production time and cost. High coverage densities are also difficult to obtain owing to the large size of the streptavidin/avidin.[266] Other biofunctionalization techniques can also be mentioned such as the antigen-antibody and the His-tag approaches.[257] The latter relies on the introduction of an affinity tag consisting of 6 to 10 consecutive histidines. The immobilization of the protein then relies on the binding between the His-tag and immobilized divalent metal ion such as nickel and cobalt.[256]

These biofunctionalization techniques are mostly used for biosensor applications but some cell culture applications can be found as well. For example, Igwe and coworkers developed a polymer-hydrogel hybrid scaffold coated with biotinylated human recombinant bone morphogenetic protein 2 (rhBMP2) for bone tissue engineering.[268] Similarly, Gorbahn *et al.* used biotin/streptavidin interactions to immobilize fibronectin on titanium to study osteogenic differentiation and showed an enhanced differentiation for immobilized FN compared with conventional adsorbed FN.[269]

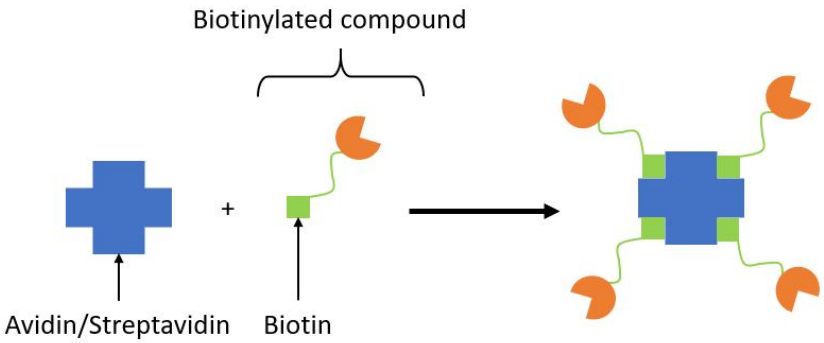

Figure 1.22.: Schematic illustration of the interaction between avidin/streptavidin and biotin.

1.5.2.4. Comparison of protein and peptide surface immobilization approaches

As a conclusion, a summary of the advantages and drawbacks of the three strategies to immobilize biomolecules on surfaces is provided in Table 1.7.

	Advantages	Drawbacks
Physical adsorption	- Easy - Inexpensive - Fast	- Weak immobilization - Random orientation
Covalent immobilization	- Strong attachment	- Need for appropriate functionalities on both surface and protein - Need for coupling agent/linker - Random orientation except for specific protocols
Bioaffinity immobilization	- Oriented immobilization - Availability of biotinylted/biotinylating agents - Good resistance to environmental conditions	- Limited coverage - Time-consuming - Costly

Table 1.7.: Overview of the advantages and drawbacks of the different surface immobilization techniques.

1.5.3 Methods to introduce surface functionalities

As covalent immobilization of biomolecules requires appropriate functionalities on both material surface and the considered biomolecule, the following section focuses on some of the most common approaches to introduce surface functionalities. The principle, synthesis and biomedical applications of self-assembled monolayers (SAMs), polymer brushes and layer-by-layer (LbL) technique are thus detailed below.

1.5.3.1. Self-assembled monolayer

Principle. Self-assembly is a process by which a disordered system of components forms an organized structure as a consequence of specific, local interactions among the components themselves, without external direction.[270] More specifically, the basic structure of molecules that form SAMs is composed of an anchoring headgroup, an organic chain backbone, and a functional endgroup, as depicted in Figure 1.23. [271, 272]

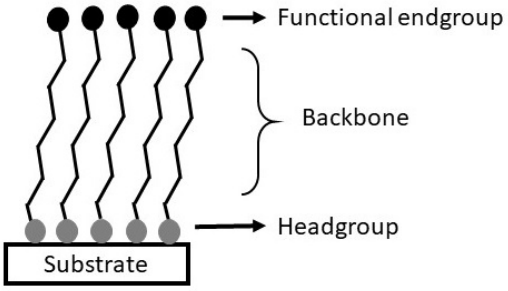

Figure 1.23.: Schematic illustration of SAM. Adapted from [272].

The assembly of these molecules into highly ordered structures is driven by two processes : a strong adsorption of the anchoring headgroup on the surface (typically 30–100 kcal/mol) and van der Waals interactions between the backbone alkyl chains.[260, 273] The surface functionality resulting from the SAM formation depends on the nature of the functional endgroup of the SAM.[274] Prominent examples of SAMs include alkylsilanes on hydroxylated surfaces such as silica, glass and alumina (Figure 1.24a), and alkylthiols on gold (Figure 1.24b).[260, 273]

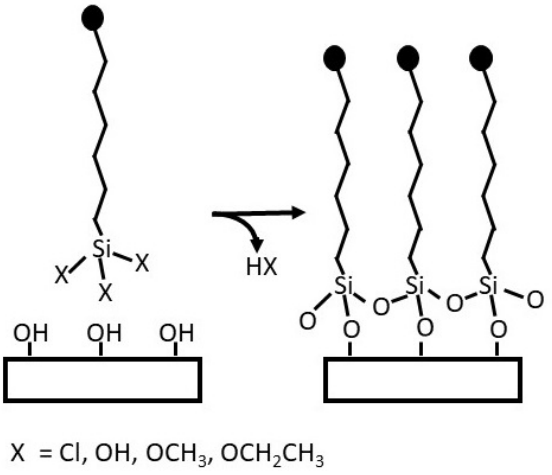

(a)

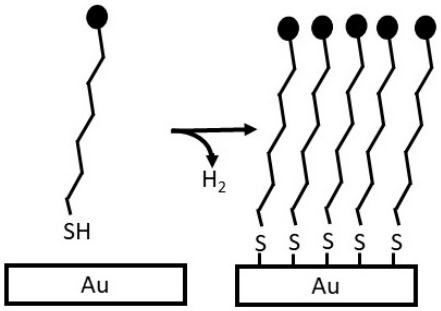

(b)

Figure 1.24.: Formation of (a) silane monoloayer on hydroxylated surface and (b) thiol monolayer on gold surface. Adapted from [275].

Coatings consisting of SAMs have gained significant attention as robust surface modification agents as they form well-defined surfaces, with a relatively good chemical stability and provide a wide range of surface functionalities.[260] SAMs are compatible with flexible substrates and can be obtained at low processing cost.[270] They also allow to obtain complex surfaces when coupled to patterning techniques. Specific patterns can be obtained either by the selective removal or placement of molecules, by the selective reaction of components

or by their destruction with energetic beams. The remaining areas can be left bare or backfilled with other molecules.[276]

Synthesis. SAMs can easily be obtained by a solution deposition process which relies on the dipping of a cleaned substrate into the corresponding solution for a certain time, allowing the monolayer to assemble. This method is straightforward and cheap and is an important reason for the popularity of SAMs. However, the cleanliness of both substrate and solution are of critical importance.[272] While most SAMs are prepared from solution, gas phase deposition constitutes a viable alternative.[272, 277] The principle of gas phase deposition is also very simple. In this case, deposition is not achieved by immersion in a solution but rather by exposing the substrates to the corresponding vapour, provided that the vapour pressure of the deposited molecule is sufficiently high. Extended deposition times may possibly be necessary depending on the chosen molecule. Besides resulting in less dense SAMs, this method is substantially more demanding and expensive.[277]

Biomedical applications. SAMs have been widely used to study and control interactions between solid substrates and biological systems, including the influence of surface chemistry on protein adsorption and cell adhesion.[274] For example, Faucheux *et al.* studied protein adsorption and fibroblast adhesion on alkylsilane SAMs displaying different functional end groups such as amine (NH_2), carboxyl (COOH), hydroxyl (OH), methyl (CH_3) and polyethylene glycol (PEG). They evidenced that SAMs in contact with bovine serum showed less protein adsorption to PEG and OH terminated SAMs than to CH3, NH_2 and COOH terminated SAMs. Significantly more cells adhered to SAMs terminated with NH_2 and COOH with a higher cell spreading and cell proliferation of human fibroblasts on these two samples.[278] In another study by Gallant *et al.*, microcontact printing was used to pattern alkanethiol SAMs into arrays of circular CH_3-ended adhesive islands within a nonadhesive background. They showed that FN adsorbed only on the islands and that cells seeded onto this patterned substrates maintained a round morphology, as they remained constrained to the available spreading area.[279]

1.5.3.2. Polymer brush

Principle. Polymer brushes refer to an assembly of polymer chains which are tethered by one end to a surface in sufficient proximity so that the polymer chains are crowded and forced to stretch away from the surface to avoid overlapping.[280] Polymer brushes can be easily synthesized from a wide range of monomers and are adaptable to a range of substrates. Based on their chemical composition, polymer brushes can be classified in four categories: homopolymer brushes (one type of repeat unit per polymer chain), mixed homopolymer brushes (two or more types of polymer chains), random copolymer brushes (two different repeat units randomly distributed along the polymer chain) and block copolymer brushes (two or more homopolymer chains covalently connected to each other at one end).[281] Polymer brushes also offer a high mechanical and chemical robustness, ensuring long-term stability.[282] Another interesting feature of polymer brushes arises from the fact that specific systems can undergo conformational changes upon exposure to external triggers such as temperature, solvent, pH, ionic strength, light, and electrical and magnetic fields.[283] For example, polymer brushes displaying a thermoresponsive behaviour related to a lower critical solution temperature (LCST) exhibit an extended conformation below their LCST while raising the temperature above the LCST induces a phase transition to a collapsed state.[284] PNIPAM, with a LCST in the physiological range (32 °C) has been widely studied for biomedical applications.[285] Similarly, polymer brushes based on polyelectrolytes (PEs) are responsive towards pH and ionic strength variations that can affect their charge and thus their chain conformation. Stimuli-responsive polymer brushes have been widely used for applications such as drug delivery, biosensing, cell culture and anti-fouling coatings.[284] Finally, polymer brushes can also be combined with patterning techniques such as UV photolithography, electron beam lithography, soft lithography, AFM lithography in order to produce brushes with defined patterns useful for various applications such as integrated circuits, biochips, or the study of cell-material interactions.[284, 285]

Synthesis. Two approaches can be used to synthesise polymer brush.[280, 281] The first one is a physisorption approach which consists of the selective adsorption of one block of a diblock copolymer to a surface. This approach is rather simple as no chemical reaction is needed. However, the polymer brush can be unstable under certain conditions of solvent, temperature, shear

stresses,... or can be displaced by other adsorbents since the physisorption is reversible. An alternative approach consists of the covalent binding of polymer chains at the surface which leads to a better stability of the tethered polymer chains. This approach is known as chemisorption. These covalently attached polymer chains can be synthesized by two different methods. The "grafting-to" approach involves the chemical reaction of preformed, functionalized polymers with surfaces containing complementary functional groups. This approach is technically simple and leads to a more precise characterization of the preformed polymer. On the other hand, it is not possible to produce very dense and thick polymer brushes because the attachment of chains may be impeded by the existence of previously attached chains which cause steric hindrance. On the opposite, the "grafting-from" approach, also called surface-initiated polymerization, involves an in situ polymerization from an initiator functionalized surface. The introduction of initiators on the surface can be achieved by treating the substrate with plasma or glow- discharge in the presence of a gas or by using initiator-containing SAMs.This technique produces polymer brushes of high grafting density. Indeed, since the chains are polymerized from the surface, there is less steric hindrance caused by adjacent chains. Interestingly, a good control over grafting density, polydispersity, brush thickness and composition can be obtained by using a controlled/living surface-initiated polymerization. Controlled surface-initiated polymerization techniques include living cationic and anionic polymerization, ring opening polymerization (ROP), reversible addition-fragmentation chain transfer polymerization (RAFTP), nitroxide-mediated radical polymerization (NMRP) and atom transfer radical polymerization (ATRP).[286] Among these, cationic, anionic and ring opening polymerization techniques require stringent experimental conditions and sensitive catalysts. RAFTP, NMRP and ATRP constitute flexible and less constraining techniques allowing the preparation of polymer brushes with controlled structures. All of them are based on the reversible dynamic equilibrium between dormant and active (radical) species. However, NMRP is not applicable to methacrylate-based monomers and usually requires high temperatures while chain transfer agents used in RAFTP are not commercially available. As a result, ATRP is the most used technique to obtain suface-initiated polymer brushes.[286] This technique, relying on the reversible activation–deactivation reaction between a growing polymer chain and a copper–ligand species, has several advantages including ease of preparation, commercially available and inexpensive catalysts, ligands and initiators. Moreover, it does not require stringent experimental conditions and

allows the polymerization and block copolymerization of a wide range of functional monomers.[287] The three different strategies to synthesize polymer brushes are illustrated in Figure 1.25.

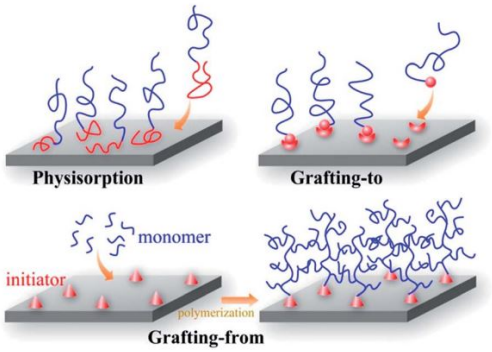

Figure 1.25.: Schematic illustration of different methods to synthesize polymer brushes on material surface: physisorption, "grafting-to" and "grafting-from".[288].

Biomedical applications. Polymer brushes have been widely used for their antifouling properties in order to prevent biofilm formation or protein adsorption. They also have been combined with several CAPs such as RGD, PHSRN and GFOFER to promote cell adhesion on brush coated surfaces.[285] More specifically, thermoresponsive polymer brushes have attracted great interest as they allow the harvesting of cells without using any enzymatic treatment. Cell detachment relies on the reversible transition of thermoresponsive brushes from hydrophilic to hydrophobic when temperature is reduced below their LCST, for instance. PNIPAM has been widely used for this purpose, as its LCST lies in the physiological range.[289] A wide range of cell types including fibroblasts, epidermal cells, chondrocytes, aortic endothelial cells, muscle cells, kidney cells, cardiac myocytes, hepatocytes, human ASCs and ESCs have been detached using this technique both from flat surfaces and MCs.[285, 289] More specifically for MCs, Tamura *et al.* reported a PNIPAM grafted PS MC that showed an efficient cell proliferation and subsequent thermally-induced cell detachment (Figure 1.26) thanks to the precise regulation of both the density of PNIPAM and diameter of bead.[136]

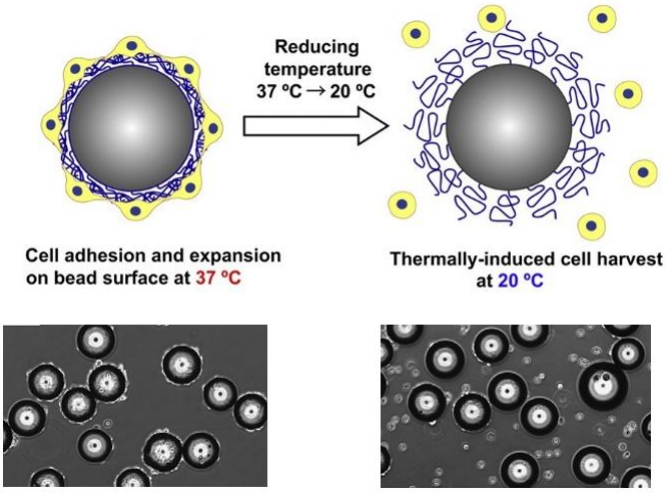

Figure 1.26.: Principle of cell harvesting on MCs that are surface-modified with a thermoresponsive PNIPAM polymer brush. Adapted from reference [136].

1.5.3.3. Layer-by-layer assembly

Principle. The LbL assembly is a thin film fabrication technique developed by G. Decher in the nineties.[290] It consists of the deposition of alternating layers of positively and negatively charged materials, as illustrated in Figure 1.27.[291] The driving force for the multilayer buildup thus relies on electrostatic interactions between opposite charges.[290] Secondary, shorter range forces also influence film properties such as thickness, morphology, structure and surface properties, and in some cases, can determine whether or not stable multilayers form at all. These secondary interactions can be strong interactions such as hydrogen bonding or weak interactions like hydrophobic interactions and Van der Waals forces.[292] Since the emergence of the LbL technique, other types of intermolecular interactions have been investigated as the basis for multilayer film formation including hydrophobic interactions, hydrogen bondings or even biological specific interactions. The electrostatic interaction remains, however, the most studied and extensively used mechanism within the LbL approach.[293]

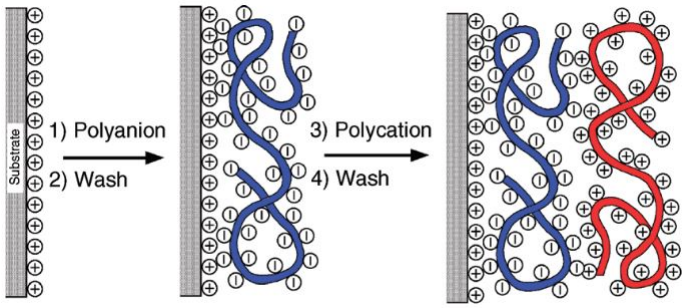

Figure 1.27.: Illustration of the first two steps of LbL technique based on the alternate deposition of oppositely charged polymer chains.[291].

This technique is easy, cheap and very versatile as it can be used on a wide range of substrates of different shapes, sizes and porosity, going from simple membranes to the most complicated surfaces, also including colloidal particles.[291] The only requirement is that the substrate carries a surface charge. This charge can be inherent or induced by surface treatment. The most diverse charged materials, such as PEs, proteins, polysaccharides, deoxyribonucleic acid (DNA) or nanoparticles can be combined with one another to form the multilayer film.[291, 294, 295] LbL assemblies are performed under mild conditions in aqueous solutions requiring no exposure to organic and harmful solvents, high temperatures, or extreme pH values, making this technique an environmentally friendly fabrication process.[293]

Fabrication. Traditionally, LbL assemblies on substrates are carried out using a solution dipping method, also called immersive assembly method, as illustrated in Figure 1.28. In this case, the substrate is alternatively dipped into different solutions containing PEs and rinsing solutions. The solution dipping method has been automated using a variety of commercially available instruments. The simplicity of immersing substrates of almost any shape or size into containers makes this technology easily accessible. However, the time required for this technique is something to improve as the immersion time for each layer can vary between 1 and 15 minutes, depending on the nature of PE used.[295]

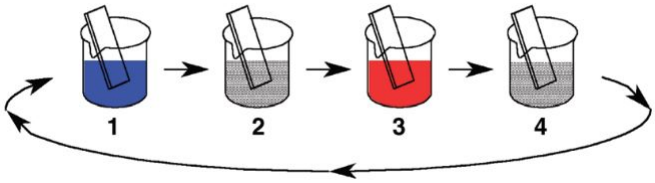

Figure 1.28.: Schematic illustration of the dipping process used to produce LbL assemblies.[291].

Alternative methods include the spin and spray assembly technologies.[294, 295] The spin assembly technology was demonstrated by the groups of Hong [296, 297] and Wang [298] and relies on the common technology of spinning a substrate to facilitate the deposition of materials onto this substrate. The spinning process allows the amount of material and the time needed to build a film to be reduced. Only 30 seconds are required for each layer deposition. Furthermore, the use of commercially available spin coaters allows the coating of large substrates (up to 10 cm in diameter) and the obtention of more homogeneous films than the immersive technology.[295] The spray assembly, introduced by Schlenoff *et al.*,[299] uses different aerosolized polymer solutions and sequentially sprays them onto the substrate. The spray assembly technology is a really fast process that only requires 6 seconds per layer making this process widely used for industrial applications.[295] Compared to the immersive technology, both processes require less sample and are less time-consuming but are not suitable for the complex shapes accessible to immersive assembly.[294, 295, 300] Another way to perform LbL deposition is by electromagnetic assembly. This process is based on the use of an applied electric or magnetic field to allow the film buildup.[295] Finally, the last technology available for LbL deposition is the fluidic assembly which is based on a pump or capillary forces to transport the liquid polymer through fluidic channels which allows the deposition of different layers by coating a substrate placed in fluidic channel. This method looks strongly like the immersive assembly method since the polymer solutions have to stay in a static contact with the substrate to adsorb onto it. Fluidic assembly is useful to obtain a specific and precise pattern for the LbL film.[295]

Growth behavior of PEMs. Two kinds of growth regimes have been identified for polyelectrolyte multilayers (PEMs): linear or exponential. Linear growth takes place if the increment in thickness per deposited bilayer is constant. For exponentially growing multilayers, the increment increases with the number of deposited layers.[301, 302] The first investigated PEs systems, such as poly(styrene sulfonate)/poly (allylamine hydrochloride) (PSS/PAH) and PSS/ polydiallyldimethylammonium chloride (PDADMAC) films exhibited a linear growth of both mass and film thickness with the number of deposited layers.[173, 301] This kind of films showed a stratified structure, with limited interpenetration between the different layers. More recently, a new type of PEM characterized by an exponential growth of both film mass and thickness with the number of deposition steps was described by several groups.[303, 304] Poly-L-lysine/hyaluronan (PLL/HA), PLL/alginate (PLL/ALG) and chitosan/HA (CHI/HA) are examples of exponentially growing films. While linearly growing films typically show thickness of about 100 nm for films constituted of 20 bilayers, this thickness can reach up to 3 µm for exponentially growing films.[173] According to the diffusion model, the type of growth is linear if polymers are not able to diffuse inside the film. If at least one PE is able to diffuse into the entire multilayer, the film grows exponentially. Indeed, during adsorption of oppositely charged PE, the excess PE within the multilayer will move to the interface of PEM and PE solution and will form complexes with the freshly adsorbing oppositely charged PE. With increasing thickness of the PEM, its capacity for PE uptake increases. As a result, the thickness increment per bilayer increases with increasing number of layers.

Post-treatments. Controlling the mechanical properties of LbL films is of great importance especially for films composed of polysaccharides and polyaminoacids, which are rather soft compared to synthetic PEs.[173] More specifically for the field of biomedical application, films needs to be stable in physiological conditions which are not always the conditions in which the film was built. The film also need to withstand shear stresses that can be induced by rinsing, agitation or even the cells themselves depending on the application. Finally, it is now well recognised that surface mechanical properties play an important role in various cellular processes such as adhesion, proliferation, and differentiation.[305] Depending on the structural properties of the films, the stiffness can be modulated from a few kPa to several GPa.[306] Several techniques have been reported to tune PEM stiffness.[173, 306] Obviously, the stiffness strongly depends on the

components of the film. Thus, incorporating components such as strong PEs or nanoparticles (carbon nanotubes, metalic nanoparticles, clay,...) is an easy way to improve the film stiffness.[173, 306] For a given film composition, introducing ionic crosslinks by playing on ionic strength and pH is another way of modulating the film mechanical properties.[306] Finally, the mechanical properties can be adjusted through chemical ways by creating covalent links within the film. For example, it was reported that high temperatures (130 °C) could lead to the formation of imide or amide bonds in PAA/PAH films.[307] Similarly, photocrosslinking of multilayer films has been reported, introducing the possibility of patterning.[306] Finally, an alternative method based on the carbodiimide chemistry was proposed by Richert *et al.* and Schuetz *et al.*[308, 309] It relies on the formation of amide bonds following the reaction between carboxyl groups with amine groups in mild conditions (room temperature, salt-containing medium).[173, 306]

Alternatively, other post-treatment strategies include the biochemical functionalization of the film. For example, a wide range of LbL films have been modified using ECM molecules with the aim of providing specific attachment to the cells via integrin receptors.[310] For example, Semenov *et al.* functionalized PLL/HA film by either adsorbing or grafting FN. They showed that covalent fixation of FN to PLL/HA coatings proved necessary to maintain densely grown MSCs. PEMs can also be grafted using ECM-derived peptides such as the RGD peptide.[310] For this, two different strategies have been developed. The first consists of grafting the peptide to one of the polyelectrolytes and then adsorbing the modified polyelectrolyte as a regular layer. It was shown that human osteoblasts adhesion increased up to 10-times on poly(L-glutamic) acid (PGA)/PLL films for which the PGA had been grafted with a RGD peptide.[311, 312] The second strategy consists of directly coupling the RGD peptide onto the film, using the carbodiimide EDC as a coupling agent.[310] For example, (HA/CHI) films deposited on titanium were grafted with RGD peptides and showed an enhanced osteoblast cell adhesion and proliferation compared to non-grafted films.[240]

Biomedical applications Thanks to its simplicity and versatility, the LbL technique has led to considerable developments of biological applications within the past decades, including biofunctionalization of cardiovascular devices, wound healing dressing, bone grafts, micro- and nano-carriers, *etc*.[313] This biofunctionalization allows to immobilize biomolecules with preserved bioactivity,

which is critical for drug delivery applications.[310] PEMs also allow to control surface properties in order to either improve protein adsorption as well as bacteria and mammalian cell adhesion or, on the contrary, restrict their adhesion in the case of antifouling coatings.[314]

More specifically, several authors used crosslinking strategies to improve cell adhesion and control cell differentiation. For example, Schneider *et al.* crosslinked PLL/HA PEM using carbodiimide chemistry and showed that they could modulate PEM stiffness by over 2 orders of magnitude (from 3 to 400 kPa) which in turn improved the adhesion and spreading of human chondrosarcoma cells, as seen in Figure 1.29.[315] Using the same combination of PLL/HA film and carbodiimide chemistry, Ren *et al.* showed that, unlike native films (Young's Modulus of 3 kPa), crosslinked films (Young's Modulus of 382 kPa) promoted formation of focal adhesions and organization of skeletal muscle cell cytoskeleton and enhanced proliferation.[316] Regarding differentiation, they also showed that stiff films led to significantly more elongated and thinner myotubes and that myotube striation was only visible on these crosslinked films. Still using PLL/HA films, Semenov *et al.* showed that native films were poorly adhesive for MSCs while highly crosslinked films became efficient substrates for MSC adhesion and proliferation.[317] Moreover, MSCs were capable of differentiating into osteocytes and chondrocytes upon culture with induction factors. The effect of film crosslinking was also investigated using other systems and led to similar conclusions. For example, chitosan (CHI)/alginate (ALG) films were crosslinked using genipin and showed an increase in cell number and spread area following an increase in crosslinker concentration.[318] In another work, chondroitin sulfate A (CSA)/PLL films crosslinked with genipin significantly promoted adhesion, proliferation, and early and late differentiation of preosteoblasts.[319]

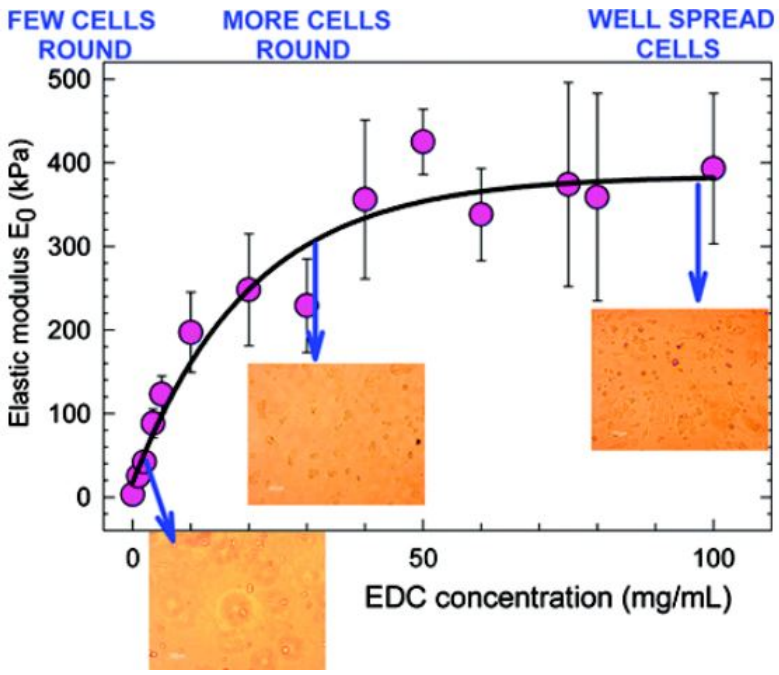

Figure 1.29.: Modulation of PLL/HA film stiffness following crosslinking improves chondrosarcoma cell adhesion and spreading.[315].

1.5.3.4. Comparison

To conclude this section on the different methods to introduce specific functionalities on the surface of materials, an overview of the advantages and drawbacks of the presented methods is provided in Table 1.8.

	Advantages	Drawbacks
SAM	- Easy - Molecularly well-defined - End groups can be used to tailor surface properties and anchor biological liands	- Thin (one molecular layer) - Limited long-term stability
Polymer brush	- Long-term stability - Tunability through choice of monomer - Variety of polymerization methods - Control over thickness	- Complex procedure - Harsh conditions
LbL	- Versatility - Aqueous conditions - Control of thickness -Control of mechanical properties	- Limited coverage - Time-consuming - Costly

Table 1.8.: Overview of the advantages and drawbacks of methods allowing to introduce surface functionalities.

2

Aim of the thesis

Cell-based medicine is a rapidly progressing scientific and medical discipline which aims to develop therapeutics to treat a variety of diseases such as cancer, diabetes, myocardial infarction, bone defects, *etc.* using a wide variety of cell types (*e.g.*, fibroblasts, lymphocytes, endothelial cells, insulin producing cells, stem cells).[28, 29] However, regardless of the specific application, one major challenge that still impedes the industrial development of cell-based therapies is the large number of cells required to treat a single patient.[89] For example, in the case of human MSCs, which are considered as especially promising candidates with over 914 clinical trials reported since 2008, doses ranging from 100 to 150 million cells per patient are usually required.[32] This highlights the critical need for efficient cell expansion technologies to ensure the full development of cell-based therapies. The cell expansion step usually involves the culture of cells as a monolayer inside plastic flasks in static conditions.[47–50] When large number of cells are not required, this technique offers the advantages of simplicity and easy-handling. To increase the expansion potential, multi-layered vessels have been developed by different companies in an effort to provide both a space and labor-saving solution (Corning CellSTACK™, Nunc Cell Factory™ [49]). However, as those culture vessels grow in size and weight, they become more difficult and time consuming to handle and may even require reinforced incubators and often mechanical assists to support media changes.[53] The large number of flasks required to produce clinically-relevant cell doses also generates significant plastic waste. The limited possibility to monitor cell growth as well as the static nature of the culture which leads to concentration gradients (pH, dissolved oxygen, nutrients, metabolites, *etc*.) also constitute known drawbacks of 2D culture.[49] Finally, those systems also offer limited scalability as only scaling-out is possible, by increasing the number of culture units.[48] Scaled-up manufacturing of cells using MCs in suspension cultures is a promising tool to overcome the limitations of monolayer culture. Indeed, the main asset of cell culture on MCs is to provide a large solid surface for cell proliferation within a limited volume of medium, while keeping relatively homogeneous and

controlled environmental culture conditions. Nowadays, a wide variety of MCs are commercially available (section 1.3.4). They can be distinguished according to several criteria: rigidity, porosity, density, charge, presence and nature of coating, size, core material, *etc*. However, these commercial MCs have been designed with the aim of propagating anchorage-dependent cell lines used in production of vaccine and biopharmaceuticals and are not optimized for cells directly used as therapeutic agents, notably stem cells. Indeed, most MC fabrication techniques offer poor control over MC characteristics such as porosity, surface roughness or mechanical properties. This is disadvantageous, not only because these parameters are known to affect stem cell behaviour,[140] but also because dynamic culture, which is a multiparameter approach, requires MCs with specific characteristics (*i.e.*, density, size, mechanical resistance) that are optimized according to the culture conditions such as agitation type and rate, bioreactor type, cell type, *etc.* Their fabrication also relies on the use of toxic organic solvents limiting their application for medical purposes. Moreover, these MCs are frequently coated with animal-proteins to ensure cell adhesion, which constitutes a drawback from a regulative point-of-view. Among the commercial animal-protein free MCs, only two of them present specific sequences recognised by cell adhesion receptors (Synthemax™ and Pronectin F) while the others mostly rely on electrostatic interactions to ensure cell adhesion.

In this context, the aim of this thesis was to develop new MCs specifically dedicated for the *in vitro* expansion of stem cells in the scope of cell-based therapies. More precisely, compostable MCs obtained through a green production process avoiding the use of organic-solvent should be fabricated in an effort to limit the amount of waste produced during the cell expansion process. We also aim to be able to tune easily MC characteristics such as size, density, surface roughness, *etc*. while keeping the material core constant. This versatility would allow us to select the most suitable MC according to our culture conditions (cell type, type of spinner flask, *etc*.). Moreover, developing a magnetic version of these MCs would facilitate cell culture handling (medium change) and monitoring (in line sampling) as well as cell-MC separation at the end of the culture.

According to these objectives, chapter 3 presents a green fabrication process of MC cores suitable for cell expansion. The impact of process parameters on MC characteristics such as size, morphology and mechanical resistance is highlighted and serves as the basis for the subsequent optimization of this MC core. The preparation of magnetic MCs facilitating culture handling is

also investigated. An overview of the MC cores selected for cell assays is finally provided. Chapter 4 focuses on the biofunctionalization of MC surface in order to ensure optimal cell adhesion, critical in dynamic condition. In chapter 5, exploratory cell assays are performed in semi-static condition to optimize various culture parameters and MC characteristics. More precisely, the cell seeding density is explored and the effect of both MC surface morphology and composition of bioadhesive coating on cell adhesion and proliferation is investigated. A comparison between one of our MCs and a widely-used commercial MC is also provided. Moreover, the performance of magnetic MCs are evaluated against non-magnetic MCs. Chapter 6 focuses on the use of our MCs to perform cell expansion in dynamic condition using spinner flasks. The feasibility of using our MCs for dynamic cell expansion is thus investigated as well as the possibility of bead-to-bead transfer to improve the yield of expanded cells. Finally, chapter 7 summarizes the main results obtained in the present thesis and points out some future prospects.

3

Microcarrier production, characterization and optimization

3.1 Introduction

The aim of this chapter was to produce, characterize and optimize MC cores suitable to be used for cell culture. These MC cores must be biocompatible and should ideally be composed of a biosourced and industrially-compostable polymer, thus limiting energy consumption and waste. The fabrication process should avoid the use of organic solvents and toxic reagents. More specifically, as dynamic culture using MCs is a complex and multiparameter approach that requires a careful selection of the appropriate MC depending on the type of vessel, stirring regime and cell type,[78] having a fabrication process allowing to easily modulate MC characteristics would be valuable. Indeed, MC cores need to meet three stringent specifications in order to be used as MCs for dynamic cell expansion: an optimal size for cell growth and maximization of available surface area, an appropriate sedimentation rate to avoid accumulation at the bottom of the reactor for reasonable stirring rates, and sufficient mechanical resistance to withstand stirring in aqueous medium. The existence of an appropriate size range results from a compromise between the maximization of the total surface area, the stability of the suspension (both in favor of a smaller size) and a minimal area per microcarrier, which is required to provide enough space for cells to adhere and grow. Then, for dynamic cell expansion, MCs also need to be well suspended in the medium to optimize nutrient and waste-product transfers between cells and the surrounding medium as well as to avoid MC aggregation which again can lead to poor transfer of oxygen and nutrients to cells, compromising their viability.[95] An appropriate sedimentation rate of MCs is thus of critical importance. On the one hand, MCs should not float but on the

other hand, if they settle too fast, a higher level of agitation would be required, causing higher shear stress that can have harmful effects on cells. Finally, MCs need to be able to withstand the mechanical stress induced by the agitation in dynamic conditions as breakage products would be detrimental to the final cell product.[48]

In this chapter, the strategy developed to produce MC cores is first described. The precise experimental protocols are then provided. The result section is further divided into four parts. In the first part, the influence of process parameters on spherulites characteristics is reviewed. Then, the production of magnetic MCs and their properties are discussed. In the following part, spherulites characteristics are optimized to obtain MC suitable for dynamic culture. Finally, a summary of the MCs selected for semi-static and dynamic cell culture assays is provided.

3.2 Strategy

Poly(lactide) (PLA) was chosen as the core material of the MCs. PLA is a thermoplastic polymer belonging to the family of aliphatic polyesters.[320, 321] It is obtained from the 2-hydroxypropionic acid monomer, also known as lactic acid. The monomer exists as two optical isomers, L and D, illustrated in Figures 3.1a and 3.1b, respectively.[321, 322] An interesting property of PLA is that its stereochemical structure can easily be modified by using different ratios of L- and D-isomers. For example, the homopolymerization of L-lactic acid or D-lactic acid forms isotactic semicrystalline polymers (PLLA and PDLA, respectively) exhibiting a melting point around 180°C. On the other hand, polymerization of a racemic mixture of L- and D-lactic acid, usually leads to the synthesis of poly-DL-lactide (PDLLA), which is amorphous. Thus, various structures exhibiting different properties can be obtained from polymerization of lactic-acid. However, so far, only PLLA and PDLLA have been extensively studied and showed promises in the biomedical field.[323]

Figure 3.1.: (a) L-lactic acid monomer; (b) D-lactic acid monomer.

This polymer was chosen for its numerous advantages. First, PLA is biocompatible. This makes PLA very attractive for biomedical applications. The polyester backbone degrades by simple hydrolysis to form non-toxic compounds. It is worth noting that the Food and Drug Administration (FDA) has approved PLA for direct contact with biological fluids [321] and *in vivo* applications.[324] Secondly, it is eco-friendly. PLA can be derived from renewable resources such as corn, wheat or rice and requires 25–55% less energy to produce than petroleum-based polymers.[321] It is also biodegradable, recyclable and compostable. PLA exhibits a rather slow degradation rate which depends on crystallinity, molar mass, molar mass distribution, morphology, water diffusion rate into the polymer, and the stereoisomeric content.[321] PLA is also easily processable by a variety of methods including injection molding, film extrusion, blow molding, thermoforming, fiber spinning, *etc*.[321] Besides its various advantages, PLA has also some drawbacks. First, PLA is considered to be very brittle. It is also known to be hydrophobic with a water static contact angle of $80°$, resulting in low cell affinity and even inflammatory response elicitation.[321] Also, due to its slow degradation, PLA might not be suitable for some applications. Finally, PLA is chemically inert as it lacks reactive side chains. As a result, surface modifications are rather challenging.[321]

To produce PLLA-based MCs cores, we used a fabrication process previously developed in our lab and based on the crystallization of PLLA (Figure 3.2a) in a miscible blend with PEG (Figure 3.2b).[135]

(a) **(b)**

Figure 3.2.: (a) Poly(L-lactide) structure, (b) Poly(ethylene glycol) structure.

PEG is a semi-crystalline polymer which is soluble in water and has a low immunogenicity and toxicity.[325] Thanks to its biocompatibility, it is widely used, not only for pharmaceutical applications such as drug delivery but also in daily consumer products such as shampoo, toothpaste, body soap, eye shadow, *etc*. Its successful use for biomedical applications is reflected by the commercialization of numerous FDA and EMA-approved pharmaceuticals products. For example, a range of PEGylated products can be found on the market [326] and PEG of about 3 kDa to 4 kDa is commonly given orally as a laxative (as GoLYTELY® and MoviPrep®).[327] However, a study performed in 2007 with 350 healthy blood donors found occurrence of PEG antibodies in 22 %-25 % of the donors [328] whereas a very low occurrence of 0.2 % was initially reported in 1984.[329] This increase may be due to an improvement of the limit of detection of antibodies with time but it was also hypothesized that it could be related to a greater exposure to PEG in cosmetics, pharmaceuticals and processed food products.[330] The understanding of the mechanisms of anti-PEG immunity and characteristics of anti-PEG antibodies are however still very limited [331] and some authors even claim that most, if not all assays for anti-PEG antibodies are flawed and lack specificity.[332] Thus, according to them, as long as well-validated assays for anti-PEG antibodies are not available, any conclusion regarding the immunogenicity of PEG is premature.[332]

The selected fabrication process offers a fine control over MC properties while keeping a constant core material and surface biochemistry, avoids the use of toxic reagents and can easily be scaled-up for industrial production using the standard tools of plastics technology.

After the expansion step on MCs, cells usually need to be detached and separated from MCs.[49] As of now, the separation step has received little attention and usually involves the use of filtration or centrifugation.[80] Alternatively, MCs

displaying magnetic properties could facilitate MC handling during MC-cell separation by allowing to immobilize MCs using a magnet. This feature could also ease MC handling during culture such as for medium replenishment. MNPs are thus incorporated into MCs in order to make them superparamagnetic and thus easier to handle. Superparamagnetism is a type of magnetism that occurs in small ferromagnetic or ferrimagnetic nanoparticles (NPs). If the size of these NPs is small enough (typically a few nanometers to a couple of tens of nanometers), their magnetization can randomly flip direction under the influence of temperature. When no external field is present, superparamagnetic NPs will thus exhibit no net magnetization due to rapid flipping of the magnetic moment.[333] In particular, superparamagnetic iron oxide nanoparticles (SPIONs), typically composed of either magnetite (Fe_3O_4) or maghemite (Fe_2O_3), have attracted great interest thanks to their various applications such as MRI contrast enhancement, tissue repair, immunoassay, detoxification of biological fluids, hyperthermia, drug delivery, and cell separation.[334, 335] Those SPIONs are especially well-suited for biomedical applications for two reasons.[336] First, their superparamagnetic nature implies that the particles will not be attracted to each other, and so the risk of agglomeration in a medical setting is minimised. Then, iron is a naturally occurring metal in the human body (ferritin) making iron-containing nanoparticles biocompatible since the body is adapted to metabolising the particles into its elements.[336] In view of the extended use of SPIONs for *in vivo* applications, these magnetic MCs are expected to remain biocompatible while allowing an easier handling of the MCs.

The overall strategy to fabricate magnetic MCs is illustrated in Figure 3.3. The first step is thus the preparation of a PEG powder containing MNPs (PEG-MNP). Indeed, MNPs are usually conditioned in aqueous solution which may cause polymer degradation at the high temperature needed to melt PLLA. Hence, in order to eliminate water, the MNPs solution is mixed with a PEG aqueous solution. For this, dextran coated iron oxide MNPs were chosen as they offer a good compatibility with PEG. The resulting mixture is subsequently freeze-dried leading to a PEG-magnetic NPs powder. In the next step, this powder is mixed with PLLA pellets to get the desired PLLA/PEG ratio. The resulting powder is heated at $230\,^{\circ}\mathrm{C}$ for 5 minutes to obtain a melt. Then, the isothermal crystallization of PLLA takes place overnight at the chosen crystallization temperature ($\mathrm{T_c}$). The polymer crystallization process results in spherulites following the random formation of nuclei and the radial growth of bundles of crystalline lamellae from these nuclei.[337] Finally, after cooling

to room temperature, the PEG is dissolved with water and individual porous spherulites are obtained.

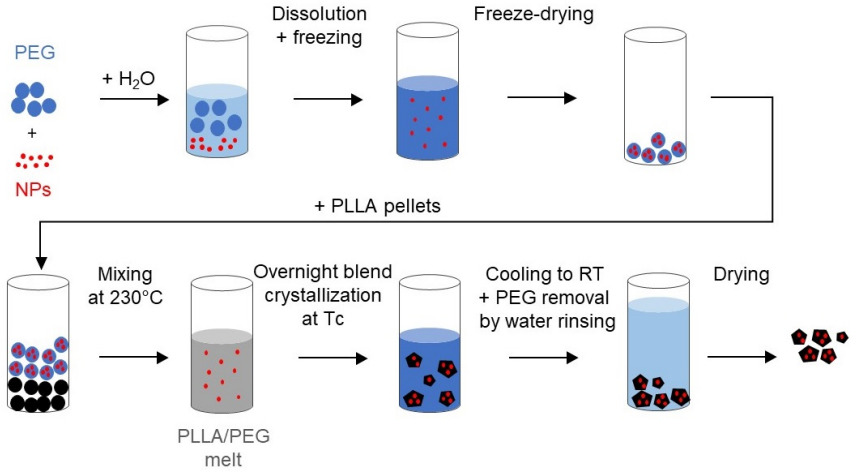

Figure 3.3.: Description of the fabrication process of magnetic MCs via spherulitic crystallization of PLLA.

3.3 Experimental section

3.3.1 Materials

Poly-(L-lactide) (20 000 g/mol, Đ$\leq$ 1.1) (PLLA20), PEG (3 500 g/mol) were obtained from Sigma-Aldrich. PLLA40 (40 000-70 000 g/mol) was obtained from Polysciences. Dextran coated iron oxide magnetic nanoparticles were purchased from Ocean Nanotech. Fluorescent nanoparticles (Molday ION™Rhodamine B) were bought from BioPAL. Milli-Q grade (resistivity of 18.2 mΩ) was produced by a Milli-Q® Reference system of Merck Millipore.

3.3.2 Preparation of PLLA microcarriers

3.3.2.1. Preparation of polyethylene glycol powder containing magnetic nanoparticles

PEG was first dissolved in Milli-Q water (0.66 g/mL) and vortexed for 30 sec. An appropriate quantity of either fluorescent (from BioPAL) or non-fluorescent (from Ocean nanotech) MNPs solution was added, depending on the desired Fe/PLLA and PEG/PLLA ratio. The solution was thoroughly mixed and frozen for at least 24 h at −20 °C prior to the freeze-drying process.

3.3.2.2. Isothermal crystallization of PLLA spherulites

PLLA microcarriers were prepared via isothermal spherulitic crystallization of PLLA from PLLA/PEG blends as described in Figure 3.3. PLLA of two different molar masses (PLLA20 and PLLA40) were used. PLLA and PEG in the form of dry powders were first combined with the desired PLLA/PEG ratio (ranging from 10/90 to 70/30) and melt-mixed at 230°C for 5 min under dry argon, followed by vortexing to obtain a homogeneous melt. The melt was then isothermally crystallized overnight under inert atmosphere in a glass tube fitted with a rubber septum to limit thermal degradation of the polymers. The temperature was comprised between 103 ± 0.1 °C and 130 ± 0.1 °C and was fixed by a heated oil bath. After crystallization, the blend was cooled down to room temperature then repeatedly washed with Milli-Q water to remove PEG and collect the insoluble PLLA microcarriers. To obtain magnetic MCs, regular PEG was replaced with the PEG powder containing MNPs as described in section 3.3.2.1. Samples prepared with different PLLA/PEG ratio are named according to the PLLA content in the blend (*i.e.*, MC30, MC50, MC70 are prepared with 30, 50 and 70 % of PLLA, respectively).

3.3.3 Characterization of PLLA microcarriers

3.3.3.1. Characterization of microcarrier morphology

MCs dried overnight at room temperature then sputter-coated with a 8 nm-thick layer of chromium under high vacuum, were observed using a JEOL 7600F scanning electron microscope (SEM) operated at an acceleration voltage of 15 kV.

3.3.3.2. Characterization of microcarrier size

MCs suspended in water were imaged by bright field microscopy using an Olympus epifluorescence IX71 microscope. The MC average size was obtained as the geometric average between the longest and shortest dimension of fifty randomly selected MCs, as measured using the microscope software (CellSensDimension).

3.3.3.3. Evidence for the presence of magnetic nanoparticles in microcarriers

Rhodamine-labelled MNPs were used during MC production instead of the regular non-labelled MNPs. MCs dried overnight at room temperature were imaged with an Olympus epifluorescence IX71 microscope equipped with a blue filter U-MNUA2 (excitation 360-370 nm and emission 420-460 nm), a green filter U-MWIBA3 (excitation 460-495 nm and emission 510-550 nm) and a red filter U-MNIGA3 (excitation 540-550 nm and emission 575-625 nm). The UV light is provided by an X-cite module, series 120PCQ from Lumen Dynamics.

3.3.3.4. Characterization of magnetic nanoparticle spatial distribution at the nanoscale

Dried MCs were embedded in a two-components epoxy resin (2.5 g EPOXY embedding mixed with 0.3 g EPOXY hardener) in a mold and cured at room temperature for 48 h. Ultrathin sections (approximately 90 nm thickness) of the embedded samples were obtained at room temperature using a Reichert

FCS cryomicrotome fitted with a diamond knife. These sections were placed on a carbon coated mesh (Q250-CR13, EMS) and imaged using a Leo 922 (Zeiss) transmission electron microscope (TEM) equipped with a LaB6 cathode operating at an accelerating voltage of 120 kV.

3.3.3.5. Determination of magnetic nanoparticle content in microcarriers

The content of MNPs in PLLA MCs was evaluated by inductively coupled plasma atomic emission spectrometry (ICP-AES). MCs prepared with 1 or 3 mg Fe /g PLLA were mashed then calcined at 500 °C before being diluted in 1 mL of concentrated HCl and 9 mL of water, diluted 10 times in water and, finally, analyzed using an ICAP 6500 (Thermo Scientific).

3.3.3.6. Study of magnetic nanoparticle release over time

Triplicate samples consisting of 100 mg of MCs prepared with 3 mg Fe /g PLLA were placed in 5 mL of phosphate buffer saline (PBS) (0.01 M, pH 7.4) and agitated at 100 rpm on an orbital shaker at room temperature for 6 days. At each time point (day 1, 2, 5 and 6), the supernatant was retrieved and replaced by 5 mL of fresh PBS. The iron content in the supernatant was assessed by ICP-AES. Briefly, the samples were calcined at 500 °C before being diluted in 1 mL of concentrated HCl and 9 mL of water, diluted 10 times in water and, finally, analyzed using an ICAP 6500 (Thermo Scientific).

3.3.3.7. Characterization of microcarrier magnetic properties

Magnetization curves of MCs containing MNPs were obtained using a MicroMag 2900 alternating gradient magnetometry (AGM). For this, 1 mg of dry MCs was placed on adhesive tape to immobilize them. The sample was analyzed and the signal of the tape was substracted from the total signal.

3.3.3.8. Measurement of microcarrier sedimentation rate

Wet MCs prepared at different crystallization temperatures and PLLA40/PEG ratios were deposited on the top surface of a water column. The time needed for them to sink over 20 cm was recorded five times, with t_0 and t_f the times for the first and the last MC reaching the bottom point, respectively. For each condition, the sedimentation rate was estimated as the median of t_0 and t_f.

3.3.3.9. Estimation of the surface area of microcarriers

One mg of MCs prepared with PLLA40/PEG ratio of 30/70, 50/50 and 70/30 (MC30, MC50, MC70) at $110\,°C$ and MC50 prepared at 103°C suspended in 200 µL Milli-Q water were placed on a glass slide and observed with a bright field microscope at a 4X magnification. Using the CellSensDimension software, a 2D reconstructed image of each entire sample was obtained and MCs were manually counted on this image using the cell counting plug-in provided in the ImageJ software. The operation was repeated five times to obtain an estimation of the number of MCs per mg of MC (for each type of MC). By measuring the median size of the MCs (section 3.3.3.2), the average surface area provided per mg of MCs was estimated, by assuming MCs as spheres. Obtaining a more precise evaluation of MC surface area would have been highly complex. Indeed, as PLLA MCs are faceted, the computation of a precise surface area would require to characterize the 3D shape of MCs which is not possible using confocal microscopy due to the opacity of MCs or SEM. An alternative is to use micro-computed tomography but this would be extremely time-consuming both in terms of data acquisition but also data analysis.[135] Also, as MC size was computed by taking the geometric average between the longest and shortest dimension, the non-spherical nature of MCs is partly taken into account.

3.3.3.10. Qualitative observation of microcarrier mechanical resistance under stirring

In order to qualitatively assess the resistance to stirring of MCs prepared using different processing parameters, 50 mL of MC suspension (1 mg/mL) was placed in a spinner flask stirred by a bulb at 45 rpm for up to seven days. MCs were then observed by bright field microscopy. Due to the geometrical

characteristics of MCs (shape and size), measuring the mechanical properties of MCs such as their elastic modulus or even worse their fracture toughness is hard to perform with conventional equipments (AFM, nanoindenter...).[79] As a result, only the qualitative evaluation of MC resistance is provided here.

3.3.3.11. Surface roughness evaluation

The surface roughness of MCs crystallized at 110 °C using different PLLA40/PEG ratios (MC30, MC50, MC70) and MC50 crystallized at 103 °C was evaluated following observation with a laser scanning confocal microscope (Keyence VK-X series). The average peak to valley height (R_a) was computed from two different samples using Igor Pro.

3.4 Results and discussion

3.4.1 Characterization of PLLA spherulites according to processing parameters

The characteristics of PLLA/PEG blends have been studied by several authors. They showed that key parameters influencing the spherulitic crystallization of PLLA in PLLA/PEG blends are blend composition, crystallization temperature and polymer molar mass.[338–341] The effect of these three parameters on PLLA spherulite morphology was thus investigated in order to provide a basis for the subsequent optimization of PLLA spherulites to serve as MCs for cell expansion.

3.4.1.1. Influence of the PLLA/PEG ratio

Younes and Cohn characterized PLLA/PEG blend ranging from 10/90 to 90/10 ratios. According to their findings, if one component represents more than 20% of the blend, it crystallizes leading to two partially segregated crystalline phases dispersed in an amorphous matrix. For more dilute compositions, crystallization is possible only for the dominant component, resulting in a non-crystalline matrix

composed of the minor component and the non-crystallized fraction of the semi-crystalline dominant component.[339] Several authors also reported that PEG contents lower than 10% did not result in a crystallization-induced phase separation.[130, 342, 343] Based on these observations, theoretical PLLA/PEG blend compositions leading to crystallization-induced phase separation can range from 10/90 to 80/20. The influence of blend composition on spherulite morphology for PLLA/PEG ratios ranging from 10/90 to 30/70 was described by Kuterbekov *et al*.[135] They reported that a higher PLLA content led to denser spherulites with smaller pores. However, they did not investigate the properties of these MCs in aqueous solution.

SEM images of spherulites prepared at a crystallization temperature of 110 °C from different PLLA20/PEG ratios (using a PLLA of a lower molar mass 20 000 g/mol), including much higher PLLA20 concentrations than reported by Kuterbekov *et al.*, are shown in Figure 3.4. As expected, a higher PLLA content leads to denser MCs showing a reduced pore size, but also to MCs presenting a better-defined shape with an increasing number of facets as the PLLA content increases. This polyhedral shape results from the impingement of adjacent spherulites due to the competing spherulitic growth inside the blend.[337] By changing the blend composition, it is thus possible to obtain a variety of morphologies ranging from irregularly shaped and highly porous spherulites to denser and well-faceted spherulites. While less dense spherulites could have an appropriate sedimentation rate for dynamic culture applications, they may lack the mechanical resistance required to withstand the agitation necessary to dynamic cell culture. Also, the non-spherical morphology of spherulites could reveal interesting for cell culture, as cells have been shown to avoid convexe surfaces (section 1.4.2.2).

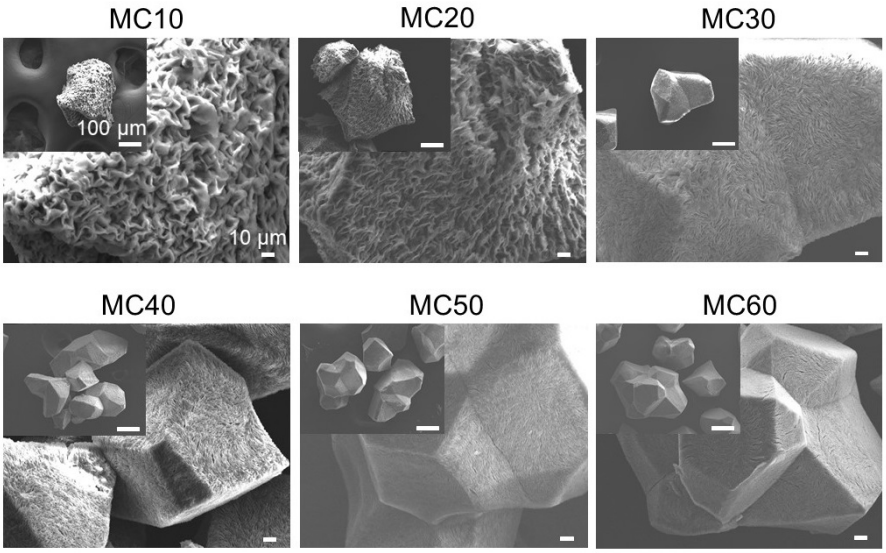

Figure 3.4.: SEM images illustrating the influence of PLLA20 content in the blend (indicated in sample name) on MC morphology. The MCs were obtained at a crystallisation temperature of 110° C. The scale bars are identical in the six panels.

3.4.1.2. Influence of the crystallization temperature

It was shown by Kuterbekov *et al*. that the crystallization temperature influences spherulite size, with lower temperatures leading to smaller spherulites.[135] This is due to the strong temperature dependence of the spherulite nucleation process, higher temperatures corresponding to less numerous nucleation seeds and therefore larger spherulites. The inspection of SEM images of MC20 prepared using PLLA20 and different crystallization temperatures of 103, 110, 120 and 130°C (as well as a boxplot with quantitative measurements of spherulite size) showed that the higher the crystallization temperature, the larger the size of the MCs, as expected (Figure 3.5). Indeed, due to a larger rate of nucleation, spherulite size decreases at lower temperatures whereas their number per unit volume increases. Notably, by selecting the crystallization temperature in a range narrower than 30°C, the average spherulite size can be varied by a factor as large as four, showing the considerable versatility of the fabrication process. We noticed also that the MC morphology remained very similar for the different

tested crystallization temperatures, demonstrating that this parameter does not affect the MC microstructure.

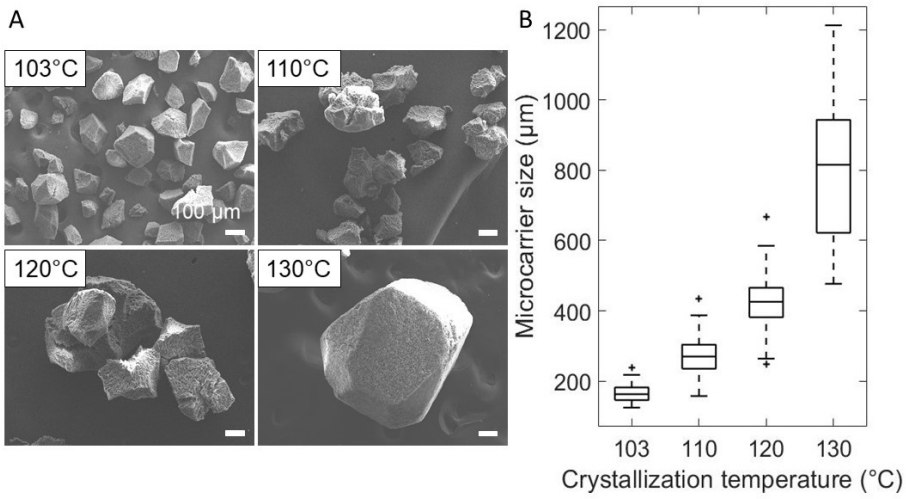

Figure 3.5.: (A) SEM images of MC20 prepared with PLLA20 at different crystallization temperatures. The scale bars are identical in all panels. (B) Boxplot showing the variation of MC20 size versus crystallization temperature (N=50)."+" signs indicate outliers.

3.4.1.3. Influence of PLLA molar mass

The influence of PLLA molar mass on spherulite morphology was also investigated using two PLLA samples of 20 000 (PLLA20) and 40 000-70 000 g/mol (PLLA40), respectively, whereas the PEG molar mass, the composition of the PLLA/PEG blend (50/50) and the crystallization temperature (110 °C) were kept constant. The morphology of MC50 observed by SEM was very similar whatever the PLLA molar mass, showing multiple faceted particles of similar porosity (Figure 3.6.A). The increase of PLLA molar mass led to a slight decrease of MC size (Figure 3.6.B). This slight effect of the PLLA molar mass on MC size was confirmed for other processing parameters (crystallization temperature of 103 °C and PLLA/PEG ratio of 20/80) as seen in Figure 3.15 in Appendix 3.6.1.

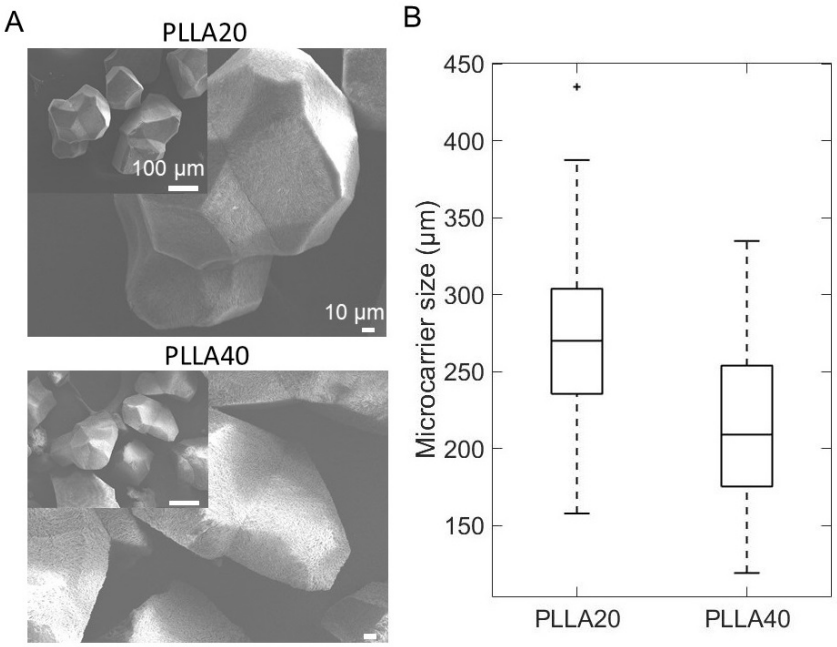

Figure 3.6.: SEM images (A) and Boxplot (N=50) of size (B) of MC50 prepared at a crystallization temperature of 110°C, using the same PLLA/PEG ratio (50/50) but different PLLA molar masses (*i.e.*, PLLA20 and PLLA40). The scale bars are identical in the two panels. "+" signs indicate outliers.

3.4.2 Production and characterization of magnetic microcarriers

To prepare MCs showing magnetic properties, varying amounts of MNPs were incorporated in MCs. These quantities were chosen to be rather low, ranging from 0.001% to 0.3% of MC weight. Indeed, while magnetic properties are desirable to ease handling of MCs, a strong magnetization could disrupt MC agitation with magnetic stirrer, often used in spinner flasks.

The following sections focus on the quantification of the amount of MNPs incorporated in MCs, the characterization of their distribution in the spherulites, the measurement of magnetic properties of the resulting MCs and the release of MNPs from MCs.

3.4.2.1. Evidence for the presence of magnetic nanoparticles in microcarriers

In order to visualize the presence of MNPs in MCs, MNPs labeled with fluorescent rhodamine were used. These MNPs were incorporated in a PEG aqueous solution that was subsequently freeze-dried. Different amounts of fluorescent MNPs were added in the PEG solution to obtain a final iron concentration in the 20/80 PLLA20/PEG blend ranging from 0.01 to 3 mg Fe/g PLLA20. First, the successful incorporation of these fluorescent NPs in the PEG powder was observed by epifluorescence microscopy (Figure 3.16.A in Appendix 3.6.2) and the resistance of the fluorophore to a temperature of 230 °C was also verified (Figure 3.16.B in Appendix 3.6.2), as this elevated temperature is required to produce the MCs.

Then, MCs prepared with different MNP concentrations were observed using epifluorescence microscopy (Figure 3.7). A strong fluorescent signal was observed for samples prepared with 3 and 1 mg Fe/g PLLA20, with a higher intensity seen for the higher Fe concentration. A sligth signal was observed for MCs prepared with 0.1 mg Fe/g PLLA20 and no fluorescence for those prepared with 0.01 mg Fe/g PLLA20. Samples containing 1 mg and 3 mg Fe/g PLLA20 were the only ones showing sufficient magnetic properties to be influenced by the presence of a magnet of 1.4 Tesla. For this reason, only these two concentrations were further characterized.

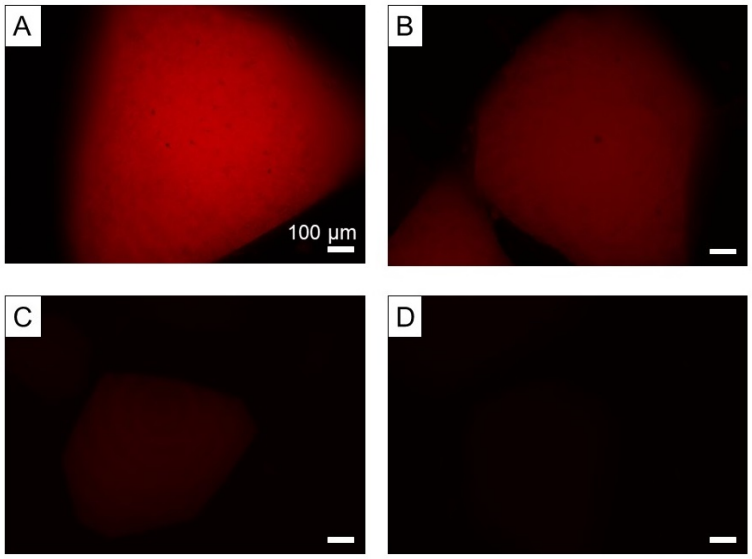

Figure 3.7.: Epifluorescence microscopy images showing MC20 (prepared with PLLA20 and crystallized at 130 °C) containing different concentrations of fluorescent MNPs: (A) 3; (B) 1; (C) 0.1 and (D) 0.01 mg Fe/g PLLA20. The scale bars are identical in all panels.

3.4.2.2. Characterization of magnetic nanoparticle spatial distribution at the nanoscale

As seen on epifluorescence images (Figure 3.7), MNPs are homogeneously distributed at the macroscopic scale. TEM analysis was thus performed on MC20 loaded with 3 mg Fe /g PLLA20 in order to investigate the distribution of MNPs at the nanoscale. It can be seen in Figure 3.8 that MNPs form clusters of aggregates of about 100 nm of diameter. These aggregates could lead to the loss of the superparamagnetic behaviour.

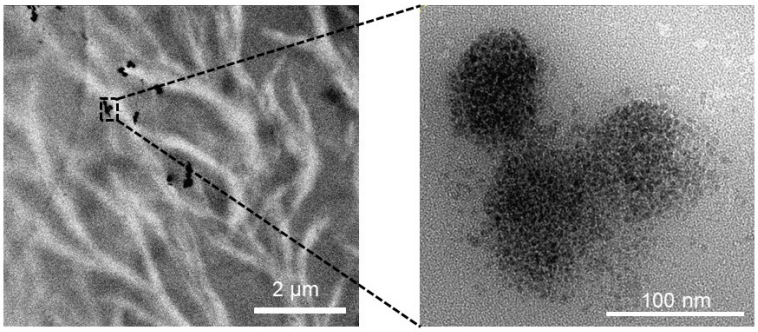

Figure 3.8.: TEM images showing MNPs distribution in MC20 (prepared with PLLA20 and crystallized at 110 °C) and loaded with 3 mg Fe /g PLLA20 at two magnifications.

3.4.2.3. Determination of the amount of magnetic nanoparticles incorporated in microcarriers

The amount of MNPs incorporated in MCs was measured by ICP-AES for MCs crystallized at 110 °C using two PLLA20/PEG ratios (20/80 and 50/50) with either 1 or 3 mg Fe/g PLLA20. The results are summarized in Table 3.1.

First, focusing on samples prepared with 20/80 PLLA20/PEG ratio (MC20), it can be noticed that the incorporation yield for both samples prepared using 1 and 3 mg Fe/g PLLA20 was found to be around 80% indicating that for this range of concentrations, the amount of iron incorporated in MCs was essentially proportional to the amount of iron present in the blend. For the sample prepared with a lower amount of PEG (MC50 obtained using 50/50 PLLA20/PEG) and using 3 mg Fe/g PLLA20, the incorporation yield was lower, with approximately 56% of iron incorporated. Interestingly, the incorporation yield seems to be close to the PEG fraction in the blend for both types of MCs (MC20 and MC50).

	Type of MC (PLLA20/PEG ratio)		
	MC20 (20/80)		MC50 (50/50)
Theoretical Fe content (mg Fe/g PLLA)	1	3	3
Measured Fe content (mg Fe/g PLLA)	0.78 ± 0.04	2.45 ± 0.2	1.70 ± 0.06
Incorporation yield (%)	78 ± 0.04	81 ± 6	56 ± 2

Table 3.1.: Amount of MNPs incorporated in MCs prepared from different PLLA20/PEG ratios at 110 °C as measured by ICP-AES.

3.4.2.4. Measurement of magnetic nanoparticle release in solution

MNP release from MC20 prepared with 3 mg Fe/g PLLA20 was evaluated over 5 day incubation in PBS at room temperature and under agitation by measuring the amount of iron in the supernatant using ICP-AES (Figure 3.9). Results indicate a continuous release over 5 days. However, the released amount was found to be negligible as it represents less than 1% of the initial MNPs content loaded in MCs. Considering a MC concentration of 1 mg/mL for cell culture, the concentration of iron in the culture medium could increase by about 15×10^{-3} µg/mL (or 6.5×10^{-8} M) by day 5 without taking into account any medium change. This amount is well below the reported iron concentration detrimental for cells. Indeed, Gokduman *et al.* reported significant effect on the viability of primary rat hepatocytes upon treatment with Fe_3O_4 NPs using iron concentration of 200 and 400 µg/mL.[344] Jarockyte and coworkers found no evidence of cytoxicity on NIH3T3 cells using lower iron concentrations (32.5×10^{-3} µg/mL or 65×10^{-3} µg/mL).[345]

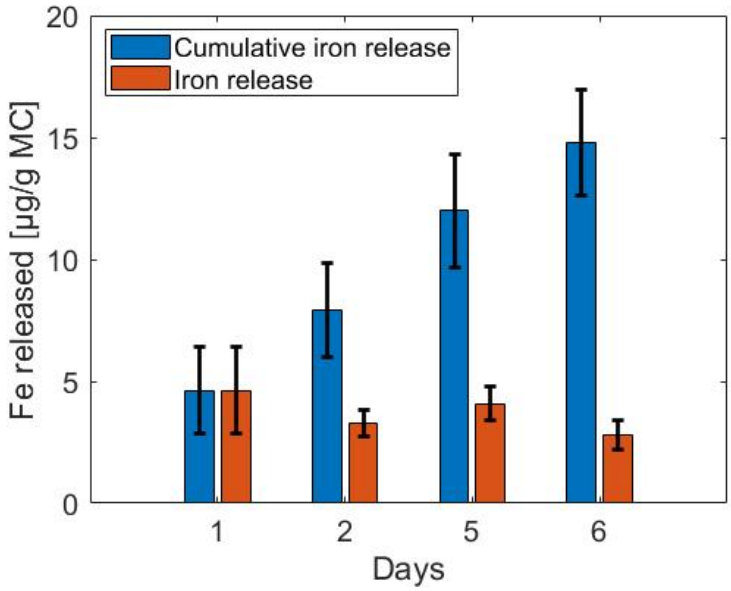

Figure 3.9.: Amount of iron (measured by ICP-AES) released from MC20 prepared from PLLA20 and crystallised at 110 °C as a function of the incubation time in PBS buffer at room temperature and under agitation.

In order to investigate whether this iron release was continuous over time or whether it would stabilize, the iron content of MC20 prepared with 3 mg Fe/g PLLA20 was evaluated by ICP-AES directly after production and after an incubation time of six months in PBS at room temperature. While the initial iron content was evaluated to be 2.45 $\pm$ 0.2 mg Fe/g MC, an iron content of 2.41$\pm$ 0.11 mg Fe/g MC was detected after 6 months in solution. No statistical difference was observed between these two values suggesting no significant loss of MNPs over longer periods in solution. From these observations, it can be concluded that magnetic MCs are stable in solution and should be appropriate for contact with cells.

3.4.2.5. Characterization of the magnetic properties of microcarriers entrapping magnetic nanoparticles

Magnetic properties of MC20 prepared with 1 or 3 mg Fe/g PLLA20 were assessed by AGM (Figure 3.10). The results obtained clearly show that MCs

loaded with MNPs retain the superparamagnetic properties of the MNPs as no hysteresis loop is visible, indicating that the formation of small aggregates (such as those observed in Figure 3.8 in section 3.4.2.2) does not lead to a loss of the superparamagnetic properties. Moreover, the magnetic moment measured for MCs prepared with 1 and 3 mg Fe/g PLLA20 are proportional by a factor 3 which is in good agreement with the quantitative results obtained in section 3.4.2.3.

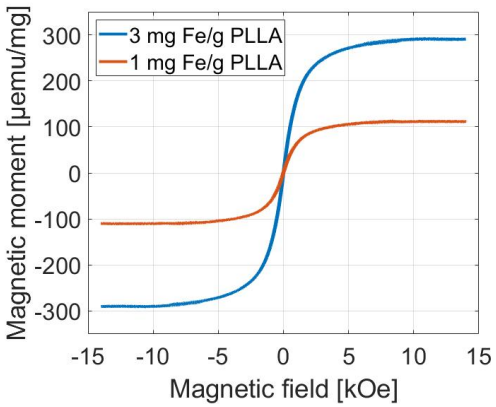

Figure 3.10.: AGM hysteresis curves measured for MC20 prepared from PLLA20 and crystallised at 110 °C with 1 mg Fe/g PLLA20 and 3 mg Fe/g PLLA20 incorporated in the blend.

3.4.3 Optimization of spherulite properties for use in dynamic condition

To be suitable for cell culture in dynamic condition, our PLLA spherulites need to meet three important requirements. They must show an appropriate size and sedimentation rate and show sufficient mechanical resistance to sustain dynamic stirring.

As shown is section 3.4.1.2 and 3.4.1.3, MC size is mainly controlled by the crystallization temperature selected for the process and to a lesser extent by the PLLA molar mass. For microporous MCs, diameters of 100 – 230 µm are reported to be the optimal size,[46] but diameters between 125 and 255 µm are

usually reported for commercial MCs.[79, 80, 137] The sedimentation rate is a function of both the medium and MC characteristics. Indeed, it depends on medium density and viscosity but also on MC density, size, shape and porosity. As PLLA density is reported to be $1.24\,g/cm^3$ [346] and MC shape is defined by the crystallization process, the only parameters than can be modified to tune the sedimentation rate are MC size and MC porosity, which depends on the PLLA/PEG ratio in the blend, as demonstrated in section 3.4.1.1. Finally, the possibilities to improve the mechanical resistance of MCs relies on reducing the porosity and increasing PLLA molar mass.

Those three important parameters, namely the crystallization temperature, the PLLA/PEG ratio and the PLLA molar mass thus need to be optimized to ensure the best MC properties for cell culture in spinner flask. A compromise has to be found as some parameters have conflicting impacts. For example, increasing the porosity helps to reduce the sedimentation rate but also decreases the mechanical resistance.

The possibility to prepare MCs which can be well-suspended in aqueous medium and resisting to stirring was investigated. For this, the suspension and mechanical resistance under agitation at 40 rpm of PLLA20 MCs produced at different crystallization temperatures (from 110 to $130\,°C$) and with blends of different PLLA20/PEG ratios (MC20, MC30, MC50 and MC70) were first tested in spinner flasks in order to select the optimal MC cores for dynamic cell culture. Some of these PLLA20 MCs suspended well in aqueous solution under agitation. However, their mechanical resistance was limited as they broke after only two days of agitation (Figure 3.11.A). To overcome this problem, PLLA40 cores prepared with a PLLA sample of higher molar mass were tested. Indeed, a higher molar mass is expected to result in an increased proportion of tie molecules bridging different lamellar crystals within the spherulites, which should contribute to reinforce their mechanical resistance. The sedimentation rates of such MCs prepared from different PLLA40/PEG ratios (MC30, MC50, MC70) and with different crystallization temperatures (103, 110, 120 and $130\,°C$) were first measured in aqueous solution (Figure 3.11.B). Commercial microporous MCs used for cell culture in spinner flask typically show sedimentation rates comprised between 12 and 19 cm/min.[55, 347] The values obtained here varied between 15 and 85 cm/min, with the MC30 crystallized at $110\,°C$ and MC50 crystallized at 110 or $103\,°C$, being close to this requirement. Other MCs had a higher sedimentation rate due to their larger size or lower porosity. Crucially, MC50

crystallized at 110 and 103 °C were significantly more mechanically resistant than MC30, as they did not break even after seven days of stirring in aqueous solution (Figure 3.11.C). This increased mechanical resistance for MCs prepared with a higher PLLA content can be explained by a lower MC porosity. Therefore, MC50 prepared with PLLA40 and a crystallization temperature of 103 °C were selected for the dynamic cell culture assays. MCs prepared at 110 °C with various PLLA40 content (MC30, MC50 and MC70) were also assessed in semi-static condition. A summary of the characteristics of the MCs used for semi-static and dynamic cell culture assays is provided in the following section.

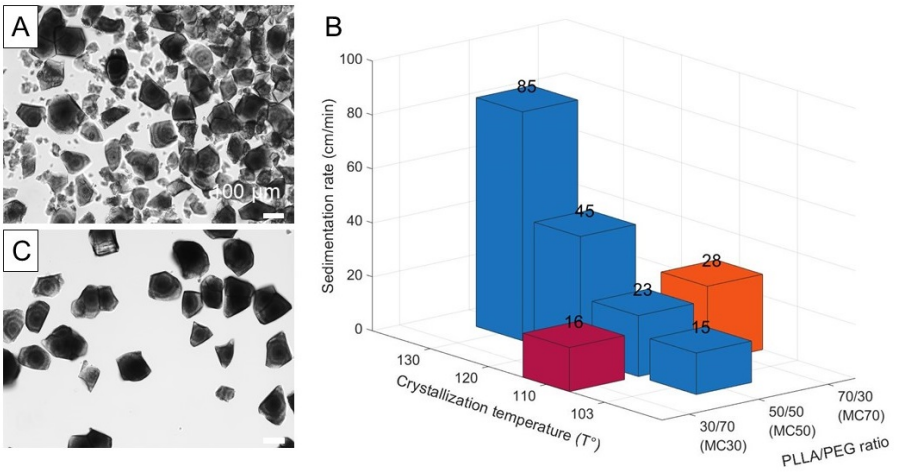

Figure 3.11.: (Left) optical microscopy images of MC50 crystallized at 110°C, using PLLA20 (A) and PLLA40 (C), after two days and seven days of stirring at 40 rpm in a spinner flask, respectively. The scale bars are identical in both panels. (Right, B) Variation of the sedimentation rate of PLLA40 MCs measured in water as a function of the processing parameters used for their fabrication, *i.e.*, crystallization temperature and PLLA40/PEG ratio.

3.4.4 Summary of the characteristics of microcarriers selected for cell culture

3.4.4.1. Microcarriers for semi-static cell culture assays

For semi-static cell culture assays, the mechanical resistance of MCs is less critical as they are not submitted to continuous agitation. MCs crystallized at $110\,°C$ using three different PLLA40 content (MC30, MC50 and MC70) were thus prepared to investigate the effect of the surface morphology and porosity (Figure 3.12.A, B, C) on cell adhesion. All these MCs were sieved using two sieves of 150 µm and 300 µm to reduce slightly their size distribution range from 220 ± 56 µm to 228 ± 42 µm (Figure 3.12.D).

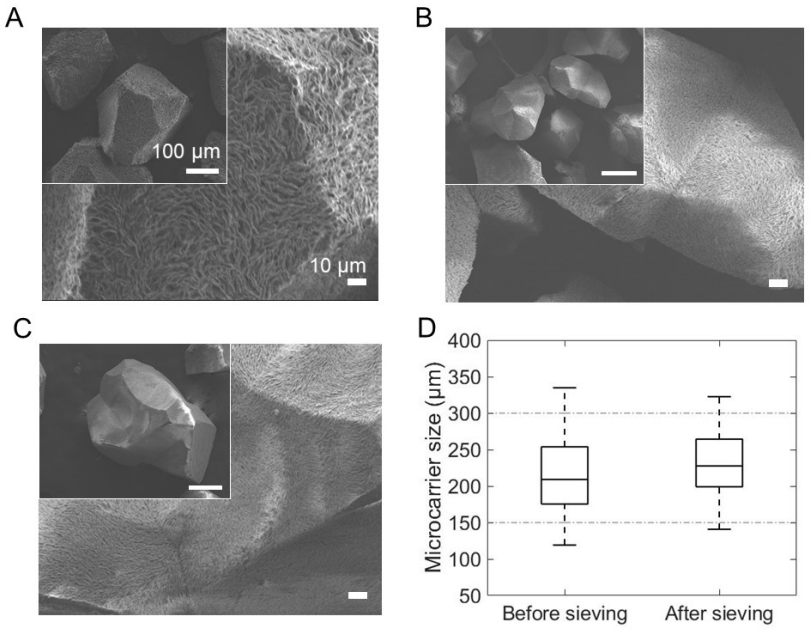

Figure 3.12.: SEM images of MCs crystallized at $110\,°C$ using different PLLA40 content: (A) MC30, (B) MC50 and (C) MC70 for semi-static cell assays. (D) Size distribution of MCs prepared at $110\,°C$ before and after sieving, (N=50). The scale bars are identical in all panels.

The surface area of these different MCs obtained after sieving was estimated based on their size and their number per mg, both obtained by optical microscopy, and assuming a spherical shape. Table 3.2 shows the number of particles per mg for each type of MC. Using the median diameter (228 µm) of MCs prepared at 110 °C[1], the surface area available per mg of MC was also computed.

Type of MC	MC30	MC50	MC70
Number of MCs per mg (dry weight)	694 ± 80	500 ± 25	317 ± 40
Surface area per mg (cm^2/mg)	1.13	0.81	0.51

Table 3.2.: Number of MCs per mg as counted by optical microscopy and estimated surface area per mg of MC.

MC average surface roughness (R_a) was computed by analyzing images recorded by optical confocal microscope, for the different MCs considered for semi-static assays. Indeed, surface roughness is known to influence cell adhesion (section 1.4.2.2) and could explain different cell behaviour on the three types of MCs. The surface roughness was markedly higher for MC30 (Table 3.3) with large variations of the R_a value even on a single MC. No significant difference was observed between MC50 and MC70, which both showed a surface roughness about four times lower compared to MC30. This is in good agreement with SEM images (Figure 3.12).

Type of MC	MC30	MC50	MC70
Surface roughness R_a (µm)	1.76 ± 1.33	0.39 ± 0.11	0.40 ± 0.02

Table 3.3.: Surface roughness of MC30, MC50 and MC70 crystallized at 110 °C from PLLA40 and used for semi-static cell assays.

Futhermore, magnetic MC50 were also prepared (T_c = 110 °C , PLLA40) in order to investigate whether the incorporation of MNPs would influence cell behaviour. These MCs could be attracted and immobilized using a 1.4 T magnet as shown in Figure 3.13

[1] As it was shown that the PLLA/PEG ratio does not influence MC size, the same median diameter was used for the three types of MCs.

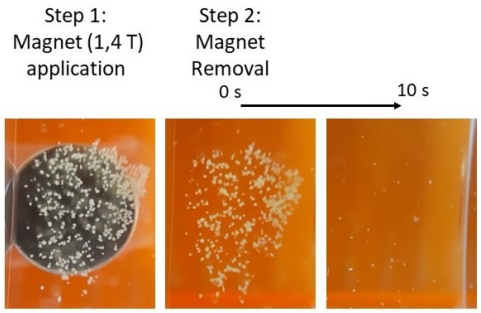

Figure 3.13.: Magnetic MC50 can be immobilized in solution by using a magnet and quickly released after magnet removal.

3.4.4.2. Microcarriers for dynamic cell culture assays

For dynamic culture in spinner flask, MC50 crystallized at $103\,°C$ using PLLA40 (see Figure 3.14) were prepared as they showed an appropriate suspension and mechanical resistance in dynamic conditions (section 3.4.3). These MCs were further sieved using two sieves of 100 and 150 µm to reduce their size distribution range from 167 ± 26 µm to 118 ± 18 µm. The number of sieved MC50 per mg was estimated to be 2 390 ± 157 resulting in a total surface area of 0.85 cm^2/mg. The surface roughness was also evaluated to be 0.52 $\pm$ 0.07 µm, which was close to the value obtained for MC50 prepared at $110\,°C$.

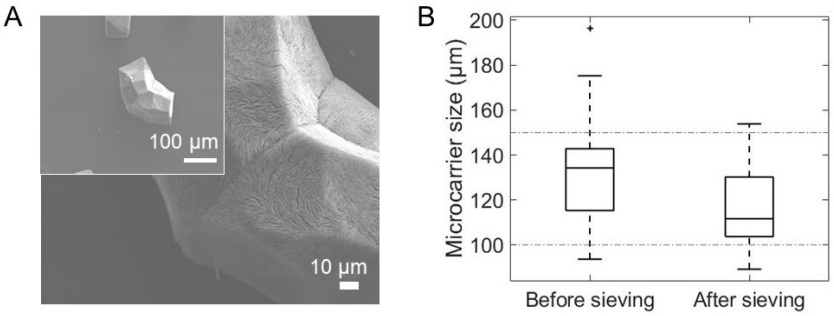

Figure 3.14.: A) SEM images of MC50 used for dynamic culture assays. B) Size distribution of M50 prepared at $103\,°C$ before and after sieving, (N=50). "+" signs indicate outliers.

3.5 Conclusion

Among the various MC production processes, a majority of them relies on organic solvents, which constitutes a serious drawback to their large-scale development due to safety, environmental and economical considerations. Other techniques, while avoiding the need for organic solvents, offer poor control over MC characteristics other than their size. In this chapter, a versatile and easy solvent-free fabrication process to prepare MCs made of PLLA, a biosourced polymer, and showing a tunable density, porosity and size, while keeping a constant core material and surface biochemistry was described. The influence of process parameters on PLLA spherulites characteristics such as morphology, porosity, size, mechanical resistance, *etc*. showed that these characteristics can easily be optimized by tuning trivial processing parameters such as crystallization temperature, PEG content and PLLA molar mass, without impacting the global process. Indeed, it was showed that MC size is mostly controlled by the crystallization temperature and to a lesser extent by the PLLA molar mass. The porosity and surface morphology depend only on the composition of the blend while mechanical resistance is improved by using a higher PLLA molar mass and/or a higher content of PLLA in the blend.

Adding to the versatility of the process, MNPs were easily incorporated in MCs by simply replacing the PEG by a PEG containing MNPs. MNPs are present as aggregates of about 100 nm homogeneously distributed in MCs and the incorporation yield is directly related to the PEG content. The stability of the magnetic MCs in solution was tested by measuring the release of iron with time, which was found negligible, evidencing the stability of these MCs. Moreover, these MCs display a superparamagnetic behaviour allowing to easily harvest them using a magnet.This feature will significantly facilitate MC sampling and separation during the cell culture.

3.6 Appendix

3.6.1 Influence of PLLA molar mass

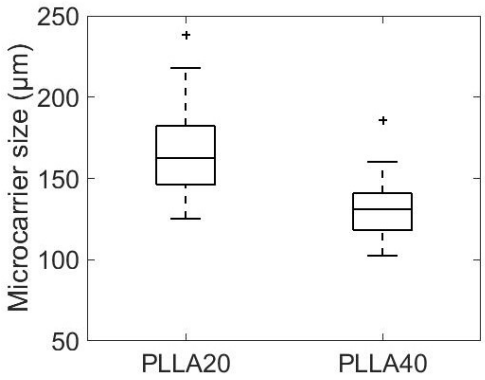

Figure 3.15.: Size of MC20 prepared at a crystallization temperature of 103 °C, using the same PLLA/PEG ratio (20/80) but different PLLA molar masses (*i.e.*, PLLA20 and PLLA40), (N=50). "+" signs indicate outliers.

3.6.2 Characterization of PEG containing magnetic nanoparticles

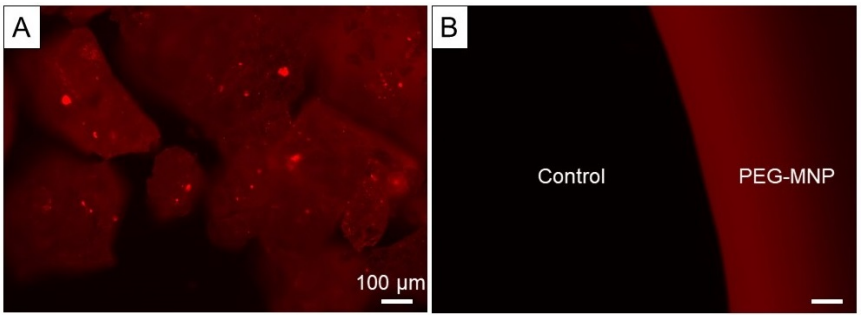

Figure 3.16.: A) PEG powder containing fluorescent NPs after freeze-drying. B) PEG containing fluorescent NPs molten at 230 °C confirms that NPs remain fluorescent even after exposure to a high temperature. The control consists of an area without any molten PEG-MNP. The scale bars are identical in both images.

4

Surface biofunctionalization of microcarriers

4.1 Introduction

The objective of this chapter was to elaborate a bioadhesive coating to improve cell adhesion on MCs. Indeed, while PLLA is a biocompatible polymer widely used for biomedical applications, its hydrophobicity does not favor cellular adhesion, growth, and matrix deposition in its pristine unmodified state.[321] For this reason, PLLA surface usually has to be modified to improve cell-material interaction. Several strategies to improve PLLA bioaffinity were reported in the literature including plasma treatment or hydrolysis to improve hydrophilicity, copolymerization or blending, addition of nanocomposites or surface biofunctionalization using proteins or peptides.[348, 349] For this work, the selected process is required to be biocompatible and ideally, should fit in the green approach developed to produce MC cores, thus prohibiting the use of any toxic reagents and organic solvents. Also, animal proteins should be avoided to limit the downsides associated with their use (*e.g.*, batch-to-batch variability, contaminations, *etc.*). Finally, the possibility to tune coating properties such as bioadhesiveness, thickness and stiffness would be highly valuable, allowing to optimize the coating characteristics depending on the cultured cell line.

The LbL technique was thus chosen for its numerous advantages : simplicity, low-cost, versatility, aqueous solution-based process, *etc*. This technique has been extensively used to modify material surfaces in order to control cell adhesion.[350] LbL films can promote the non-specific adhesion of mammalian cells by modification of the physicochemical properties of the substrate surface such as stiffness (*e.g.*, poly(acrylic acid) (PAA)/poly(allylamine hydrochloride) (PAH), PLL/HA) and surface charge (*e.g.*, poly(styrenesulfonate) (PSS)/PAH,heparin

(HEP)/COL, CHI/HA) but can also enhance specific cell adhesion following the incorporation of cell recognition moieties.[310, 350]

In this chapter, the strategy chosen to biofunctionalize MC surface is first described, followed by a detailed explanation of the experimental protocols. The results are then presented with the first part focusing on the fabrication of the LbL film and the second one detailing its grafting with a bioadhesive peptide. Finally, a short conclusion closes the chapter.

4.2 Strategy

Films composed of PLL and HA have been extensively characterized both in terms of their properties (thickness, charge, stiffness, *etc.*),[304, 308, 351] as well as their influence on cellular behaviour such as adhesion, proliferation and differentiation.[316, 317, 352] HA, also known as hyaluronan or sodium hyaluronate in its salt form, is a high molar mass natural polysaccharide which was discovered in 1934 by Karl Meyer. Its structure, shown in Figure 4.1a, consists of a linear polyanion containing alternating N-acetyl-D-glucosamine and D-glucuronic acid residues linked by β(1-4) and β(1-3) bonds.[353] From a general point of view, it belongs to a group of substances known as GAGs along with chondroitin sulfate, dermatan sulfate, keratan sulfate, heparan sulfate and heparin, HA being the simplest among them.[354] Indeed, HA is not sulfated, and is not covalently linked to a protein core in the form of a proteoglycan. While most GAGs are made in the cell's Golgi networks, HA, however, is synthesized by HA synthases located in the cell membrane and immediately extruded out of the cell and into the ECM.[355, 356] HA is omnipresent in the body of all vertebrates, including humans and its simple structure is conserved throughout all mammals, suggesting the considerable importance of this biomolecule.[355, 356] In the body, HA is mainly found in the extracellular matrix and pericellular matrix, but has also been shown to occur intracellularly.[357] It plays multiple roles including space filler, lubricant, free radical scavenger and regulation of cellular activities.[353] Commercial production of HA commonly involves its extraction from rooster comb and human umbilical cord as well as its production in larger quantities by bacterial fermentation.[355, 358] For this reason, HA is used in a broad range of biomedical applications. For example, a major application of HA consists of the viscosupplementation of joints affected by

arthritis. Other applications include the use of crosslinked HA in drug delivery or to fill facial wrinkles and depressed scars.[358]

The counter polycation PLL is widely used in cell culture to promote cell adhesion to solid substrates.[317] However, poly-L-ornithine (PLO), a synthetic amino acid chain whose structure can be seen in Figure 4.1b is now considered as an alternative to PLL to increase cell attachment on plastic and glassware.[359] For example, PLO used to coat alginate microcapsules was associated with better in vivo biocompatibility [360] and less immunogenicity [359] than PLL . Similarly, PLO was used as a coating layer on PLA/polypyrrole nanofibers and improved cell adhesion without any toxicity.[361] PLO-coated poly(D,L-lactide-co-glycolide) (PLGA) microspheres were also reported to improve ASC adhesion compared to PLL-coated microspheres.[362]. This specific polyelectrolyte association was also successfully deposited on microparticles used as scaffold for bone regeneration.[135] For this reason, PLO was preferred over PLL for this work.

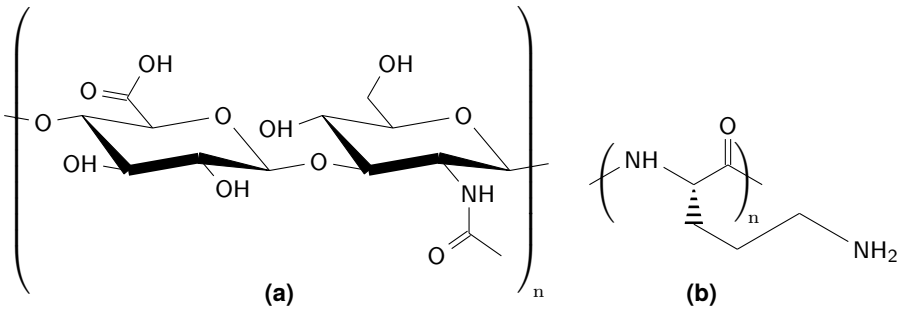

Figure 4.1.: Chemical structure of (a) HA and (b) PLO used for LbL deposition onto PLLA MCs.

As pointed out in the state of the art, the mechanical properties of the film are crucial to ensure good cell adhesion but also to control cell differentiation.[305, 306] The PLO/HA film was thus further crosslinked allowing to stabilize it as well as to control its rigidity.[308] As Picart *et al.* showed that is was possible to combine the positive effect of crosslinking and post-functionalization using bioadhesive peptide to improve cell adhesion,[311] a bioadhesive RGD peptide was grafted on the crosslinked PLO/HA film to further increase cell adhesion, challenged by the shear stress occurring in dynamic culture condition.[95] The RGD sequence is by far the most used sequence to improve cell adhesion [254] and has demonstrated its efficiency on a wide range of materials such as

titanium implant,[240–243] hydrogels,[244–246] hydroxyapatite scaffolds,[247, 248] electrospun scaffolds,[249, 250] or MCs.[117, 251, 252] The biofunctionalization process is illustrated in Figure 4.2. Using this strategy, the bioadhesive coating would be devoid of any animal protein, which constitutes an asset with respect to current regulations.

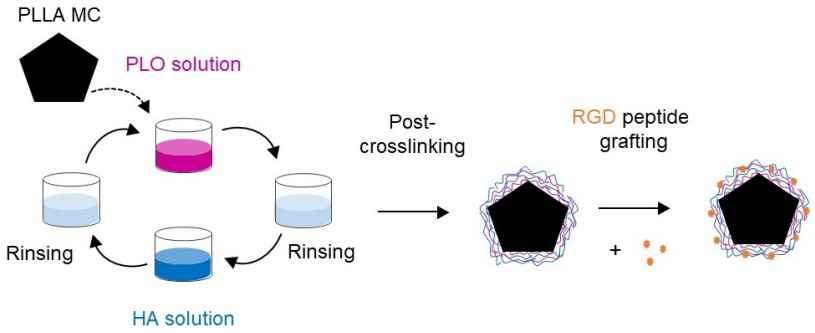

Figure 4.2.: Surface biofunctionalization of PLLA MC by LbL assembly of PLO and HA followed by post-crosslinking and grafting of a bioadhesive RGD peptide.

4.3 Experimental section

4.3.1 Materials

Sodium hyaluronate (HA) (360 000 g/mol) was obtained from Lifecore Biomedical. Poly-L-ornithine hydrobromide (PLO) (78 000 g/mol) was purchased from Alamanda Polymers. Rhodamine-labeled poly(allylamine) (15 000 g/mol) was purchased from Surflay Nanotec GmbH. Poly(ethyleneimine) (PEI) (60 000 g/mol), Sulfo-NHS (98 %), EDC (98 %), 4-(2-hydroxyethyl)piperazine-1-ethanesulfonic acid (HEPES) (99.5 %), sodium chloride (NaCl) (99.5 %), dimethylsulfoxide (DMSO), Rhodamine red were bought from Sigma-Aldrich. 2-(N-morpholino)ethanesulfonic acid (99 %) (MES) and absolute ethanol (95 %) were obtained from Acros. GRGDS peptide (98 %) and fluorescent RGDK-FITC (95 %) were provided by Genecust. Single-side-polished (100) silicon

wafers were purchased from TOPSIL. Milli-Q grade (resistivity of 18.2 $m\Omega$) was produced by a Milli-Q® Reference system of Merck Millipore.

4.3.2 Deposition and crosslinking of PLO/HA films

The deposition of PLO/HA films was carried out according to protocol already published for PLL/HA films.[304, 315] PLO and HA dissolved in 0.15 M NaCl (pH 7.4) at a concentration of 0.5 and 1 mg/mL, respectively, were adsorbed alternately on MCs by immersing the sample for 5 min in the polyelectrolyte solutions. Then, three washing steps were performed in 0.15 M NaCl (pH 7.4), consisting respectively of one sec dipping for ten times, five sec dipping for five times and 10 sec dipping for one time. An anchoring PEI layer was deposited as a first layer in place of PLO. The resulting films are denoted as $(PLO/HA)_n$, where n is the number of PLO/HA deposited bilayers. (PLO/HA) films were also built onto silicon wafers used as model surfaces. For this, silicon wafers were first cleaned by immersion in freshly prepared piranha mixture [H_2O_2 (35 %):H_2SO_4(98 %) (1:1 v/v)] for 20 min, rinsed extensively with Milli-Q water and dried under an argon stream. The LbL films were deposited on the samples using an automated dipping machine (Riegler and Kirstein GmbH). For LbL deposition on MCs, wet MC50 crystallized at 110°C were placed in porous cell culture inserts (Corning Netwell, 74-µm mesh size) (see Figure 4.3) that were fixed on the arm of the dipping robot.

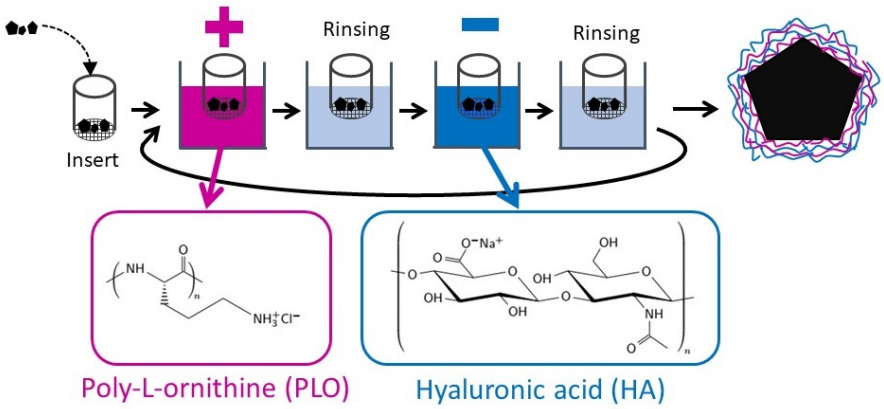

Figure 4.3.: Deposition of LbL film composed of PLO and HA on MCs.

After LbL deposition, (PLO/HA) films were crosslinked through an overnight incubation at 4°C in a freshly prepared crosslinking solution containing 70 mg/mL of EDC and 11 mg/mL of Sulfo-NHS in 0.15 M NaCl (pH 5.5). Then, the samples were rinsed five times for 20 min in HEPES buffer (20 mM in 0.15 M NaCl, pH 7.4).[308]

4.3.3 Grafting of bioadhesive peptide on crosslinked LbL film

The bioadhesive GRGDS peptide was grafted on the crosslinked $(PLO/HA)_8$ films using the same EDC/Sulfo-NHS chemistry as for the crosslinking step. Briefly, MC50 or silicon wafers covered by a crosslinked $(PLO/HA)_8$ film were incubated for 15 min at 4°C in a freshly prepared 0.1 M MES solution (pH 6.5) containing 70 mg/mL of EDC and 11 mg/mL of Sulfo-NHS. Samples were then rinsed thoroughly with MES solution before being incubated overnight at 4°C in peptide solution at a concentration of 0.1 mM or 1 mM in MES buffer. Following the grafting, flat samples were rinsed eight times for 20 min in HEPES buffer (20 mM in 0.15 M NaCl, pH 7.4), thrice for 20 min in ethanol/Milli-Q (50:50 v:v) solution and twice for 20 min in Milli-Q water to completely remove the non-grafted peptide. For MC50, an additional overnight wash in HEPES was performed before the ethanol/Milli-Q washing step to ensure a complete removal of the non-grafted peptide. The same conditions were used to graft the fluorescent RGDK-FITC peptide on crosslinked $(PLO/HA)_8$ films. Control samples were also prepared by omitting the EDC/Sulfo-NHS activation step prior to incubation in peptide solution. MC50 grafted with 0.1 mM and 1 mM peptide concentration are denoted MC50-RGD-0.1 and MC50-RGD-1 in the sequel, respectively.

4.3.4 Characterization of biofunctional films

4.3.4.1. Characterization of LbL film deposited on flat model surfaces

The thickness of $(PLO/HA)_n$ with n varying from 2 to 10 and deposited on flat silicon wafers then crosslinked and dried, was measured by ellipsometry using

an Accurion EP4 single-wavelength ellipsometer. The wavelength of the laser was 658 nm and the incidence angle ranged from 60° to 80° (2° increment). Film thickness was determined by fitting a one-layer model with the built-in software. The refractive index of (PLO/HA) films was fixed at 1.5 and the one of the silicon substrate to the value tabulated by the manufacturer.

4.3.4.2. Characterization of LbL film deposition on microcarriers

Bare and $(\mathrm{PLO}/\mathrm{HA})_8$-coated MC50 were dipped in rhodamine solution for 10 min, rinsed 5 times for 5 min in PBS (0.01 M, pH 7.4) film then imaged with a Zeiss LSM 700 confocal laser scanning microscope (CLSM) in order to visualize the coverage of the microcarrier surface by the LbL coating. The average fluorescence intensity was computed for bare and $(\mathrm{PLO}/\mathrm{HA})_8$-coated MC50. For this, the average fluorescence intensity of one facet of each type of MC was evaluated after graying the image, computing the histogram of grey values and subtracting the fluorescence intensity of the background. The fluorescence intensities are presented as mean values $\pm$ standard deviation. Statistical analyses were performed using one-way analysis of variance (ANOVA) followed by post hoc Tukey test with a significance level set at alpha = 0.05.

4.3.4.3. Evidence for the peptide grafting

The grafting of fluorescent RGDK-FITC peptide on both flat model films and surface-modified MC50 was evidenced by imaging the samples with an Olympus epifluorescence IX71 microscope equipped with a blue filter U-MNUA2 (excitation 360-370 nm and emission 420-460 nm), a green filter U-MWIBA3 (excitation 460-495 nm and emission 510-550 nm) and a red filter U-MNIGA3 (excitation 540-550 nm and emission 575-625 nm). The UV light was provided by an X-Cite module, series 120PCQ from Lumen Dynamics. On flat surfaces, a deliberate scratch was made to evaluate the background fluorescence. The average fluorescence intensity was computed for all samples (flat model surfaces and MCs) For this, the average fluorescence intensity of one facet of each MC sample was evaluated after graying the image, computing the histogram of grey values and subtracting the fluorescence intensity of the background. The fluorescence intensities are presented as mean values $\pm$ standard deviation. Statistical analyses were performed using one-way analysis of variance

(ANOVA) followed by post hoc Tukey test with a significance level set at alpha = 0.05.

4.4 Results and discussion

4.4.1 Characterization of PLO/HA films

The coating deposited on PLLA MCs is obtained through the LbL method and is composed of HA as negative polyanion and PLO as polycation. This (PLO/HA) film was subsequently crosslinked using a biocompatible crosslinking reaction based on carbodiimide chemistry (EDC/Sulfo-NHS) in order to improve the stability and the mechanical properties of the coating towards cells.[172, 308, 315] The coupling reaction is depicted in Figure 4.4a.

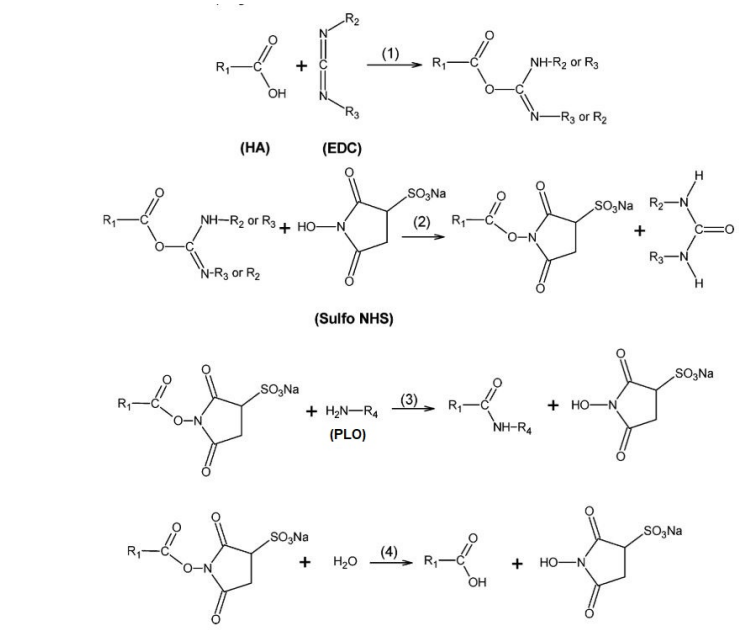

(a)

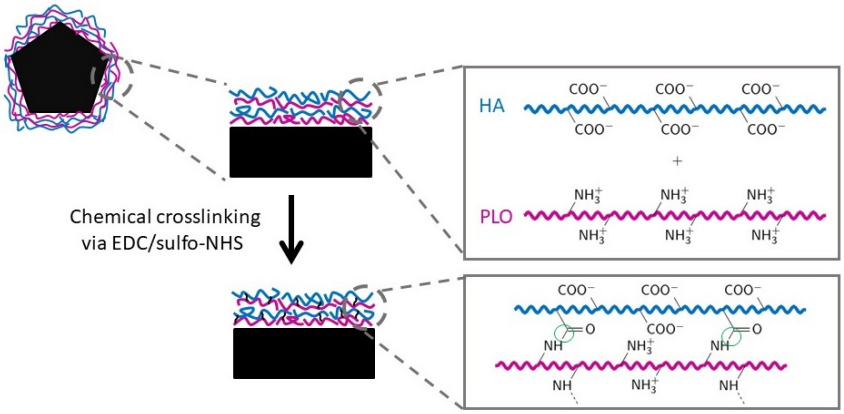

(b)

Figure 4.4.: (a) EDC/Sulfo-NHS coupling scheme: (1) EDC reacts with a carboxylic group and activates it to give a O-acylisourea intermediate; (2) The activated complex is converted into an active ester with sulfo-NHS; (3) The active ester reacts with primary amine to form an amide bond; (4) The unreacted sites are hydrolyzed to give a regeneration of the carboxylic groups. Scheme adapted from [308]. (b) Crosslinking of PLO/HA film by formation of amide bonds following the reaction of activated carboxylic sites coming from HA with primary amine groups coming from PLO.

The reaction leads to the formation of amide bonds following the reaction of activated carboxylic sites coming from HA with primary amine groups coming from PLO in the presence of EDC and Sulfo-NHS (Figure 4.4b).[308] EDC (70 mg/mL) and Sulfo-NHS (11 mg/mL) concentrations were chosen based on the literature as they were reported to be optimal for cell adhesion on PLL/HA films. Indeed, the film Young's modulus would increase from 3 to 400 kPa and showed increased adhesion and spreading of human chondrosarcoma [315], myoblast cells,[316] and ASCs [317] (section 1.5.3.3).

The variation of the thickness of dry crosslinked (PLO/HA) film as a function of the number of deposited (PLO/HA) bilayers on planar model surfaces was measured by ellipsometry (Figure 4.5.A). The film thickness follows an exponential growth which is typical for this kind of system based on biopolymers. The exponential growth is due to the diffusion of PLO in and out of the film during the build-up process.[302]

It was previously demonstrated that eight bilayers were sufficient to obtain a homogeneous film in a similar system.[304] From our results, $(\mathrm{PLO/HA})_8$ films possess a dry thickness of about 50 nm. However, this kind of film is known for its high swelling capacities and hydrated $(\mathrm{PLO/HA})_8$ films have been shown to present thickness of about 1 µm.[308] MC50 coated with $(\mathrm{PLO/HA})_8$ were thus dipped in a rhodamine solution to visualize the film distribution. This allowed to confirm that MC50 were uniformly covered at the micrometer scale by the LbL film (Figure 4.5.B). By contrast, bare MC50 dipped in rhodamine solution only showed a slight fluorescence that may be due to the presence of residual rhodamine solution in the pores of the MC50 or slight adsorption of rhodamine on PLLA surface (Figure 4.5.C). This difference of fluorescence intensity evidences the strong interaction between rhodamine dye and (PLO/HA) film. This interaction allows us to visualize the distribution of the coating on MC50 surface. It can be concluded that the MC50 surface is homogeneously and continuously covered by the LbL coating at the micrometer scale.

It has been previously reported that for some systems based on biopolymers such as CHI/HA [363] or PLL/alginate,[303] cell adhesion was strongly decreased when the number of layers of the film increased. This effect was attributed to the "gel-like" character of those films.[363] Therefore, as it seemed sufficient to cover the surface of the MC50, (PLO/HA) films made of eight bilayers were thus used to modify MC surface. HA was used as the final layer of the film. While HA is known to bind to specific cell surface receptors (*e.g.* CD44)

and modulate cell motility, adhesion, proliferation and gene expression,[364] it also leads to a negative surface charge that could impair cell adhesion due to electrostatic repulsion with the negatively-charged cell membrane. Using PLO as a last layer would theoretically lead to a positively charged surface that could attract the cells. However, Richert *et al.* showed that for PLL/HA systems, both PLL-ending and HA-ending films demonstrated a negative surface charge following the crosslinking step.[308] This seems to indicate that the outer layer is essentially formed of HA following the crosslinking step, regardless of the final layer used during the build-up of the film.

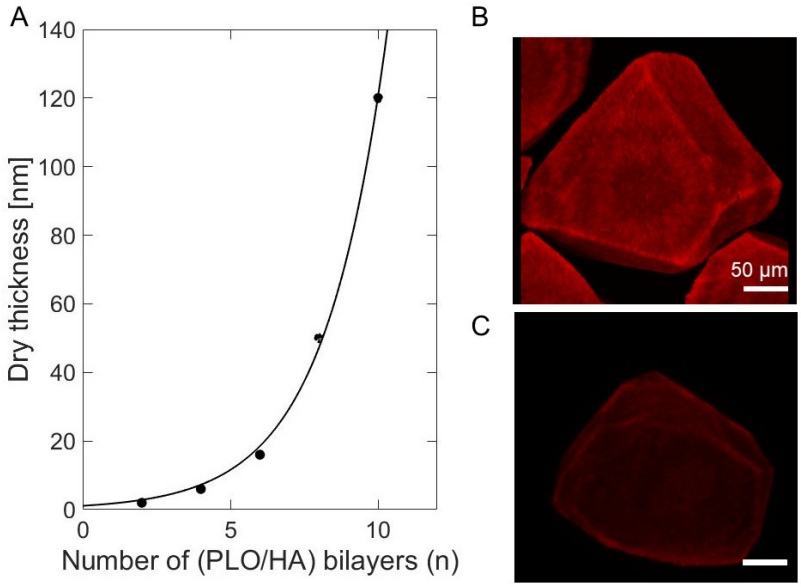

Figure 4.5.: (A) Variation of the dry thickness of crosslinked PLO/HA films grown on silicon substrate, as a function of the number of deposited bilayers n (ellipsometry measurements); CLSM images of $(\mathrm{PLO}/\mathrm{HA})_8$-coated (B) and bare (C) MC50 dipped in rhodamine solution. Fluorescence intensity quantification is provided in Figure 4.8 in appendix 4.6.1.

4.4.2 Evidence for the peptide grafting

In order to enhance the effect of the LbL coating, a bioadhesive RGD peptide was grafted on the crosslinked LbL film to strengthen cell adhesion. This grafting was performed using the same EDC/Sulfo-NHS chemistry as for the LbL crosslinking. The peptide is thus grafted following the formation of amide bonds between the activated carboxylic sites coming from HA with amine groups in the peptide sequence (Figure 4.6).

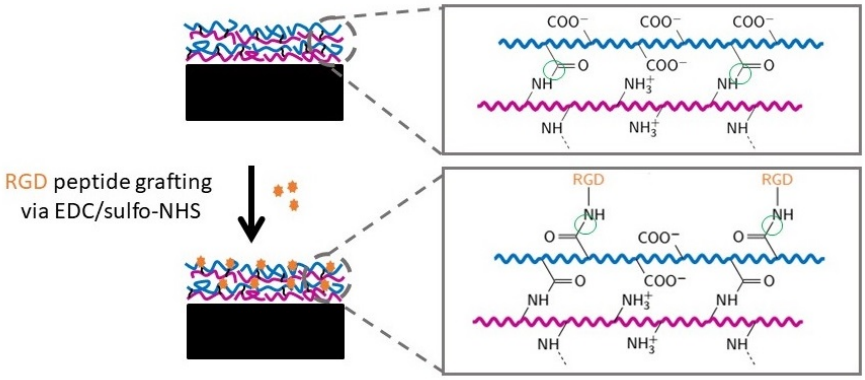

Figure 4.6.: RGD peptide grafting on crosslinked PLO/HA films is performed through the formation of amide bonds between the activated carboxylic sites coming from HA with amine groups in the peptide sequence following the action of EDC and sulfo-NHS.

As of now, no consensus has been reached on the optimal RGD concentration. While a higher RGD surface density is usually related to cell spreading, survival and proliferation,[141] it has also been reported that a large adhesion strength tends to reduce cell migration/proliferation and induce cell differentiation instead.[140] Thus, the peptide grafting step was performed using two RGD concentrations (0.1 mM and 1 mM), allowing us to investigate the effect of RGD peptide concentration on cell adhesion and proliferation in the next chapter.

The grafting of RGD peptide on $(\mathrm{PLO/HA})_8$ films deposited on planar surfaces was first investigated by using a fluorescent RGD-FITC peptide at two concentrations following EDC/sulfo-NHS activation step. A control sample prepared without activation step was also produced. The imaging by epifluorescence microscopy of the samples grafted using 1 and 0.1 mM RGD (Figure 4.7.A and

4.7.B, respectively) revealed the successful grafting of the peptide. As seen from the difference of fluorescence intensity between these two images, the higher the peptide concentration used for the grafting, the higher the fluorescence intensity on the film, which means a higher amount of grafted peptide in the film (qualitative evaluation). Moreover, as evidenced by the much lower fluorescence intensity observed when the activation step was omitted (Figure 4.7.C), the chemical grafting of the peptide on the $(PLO/HA)_8$ films required the activation of the carboxylic groups present on HA chains. Otherwise, the peptide was simply slightly adsorbed into the film and rinsed away in subsequent steps. Similar experiments were performed to evaluate the grafting of the peptide on $(PLO/HA)_8$-modified MC50 (Figure 4.7.D, E, F) confirming that the activation step is required to chemically graft the peptide on the film and that a higher peptide concentration led to a larger amount of peptide grafted on the film.

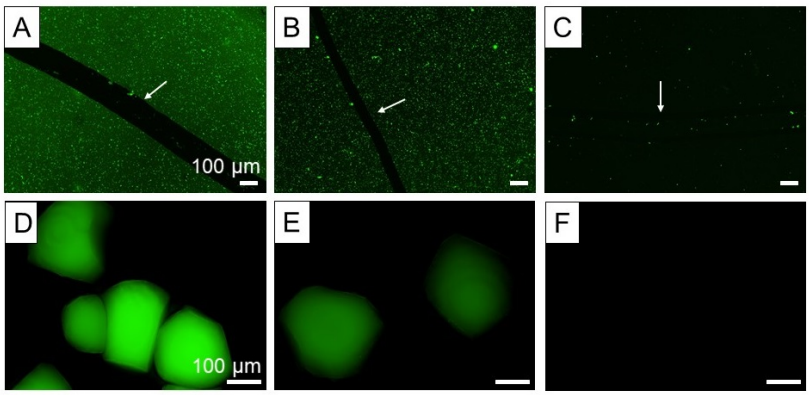

Figure 4.7.: (Top) Fluorescence microscopy images of crosslinked $(PLO/HA)_8$ films deposited on flat model surfaces (A) activated by sulfo-NHS/EDC and incubated in 1 mM or (B) 0.1 mM RGD-FITC solution; (C) control consisting of crosslinked $(PLO/HA)_8$ film incubated in 0.1 mM RGD-FITC solution without any prior activation. Deliberate scratches (see white arrows) were made on the films to visualize the fluorescence background. (Bottom) Fluorescence microscopy images of MC50 coated with crosslinked $(PLO/HA)_8$ (D) activated and incubated in 1 mM or (E) 0.1 mM RGD-FITC peptide solution; (F) control without any prior activation then incubated in 0.1 mM RGD-FITC solution. The scale bars are identical in each line. Fluorescence intensity quantification is provided in Figures 4.9 and 4.10 in appendix 4.6.1.

4.5 Conclusion

Due to PLLA low bioaffinity, PLLA MCs required a surface biofunctionalization in order to improve cell adhesion which is of critical importance for cell culture, notably in dynamic conditions. In this chapter, MC surface was easily functionalized with a bioadhesive coating devoid of animal proteins. For this, a film built from PLO and HA using the LbL technique was deposited on the MC50 surface then chemically crosslinked and grafted with a RGD peptide. The absence of animal proteins constitutes an asset with respect to current regulations, as animal proteins are often associated with batch-to-batch variability and most importantly, elicitation of immune response. The build-up of the LbL film was followed by ellipsometry on a flat model surface, which confirmed its successful deposition and showed that the film growth was exponential, as expected for that kind of system. A number of eight bilayers was selected as this was sufficient to obtain a homogeneous coverage of MC50. The successful grafting of the peptide at two concentrations was also evidenced both on flat model surfaces and MC50.

In the following chapter, the effect of the bioadhesive coating on cell adhesion and proliferation has been systematically assessed in semi-static conditions to better understand the contribution of the (PLO/HA) film as well as the RGD peptide and its concentration to cell adhesion.

4.6 Appendix

4.6.1 Fluorescence intensity quantification

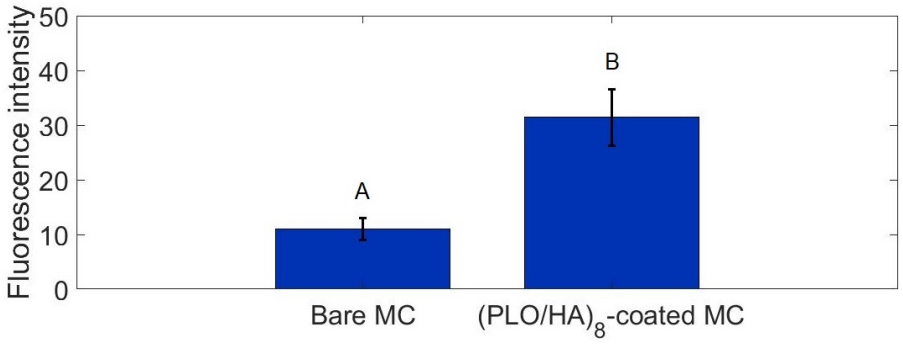

Figure 4.8.: Fluorescence intensity of $(\mathrm{PLO}/\mathrm{HA})_8$-coated and bare MC50 dipped in rhodamine solution. Bars topped with different letters indicate significant difference (p-value < 0.05).

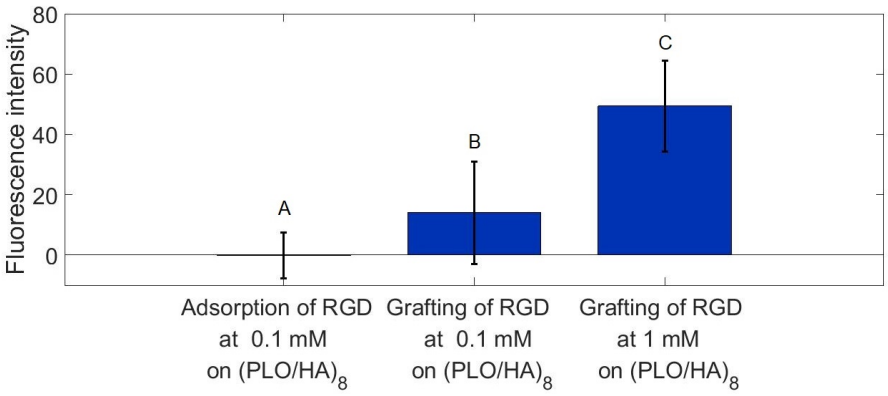

Figure 4.9.: Fluorescence intensity of crosslinked $(\mathrm{PLO}/\mathrm{HA})_8$ films deposited on flat model surfaces either adsorbed with 0.1 mM RGD-FITC (no activation through sulfo-NHS/EDC) or grafted with 0.1 mM or 1 mM RGD-FITC solution following sulfo-NHS/EDC activation. Bars topped with different letters indicate significant difference (p-value < 0.05).

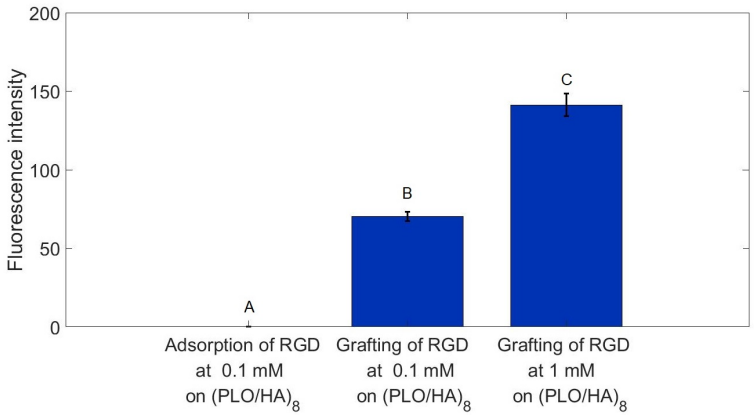

Figure 4.10.: Fluorescence intensity of crosslinked $(\mathrm{PLO}/\mathrm{HA})_8$ films deposited on MC50 either adsorbed with 0.1 mM RGD-FITC (no activation through sulfo-NHS/EDC) or grafted with 0.1 mM or 1 mM RGD-FITC solution following sulfo-NHS/EDC activation. Bars topped with different letters indicate significant difference (p-value < 0.05) .

5

Stem cell culture on microcarriers in semi-static condition

5.1 Introduction

Human adipose-derived stromal/stem cells (hASCs) have gained increasing prominence in the cell therapy field thanks to their multipotency, ease of access and isolation yield.[16, 18] These cells were thus selected to assess MC performance for cell expansion as they are progressively replacing bone-derived MSCs as the gold standard for MSC-based therapy.[10, 18] However, similarly to other types of stem cells, hASC adhesion, proliferation and differentiation potential is particularly sensitive to different factors such as the medium composition [365, 366] and choice of serum,[367] cell seeding density,[368] as well as culture substrate characteristics such as surface stiffness [369], functionalities,[370] roughness [196] or presence of biochemical cues such as bioadhesive peptides.[371, 372] A challenge also lies in the fact that different cell lines interact differently with MCs and screening of various MCs in static condition is usually recommended when establishing a MC-based culture of a new cell line.[78, 82]

As the MCs presented here are novel, no information on how they would interact with cells are available. MC culture using hASCs was thus performed in well-plates in semi-static condition, which consists of intermittent agitation performed only during the initial adhesion step to favour cell-MC contacts. As dynamic culture involves additional parameters compared to static culture (*e.g.*, type and rate of stirring, *etc.*), preliminary assays are usually performed in (semi) static condition avoiding the need to optimize too many parameters at a time. This small-scale set-up thus allowed us to investigate the effect of various parameters on cell adhesion and proliferation, without considering dynamic culture related

factors. Cell seeding density on MCs was optimized based on visual observation of cell adhesion and proliferation. The effect of MC morphology described in chapter 3 and composition of the bioadhesive coating described in chapter 4 were also investigated, in an effort to better understand cell-MC interactions and to optimize the conditions for *ex vivo* hASC expansion. The objective here was to set up the basis for a successful dynamic MC culture.

Based on these results, the most efficient surface-modified MC in terms of cell expansion was selected to be compared to a commercial MC (Cytodex® 3) regarding proliferation and detachment efficiency. This MC, which relies on animal derived-proteins is widely used to expand various cell types,[55] and is thus interesting to compare to our animal protein-free alternative. Preliminary differentiation assays were also performed to verify the propensity of hASCs to commit to osteogenic and adipogenic lineages while cultured on these two MCs. Finally, the suitability of magnetic MCs for hASC expansion was evaluated by comparing cell proliferation on magnetic and non magnetic MCs.

5.2 Experimental section

5.2.1 Materials

Mesenchymal Stem Cell Growth Medium 2 (basal medium supplemented with supplement mix), Mesenchymal Stem Cell Adipogenic Differentiation Medium 2 and Mesenchymal Stem Cell Osteogenic Differentiation Medium were purchased from Promocell. Dulbecco's phosphate buffered saline devoid of calcium and magnesium (DPBS)), DMEM (high glucose, GlutaMAX™ Supplement), StemPro™ Accutase Cell Dissociation Reagent, Alexa Fluor™ 488 phalloidine, CyQUANT™ Cell Proliferation Assay Kit, Calcein AM, and PrestoBlue™ Cell Viability reagent were provided by Thermo Fisher Scientific. Penicillin/streptomycin (PEST) was obtained from Life Technologies. FBS, Triton™ X-100, BSA (96 %), glutaraldehyde aqueous solution (25 %), 4',6-Diamidine-2'-phenylindole dihydrochloride (DAPI) (98 %) and Oil red O were purchased from Sigma-Aldrich. Corning® Costar® Ultra-Low Attachment Multiple Well Plates and Alizarin Red were purchased from VWR. Cellstar® 24-well cell culture plates were obtained from Greiner Bio-one. Ethidium bromide was

purchased from Biotium. Milli-Q grade (resistivity of 18.2 $m\Omega$) was produced by a Milli-Q® Reference system of Merck Millipore. hASCs were collected from lipoaspirates harvested from 1 adult donor who had provided his/her informed consent. Adipose tissues were enzymatically digested and ASCs were isolated by density gradient centrifugation and adherence to tissue culture plastic as previously described.[373]

5.2.2 Selection of growth medium and characterization of cells grown in monolayer culture

hASCs were grown in flasks in either Mesenchymal Stem Cell Growth Medium 2 from Promocell supplemented with 1% (v/v) PEST or DMEM (high glucose, GlutaMAX™ from Thermo Fisher Scientific supplemented with 1% (v/v) PEST and 10 % FBS. Cell were seeded in T75 flasks at a cell density of 4 300 cells/cm^2. Phase contrast images were taken at various time points during the culture to follow cell proliferation. Cells were subcultured using Accutase and counted using a Burker counting chamber, allowing to quantify cell expansion defined as the fold-increase between the number of harvested and seeded cells. Cell growth kinetics was also quantified in the selected medium by measuring the metabolic activity change. For this, cells were seeded at 4 300 cells / cm^2 in 24-well plates and cultured for five days. Metabolic activity assays were carried out on day 0, 1, 2, 4 and 5 as described in section 5.2.6.1.

5.2.3 Routine culture of hASCs

hASCs were routinely cultured in cell culture flasks in reconstituted Mesenchymal Stem Cell Growth Medium 2 from Promocell supplemented with 1% (v/v) PEST in an incubator (Binder CB170 E7) at 37 °C and in a humidified 5% CO_2 atmosphere. The supplemented culture medium was renewed three times per week and confluent cells were subcultured using Accutase and counted using a Burker counting chamber. Cells were used from passage four to passage eight.

5.2.4 Microcarrier preparation and conditioning

PLLA MCs surface-modified with a coating or not, were first rinsed in ethanol 70% then transferred in sterile PBS. They were then placed in the wells of ultra-low adhesion well-plates (1 mg MC/well unless stated otherwise) and subsequently sterilized by exposure to UV light for 30 min. The supernatant was removed and replaced by 300 µL of cell culture medium and the samples were conditioned in the incubator at 37 °C in a humidified 5% CO_2 atmosphere for 30 min.

The commercial Cytodex® 3 MCs were prepared according to manufacturer's instructions. Briefly, Cytodex® 3 were swollen in PBS (50–100 mL/g Cytodex) in a suitably siliconized glass bottle for at least 3 h at room temperature with occasional gentle agitation. The supernatant was removed and MCs were washed once with PBS (30–50 mL/g Cytodex MC). The PBS was discarded and replaced with fresh PBS (30–50 mL/g Cytodex). MCs were sterilized by autoclaving with steam and washed once more using sterile PBS. MCs were then placed in the wells of ultra-low adhesion well-plates (0.3 mg MC/well) from which the supernatant was removed and replaced by 300 µL of cell culture medium. The samples were conditioned in the incubator at 37 °C in a humidified 5% CO_2 atmosphere for 30 min.

5.2.5 Culture on microcarriers in semi-static condition

5.2.5.1. General procedure

The general procedure for hASC culture on MC in semi-static condition is illustrated in Figure 5.1. On day 0 of the experiment, MCs were prepared as described in section 5.2.4. During MC conditioning, hASCs cultured in cell culture flasks were detached from the flask using Accutase and counted using a Burker cell counting chamber. The supernatant was removed from each well and 300 µL of cell suspension was added (3 500 cells/well). Well-plates were placed in the incubator and manually agitated for 2 min every 28 min for four h. Then, each well was rinsed two times with 500 µL of PBS to remove non adhered cells. Three hundreds µL of supplemented medium was added in each

well and the plates were incubated for five days. The medium was replaced by 500 µL of fresh supplemented medium on the second day of the culture.

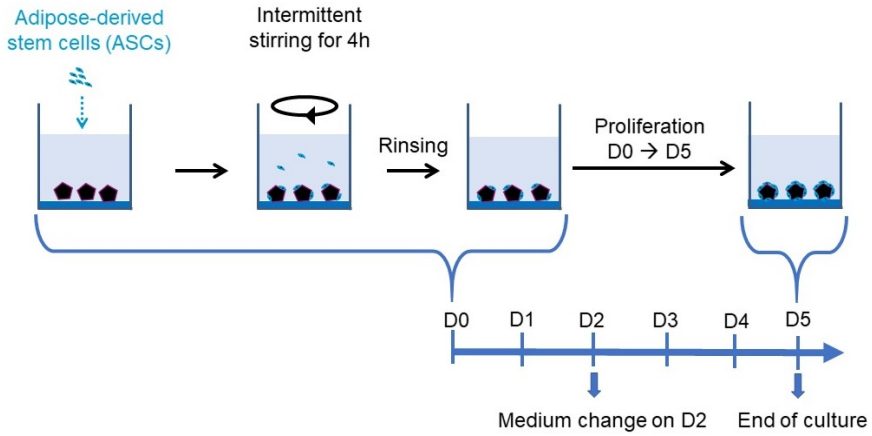

Figure 5.1.: General procedure for hASC culture on MCs in semi-static condition.

5.2.5.2. Cell seeding density optimization

Cell culture assays using different cell densities were performed to optimize this parameter towards cell proliferation. This experiment was performed using MCs prepared at 110 °C from a 50/50 PLLA40/PEG ratio and surface-biofunctionalized with a LBL film grafted using RGD at a concentration of 1 mM (MC50-RGD-1). The culture protocol is described in section 5.2.5.1. Cells were seeded at concentration of either 2 500, 3 500, 5 000 or 7 500 cells/well. On day 1, 3 and 5 of the experiment, Live/Dead staining was performed (section 5.2.6.3) to visualise the distribution and viability of cells grown on MCs.

5.2.5.3. Influence of coating and microcarrier morphology on cell behaviour

To assess the effect of MC morphology and the composition of MC coating on hASC behaviour, culture experiments were performed using MCs crystallized at 110 °C using three PLLA40 contents (MC30, MC50 and MC70 crystallized

from 30/70, 50/50 and 70/30 PLLA40/PEG ratio, respectively) and presenting four types of surfaces: bare MCs (MC-bare), MCs coated with crosslinked $(PLO/HA)_8$ (MC-LbL) and MCs coated with crosslinked $(PLO/HA)_8$ grafted with RGD moities using 0.1 mM (MC-RGD-0.1) or 1 mM (MC-RGD-1) RGD solution (Table 5.1). In order to keep the MC surface area per well constant between the different types of samples, and thus inoculate the same number of cells in each well (3 500 cells/well), MCs were placed in wells according to the following quantities : 0.72 mg for MC30, 1 mg for MC50 and 1.57 mg for MC70. These numbers were computed based on the estimated surface area provided in section 3.4.4.1. The general cell culture protocol described in section 5.2.5.1 was then performed. On day 0, 2 and 5 of the experiment, metabolic assays were performed in triplicate (section 5.2.6.1). At each time point, one sample of each condition was also retrieved, rinsed twice with 500 µL of PBS then stained for Live/Dead imaging (section 5.2.6.3). Another set of samples was kept for further nucleus and cytoskeleton staining (section 5.2.6.4).

		Type of MC (PLLA40/PEG ratio)		
		MC30 (30/70)	MC50 (50/50)	MC70 (70/30)
		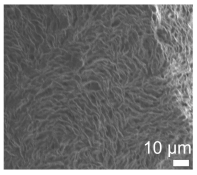	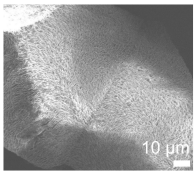	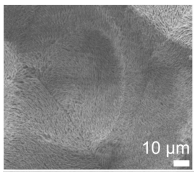
MC surface functionalization	Bare (MC-bare) 	MC30-bare	MC50-bare	MC70-bare
	LbL (MC-LbL) 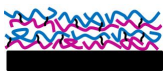	MC30-LbL	MC50-LbL	MC70-LbL
	RGD 0.1 mM (MC-RGD-0.1) 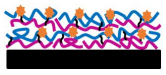	MC30-RGD-0.1	MC50-RGD-0.1	MC70-RGD-0.1
	RGD 1 mM (MC-RGD-1) 	MC30-RGD-1	MC50-RGD-1	MC70-RGD-1

Table 5.1.: Summary of the samples used to assess the influence of the coating and MC morphology on cell adhesion and proliferation. The percentage of PLLA40 used to prepare each sample is clearly indicated in the name of the samples. Uncoated MCs are referred to as MC-bare, MCs coated with crosslinked $(PLO/HA)_8$ are referred to as MC-LbL, and MCs coated with crosslinked $(PLO/HA)_8$ then grafted using 0.1 and 1 mM RGD peptide are referred to as MC-RGD-0.1 and MC-RGD-1, respectively.

5.2.5.4. Comparison of performance of MC50-RGD-1 with a commercial microcarrier

Proliferation. The objective of this experiment was to compare our MC to a commercial MC widely used to expand various cell lines.This experiment was thus performed with MC50-RGD-1 and Cytodex® 3 (Table 5.2 for MC characte-

ristics) following the protocol described in section 5.2.5.1. MC concentration was 1 mg MC/well for MC50-RGD-1 and 0.3 mg MC/well for Cytodex® 3 to keep the surface area constant for both types of MCs. MCs were inoculated using 3 500 cells/well. On day 0, 1, 2, 4 and 5 of the experiment, metabolic assays were performed in triplicate (section 5.2.6.1). At each time point, some MCs were also retrieved, rinsed twice with 500 µL of PBS then stained for Live/Dead imaging (section 5.2.6.3).

On the last day of the culture, cells were detached from MCs to qualitatively assess the harvesting efficiency on both types of MCs. Briefly, MCs were rinsed with PBS twice and incubated for ten min in Accutase at 37 °C. A quick manual agitation was performed after five min. The supernatant was retrieved to recover the floating cells. Two washing steps with PBS were performed to recover any remaining floating cells. MCs were then stained for Live/Dead imaging (section 5.2.6.3) to visualize the remaining attached cells.

	MC50-RGD-1	Cytodex® 3
Core	PLLA	Crosslinked dextran
Surface	$(PLO/HA)_8$ crosslinked then grafted using a 1mM RGD solution	Crosslinked gelatin
Size	150-300 µm	141-211 µm
Surface area	0.81 cm/mg	2.7 cm/mg

Table 5.2.: Overview of the characteristics of MC50-RGD-1 and Cytodex® 3.

Preliminary differentiation assays. hASCs were cultured on MC50-RGD-1 and Cytodex® 3 until day 5 following the protocol described in section 5.2.5.1. MC concentration was 1 mg MC/well for MC50-RGD-1 and 0.3 mg MC/well for Cytodex® 3 to keep the surface area constant for both types of MCs. MCs were inoculated using 3 500 cells/well. Cell cultured in regular 24-well plates and inoculated at 8 160 cells/well were used as a 2D control. According to these conditions, a constant cell density of 4 300 cells/cm^2 was thus used for the three systems. After the regular 5 day culture, cell culture medium was switched to either hASC osteogenic and adipogenic medium, which were changed every three days. After 21 days, the culture was stopped and cell-laden MCs as well as cell grown in monolayer were stained using Oil red O (section 5.2.6.5) and

Alizarin red (section 5.2.6.6) to detect lipid droplets and matrix mineralization, respectively. The different steps of the experiment are summarized in Figure 5.2.

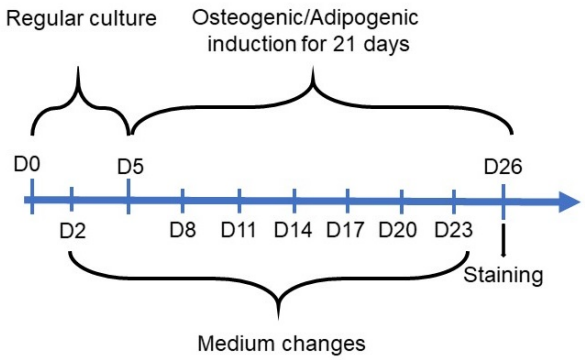

Figure 5.2.: Methodology used to assess hASC differentiation potential.

5.2.5.5. Influence of magnetic nanoparticles on cell adhesion and proliferation

Magnetic and non magnetic MC50-RGD-1 prepared according to the protocol described in section 5.2.4 were used to culture hASCs until day 5 following the protocol described in section 5.2.5.1. On day 0, 2 and 5 of the experiment, metabolic activity assays were performed in triplicate (section 5.2.6.1).

5.2.6 Cell characterization

5.2.6.1. Metabolic activity

Metabolic activity assays were performed by incubating the samples for three h in 250 µL of growth medium containing 10 % of PrestoBlue™ Cell Viability Reagent. One hundred µL of supernatant was transferred to a flat bottom black 96-well plate and fluorescence intensity was measured using a TECAN Infinite M1000 microplate reader (560 nm/590 nm excitation/emission).

5.2.6.2. DNA quantification

DNA content was quantified using CyQuant™ Cell Proliferation Assay kit. After the desired proliferation period, cell-laden MCs were retrieved, washed twice with PBS and frozen at $-80\,°C$. Reagents were prepared according to manufacturer instructions. Two hundreds µL of CyQuant dye/cell-lysis buffer were added to each sample. Samples were then vortexed for 15 seconds and incubated for 5 minutes protected from light. One hundred µL of the supernatant was deposited in a new 96-well cell culture microplate. The fluorescence intensity was read using a microplate reader (TECAN Infinite®Pro M Nano+) at 480/520 nm (excitation/emission).

5.2.6.3. Cell viability

Live/Dead staining was performed by incubating the samples in a combined solution of Calcein AM (2 µL/mL in PBS) and ethidium bromide (1 µL/mL in PBS) for 30 min at room temperature. Stained cells were then imaged using an Olympus IX71 epifluorescence microscopy.

5.2.6.4. Cell nucleus and cytoskeleton staining

Cells grown on MCs were fixed in glutaraldehyde aqueous solution (1 %) overnight then permeabilized in 0.1 % Triton™ X-100 and blocked by incubation in PBS containing 5 % BSA for 45 min. Staining of actin filament by Alexa fluor™ 488 Phalloidine (10 µL/mL in PBS supplemented with 1% BSA) was performed for 30 min. Then the samples were rinsed two times for 5 min in PBS supplemented with 1 % BSA followed by nucleus staining using DAPI (0.1 µL/mL in PBS supplemented with 1 % BSA) for 10 min. Samples were rinsed again two times for 5 min in PBS before being imaged using a Zeiss LSM 700 CLSM.

5.2.6.5. Oil red O staining

A stock solution was prepared by dissolving Oil red O in isopropanol (5 g/L), followed by incubation for one hour at room temperature and filtering using

a 0.2 mm filter. The working solution was prepared by mixing 6 mL of stock solution with 4 mL of milli-Q water, incubating for one hour at room temperature and filtering again with a 0.2 mm filter.

Samples to be stained were washed twice with PBS and fixed with 4 % paraformaldehyde (PFA) for 30 min at room temperature. They were washed again twice with PBS and incubated in Oil red O working solution (200 µL/well) for 15 min at room temperature. Samples were rinsed with milli-Q water until they became clear and observed in bright field using an Olympus IX71 microscope.

5.2.6.6. Alizarin red staining

Alizarin red stock solution was prepared by dissolving it in milli-Q water (12.5 g/L). The pH was set to 4.1 and the volume was increased to 50 mL to obtain a 40 mM solution. The solution was filtered with a 0.2 mm filter.

Samples to be stained were washed twice with PBS and fixed with 4 % PFA for 30 min at room temperature. They were washed again twice with PBS and incubated in Alizarin Red solution (200 µL/well) for 20 min at room temperature. Samples were rinsed with milli-Q water until they became clear and observed in bright field using an Olympus IX71 microscope.

5.2.7 Statistical analysis

Numerical data are presented as mean values $\pm$ standard deviation. Depending on the experiment, statistical analyses were performed using T-tests, as well as one and two-way analysis of variance (ANOVA) (Matlab) followed by post hoc Tukey (HSD) test with a significance level set at alpha = 0.05 for comparison of multiple means.

5.3 Results and discussion

5.3.1 Selection of growth medium and characterization of cell proliferation in monolayer culture

As the proliferation of cells relies heavily on the choice of growth medium and its supplementation, two different media were tested in an effort to maximize cell proliferation rate in classical monolayer culture, hoping this would also provide us with the best conditions for culture on MCs. The first tested medium was the Mesenchymal Stem Cell Growth Medium 2 provided by PromoCell. It consists in a low-serum cell growth medium designed to robustly support the standardized expansion of human MSCs. The second tested medium was constituted of DMEM from Thermo Fisher Scientific supplemented with a high content of glucose and GlutaMax^{TM} which is a substitute for L-glutamine mimimizing the production of toxic ammonia and other byproducts during the culture. As DMEM does not contain any proteins, lipids, or growth factors, it was also supplemented with 10% FBS provided by Sigma-Aldrich. Cells were grown in flasks and the total fold-increase between the number of harvested and seeded cells was computed. Cell proliferation was considerably higher in PromoCell growth medium (33.7 ± 1.7 fold increase over five days) compared to DMEM (2.5 ± 0.5 fold increase over seven days), which was confirmed by visual inspection (Figure 5.3). Indeed, in PromoCell medium, cells reached confluency after five days and looked small and thightly packed allowing to reach very high cell density. On the opposite, cells grown in DMEM looked widely spread and were not even confluent after seven days of culture. The higher effectiveness of PromoCell growth medium regarding cell proliferation is not a surprise, as it was specifically design for the expansion of MSCs. Thus, the PromoCell medium ($\approx$ 228 €/500 mL), while much more expensive than DMEM supplemented with 10 % FBS ($\approx$ 22 €/500 mL), was chosen for its impressive performance. It is worth noting that, with a yield more than ten times higher compared to DMEM, cell culture using PromoCell medium will lead to reduced consumable consumption (flasks, growth medium, *etc.*) thus reducing other costs.

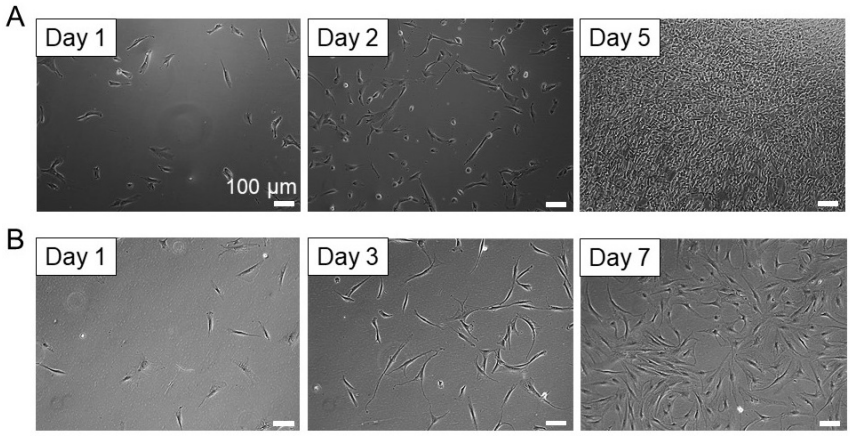

Figure 5.3.: Phase contrast images of cell grown in (A) Mesenchymal Stem Cell Growth Medium 2 from PromoCell and (B) DMEM from Thermo Fisher Scientific supplemented with 10 % FBS bought from Sigma-Aldrich. Scale bars are identical in all panels.

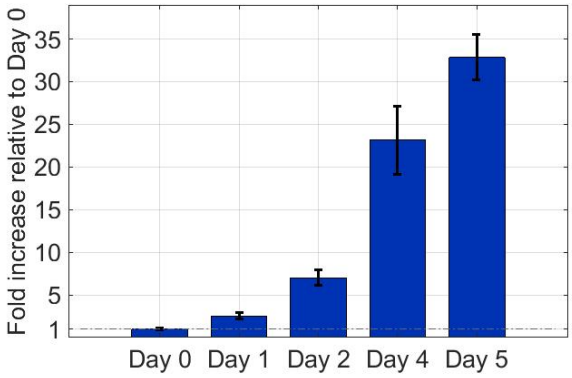

Figure 5.4.: Proliferation of hASCs grown in monolayer culture in Mesenchymal Stem Cell Growth Medium 2 (Promocell) as measured via the metabolic activity change relative to D0. (N=2, n=3).

The metabolic activity of cell grown as monolayer in PromoCell medium was also quantified to characterize cell growth kinetics in this medium, which demonstrated an exponential growth leading to a 32.8 $\pm$ 2.8 fold increase after five days of culture corresponding to a doubling time of 23.8 h (Figure 5.4). This

metabolic activity fold increase obtained after five days (32.8 $\pm$ 2.8) is comparable to the fold increase obtained by counting cells grown in flasks ((33.7 $\pm$ 1.7), suggesting the validity of this method to estimate the cell number.

5.3.2 Cell seeding density optimization

Cell seeding density is a critical parameter to ensure optimal expansion. Indeed, a too low cell to MC ratio could lead to an extensive lag phase but also to an uneven cell distribution on MCs. On the opposite, a ratio that is too high may results in a large number of unattached cells leading to a waste of inoculum, and a reduced surface area available for cell growth limiting the yield of expanded cells.[374]

From a theoretical point of view, the number of adhered cells per MC can be predicted using a Poisson distribution as cell adhesion events are random events.[375] A theoretical cell concentration ranging from 3 to 5 cells per MC regardless of the cell type is reported based on this Poisson distribution.[56, 374, 375] However, this optimal cell number clearly depends on cell types with various numbers being reported by different groups : 6 for foreskin fibroblasts, 8 and 30 for Vero cells, from 3 to 5 for hMSCs and 7 for MDCK cells.[374]

Different cell seeding densities, shown in Table 5.3, were tested using the MC50-RGD-1. As demonstrated in a subsequent section (section 5.3.3), this MC was the most appropriate for cell culture, thanks to the presence of the RGD peptide. The number of cells was varied from 2 500 to 7 500 per mg of MC. Based on the number of MCs per mg and surface area previously estimated, these densities corresponds to approximately 5 to 12.5 cells per MC or 3 100 to 9 250 cells per cm^2 of MC surface (section 3.3.3.9 for more details about the surface area estimation). As a reference, cells were routinely cultured in flasks using a cell seeding density ranging from 3 000 to 4 300 cells/cm^2.

Number of cells/mg MC	Number of cells/MC	Number of cells/cm^2 of MC
2 500	5	$\approx$ 3 100
3 500	7	$\approx$ 4 300
5 000	10	$\approx$ 6 170
7 500	12.5	$\approx$ 9 250

Table 5.3.: Overview of the different seeding densities tested in semi-static condition.

Figure 5.5 shows Live/Dead images of MCs inoculated using these different seeding densities at different time points (day 1, day 3 and day 5). On day 1, living cells could be found on MCs for all seeding densities. However, a large number of unattached cells (white arrows) were observed for the two highest seeding concentrations (*i.e.*, 5 000 and 7 500 cells/mg MC) which was not the case for the two lowest concentrations. Cell distribution on MCs seemed qualitatively more homogeneous using 3 500 cells/mg MC compared to 2 500 cells/mg MC, as MCs without adhered cells were not observed for this concentration. On day 3 of the culture, cell proliferation could be observed for all tested cell densities. MCs inoculated with 7 500 cells/mg were almost fully confluent with formation of large MC-cell aggregates. On day 5, all cell densities except for 2 500 cells/mg led to 100 % confluent MCs showing MC-cell aggregates of increasing size with increasing initial cell density.

As the two highest concentrations led to significant waste of cell inoculum, these cell densities were not considered for the next experiments. The cell density of 3 500 cells/mg was finally chosen as it led to a more homogeneous culture. Moreover, taking into account the inevitable cell loss during inoculation, this cell density is close to the one used for routine culture in flasks.

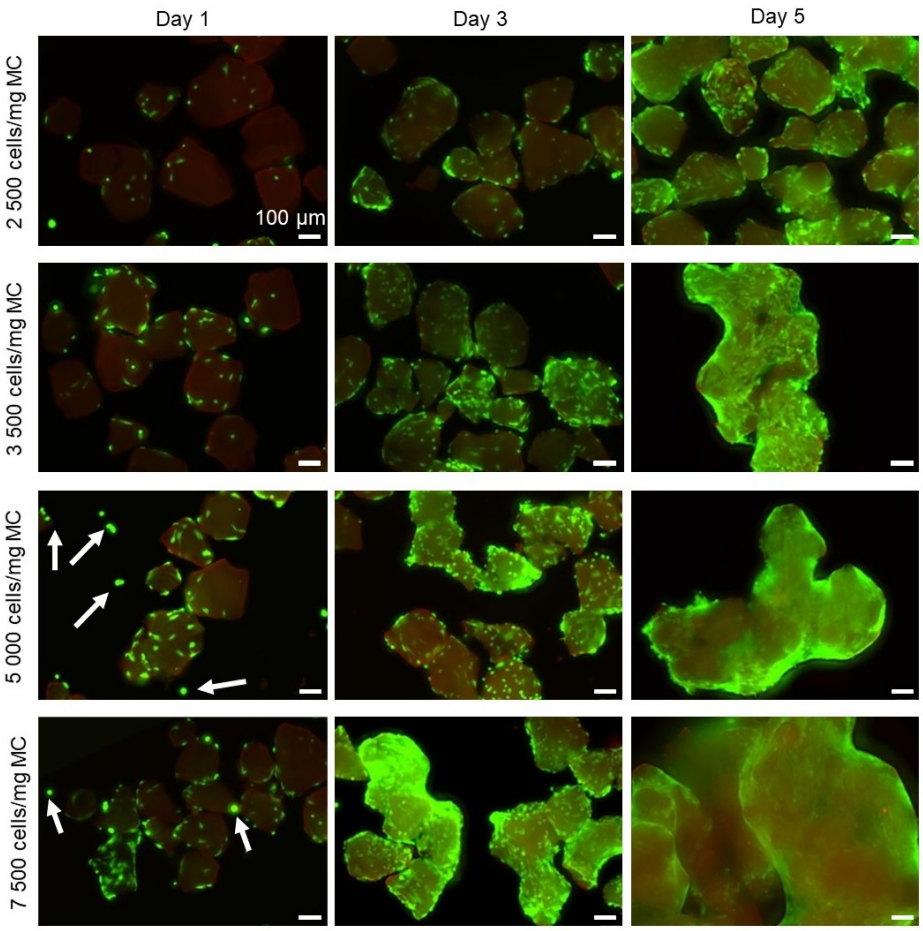

Figure 5.5.: Live/Dead images of MC50-RGD-1 inoculated with hASCs at densities of 2 500, 3 500, 5 000 and 7 500 cells/mg of MC on day 1, 3 and 5. White arrows indicate floating cells. Scale bars are identical in all panels. Magnified images can be visualized in the electronic version.

5.3.3 Influence of coating and microcarrier morphology

5.3.3.1. Cell adhesion and proliferation

The influence of MC morphology and bioadhesive coating on cell adhesion and proliferation was systematically investigated. For this, MCs were prepared using three PLLA40 contents (MC30, MC50 and MC70). As a reminder, MCs prepared with a higher PLLA40 content show a smoother surface compared to MCs prepared with a lower PLLA40 content. For each MC morphology, samples consisted of bare MCs, MCs coated with crosslinked $(PLO/HA)_8$, MCs coated with $(PLO/HA)_8$ crosslinked then grafted using RGD peptide at concentrations of 0.1 and 1 mM RGD. Table 5.1 gives an overview of the samples used.

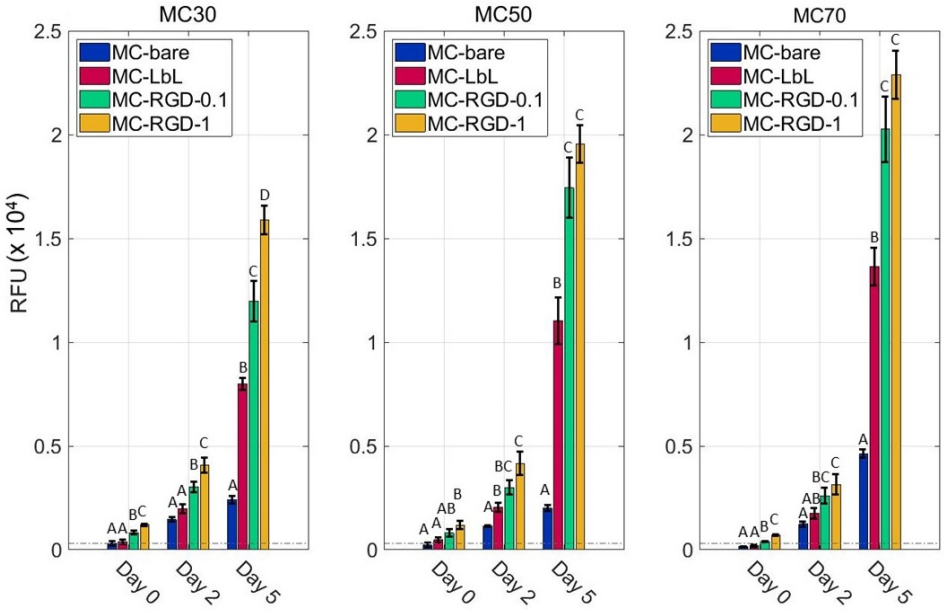

Figure 5.6.: hASC proliferation performed in semi-static condition on MCs with different surface morphologies and coatings. Bars represent the mean ± standard deviation. Bars topped with different letters indicate significant difference (p-value < 0.05). Horizontal dashed lines indicate the limit of detection. (N=2, n=3).

The adhesion and proliferation of cells on MCs was followed by measuring cell metabolic activity [85, 376–378] as shown in Figure 5.6. Cell metabolic activity was correlated to cell number. DNA content quantification was also performed to measure cell proliferation. However, the kit reagents interacted with MCs whatever the experimental settings, precluding any accurate quantification (Figure 5.16 in appendix 5.5.1). Images of Live/Dead staining are also provided in Figures 5.7, 5.8 and 5.9 for day 0, 2 and 5, respectively.

On day 0, the initial adhesion was quantified after four h of adhesion in semi-static condition. Regarding coating influence, the same tendency was observed regardless of MC morphology. Initial cell adhesion was really low for bare and LbL samples with values below the limit of detection. No significant improvement of cell adhesion was obtained with the LbL coating alone compared to bare MCs. However, adding the RGD peptide greatly improved cell adhesion in a concentration dependent manner, with cell adhesion being significantly higher for the highest RGD concentration. Regarding MC morphology, no clear difference was observed between MC30 and MC50 while MC70 showed an overall decreased adhesion compared to the other samples. These quantitative results were consistent with qualitative observation of cell adhesion on MCs through Live/Dead staining shown in Figure 5.7. It should be noted that, due to their opacity, only one side of MCs is visible. An increasing number of cells was observed when going from bare MCs to RGD grafted MCs with no empty MC observed at the highest RGD concentration. At this point, cells showed a rounded shape on all samples, most likely due to the short adhesion time (four h). The absence of red-stained cells indicated the lack of major cytotoxicity of the MCs, whatever their surface treatment.

On day 2, cells had proliferated on all samples compared to day 0. Similarly to that day, cell number was not significantly higher for MC-LbL compared to MC-bare. The addition of RGD peptide led to an increased cell number with a significant positive effect of higher peptide concentration. At this time point, no effect of MC surface morphology on cell number was observed. Figure 5.8 confirms the trends described above regarding cell number and viability. It can also be seen that cell shape stayed round on all MC-bare and only some elongated cells could be observed on MC-LbL. In contrast, cells showed an elongated morphology for all samples grafted with RGD peptide.

Finally, on day 5, cells continued to grow on all samples with the same trend as for day 2. Cell numbers were significantly different on all types of MC coating

with MC-RGD-1 showing the highest cell number. Regarding MC morphology, contrarily to prior days, the cell number was higher in the following order : MC70 $>$ MC50 $>$ MC30. This might indicate that MC surface morphology had opposite influence over cell adhesion and proliferation. Indeed, MC70, which shows a lower surface roughness compared to MC30, showed a significantly lower amount of cells on day 0 but a significantly higher amount of cells on day 5 compared to MC30. This indicates that a higher surface roughness, as obtained for MC30, improves cell adhesion while a lower surface roughness, as obtained for MC70, induces a quicker cell proliferation. For example, a fold-increase of 32.9 $\pm$ 4, 16.4 $\pm$ 1.8 and 13.2 $\pm$ 1.4 were measured for MC70-RGD-1, MC50-RGD-1 and MC30-RGD-1, respectively. These numbers correspond to doubling times of 23.8, 29.7 and 32.2 h, respectively. It is noteworthy that the total cell expansion obtained on MC70-RGD-1 is close to the one obtained in monolayer culture (section 5.3.1). However, the larger amount of cells observed on MC70 compared to MC50 on day 5 cannot be attributed to a surface roughness effect (here defined by the average peak-to-valley height R_a) as both samples showed approximately the same R_a value (0.39 $\pm$ 0.11 and 0.40 $\pm$ 0.02 µm for MC50 and MC70, respectively). A deeper characterization of the surface roughness including shape, spacing and organization of features [142, 187] might be required to understand this effect.

Figure 5.9 showing Live/Dead images of cells on MCs confirms the quantitative data. Indeed, on MC30-bare and MC50-bare, cell kept a round shape and proliferated mostly as aggregates. Some elongated cells could however be seen on MC70-bare. MC-LbL showed more elongated cells and a larger number of cells was observed going from MC30-LbL to MC50-LbL and MC70-LbL but cell coverage was mostly inhomogeneous with MCs without cells being seen. A larger amount of cells was observed on MC-RGD-0.1 compared to MC-LbL. Only MC50-RGD-1 and MC70-RGD-1 reached confluency, indicating that the lower growth rate observed on MC30-RGD-1 cannot be attributed to cell contact inhibition. When cells reached confluency, aggregates of several MCs covered with cells could be observed. Finally, there was no sign of reduced cell viability even after five days of culture.

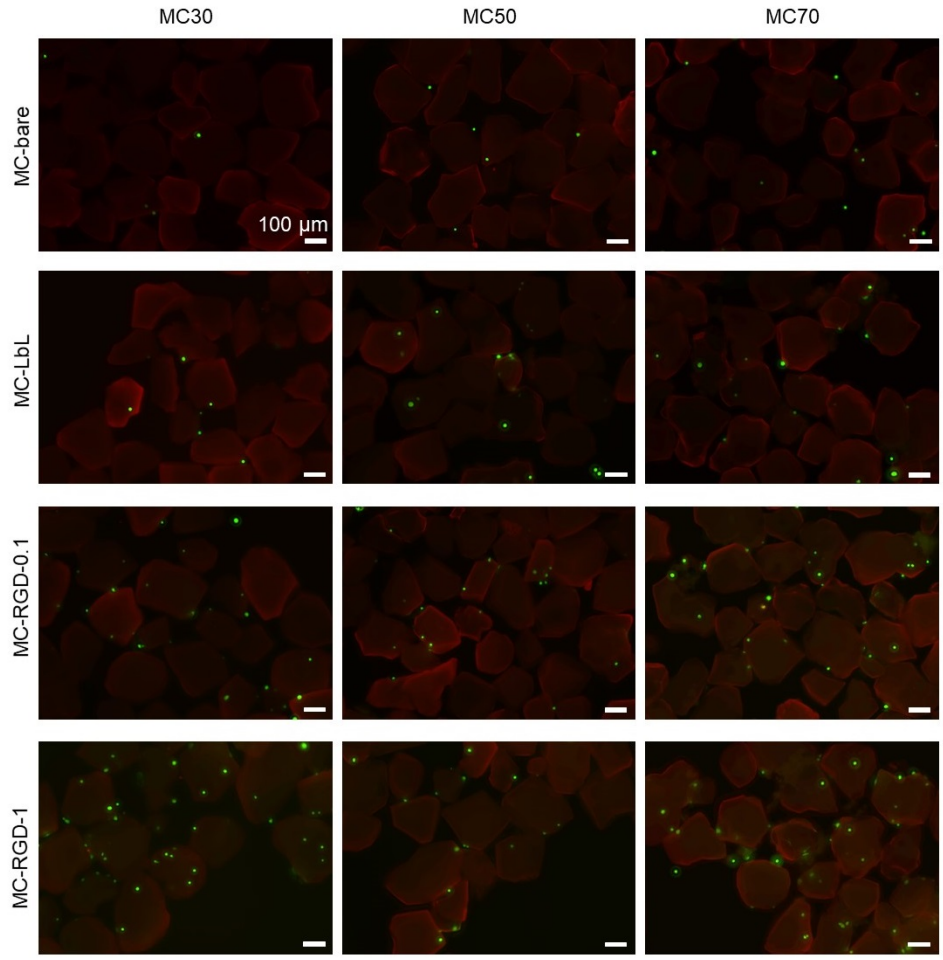

Figure 5.7.: Live/Dead images of cells on MCs with different surface morphologies and coatings on D0. Scale bars are identical in all panels. Magnified images can be visualized in the electronic version.

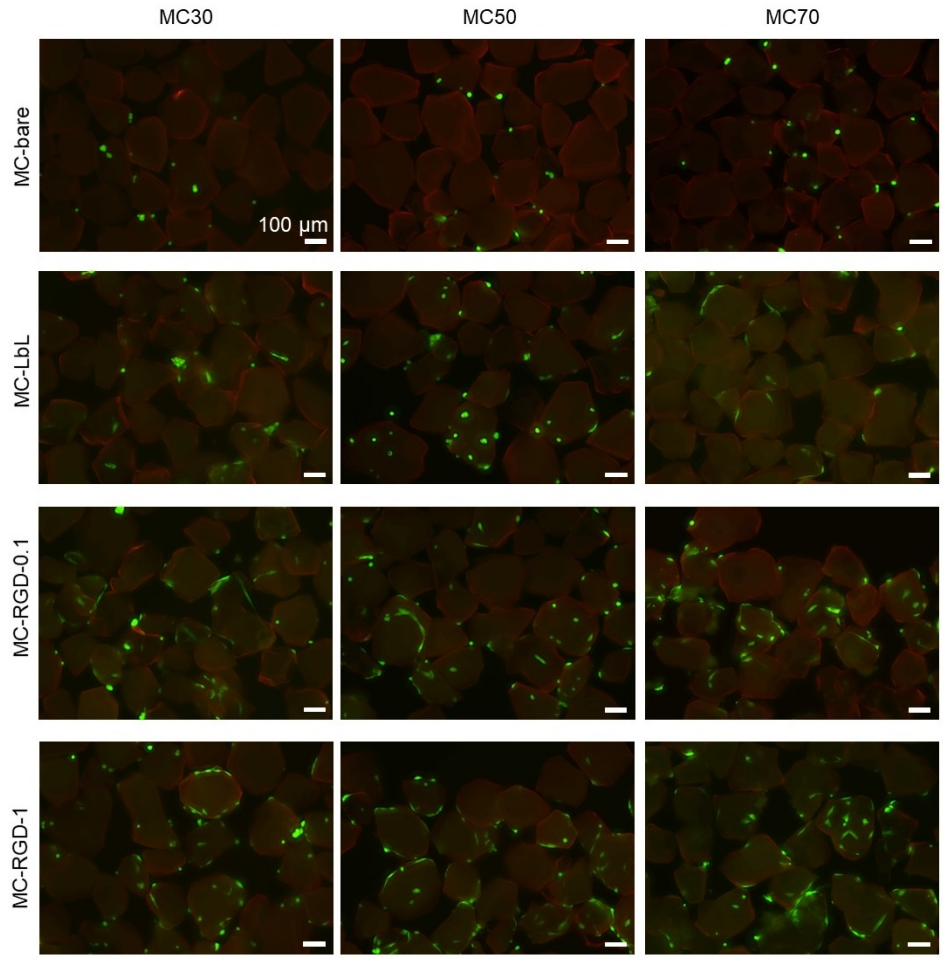

Figure 5.8.: Live/Dead images of cells on MCs with different surface morphologies and coatings on D2. Scale bars are identical in all panels. Magnified images can be visualized in the electronic version.

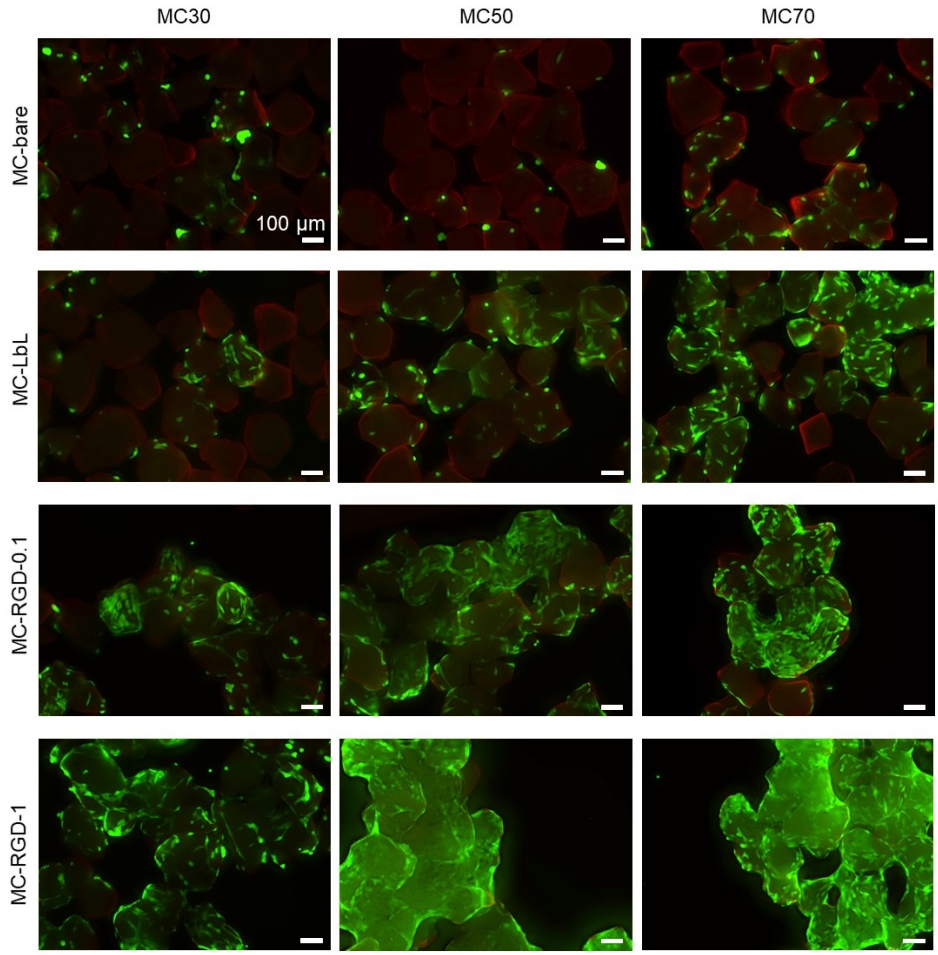

Figure 5.9.: Live/Dead images of cells on MCs with different surface morphologies and coatings on D5. Scale bars are identical in all panels. Magnified images can be visualized in the electronic version.

5.3.3.2. Cell morphology

In order to better analyze cell morphology on the different MCs, cell-laden MCs were fixed to be stained for nucleus and cytoskeleton visualization. Unfortunately, due to the Covid-19 pandemic and the subsequent closing of the lab, samples could not be handled in time. As a result, only MC50 could be imaged on day 0 and 4, as seen in Figure 5.10.

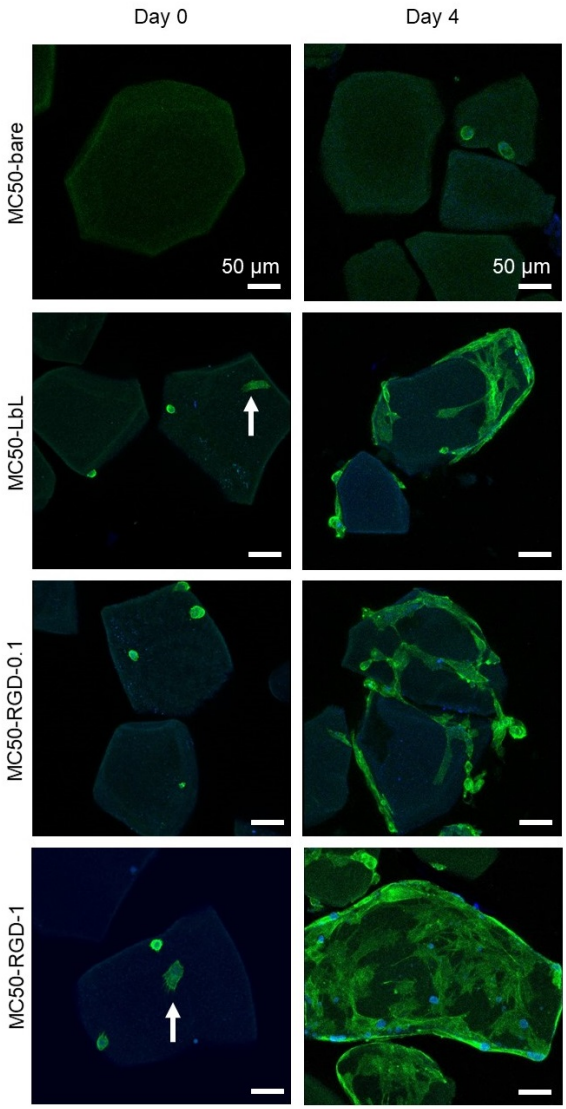

Figure 5.10.: CLSM images of cytoskeletal organization and spreading of hASCs grown on MC50 with different coatings on day 0 (left) and day 4 (right). Phalloidin stains actin filaments (green) and DAPI stains cell nuclei (blue). White arrows indicates spreading cells on day 0. Scale bars are identical in all panels. Magnified images can be visualized in the electronic version.

On day 0, no cells could be found on MC50-bare. Approximately two to three cells per MC were observed on surface-biofunctionalized samples but as stated

before, all cells cannot be observed due to the opacity of the MCs. Cells remained mostly rounded on all samples, due to the short adhesion time (four h) but some cells starting to spread could nevertheless be seen (white arrows). On day 4, barely any cells were observed on MC50-bare and they were rounded, indicating poor affinity for the surface. On the contrary, cell were well-spread on the three biofunctionalized MCs with larger number of cells observed going from MC50-LbL to MC50-RGD-0.1 and MC50-RGD-1.

5.3.4 Comparison of MC50-RGD-1 with a commercial microcarrier

In this section, the performance of the MC50-RGD-1 is compared to a commercial MC in semi-static condition. While MC70-RGD-1 led to a higher cell number at the end of the culture, it is unfortunately not suitable for dynamic cell culture due to a too high sedimentation rate (section 3.4.3). Therefore, MC50-RGD-1 was thus selected in its place. Cytodex® 3 is a MC provided by GE Healthcare which consists of a surface layer of denatured collagen covalently bound to a matrix of crosslinked dextran and was specifically designed for cells that may be difficult to grow in vitro.[133] As several types of MSCs were successfully expanded on Cytodex® 3,[137] it was deemed a good candidate to compare to our MC.

5.3.4.1. Proliferation assays

Figure 5.11A displays cell proliferation for the two types of MCs. Exponential growth was observed for both systems. No significant difference was observed for initial cell adhesion but cell proliferated more on Cytodex® 3. Figure 5.11B also provides the proliferation expressed as fold-increase. MC50-RGD-1 and Cytodex® 3 showed a proliferation of 17.6 $\pm$ 2.9 and 22.8 $\pm$ 3.6 fold-increase, respectively, which correspond to a doubling time of 26.6 and 29 h, respectively. While MC50-RGD-1 demonstrated a lower cell expansion by day 5 compared to Cytodex® 3, its performance is still valuable considering it does not rely on animal proteins. Live/Dead images of cell on both MCs are provided in Figure 5.12 and allow to visually follow cell proliferation. By day 5, all systems were

confluent and both types of MCs formed aggregates. Cells remained viable on all MCs throughout the culture.

A qualitative assessment of cell detachment efficiency was also performed on day 5. The detachment protocol was the same as for cells in monolayer culture. Live/Dead images of MCs after the detachment procedure are provided in Figure 5.12, allowing to visualize the remaining attached cells. Very few cells could be seen on MC50-RGD-1 after the detachment treatment, indicating that cells could be easily harvested from our MC at the end of the culture. On the opposite, a large number of cells was still visible on Cytodex® 3, even if these cells were rounded as if they were starting to detach. These results clearly demonstrate the superiority of our MC compared to the commercial alternative regarding the harvesting efficiency. The detachment efficiency on Cytodex® 3 has already been reported to be quite low for human MSCs with harvesting yield of less than 20 % following a ten min incubation in accutase or trypsin.[104] This harvesting efficiency could possibly be improved by either using longer incubation times in enzyme or by applying some shear stress as cells could stick to Cytodex® 3 due to its gelatinous nature. However, both approaches could have detrimental effects on cells. Quantitative results regarding detachment efficiency proved to be difficult to obtain due to the impossibility to perform DNA quantification for cells in contact with MCs (Appendix 5.16).

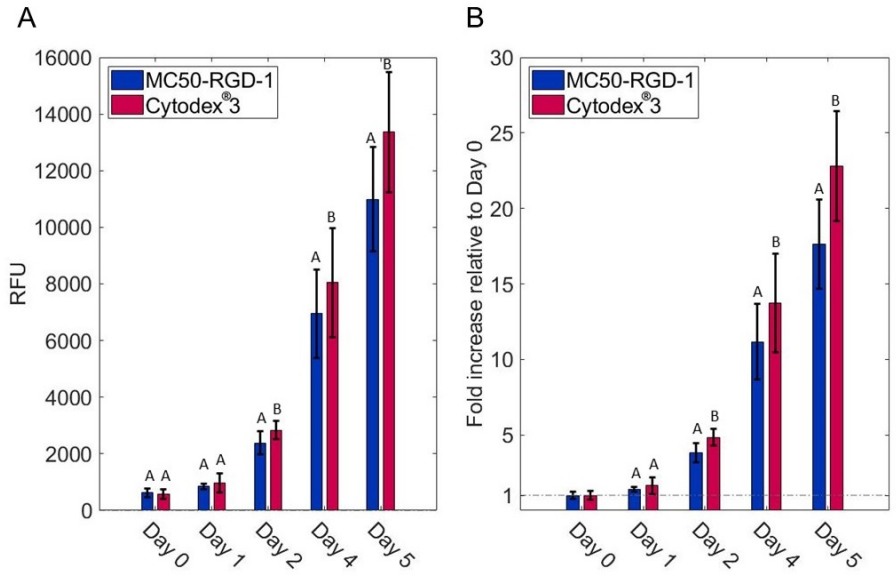

Figure 5.11.: Cell proliferation on MC50-RGD-1 and Cytodex® 3: (A) relative fluorescence intensity (RFU); (B) metabolic activity change. Bars topped with different letters indicate significant difference (p-value < 0.05). (N=2, n=3)

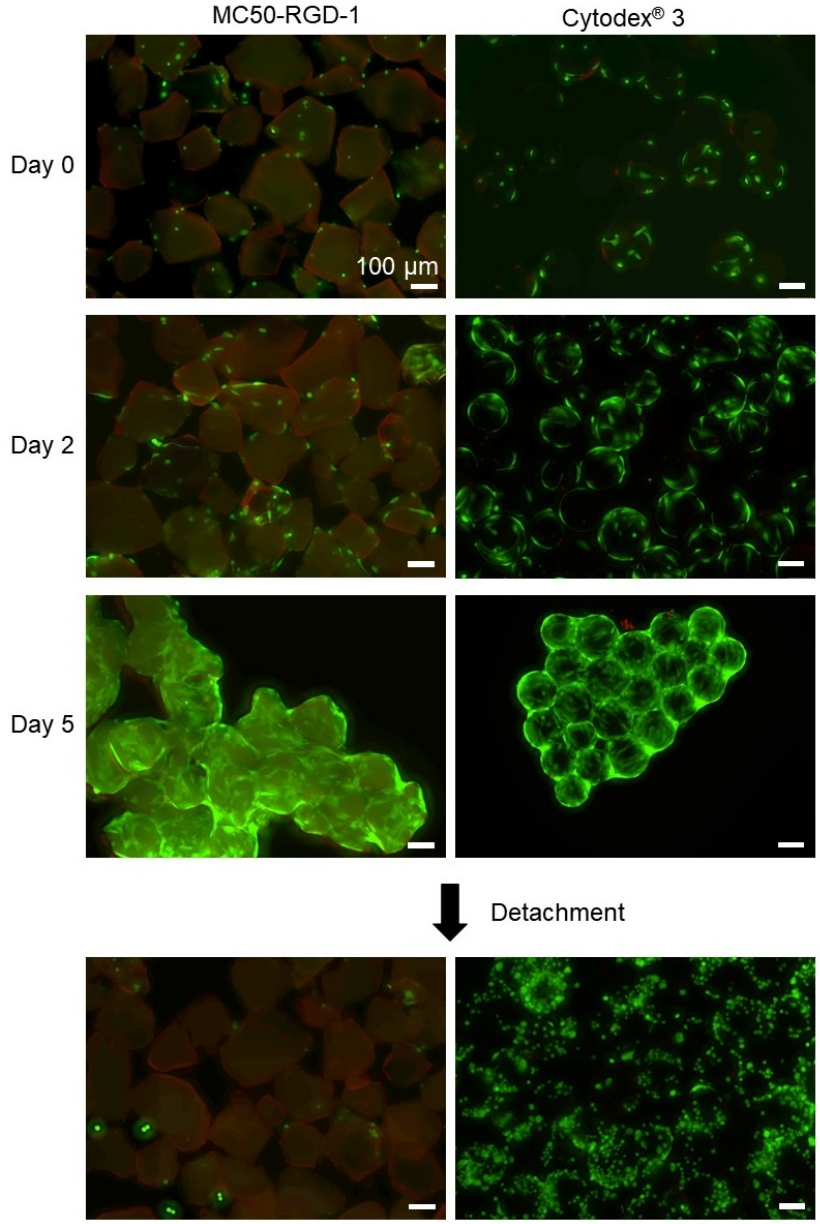

Figure 5.12.: Live/Dead images of cell grown on MC50-RGD-1 and Cytodex® 3 on day 0, day 2 and day 5, as well as a qualitative evaluation of the detachment efficiency. Scale bars are identical in all panels. Magnified images can be visualized in the electronic version.

5.3.4.2. Preliminary differentiation assays

The results presented in this section were obtained in collaboration with Dr A. Ajith Kumar within the frame of the project.

The ability of hASCs grown on MC50-RGD-1 and Cytodex® 3 to undergo osteogenic and adipogenic differentiation following culture for 21 days in induction medium was qualitatively studied. Cell differentiation in 2D was used as a control. The osteogenic differentiation was assessed by visualizing matrix mineralization (calcium deposits) via Alizarin Red staining while the adipogenic differentiation was assessed by visualizing lipid droplets in cells via Oil red O staining. Figure 5.13 provides macro and microscopic observations of samples stained for osteogenic and adipogenic differentiation. However, microscopic observation of both types of MCs was problematic due to the formation of large aggregates after such long culture times.

The ability of hASCs to undergo osteogenic differentiation, when supplemented with an appropriate medium, was confirmed for all three systems with calcium deposits clearly visible, except for MC50-RGD-1 due to imaging issues related to the size of MC-aggregates (Figure 5.13A). Macroscopically, both MCs appeared red even if Cytodex® 3 was darker, suggesting higher mineralization. Further assays would be required to confirm whether this higher mineralization stems from a higher amount of cells or a higher differentiation capacity. Indeed, Cytodex® 3 led to higher cell expansion than MC50-RGD-1 (section 5.3.4.1) and several authors also reported that cells differentiated on the surface of Cytodex® 3 displayed enhanced osteogenic differentiation as compared with MSCs cultured on monolayer surfaces.[91, 122, 379]

Cells on all three types of systems also demonstrated the capacity to differentiate towards adipogenic lineages with lipids droplets visible (Figure 5.13B). Macroscopically, no colour difference was observed between both types of MCs but quantitative data would be required to confirm this first observation.

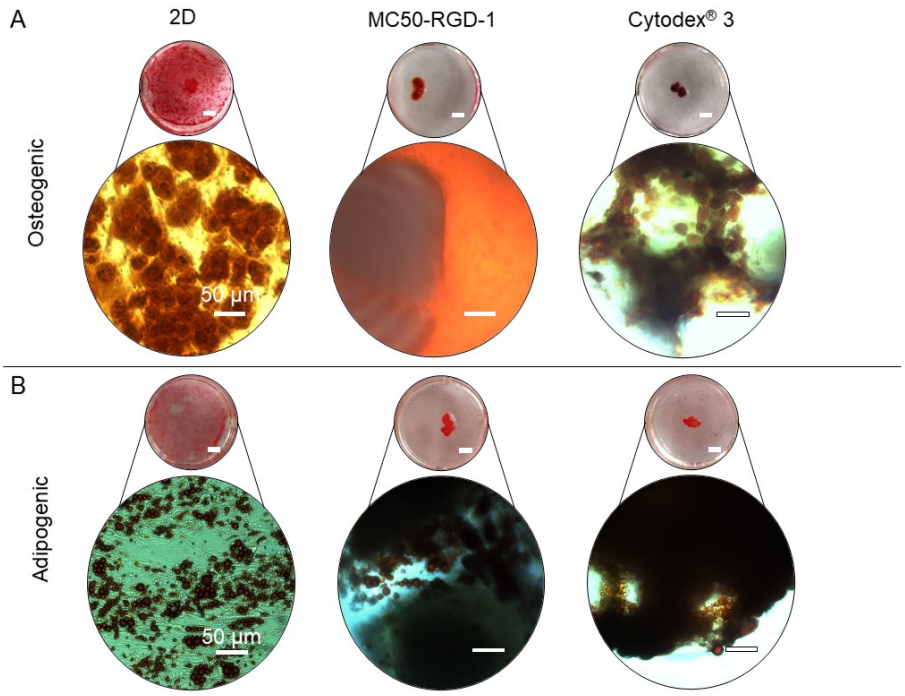

Figure 5.13.: Osteogenic and adipogenic differentiation of hASCs grown in 2D and on MC50-RGD-1 and Cytodex® 3. (A) Visualization of the matrix mineralization by Alizarin Red staining after 21 days of osteogenic induction. (B) Visualization of the lipid droplets by Oil red O staining after 21 days of adipogenic induction. Scale bars in whole-well images represent 2 mm.

5.3.5 Comparison of cell adhesion and proliferation on magnetic and non-magnetic microcarriers

Cell proliferation was assessed on MC50-RGD-1 prepared with and without MNPs using a concentration of 3 mg Fe/ g PLLA (Figure 5.14). Both systems led to an exponential cell growth. Except for a slightly lower amount of cells on non-magnetic MCs on day 0, no statistical difference was observed between the two samples at other time points. By day 5, the fold increase reached 18.4 $\pm$ 6 and 14.3 $\pm$ 5 for non-magnetic and magnetic MCs. The higher fold increase observed on non-magnetic MCs is explained by the slightly lower cell number on day 0. The doubling time was estimated to be 28.5 h for non-magnetic MCs

and 31 h for magnetic MCs. This highlights the fact that magnetic MCs can be used to facilitate culture handling without compromising cell expansion. Indeed, the movement of cell-laden MCs was qualitatively assessed as shown in Figure 5.15, which demonstrates the feasibility of magnetic manipulation.

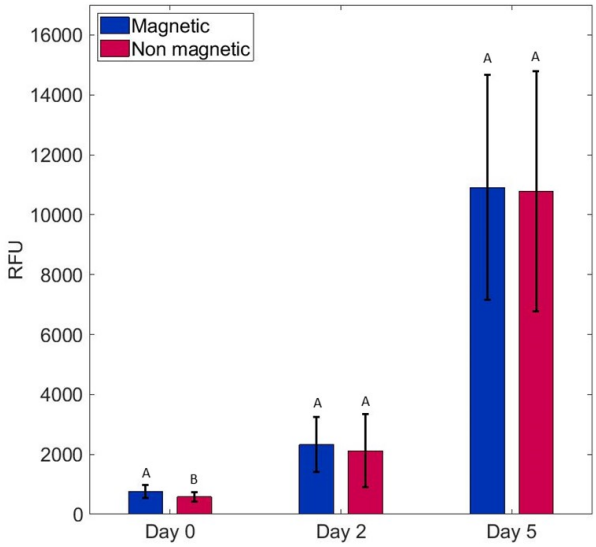

Figure 5.14.: Cell proliferation of hASCs on magnetic and non magnetic MC50-RGD-1 as measured by metabolic activity. Bars topped with different letters indicate significant difference (p-value < 0.05). (N=2, n=3)

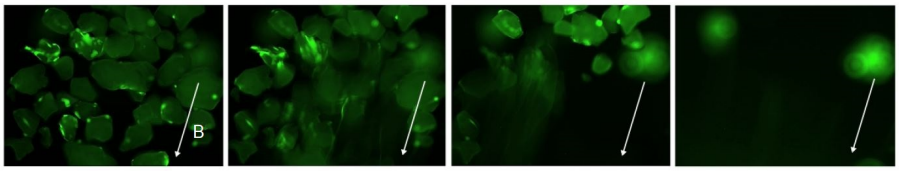

Figure 5.15.: Displacement of cell-laden magnetic MCs when submitted to a 1.4 T magnet. The arrow indicates the direction of the field. Each picture is taken approximately every three seconds.

5.4 Conclusion

Biofunctionalized MCs characterized in previous chapters were used for cell culture assays in semi-static condition. This set-up allowed us to screen a variety of parameters in an effort to select the most appropriate parameters such as cell seeding density and surface modification to then test the same parameters in dynamic condition. First, special attention was devoted to select the best growth medium (PromoCell) in order to operate further assays in optimum conditions. A cell seeding density of 3 500 cells/mg for MC50 was selected as it allowed to simultaneously minimize loss of cell inoculum and obtain an homogeneous adhesion. Then, the effect of MC morphology and composition of bioadhesive coating was investigated. Regarding the bioadhesive coating, LbL film alone did not significantly improve adhesion but led to a higher cell spreading and proliferation compared to bare MCs. Grafting the RGD peptide further improved cell adhesion and proliferation with the best results obtained when a higher RGD concentration was used for RGD grafting. MC morphology clearly has an impact on cell behaviour with opposite effect of surface roughness on adhesion and proliferation. While the more rough MC30 led to higher cell adhesion, the smoother MC70 resulted in the highest cell proliferation, followed by MC50. Unfortunately, MC70 does not demonstrate an appropriate sedimentation rate and cannot be used for dynamic culture but could reveal interesting for other applications which do not require a good MC suspension. MC50-RGD-1 were thus used for subsequent assays. In particular, this MC was compared to the commercial MC Cytodex® 3 which has been successfully used to expand MSCs.[137] We demonstrated that, while MC50-RGD-1 showed a slightly lower cell expansion after five days, the harvesting efficiency is much higher on MC50-RGD-1. Moreover, hASCs cultured on both MCs retain their osteogenic and adipogenic differentiation capacity but further assays are required to obtain a quantitative comparison. Finally, we showed that magnetic MCs supported cell adhesion and proliferation to the same extent as non-magnetic MCs. These magnetic properties can facilitate MC handling during MC-cell separation by allowing to immobilize or move MCs using a magnet. This feature could also ease MC handling during culture such as for medium replenishment. In the following chapter, the performance of MC50-RGD-1 for culture of hASCs in dynamic condition is assessed.

5.5 Appendix

5.5.1 Feasibility of DNA quantification of cells in presence of microcarriers

The feasibility of quantifiying the DNA of cells adhered on MCs was investigated (Figure 5.16). For this, MC50-RGD-1 and Cytodex® 3 were placed in eppendorfs and a suspension of either 3 000 and 30 000 cells was added to the eppendorfs. Controls consisting of the cell suspensions alone were also prepared. The DNA content of the various samples was quantified according to the protocol described in section 5.2.6.2. Results indicate an interaction between MCs and kit reagents which is even more pronounced on Cytodex® 3. This indicates that DNA quantification is not a suitable way to quantify cell number on MCs.

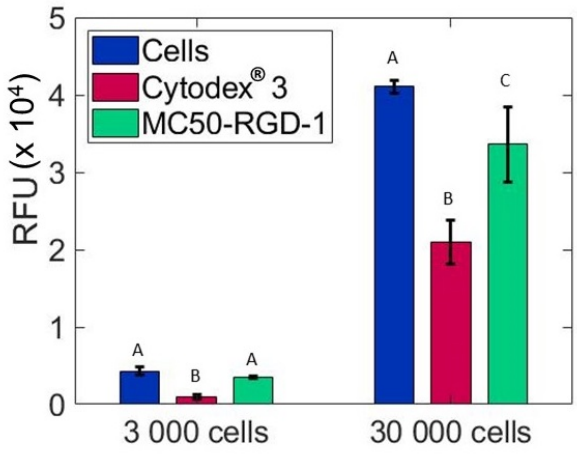

Figure 5.16.: DNA quantification of cells alone and cells in presence of MC50-RGD-1 and Cytodex® 3 using 3000 and 30000 cells. (N=2, n=3).

6

Stem cell culture on microcarriers in dynamic condition

A part of the results presented in this chapter was obtained by Dr A. Ajith Kumar with whom I was collaborating within the frame of the project.

6.1 Introduction

Dynamic cell culture using MC technology is expected to play a fundamental role in the successful development of novel and promising stem cell therapies destined to improve human health.[380] Dynamic cell culture on MCs can be implemented in conventional and well-characterized equipments such as ST bioreactors already used for non-adherent cell culture. This kind of equipment results in a homogeneous culture that can be monitored and controlled with ease, leading to more reproducible cultures.[48] The possibility of bead-to-bead transfer by addition of fresh MCs, without the need for enzymatic detachment, also contributes to the appeal of this technique. However, the potential harmful effects of shear stress and MC aggregation as well as the need for an additional downstream step for cell-MC separation and MC removal have to be considered when setting up dynamic cultures.[82]

The establishment of a successful dynamic cell culture on MCs is a complex process with a multitude of parameters requiring optimization. The selection of the appropriate MC is a fundamental component of cell expansion on MC and the following requirements need to be addressed:

1. Good stem cell adhesion
2. Efficient stem cell expansion and even differentiation on MCs

3. Facile and efficient cell harvesting from MCs

The inoculation protocol should be accurately optimized as the initial attachment efficiency is influenced by several factors such as cell and MC concentration, pH, temperature, medium composition, bioreactor configuration, and agitation protocol during the cell seeding period.[82] These parameters should also be closely controlled during the culture to ensure an optimal environment for cell growth.

Another important feature of dynamic culture is the ability of cells to detach from a specific MC and to colonize another one in a process known as bead-to-bead transfer.[35] This process is believed to be a key mechanism for rapid and efficient cell expansion in suspension cultures by allowing the addition of fresh MCs to ongoing cultures, providing additional surface area for cells to grow and thus extending culture duration while increasing the yield of produced cells.[380] This transfer of cells from the initial microcarriers to fresh ones added during the culture can be explained by two possible mechanisms.[381] The first one relies on exchange of cells during bead-to-bead contact thanks to the formation of cellular bridges between MCs during the intermittent agitation performed just after addition of the new MCs in the medium.[382, 383] The second mechanism is related to the detachment of cells from carriers and reattachment to uncolonized carriers.[384] Moreover, the addition of fresh MCs during the culture also proved to reduce the formation of MC aggregates.[90]

In the previous chapters, a novel MC consisting of a PLLA core biofunctionalized using an animal protein-free coating was developed and optimized to be used for dynamic culture. However, while culture in semi-static condition was performed using MCs prepared at 110°C, MCs crystallized at 103°C were used in dynamic condition as they have a similar morphology and density but a lower size leading to a more homogeneous suspension. In this chapter, the potential of these MCs for cell expansion in dynamic condition is thus evaluated. The possibility of performing bead-to-bead transfer to increase the yield of cell production without having to stop the culture is also investigated.

6.2 Experimental section

6.2.1 Materials

Mesenchymal Stem Cell Growth Medium 2 (basal medium supplemented with supplement mix) was purchased from Promocell. Dulbecco's phosphate buffered saline devoid of calcium and magnesium (DPBS)), StemPro™Accutase Cell Dissociation Reagent, Alexa Fluor™ 488 phalloidine, Calcein AM, and PrestoBlue™ Cell Viability reagent were provided by Thermo Fisher Scientific. PEST was obtained from Life Technologies. Triton™ X-100, BSA (96 %), glutaraldehyde aqueous solution (25 %), DAPI (98 %) and Sigmacote® were purchased from Sigma-Aldrich. Corning® Costar® Ultra-Low Attachment Multiple Well Plates were purchased from VWR. Cellstar® 24-well cell culture plates were purchased from Greiner Bio-one. 125 mL capacity spinner flasks equipped with a magnetic ball impellor (Magna-Flex™) obtained from Wheaton were used to perform cell culture in dynamic condition (Figure 6.1). Ethidium bromide was purchased from Biotium. Rhodamine-labeled poly(allylamine) (PAA) (15 000 g/mol) was purchased from Surflay Nanotec GmbH. hASCs were collected from lipoaspirates harvested from 1 adult donor who had provided his/her informed consent. Adipose tissues were enzymatically digested and ASCs were isolated by density gradient centrifugation and adherence to tissue culture plastic as previously described.[373]

Figure 6.1.: Magna-Flex™ spinner flask used for dynamic cell culture.

6.2.2 Microcarrier preparation and conditioning

MC50-RGD-1 crystallized at 103 °C were prepared for dynamic culture similarly as for semi-static culture (section 5.2.4). Briefly, they were first rinsed in ethanol 70% then transferred in sterile PBS. They were then placed in a petri dish and subsequently sterilized by exposure to UV light for 30 min. In order to prevent cell and MC adhesion on the inner surface of the spinner flask, it was siliconized with Sigmacote® reagent. After treatment, the spinner flask was thoroughly washed by Milli-Q water to remove the non-grafted product. The surface-modified spinner flask was autoclaved prior to use. MCs were then transferred to the spinner flask and the supernatant was removed and replaced by 20 mL of cell culture medium. The spinner flask was placed in the incubator at 37 °C and in a humidified 5% CO_2 atmosphere for conditioning for 30 min.

6.2.3 Cell culture on microcarriers in dynamic conditions

6.2.3.1. General procedure

MC50-RGD-1 crystallized at 103°C were used for dynamic culture assays. The general procedure for hASC culture on MC in dynamic condition is illustrated in Figure 6.2. After MC conditioning, the medium was removed and fresh culture medium was added to obtain a final MC concentration of 1 mg/mL. Cells were seeded at a density of 8 365 cells/mg MC or 3.5 cells per MC . In order to ensure cell adhesion, the spinner flask agitation was kept intermittent for 18 h, with a two min agitation at 45 rpm, followed by 28 min rest. The following day, the medium containing unattached cells was removed and fresh medium was added. The agitation was then continuous at 45 rpm throughout the culture period. The medium was completely replaced every three days. During the culture, a tiny fraction of MCs was collected at designated time points for analysis. In order to maintain consistency, the flask content was mixed by a gentle manual agitation and a representative sample was collected from the center of the culture content. One mL of the medium containing about 1 mg of MCs was transferred to individual wells of an ultra-low adhesion well-plate.

After MC settling, the supernatant was removed and MCs were rinsed with PBS for further analysis.

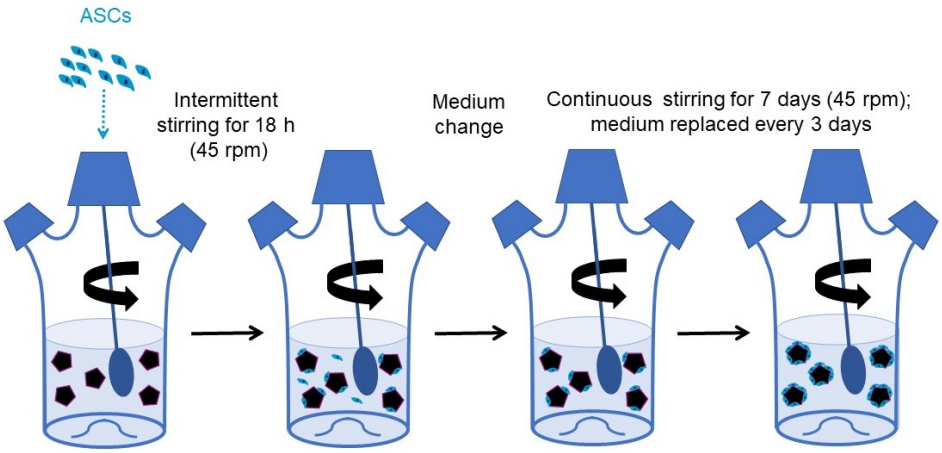

Figure 6.2.: Methodology used for hASC culture on MCs in dynamic condition.

6.2.3.2. Bead-to-bead cell transfer assays

When a first batch of cells cultured on MC50-RGD-1 in spinner flask was close to 50% confluency (at day 4), fresh MCs were added in the spinner flask at a 50% concentration of the initial MC concentration in order to perform bead-to-bead transfer. The LbL coating of these fresh MCs was labelled with PAA-Rhodamine (deposited as a first layer during the LbL deposition process) in order to discriminate them from MCs initially present in the flask. Just after the addition of fresh MCs, an intermittent agitation was applied (two min agitation at 45 rpm, followed by 28 min rest) for 12 h to encourage the transfer of cells from the initial MCs to the new MCs. The agitation was then changed to continuous mode at 45 rpm for the remaining duration of the culture. The overall procedure is summarized in Figure 6.3.

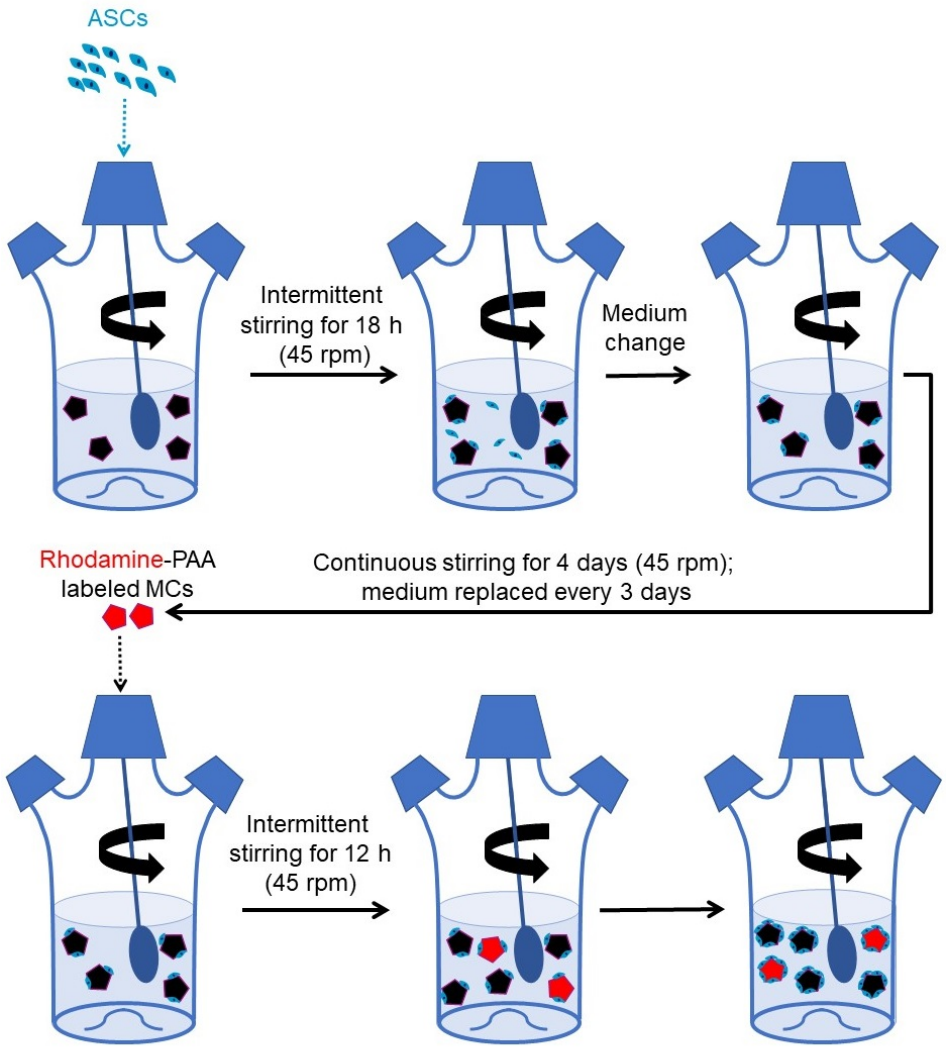

Figure 6.3.: Methodology used for bead-to-bead cell transfer assays performed with hASCs cultured on MC50-RGD-1. 50% of fresh MC50-RGD-1 (stained in red) were added to the existing culture after four days of cell expansion.

6.2.4 Cell characterization

6.2.4.1. Metabolic activity

Cell metabolic assays were performed according to the protocol described in section 5.2.6.1 for semi-static culture.

6.2.4.2. Cell viability

Live/Dead staining was performed according to the protocol described in section 5.2.6.3 for semi-static culture.

6.2.4.3. Cell nucleus and cytoskeleton staining

Morphological staining was performed according to the protocol described in section 5.2.6.4 for semi-static culture.

6.2.4.4. SEM observation

Cells grown on MC samples were fixed in 1 % (w/w) glutaraldehyde aqueous solution then serially dehydrated in 20, 40, 60, 80, 100 % (v/v) ethanol/water solutions (5 min each) followed by 10 min immersion in hexamethyldisilazane and overnight drying in fumehood. The dried samples were sputter-coated with a 10 nm-thick layer of gold and imaged by using a JEOL 7600F SEM operated at an acceleration voltage of 15 kV.

6.2.5 Statistical analysis

Numerical data are presented as mean values $\pm$ standard deviation. Statistical analyses were performed using one-way analysis of variance (ANOVA) followed by post hoc Tukey (HSD) test with a significance level set at alpha = 0.05 for comparison of multiple means.

6.3 Results and discussion

6.3.1 Cell proliferation

For the dynamic culture, PLLA cores prepared with a 50/50 PLLA40/PEG ratio crystallized at 103 °C were used. These PLLA cores showed the same morphology and porosity as the ones used for semi-static studies (Figure 3.14) but could be suspended better under gentle agitation, thanks to their lower average size. Similarly to the MCs used for semi-static culture, these MCs were also coated with a crosslinked $(PLO/HA)_8$ film postgrafted using 1 mM RGD peptide (MC50-RGD-1). An agitation speed of 45 rpm was selected as the best compromise between maintaining the MCs in suspension in the spinner flask and keeping cells on the MCs. No dead cells were observed on MC50-RGD-1, even after seven days of culture (Figure 6.4B). Cells were spindle-shaped as long as sufficient space was available on the MCs, after which they appeared very dense and clustered, probably due to cells reaching confluency. hASCs were metabolically active and continued to proliferate over time (Figure 6.4A). The number of cells on MCs increased by a 7.42 $\pm$ 0.97-fold between day 1 and day 4 and up to a 13.27 $\pm$ 2.27 fold increase between day 1 and day 7 to reach confluency (doubling time of 45 h). Slight MC aggregation was observed by day 7 due to cell-cell adhesion between MCs. MC aggregate formation was also reported for culture performed on commercial Cytodex® MCs, which caused mass transfer limitations forming stagnant cores leading to cell necrosis.[59, 90] However, in our study the MC aggregates were small-sized (250-400 µm) and did not cause cell death.

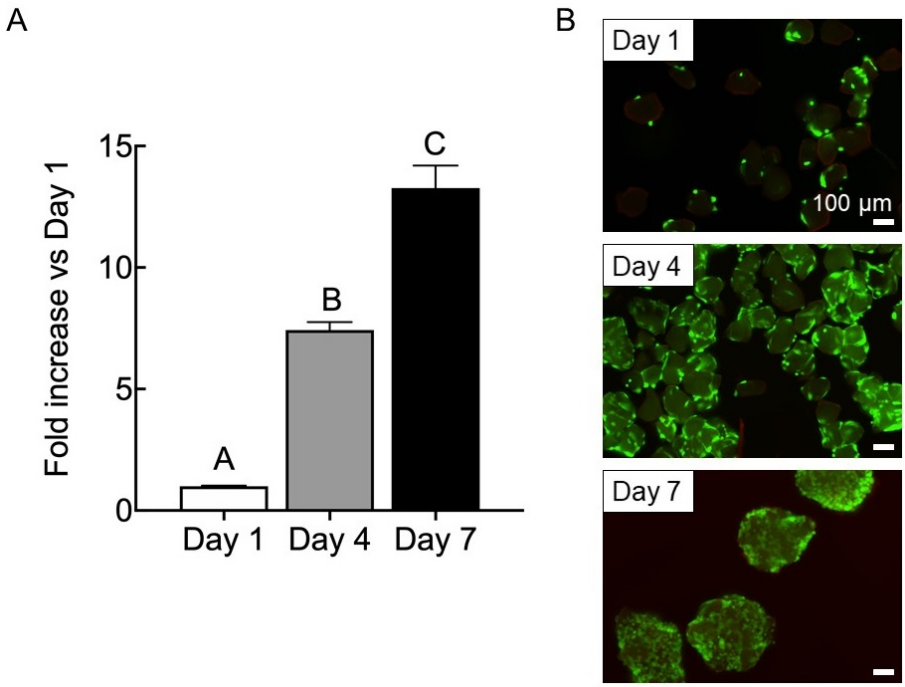

Figure 6.4.: Viability and proliferation of hASCs grown on MC50-RGD-1 in dynamic condition. (A) Quantification of cellular metabolic activity. (N=3, n=3). (B) Analysis of hASC viability by Live/Dead staining.

The morphology and cytoskeletal organization of hASCs grown on the MC50-RGD-1 surface was studied by staining of the cell cytoskeleton at different time points. The cell nucleus was simultaneously counter-stained with DAPI (Figure 6.5A). Layer-by-layer Z stacking and 3D reconstruction from the CLSM images showed that cells exhibited prominent actin fibers on the MC surface as early as on day 1 after seeding. By day 4, the cells spread on the MC surface with well-defined actin filaments which progressively increased with culture duration and covered the entire surface of the microcarriers by day 7. Additionally, SEM analysis was conducted at the same time points to characterize cell morphology on MCs. On day 1, the cells appeared rounded on the carriers (Figure 6.5B). But day 4 after seeding, cell flattened and appeared well spread over the MC surface. By day 7, the cells underwent active proliferation and formed several cell bridges with the adjacent MCs to form aggregates.

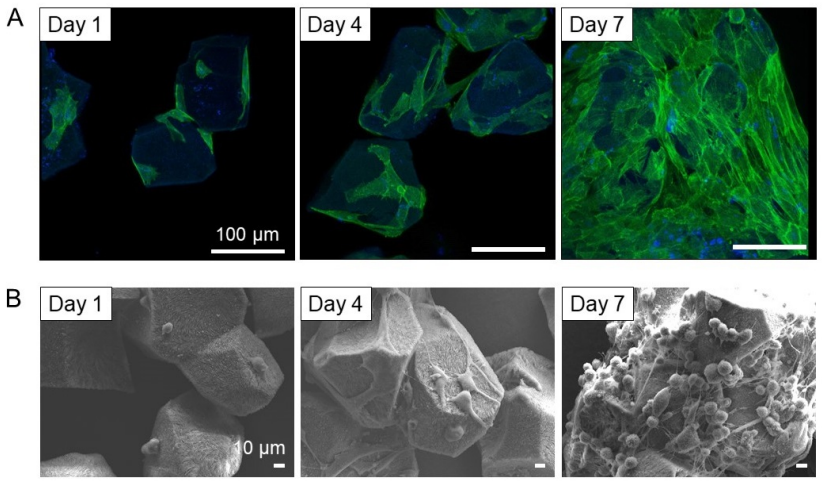

Figure 6.5.: Cytoskeletal organization and spreading of hASCs grown on MC50-RGD-1 surface: (A) CLSM micrographs of stained hASCs. Phalloidin stains actin filaments (green) and DAPI stains cell nuclei (blue). (B) SEM images of hASCs grown on MC50-RGD-1.

Several studies describing MSC expansion on various commercial MCs are available in the literature. Eibes *et al.* cultured MSCs on Cultispher®-S MCs in a spinner flask and obtained an 8.4-fold increase in the cell number on day 8.[385] A 4-fold increase in the growth rate of hMSCs was reported on Cytodex® 1 microcarriers on day 7 of spinner flask culture by Schop *et al*.[85] Similarly, a 13.6-fold expansion on Cytodex® 3 microcarriers was reported on day 11.[91] Even though a direct comparison with these earlier reports may not be accurate due to variations in cell type, cell source, methodology for cell characterization, culture medium and culture duration, it can be stated that the MCs developed in our study allowed a significantly high cell proliferation rates in dynamic culture over a short duration of seven days.

Here, we provide a proof-of-concept of dynamic culture but further improvements could be made. For example, MC concentration could be increased to offer the largest surface area per volume of culture. However, MC concentration selection requires a precise optimization as increasing MC concentration may result in damage to cells due to cell-MC and MC-MC collisions.[48] It was also reported that higher MC concentration and thus higher cell concentration per unit of volume could lead to reduced growth rate due to limited nutrient availability

[92] or accumulation of toxic metabolites and growth inhibitors produced by the cells.[386] As a result, feeding regimen might need to be adapted to avoid this phenomenon.

6.3.2 Bead-to-bead transfer

One advantage of dynamic culture on MCs is the possibility to increase the yield of cells at the end of the production period by the addition of fresh MCs during the proliferation phase to perform bead-to-bead transfer. This offers new surfaces to the cells to attach and proliferate thus extending culture duration. For example, *Hervy et al*. achieved successful expansion for 40 days with up to 10 000 fold-increase using bead-to-bead transfer.[84]

New MC50-RGD-1 were introduced into the spinner flasks at a ratio of 0.5:1 (new MCs:initial MCs), 4 days after initial seeding. To discriminate the fresh MCs from the initial ones, the coating of fresh MCs was labelled with PAA-rhodamine The culture was maintained at an intermittent mode of agitation for 12 h (*i.e.*, agitated for 2 min and then kept static for 28 min). Maintaining an intermittent agitation [387] allowed the MCs to be in close proximity with one another, which enabled transfer of cells from initial MCs to the new MCs, by a bridging effect.[382] It was observed that cell transfer started as early as one hour after the addition of fresh MCs. Twelve hours later, almost all the newly added MCs have been colonized by cells (Figure 6.6), and at this point the agitation was switched back to continuous mode. This study thus gives a direct evidence that hASCs display bead-to-bead transfer on the MC50-RGD-1.

Thanks to bead-to-bead transfer, subculturing is no longer required, reducing culture handling and minimizing the use of enzymatic agents.[380] This provides the benefits of both reducing costs and preserving cell integrity as frequent exposure to proteolytic enzymes has been shown to have adverse effects on mammalian cells such as proteome alteration [388], replicative senescence [389] and effects on cell shape and chromatin structure.[390] Interestingly, a "cells-on-bead" inoculation method has also been developed by Rafiq and coworkers, which consists in adding near-confluent MCs ($\approx$ 10 %) to inoculate a fresh MC culture, rather than using a cell suspension.[380] This technique has been reported to reduce the lag phase duration and increase cell proliferation rate.[380] This cells-on-bead inoculation method could be considered

to inoculate our new PLLA MC as it showed good results with various MCs (Hillex®, Cytodex® 3, Plastic Plus).[380]

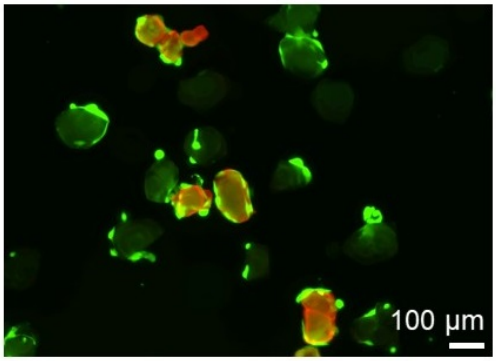

Figure 6.6.: Bead-to-bead cell transfer assay performed with hASCs cultured on MC50-RGD-1. 50% of fresh MC50-RGD-1 (stained in red) were added to the existing culture after four days of cell expansion. Images were taken after 12 h of intermittent agitation. Cells were stained with Calcein AM.

6.4 Conclusion

In this chapter, the performance of the surface-biofunctionalized PLLA MC optimized in previous chapters (MC50-RGD-1 crystallized at 103°C) for the expansion of hASCs is assessed in dynamic condition. This MC supported cell adhesion and proliferation in dynamic condition with more than a 13 fold increase observed between day 1 and day 7. We have also demonstrated qualitatively the ability of hASCs to migrate from one MC to another in order to colonize fresh MCs added during the culture. This possibility of bead-to-bead transfer offers a cost effective solution to scale up the commercial production of stem cells by extending the culture duration while minimizing culture handling and use of reagents.

7

Conclusion and perspectives

7.1 Conclusion

The aim of this thesis was to develop new biodegradable (i.e., compostable) MCs obtained through a green production process and showing tunable characteristics such as size, density, surface roughness, *etc.*, in an effort to deal with the complexity of dynamic culture. Moreover, we hoped to produce a magnetic version of these MCs in order to facilitate cell culture handling, monitoring and cell-MC separation.

Our first achievement was to successfully fabricate and characterize these MC cores composed of a biosourced, biodegradable and non-expensive polymer (PLLA), easy to produce with a scalable solvent-free process, which could even be industrially-composted after use for optimal circularity. Their preparation process which relies on the spherulitic crystallization of PLLA in a PLLA/PEG blend is extremely versatile, and the MC size, porosity and mechanical resistance can easily be optimized by tweaking trivial processing parameters such as crystallization temperature, PEG content and PLLA molar mass, without impacting the global process. Indeed, MC size was shown to depend primarily on the crystallization temperature while the PEG content dictates MC porosity and surface roughness. Different types of MC cores were thus produced in an effort to find the most suitable for dynamic culture (MC30, MC50, MC70). Adding to the versatility of the process, magnetic MC cores were also obtained by simply incorporating MNPs in the PLLA/PEG blend before crystallization. These magnetic MCs facilitate cell retrieval and separation from the MCs as well as routine culture handling.

Then, we focused on the surface biofunctionalization of the MC cores using an animal protein-free bioadhesive coating, which constitutes a supplementary

asset with respect to current regulations. For this, we used a crosslinked polysaccharide/polypeptide multilayer film composed of eight (PLO/HA) bilayers and obtained *via* the LbL technique. We demonstrated its successful deposition on PLLA surface. This coating was subsequently grafted with a bioadhesive RGD peptide for optimal cell adhesion. We qualitatively showed that a higher peptide concentration used during the grafting step led to a higher degree of peptide grafting on MC, allowing us to prepare MCs showing two different RGD grafting densities (MC-RGD-0.1 and MC-RGD-1).

Cell culture assays were then carried out in semi-static condition using the prepared MCs. This small-scale set-up gave us the opportunity to investigate the influence of various parameters in an effort to optimize culture conditions for subsequent dynamic culture. The growth medium and optimal cell seeding density were notably selected. The effect of MC surface morphology and composition of coating on cell adhesion and proliferation was investigated. We showed that the LbL coating alone had only a positive influence on cell spreading and proliferation and that the grafting of the RGD peptide at the higher concentration was necessary to obtain a higher cell number at the end of the culture. MC morphology also had an influence on cell behaviour with opposite effects on cell adhesion and proliferation: rougher MCs led to a higher initial adhesion while smoother MCs resulted in a higher cell proliferation. As it demonstrated both good cell adhesion/proliferation and appropriate characteristics for dynamic culture, MC50-RGD-1 was compared to the commercial Cytodex® 3 MC. The performance of both MCs regarding cell proliferation were comparable with a slight advantage for Cytodex® 3 while the detachment efficiency was qualitatively superior for MC50-RGD-1. hASCs were also able to differentiate towards adipogenic and osteogenic lineages on both MCs but further assays are required to obtain quantitative data. Finally, we demonstrated that the presence of MNPs in magnetic MCs did not impact cell proliferation. Magnetic MCs can thus be safely used to facilitate culture handling and cell retrieval.

Finally, our last achievement was to demonstrate that our MC50-RGD-1 supports growth and proliferation of stem cells in dynamic conditions and that the cell production yield can be increased by successful bead-to-bead transfer.

7.2 Future work

The results summarized in the previous section are promising but further researches need to be carried out for our new MCs to reach their full potential regarding dynamic cell expansion.

For example, as stated in chapter 6, MC initial concentration could be optimized to provide the highest surface area per volume of culture while limiting cell-MC and MC-MC collisions as well as nutrient depletion and accumulation of toxic metabolites. The bead-to-bead transfer protocol could also be optimized (fraction of fresh MC, agitation regimen, timing of addition) based on cell yield quantification. Similarly, exploring the cells-on-bead inoculation protocol described in section 6.4 might reveal interesting as it led to reduced lag phase and improved growth rate on other MCs.[380] Furthermore, the possibility of cryopreserving the cells adhered onto MCs should be investigated, especially if the cells-on-bead inoculation method is successful. Indeed, cryopreserving cell-MC constructs could allow to restart new cultures easily but has also perspectives for tissue engineering applications.[391]

Additional characterization of cells grown in dynamic condition could also be performed. For example, hASC differentiation potential following growth on MC in dynamic condition should be assessed as 3D dynamic culture has been reported to enhance osteogenic and adipogenic differentiation of MSCs.[88, 379] Furthermore, the immunomodulatory properties of the cells following 3D culture could be characterized as immunomodulation is believed to be one of the key mode of action of MSCs.[11, 14]

Regarding a potential industrial valorization, the scaling-up of the MC production process and surface biofunctionalization step would involve further work. For example, the large-scale production of MC cores could rely on an extrusion blending process. More importantly, the stability of the bioadhesive coating over time needs to be assessed to define optimal storage condition and shelf life, as freshly prepared MCs were systematically used in this study.

7.3 Alternative uses of microcarriers

Besides cell expansion, the MCs developed in this thesis could be considered for a wide range of applications. Thanks to the versatility of the fabrication process, MC characteristics can be tailored to suit different requirements.

First, our MCs could be used as immobilized substrates in PBRs. In this case, the reduced mechanical stress would allow to select the surface morphology leading to the best cell proliferation.

Alternatively, MCs can be used for tissue engineering applications. Microspheres are of particular interest because they are injectable and provide a localized effect to the desired site (which is not the case with a cell suspension) without hindering nutrient and waste diffusion.[392] These microspheres can act as a scaffold that prevents cell leakage and offers a solid surface for cell adhesion and growth.[392] For example, ASCs-laden MCs were used as building blocks that self-assemble into macrotissues in a bottom-up approach.[393] Using this strategy, high quality bone grafts (with a surface area of about $2\,cm^3$) were successfully engineered. In another study by Yan *et al.*, porous MCs fabricated from a strontium-substituted hydroxyapatite-graft-poly(γ-benzyl-L-glutamate) hybrid nanocomposite were developed. They allowed cells adhesion, infiltration, and proliferation and promoted the osteogenic differentiation of rabbit ASCs.[394] Successful healing of femoral bone defect was also reported following injection of these ASCs-seeded MCs in a rabbit model. In our case, as the PLLA MCs are composed of biocompatible FDA approved components and are animal- and organic solvent-free, directly implanting the cell-MC complexes is clearly a possibility. It should be noted, however, that PLLA displays a slow degradation, meaning that it can only be used for long-term applications. Also, even though they can be metabolized by the body, PLLA degradation products are acidic and can cause undesirable local changes in pH, which in turn provoke inflammation and limit tissue development.[395]

Similarly, MCs could also be exploited for drug delivery applications.[396–399] The use of porous microspheres for biomolecule delivery offers the advantages of a long-term, continuous, and controlled release of drugs or biomolecules, such as hormones, growth factors, *etc*., circumventing repetitive, timed doses that elicit a burst release upon administration.[392] For example, a therapeutic

protein (transforming growth factor β1) was encapsulated within PLGA microparticles by a novel emulsification/extraction process relying on non-volatile injectable solvents which are less toxic compared to other organic solvents.[400] The protein activity was preserved and good encapsulation as well as sustained release of the protein was achieved. In another work, the group of Jimbo demonstrated the use of PLGA microspheres loaded with either simvastatin [398] and clarithromycin [399] to enhance bone regeneration in rabbit calvaria defects. The microspheres demonstrated slow drug release for up to four weeks. This release kinetics was associated with the highest regeneration of new bone at extended healing periods. Interestingly, when MNPs are incorporated in MCs, magnetic targeting can be exploited to guide MCs to a desired location using an external magnetic field. More precisely, this technique, known as magnetic resonance navigation (MRN), relies on magnetic resonance imaging (MRI) devices and aims at navigating carriers in real-time along a pre-planned trajectory from their injection site to a targeted area. This approach minimizes systemic distribution of toxic agents loaded into the carriers and improves therapeutic efficacy by delivering a larger proportion of the drug injected.[401] For example, Pouponneau and coworkers reported the successful steering of doxorubicin-loaded magnetic PLGA microspheres both *in vitro* and *in vivo* in a rabbit model.[402] Using our porous PLLA MCs, drugs could be incorporated and then released from the LbL coating. Indeed, LbL films have been widely investigated for drug delivery purposes and have already proved their potential.[403, 404] The size and magnetic properties of our MCs may however require further optimization for MRN to be feasible.

Finally, MCs are of interest regarding the design of composite biomaterials.[405] More specifically, MCs can be easily embedded in hydrogel matrices,[406–411] and their encapsulation increases the mechanical strength of the gel, and offers a high cell-anchoring and spreading surface, thus improving cell viability.[408, 409] For example, Kandalam *et al.* integrated human marrow-isolated adult multilineage-inducible stem cells and MCs loaded with brain-derived neurotrophic factors (BDNF) into an injectable non-toxic silanized-hydroxypropyl methylcellulose hydrogel.[412] This system showed increased *in vitro* expression of neural/neuronal differentiation markers of the cells after one week as well as the secretion of various growth factors and chemokines, thus showing great promises for neural repair. Interestingly, these MCs loaded with BDNF were also combined with stem cells from the apical papilla and were injected in a rat spinal cord contusion model, resulting in improved locomotor function.[413] The com-

posite biomaterial strategy was even combined with 3D bioprinting in a work by Levato *et al.* They fabricated living constructs via bioprinting of cell-laden MCs encapsulated in gelatin methacrylamide-gellan gum bioinks.[406]. As reported before, MCs acted as a mechanical reinforcement to the soft matrix and the encapsulation of MC-MSCs complexes led to improved cell adhesion, cell–cell contacts and bone matrix deposition without compromising the printability of the bioinks.

These different examples demonstrate the large potential of our MCs for various biomedical applications, which stems from their highly versatile fabrication process.

Bibliography

1. Avasthi, S., Srivastava, R. N., Singh, A. & Srivastava, M. Stem cell : past, present and future. *Internet J. Med. Updat.* **3,** 22–30 (2008).
2. Ilic, D. & Polak, J. M. Stem cells in regenerative medicine: Introduction: *Br. Med. Bull.* **98,** 117–126 (2011).
3. Zare, S., Kurd, S., Rostamzadeh, A. & Nilforoushzadeh, M. A. Types of stem cells in regenerative medicine: A review. *J. Ski. Stem Cell* **1,** 1–5 (2014).
4. Mizuno, H., Tobita, M. & Uysal, A. C. Concise review: adipose-derived stem cells as a novel tool for future regenerative medicine. *Stem Cells* **30,** 804–810 (2013).
5. Kolios, G. & Moodley, Y. Introduction to stem cells and regenerative medicine. *Respiration* **85,** 3–10 (2012).
6. Lindroos, B., Suuronen, R. & Miettinen, S. The potential of adipose stem cells in regenerative medicine. *Stem Cell Rev. Reports* **7,** 269–291 (2011).
7. Ng., A. P. & Alexander, W. S. Haematopoietic stem cells : past, present and future. *Cell Death Discov.* **3,** 2–5 (2017).
8. Dominici, M., Le Blanc, K., Mueller, I., Slaper-Cortenbach, I., Marini, F. C., Krause, D. S., Deans, R. J., Keating, A., Prockop, D. J. & Horwitz, E. M. Minimal criteria for defining multipotent mesenchymal stromal cells. The International Society for Cellular Therapy position statement. *Cytotherapy* **8,** 315–317 (2006).
9. Friedenstein, A. J., Piatetzky-Shapiro, I. I. & Petrakova, K. V. Osteogenesis in transplants of bone marrow cells. *J. Embryol. Exp. Morphol.* **16,** 381–390 (1966).
10. Nagata, T., Mitsumori, T. & Iwaguro, H. Adipose tissue-derived stem and regenerative cells for tissue regeneration. *J. Oral Biosci.* **55,** 127–131 (2013).

11. Lavoie, J. R. & Rosu-myles, M. Uncovering the secretes of mesenchymal stem cells. *Biochimie* **95,** 2212–2221 (2013).

12. Quevedo, H. C., Hatzistergos, K. E., Oskouei, B. N., Feigenbaum, G. S., Rodriguez, J. E., Valdes, D., Pattany, P. M., Zambrano, J. P., Hu, Q., Mcniece, I., Heldman, A. W. & Hare, J. M. Allogeneic mesenchymal stem cells restore cardiac function in chronic ischemic cardiomyopathy via trilineage differentiating capacity. *Proc. Natl. Acad. Sci. U. S. A.* **106,** 14022–14027 (2009).

13. Taraballi, F., Pastò, A., Bauza, G., Varner, C., Amadori, A. & Tasciotti, E. Immunomodulatory potential of mesenchymal stem cell role in diseases and therapies: A bioengineering prospective. *J. Immunol. Regen. Med.* **4,** 100017 (2019).

14. Singer, N. G. & Caplan, A. I. Mesenchymal stem cells : mechanisms of inflammation. *Annu. Reivews Pathol. Mech. Dis.* **6,** 457–478 (2011).

15. Cheng, K. H., Kuo, T. L., Kuo, K. K. & Hsiao, C. C. Human adipose-derived stem cells: Isolation, characterization and current application in regeneration medicine. *Genomic Med. Biomarkers, Heal. Sci.* **3,** 53–62 (2011).

16. Gimble, J. M., Katz, A. J. & Bunnell, B. A. Adipose-derived stem cells for regenerative medicine. *Circ. Res.* **100,** 1249–1260 (2007).

17. Zuk, P. A., Zhu, M., Mizuno, H., Huang, J., Futrell, J. W., Katz, A. J., Benhaim, P., Lorenz, H. P. & Hedrick, M. H. Multilineage cells from human adipose tissue : Implications for cell-based therapies. *Tissue Eng.* **7,** 211–228 (2001).

18. Bajek, A., Gurtowska, N., Olkowska, J., Kazmierski, L., Maj, M. & Drewa, T. Adipose-derived stem cells as a tool in cell-based therapies. *Arch. Immunol. Ther. Exp. (Warsz).* **64,** 443–454 (2016).

19. M. Gimble, J. & E. Nuttall, M. Adipose-derived stromal/stem cells (ASC) in regenerative medicine: pharmaceutical applications. *Curr. Pharm. Des.* **17,** 332–339 (2011).

20. Mizuno, H. Adipose-derived stem cells for regenerative medicine in the field of plastic and reconstructive surgery. *J. Oral Biosci.* **55,** 132–136 (2013).

21. Barba, M., Di Taranto, G. D. & Lattanzi, W. Adipose-derived stem cell therapies for bone regeneration. *Expert Opin. Biol. Ther.* **17,** 677–689 (2017).

22. Sterodimas, A., De Faria, J., Nicaretta, B. & Pitanguy, I. Tissue engineering with adipose-derived stem cells (ADSCs): Current and future applications. *J. Plast. Reconstr. Aesthetic Surg.* **63,** 1886–1892 (2010).

23. Palumbo, P., Lombardi, F., Siragusa, G., Cifone, M. G., Cinque, B. & Giuliani, M. Methods of isolation, characterization and expansion of human adipose-derived stem cells (ASCs): an overview. *Int. J. Mol. Sci.* (2018).

24. Rada, T., Reis, R. L. & Gomes, M. E. Adipose tissue-derived stem cells and their application in bone and cartilage tissueeEngineering. *Tissue Eng. Part B* **15,** 113–125 (2009).

25. Kim Y., Kim H., Cho H., Bae Y., Suh K. and Jung J. Direct comparison of human mesenchymal stem cells derived from adipose tissues and bone marrow in mediating neovascularization in response to vascular ischemia. *Cell Physiol Biochem..* **20,** 867–876 (2007).

26. Thomas, E. D., Storb, R., Clift, R. A., Fefer, A., Johnson, L., Neiman, P. E., Lerner, K. G., Glucksberg, H. & Buckner, C. D. Bone-marrow transplantation. *N. Engl. J. Med.* **292,** 832–843 (1975).

27. Heathman, T. R., Nienow, A. W., McCall, M. J., Coopman, K., Kara, B. & Hewitt, C. J. The translation of cell-based therapies: Clinical landscape and manufacturing challenges. *Regen. Med.* **10,** 49–64 (2015).

28. Whitaker, M., Foley, L. & Ward, S. in *Bioprocess. Cell Based Ther.* (ed Connon, C. J.) (2016).

29. Nienow, W., Mccall, M. J., Coopman, K., Kara, B. & Hewitt, C. J. The translation of cell-based therapies : clinical landscape and manufacturing challenges. *Regen. Med.* **10,** 49–64 (2015).

30. Mason, C. & Dunnill, P. Assessing the value of autologous and allogeneic cells for regenerative medicine. *Regen. Med.* **4,** 835–853 (2009).

31. Squillaro, T., Peluso, G. & Galderisi, U. Clinical trials with mesenchymal stem cells : an update. *Cell Transplant.* **25,** 829–848 (2016).

32. Kabat, M., Bobkov, I., Kumar, S. & Grumet, M. Trends in mesenchymal stem cell clinical trials 2004-2018 : Is efficacy optimal in a narrow dose range ? *Stem Cells Transl. Med.* **9,** 17–27 (2020).

33. Argentati, C., Morena, F., Bazzucchi, M., Armentano, I., Emiliani, C. & Martino, S. Adipose stem cell translational applications : From bench-to-bedside. *Int. J. Mol. Sci.* **19,** 3475 (2018).

34. Blasimme, A. & Sebbag, E. R. Regulation of cell - based therapies in Europe : current challenges and emerging issues. *Stem Cells Dev.* **22,** 14–19 (2013).

35. De Soure, A. M., Fernandes-platzgummer, A., Silva, C. L. & Cabral, J. M. S. Scalable microcarrier-based manufacturing of mesenchymal stem / stromal cells. *J. Biotechnol.* **236,** 88–109 (2016).

36. European Medicines Agency. *Guideline on the use of bovine serum in the manufacture of human biological medicinal products* 2013.

37. Spees, J. L., Gregory, C. A., Singh, H., Tucker, H. A., Peister, A., Lynch, P. J., Hsu, S.-c., Smith, J. & Prockop, D. J. Internalized antigens must be removed to prepare hypoimmunogenic mesenchymal stem cells for cell and gene therapy. *Mol. Ther.* **9,** 747–756 (2004).

38. Lindroos, B., Boucher, S., Chase, L., Kuokkanen, H., Huhtala, H., Haataja, R., Vemuri, M., Suuronen, R. & Miettinen, S. Serum-free , xeno-free culture media maintain the proliferation rate and multipotentiality of adipose stem cells in vitro. *Cytotherapy* **11,** 958–972 (2009).

39. López-Beas, J., Guadix, J. A., Clares, B., Soriano-Ruiz, J. L., Zugaza, J. L. & Gálvez-Martín, P. An overview of international regulatory frameworks for mesenchymal stromal cell-based medicinal products: From laboratory to patient. *Med. Res. Rev.* **40,** 1315–1334 (2020).

40. European Medicines Agency. *Reflection paper on classification of advanced therapy medicinal products Reflection paper on classification of Advanced Therapy Medicinal Products Table of contents* 2015.

41. Mount, N. M., Ward, S. J., Kefalas, P. & Hyllner, J. Cell-based therapy technology classifications and translational challenges. *Philos. Trans. R. Soc. B Biol. Sci.* **370,** 20150017 (2015).

42. Ozdil, D. & Aydin, H. M. in *Adv. Surfaces Stem Cell Res.* (eds Tiwari, A., Garipcan, B. & Uzun, L.) 323–342 (2016).

43. Whitaker, M., Foley, L. & Ward, S. in *Bioprocess. Cell Based Ther.* (ed Connon, C. J.) First Edit, 1–33 (John Wiley & Sons, 2017).

44. Auquier, P. & Toumi, M. Advanced therapy medicinal products: current and future perspectives ´. *J. Mark. Access Heal. Policy* **1,** 1–10 (2016).

45. Cuende, N., Rasko, J. E. J. & Koh, M. B. C. Cell , tissue and gene products with marketing authorization in 2018 worldwide. *Cytotherapy* **20,** 1401–1413 (2018).

46. Markicheva, E. & Grandfils, C. in *Biomater. Cell Immobil.* 734–763 (2004).

47. Heathman, T. R., Rafiq, Q. A., Coopman, K., Nienow, A. W. & Hewitt, C. J. in *Bioprocess. Cell Based Ther.* 91–125 (Wiley-Blackwell, 2016).

48. Merten, O.-W. Advances in cell culture: anchorage dependence. *Philos. Trans. R. Soc. Lond. B. Biol. Sci.* **370,** 20140040 (2015).

49. Schnitzler, A. C., Verma, A., Kehoe, D. E., Jing, D., Murrell, J. R., Der, K. A., Aysola, M., Rapiejko, P. J., Punreddy, S. & Rook, M. S. Bioprocessing of human mesenchymal stem/stromal cells for therapeutic use: Current technologies and challenges. *Biochem. Eng. J.* **108,** 3–13 (2016).

50. Spier, M. R., Porto, L., Vandenberghe, D. S., Bianchi, A., Medeiros, P. & Soccol, C. R. in *Bioreact. Des. Prop. Appl.* (eds Antolli, P. G. & Liu, Z.) 55–90 (2011).

51. Ryan, J. A. *Growing more cells: A simple guide to small volume cell culture scale-up* 2008.

52. Halsall, J. & Davis, J. M. in *Anim. Cell Cult. Essent. Methods* 143–171 (2007).

53. Bos, C. V. D., Keefe, R., Schirmaier, C. & McCaman, M. Therapeutic human cells : manufacture for cell therapy / regenerative medicine. *Adv. Biochem. Eng. / Biotechnol.* **138,** 61–97 (2014).

54. Wezel, A. L. V. Growth of cell-strains and primary cells on micro-carriers in homogeneous culture. *Nature* **216,** 64 (1967).

55. GEHealthcare. *Microcarrier Cell Culture Technology : Principles and Methods* 2007.

56. Jossen, V., van den Bos, C., Eibl, R. & Eibl, D. Manufacturing human mesenchymal stem cells at clinical scale: process and regulatory challenges. *Appl. Microbiol. Biotechnol.* **102,** 3981–3994 (2018).

57. Mizukami, A. & Swiech, K. Mesenchymal stromal cells : From discovery to manufacturing and commercialization. *Stem Cells Int.* **2018,** 1–14 (2018).

58. Sart, S., Schneider, Y.-J., Li, Y. & Agathos, S. N. Stem cell bioprocess engineering towards cGMP production and clinical applications. *Cytotechnology* **66,** 709–722 (2014).

59. Jossen, V., Schirmer, C., Mostafa Sindi, D., Eibl, R., Kraume, M., Pörtner, R. & Eibl, D. Theoretical and practical issues that are relevant when scaling up hMSC microcarrier production processes. *Stem Cells Int.* **2016,** 1–15 (2016).

60. Singh, V. Disposable bioreactor for cell culture using wave-induced agitation. *Cytotechnology* **30,** 149–158 (1999).

61. Robb, K. P., Fitzgerald, J. C. & Barry, F. Mesenchymal stromal cell therapy: progress in manufacturing and assessments of potency. *Cytotherapy,* 1–18 (2018).

62. Meuwly, F., Ruffieux, P., Kadouri, A. & Stockar, U. V. Packed-bed bioreactors for mammalian cell culture : Bioprocess and biomedical applications. *Biotechnol. Adv.* **25,** 45–56 (2007).

63. Lund, A. W., Yener, B., Stegemann, J. P. & Plopper, G. E. The natural and engineered 3D microenvironment as a regulatory cue during stem cell fate determination. *Tissue Eng. Part B* **15,** 371–380 (2009).

64. Godara, P., Mcfarland, C. D. & Nordon, R. E. Design of bioreactors for mesenchymal stem cell tissue engineering. *J. Chem. Technol. Biotechnol.* **420,** 408–420 (2008).

65. Knazel, R. A., Wu, Y.-W., Aebersold, P. M. & Rosenberg, S. A. Culture of human tumor infiltrating lymphocytes in hollow fiber bioreactors. *J. Immunol. Methods* **127,** 29–37 (1990).

66. Vymetalova, L., Kucirkova, T., Knopfova, L., Pospisilova, V. & Kasko, T. Large-scale automated hollow-fiber bioreactor expansion of umbilical cord-derived human mesenchymal stromal cells for neurological disorders. *Neurochem. Res.* **45,** 204–214 (2020).

67. Mennan, C., Garcia, J., Roberts, S., Hulme, C. & Wright, K. A comprehensive characterisation of large- scale expanded human bone marrow and umbilical cord mesenchymal stem cells. **4,** 1–15 (2019).

68. Frank, N. D., Jones, M. E., Vang, B. & Coeshott, C. Evaluation of reagents used to coat the hollow-fiber bioreactor membrane of the Quantum ® Cell Expansion System for the culture of human mesenchymal. *Mater. Sci. Eng. C* **96,** 77–85 (2019).

69. Greuel, S., Hanci, G., Böhme, M., Miki, T., Schubert, F., Sittinger, M., Fredrik, C., Katrin, M. & Nora, Z. Effect of inoculum density on human - induced pluripotent stem cell expansion in 3D bioreactors, 1–12 (2019).

70. Tirughana, R., Metz, M. Z., Li, Z., Hall, C., Hsu, D., Beltzer, J., Annala, A. J., Oganesyan, D., Gutova, M. & Aboody, K. S. GMP production and scale-up of adherent neural stem cells with a quantum cell expansion system. *Mol. Ther. Methods Clin. Dev.* **10,** 48–56 (2018).

71. Haack-sørensen, M. & Juhl, M. Development of large-scale manufacturing of adipose-derived stromal cells for clinical applications using bioreactors and human platelet lysate. *Scand. J. Clin. Lab. Invest.* **78,** 293–300 (2018).

72. Rodrigues, C. A. V., Fernandes, T. G., Diogo, M. M., Lobato, C. & Cabral, J. M. S. Stem cell cultivation in bioreactors. *Biotechnol. Adv.* **29,** 815–829 (2011).

73. Weber, C., Freimark, D., Pörtner, R., Pino-grace, P. & Pohl, S. Expansion of human mesenchymal stem cells in a fixed-bed bioreactor system based on non-porous glass carrier – Part A : Inoculation , cultivation , and cell harvest procedures. *Int. J. Artif. Organs* **33,** 512–525 (2010).

74. Mizukami, A., Pereira, T. D., Orellana, M. D., Abreu, M., Covas, D. T., Farid, S. S. & Swiech, K. Technologies for large-scale umbilical cord-derived MSC expansion : Experimental performance and cost of goods analysis. *Biochem. Eng. J.* **135,** 36–48 (2018).

75. Morrow K.J. Disposable Bioreactors Gaining Favour: New Components and Systems Improve Process Reliability and Reduce Cost. *Genetic Engineering News* **26,** 42–45 (2006).

76. Simaria, A. S., Hassan, S., Varadaraju, H., Rowley, J., Warren, K., Vanek, P. & Farid, S. S. Allogeneic cell therapy bioprocess economics and optimization: Single-use cell expansion technologies. *Biotechnol. Bioeng.* **111,** 69–83 (2014).

77. Lam, A. T. L., Chen, A. K. L., Ting, S. Q. P., Reuveny, S. & Oh, S. K. W. Integrated processes for expansion and differentiation of human pluripotent stem cells in suspended microcarriers cultures. *Biochem. Biophys. Res. Commun.* **473,** 764–768 (2016).

78. Rafiq, Q. A., Coopman, K., Nienow, A. W. & Hewitt, C. J. Systematic microcarrier screening and agitated culture conditions improve human mesenchymal stem cell yield in bioreactors. *Biotechnol. J.* **11,** 473–486 (2016).

79. Sart, S., Agathos, S. N. & Li, Y. Engineering stem cell fate with biochemical and biomechanical properties of microcarriers. *Biotechnol. Prog.* **29,** 1354–1366 (2013).

80. Chen, A. K.-L., Reuveny, S. & Oh, S. K. W. Application of human mesenchymal and pluripotent stem cell microcarrier cultures in cellular therapy: Achievements and future direction. *Biotechnol. Adv.* **31,** 1032–1046 (2013).

81. Nilsson, K. in *Biotechnol. Genet. Eng. Rev.* 403–439 (1989).

82. Badenes, S. M., Fernandes-Platzgummer, A., Rodrigues, C. A., Diogo, M. M., Da Silva, C. L. & Cabral, J. M. *Microcarrier culture systems for stem cell manufacturing* 77–104 (Elsevier B.V., 2016).

83. Tan, K. Y., Reuveny, S., Kah, S., Oh, W. & Oh, S. K. W. Recent advances in serum-free microcarrier expansion of mesenchymal stromal cells: Parameters to be optimized. *Biochem. Biophys. Res. Commun.* **473,** 769–773 (2016).

84. Hervy, M., Weber, J. L., Pecheul, M., Dolley-Sonneville, P., Henry, D., Zhou, Y. & Melkoumian, Z. Long term expansion of bone marrow-derived hMSCs on novel synthetic microcarriers in xeno-free, defined conditions. *PLoS One* **9,** 1–8 (2014).

85. Schop, D., van Dijkhuizen-Radersma, R., Borgart, E., Janssen, F. W., Rozemuller, H., Prins, H.-J. H.-J. & De Bruijn, J. Expansion of human mesenchymal stromal cells on microcarriers: growth and metabolism. *J. Tissue Eng. Regen. Med.* **4,** 131–140 (2010).

86. Dos Santos, F., Campbell, A., Fernandes-Platzgummer, A., Andrade, P. Z., Gimble, J. M., Wen, Y., Boucher, S., Vemuri, M. C., Da Silva, C. L. & Cabral, J. M. A xenogeneic-free bioreactor system for the clinical-scale expansion of human mesenchymal stem/stromal cells. *Biotechnol. Bioeng.* **111,** 1116–1127 (2014).

87. Caruso, S. R., Orellana, M. D., Mizukami, A., Fernandes, T. R., Fontes, A. M., Suazo, C. A., Oliveira, V. C., Covas, D. T. & Swiech, K. Growth and functional harvesting of human mesenchymal stromal cells cultured on a microcarrier-based system. *Biotechnol. Prog.* **30,** 889–895 (2014).

88. Sun, L. Y., Hsieh, D. K., Syu, W. S., Li, Y. S., Chiu, H. T. & Chiou, T. W. Cell proliferation of human bone marrow mesenchymal stem cells on biodegradable microcarriers enhances in vitro differentiation potential. *Cell Prolif.* **43,** 445–456 (2010).

89. Santos, F. D., Andrade, P. Z., Abecasis, M. M., Gimble, J. M., Chase, L. G., Campbell, A. M., Boucher, S., Vemuri, M. C., Silva, C. L. D. & Cabral, J. M. Toward a clinical-grade expansion of mesenchymal stem cells from human sources: A microcarrier-based culture system under xeno-free conditions. *Tissue Eng. Part C Methods* **17,** 1201–1210 (2011).

90. Ferrari, C., Balandras, F., Guedon, E., Olmos, E., Chevalot, I. & Marc, A. Limiting cell aggregation during mesenchymal stem cell expansion on microcarriers. *Biotechnol. Prog.* **28,** 780–787 (2012).

91. Goh, T. K.-P., Zhang, Z.-Y., Chen, A. K.-L., Reuveny, S., Choolani, M., Chan, J. K. Y. & Oh, S. K.-W. Microcarrier culture for efficient expansion and osteogenic differentiation of human fetal mesenchymal stem cells. *Biores. Open Access* **2,** 84–97 (2013).

92. Chen, A. K. L., Chew, Y. K., Tan, H. Y., Reuveny, S. & Oh, S. K. W. Increasing efficiency of human mesenchymal stromal cell culture by optimization of microcarrier concentration and design of medium feed. *Cytotherapy* **17,** 163–173 (2015).

93. Schirmaier, C., Jossen, V., Kaiser, S. C., Jüngerkes, F., Brill, S., Safavi-Nab, A., Siehoff, A., van den Bos, C., Eibl, D. & Eibl, R. Scale-up of adipose tissue-derived mesenchymal stem cell production in stirred single-use bioreactors under low-serum conditions. *Eng. Life Sci.* **14,** 292–303 (2014).

94. Nienow, A. W., Rafiq, Q. A., Coopman, K. & Hewitt, C. J. A potentially scalable method for the harvesting of hMSCs from microcarriers. *Biochem. Eng. J.* **85,** 79–88 (2014).

95. Berry, J. D., Liovic, P., Šutalo, I. D., Stewart, R. L., Glattauer, V. & Meagher, L. Characterisation of stresses on microcarriers in a stirred bioreactor. *Appl. Math. Model.* **40,** 6787–6804 (2016).

96. Stolberg, S. & McCloskey, K. E. Can shear stress direct stem cell fate? *Biotechnol. Prog.* **25,** 10–19 (2009).

97. Knippenberg, M., Helder, M. N., Doulabi, B. Z., Semeins, C. M., Wuisman, P. I. & Klein-Nulend, J. Adipose Tissue-Derived Mesenchymal Stem Cells Acquire Osteogenic Stimulation. *Tissue Eng.* **11,** 1780–1788 (2005).

98. Hao, J., Zhang, Y., Jing, D., Shen, Y., Tang, G., Huang, S. & Zhao, Z. Mechanobiology of mesenchymal stem cells: Perspective into mechanical induction of MSC fate. *Acta Biomater.* **20,** 1–9 (2015).

99. Kreke, M. R., Sharp, L. A., Woo Lee, Y. & Goldstein, A. S. Effect of intermittent shear stress on mechanotransductive signaling and osteoblastic differentiation of bone marrow stromal cells. *Tissue Eng. - Part A.* **14,** 529–537 (2008).

100. Dong, J. D., Gu, Y. Q., Li, C. M., Wang, C. R., Feng, Z. G., Qiu, R. X., Chen, B., Li, J. X., Zhang, S. W., Wang, Z. G. & Zhang, J. Response of mesenchymal stem cells to shear stress in tissue-engineered vascular grafts. *Acta Pharmacol. Sin.* **30,** 530–536 (2009).

101. Zhang, J., Cui, Z., Field, R., Moloney, M. G., Rimmer, S. & Ye, H. Thermoresponsive microcarriers based on poly(N-isopropylacrylamide). *Eur. Polym. J.* **67,** 346–364 (2015).

102. Tavassoli, H., Alhosseini, S. N., Tay, A., Chan, P. P., Oh, S. K. W. & Warkiani, M. E. Large-scale production of stem cells utilizing microcarriers: A biomaterials engineering perspective from academic research to commercialized products. *Biomaterials* **181,** 333–346 (2018).

103. Global Cell Solution. *BioLevitator Cell Culture Handbook* (2009).

104. Weber, C., Kassem, M., Pohl, S., Pörtner, R., Wallrapp, C., Peter, G. & Czermak, P. Expansion and Harvesting of hMSC-TERT. *Open Biomed. Eng. J.* **1,** 38–46 (2007).

105. Luck, S., Schubel, R., Rub, J., Hahn, D., Mathieu, E., Zimmermann, H., Scharnweber, D., Werner, C., Pautot, S. & Jordan, R. Tailored and biodegradable poly(2-oxazoline) microbeads as 3D matrices for stem cell culture in regenerative therapies. *Biomaterials* **79,** 1–14 (2016).

106. Li, W., Lu, L., Jiao, Y., Zhang, C. & Zhou, C. Poly(L-lactide) crystallization topography directs MC3T3-E1 cells response. *J. Biomater. Sci. Polym. Ed.* **5063** (2016).

107. Song, K., Yang, Y., Wu, S., Zhang, Y., Feng, S., Wang, H., Wang, Y., Wang, L. & Liu, T. In vitro culture and harvest of BMMSCs on the surface of a novel thermosensitive glass microcarrier. *Mater. Sci. Eng. C* **58,** 324–330 (2016).

108. Yang, H. S., Jeon, O., Bhang, S. H., Lee, S. H. & Kim, B. S. Suspension culture of mammalian cells using thermosensitive microcarrier that allows cell detachment without proteolytic enzyme treatment. *Cell Transplant.* **19,** 1123–1132 (2010).

109. Lam, A. T. L., Li, J., Toh, J. P. W., Sim, E. J. H., Chen, A. K. L., Chan, J. K. Y., Choolani, M., Reuveny, S., Birch, W. R. & Oh, S. K. W. Biodegradable poly-ε-caprolactone microcarriers for efficient production of human mesenchymal stromal cells and secreted cytokines in batch and fed-batch bioreactors. *Cytotherapy* **19,** 419–432 (2017).

110. Zhou, A., Ye, Z., Zhou, Y. & Tan, W. S. Bioactive poly(ε-caprolactone) microspheres with tunable open pores as microcarriers for tissue regeneration. *J. Biomater. Appl.* **33,** 1242–1251 (2019).

111. Li, J., Lam, A. T.-L., Toh, J. P. W., Reuveny, S., Oh, S. K.-W. & Birch, W. R. Fabrication of uniform-sized poly-ε-caprolactone microspheres and their applications in human embryonic stem cell culture. *Biomed. Microdevices* **17,** 105 (2015).

112. Hong, Y., Gao, C., Xie, Y., Gong, Y. & Shen, J. Collagen-coated polylactide microspheres as chondrocyte microcarriers. *Biomaterials* **26,** 6305–6313 (2005).

113. Li, L., Song, K., Chen, Y., Wang, Y., Shi, F., Nie, Y. & Liu, T. Design and biophysical characterization of poly (L-Lactic) acid microcarriers with and without modification of chitosan and nanohydroxyapatite. *Polymers (Basel).* **10** (2018).

114. Gabler, F., Frauenschuh, S., Ringe, J., Brochhausen, C., Götz, P., Kirkpatrick, C. J., Sittinger, M., Schubert, H. & Zehbe, R. Emulsion-based synthesis of PLGA-microspheres for the in vitro expansion of porcine chondrocytes. *Biomol. Eng.* **24,** 515–520 (2007).

115. Li, W., Han, Y., Yang, H., Wang, G., Lan, R. & Wang, J. Y. Preparation of microcarriers based on zein and their application in cell culture. *Mater. Sci. Eng. C* **58,** 863–869 (2016).

116. Huang, L., Xiao, L., Jung Poudel, A., Li, J., Zhou, P., Gauthier, M., Liu, H., Wu, Z. & Yang, G. Porous chitosan microspheres as microcarriers for 3D cell culture. *Carbohydr. Polym.* **202,** 611–620 (2018).

117. Tan, H., Huang, D., Lao, L. & Gao, C. RGD modified PLGA/gelatin microspheres as microcarriers for chondrocyte delivery. *J. Biomed. Mater. Res. - Part B Appl. Biomater.* **91,** 228–238 (2009).

118. Staff, R. H., Schaeffel, D., Turshatov, A. & Donadio, D. Particle Formation in the Emulsion-Solvent Evaporation Process. *Small* **9,** 3514–3522 (2013).

119. Park, J.-h. & Pe, A. Microcarriers designed for cell culture and tissue engineering of bone. *Tissue Eng. Part B* **19,** 172–190 (2013).

120. Kim, T. K., Yoon, J. J., Lee, D. S. & Park, T. G. Gas foamed open porous biodegradable polymeric microspheres. *Biomaterials* **27,** 152–159 (2006).

121. Bhuptani, R. S. & Patravale, V. B. Porous microscaffolds for 3D culture of dental pulp mesenchymal stem cells. *Int. J. Pharm.* **515,** 555–564 (2016).

122. Shekaran, A., Lam, A., Sim, E., Jialing, L., Jian, L., Wen, J. T. P., Chan, J. K. Y., Choolani, M., Reuveny, S., Birch, W. & Oh, S. Biodegradable ECM-coated PCL microcarriers support scalable human early MSC expansion and in vivo bone formation. *Cytotherapy* **18,** 1332–1344 (2016).

123. Bodmeier, R. & Chen, H. Preparation of biodegradable poly (+-) lactide microparticles using a spray-drying technique. *J. Pharm. Pharmacol.* **40,** 754–757 (1988).

124. Nykamp, G., Carstensen, U. & Muller, B. W. Jet milling — a new technique for microparticle preparation. *Int. J. Pharm.* **242,** 79–86 (2002).

125. Levato, R., Mateos-timoneda, M. A. & Planell, J. A. Preparation of biodegradable polylactide microparticles via a biocompatible procedure. *Macromol. Biosci.* **12,** 557–566 (2012).

126. Li, C., Zhao, S., Zhao, Y., Qian, Y., Li, J. & Yin, Y. Chemically crosslinked alginate porous microcarriers modified with bioactive molecule for expansion of human hepatocellular carcinoma cells. *J. Biomed. Mater. Res. - Part B Appl. Biomater.* **102,** 1648–1658 (2014).

127. Li, C., Qian, Y., Zhao, S., Yin, Y. & Li, J. Alginate/PEG based microcarriers with cleavable crosslinkage for expansion and non-invasive harvest of human umbilical cord blood mesenchymal stem cells. *Mater. Sci. Eng. C* **64,** 43–53 (2016).

128. Oryan, A., Kamali, A., Moshiri, A., Baharvand, H. & Daemi, H. Chemical crosslinking of biopolymeric scaffolds: Current knowledge and future directions of crosslinked engineered bone scaffolds. *Int. J. Biol. Macromol.* **107,** 678–688 (2018).

129. Yu, C., Kornmuller, A., Brown, C., Hoare, T. & Flynn, L. E. Decellularized adipose tissue microcarriers as a dynamic culture platform for human adipose-derived stem/stromal cell expansion. *Biomaterials* **120,** 66–80 (2017).

130. Li, F. J., Zhang, S. D., Liang, J. Z. & Wang, J. Z. Effect of polyethylene glycol on the crystallization and impact properties of polylactide-based blends. *Polym. Adv. Technol.* **26,** 465–475 (2015).

131. Ji, Q., Wang, Z., Jiao, Z., Wang, Y., Wu, Z., Wang, P., Zhu, Y., Sun, S., Liu, Y. & Zhang, P. Biomimetic polyetheretherketone microcarriers with specific surface topography and self-secreted extracellular matrix for large-scale cell expansion. *Regen. Biomater.* **7,** 109–118 (2019).

132. Sun, L., Xiong, Z., Zhou, W., Liu, R., Yan, X., Li, J., An, W., Yuan, G., Ma, G. & Su, Z. Novel konjac glucomannan microcarriers for anchorage-dependent animal cell culture. *Biochem. Eng. J.* **96,** 46–54 (2015).

133. Amersham Biosciences. *Microcarrier cell culture: Principles and methods.* 7–160 (2005).

134. Arkhipova, A. Y., Kotlyarova, M. C., Novichkova, S. G., Agapova, O. I., Kulikov, D. A., Kulikov, A. V., Drutskaya, M. S., Agapov, I. I. & Moisenovich, M. M. New silk fibroin-based bioresorbable microcarriers. *Bull. Exp. Biol. Med.* **160,** 491–494 (2016).

135. Kuterbekov, M., Machillot, P., Lhuissier, P., Picart, C., Jonas, A. M. & Glinel, K. Solvent-free preparation of porous poly(L-lactide) microcarriers for cell culture. *Acta Biomater.* **75,** 300–311 (2018).

136. Tamura, A., Kobayashi, J., Yamato, M. & Okano, T. Temperature-responsive poly(N-isopropylacrylamide)-grafted microcarriers for large-scale non-invasive harvest of anchorage-dependent cells. *Biomaterials* **33,** 3803–3812 (2012).

137. Rafiq, Q. A., Coopman, K. & Hewitt, C. J. Scale-up of human mesenchymal stem cell culture: Current technologies and future challenges. *Curr. Opin. Chem. Eng.* **2,** 8–16 (2013).

138. Gupta, P., Ismadi, M. Z., Verma, P. J., Fouras, A., Jadhav, S., Bellare, J. & Hourigan, K. Optimization of agitation speed in spinner flask for microcarrier structural integrity and expansion of induced pluripotent stem cells. *Cytotechnology* **68,** 45–59 (2016).

139. Bacakova, L., Filova, E., Parizek, M., Ruml, T. & Svorcik, V. Modulation of cell adhesion, proliferation and differentiation on materials designed for body implants. *Biotechnol. Adv.* **29,** 739–767 (2011).

140. Bačáková, L., Filová, E., Rypáček, F., Švorčík, V. & Starý, V. Cell Adhesion on Artificial Materials for Tissue Engineering. *Physiol. Res.* **53** (2004).

141. Hersel, U., Dahmen, C. & Kessler, H. RGD modified polymers biomaterials for stimulated cell adhesion and beyond. *Biomaterials* **24,** 4385–4415 (2003).

142. Anselme, K., Ploux, L. & Ponche, A. Influence of Surface Chemistry and Surface Topography on Cell Adhesion. *J. Adhes. Sci. Cell / Mater. Interfaces,* 37–41 (2010).

143. Mas-Moruno, C. in *Pept. Proteins as Biomater. Tissue Regen. Repair* 73–100 (Elsevier Ltd., 2018).

144. Alberts, B., Johnson, A., Lewis, J., Raff, M., Roberts, K. & Walter, P. *Molecular Biology of The Cell* (Garland Sciences, New York, 2008).

145. Han, W. M., Jang, Y. C. & García, A. J. *The extracellular matrix and cell–biomaterial interactions* 701–716 (Elsevier, 2020).

146. Khalili, A. A. & Ahmad, M. R. A Review of cell adhesion studies for biomedical and biological applications. *Int. J. Mol. Sci.* **16,** 18149–18184 (2015).

147. Bilgen, B. & Odabas, S. in *Adv. Surfaces Stem Cell Res.* (eds Tiwari, A., Garipcan, B. & Uzun, L.) 45–65 (2016).

148. Holle, A. W. & Engler, A. J. More than a feeling : discovering , understanding , and influencing mechanosensing pathways. *Curr. Opin. Biotechnol.* **22,** 648–654 (2011).

149. Mohammed, D., Versaevel, M., Bruyère, C., Alaimo, L., Luciano, M., Vercruysse, E., Procès, A. & Gabriele, S. Innovative Tools for Mechanobiology : Unraveling Outside-In and Inside-Out Mechanotransduction. *Front. Bioeng. Biotechnol.* **7,** 1–18 (2019).

150. Sawicki, L. A., Choe, L. H., Wiley, K. L., Lee, K. H. & Kloxin, A. M. Isolation and identification of proteins secreted by cells cultured within synthetic hydrogel-based matrices. *ACS Biomater. Sci. Eng.* **4,** 836–845 (2018).

151. Ferreira, S. A. *et al.* Bi-directional cell-pericellular matrix interactions direct stem cell fate. *Nat. Commun.* **9,** 4049 (2018).

152. Mann, B. K., Tsai, A. T., Scott-burden, T. & West, J. L. Modification of surfaces with cell adhesion peptides alters extracellular matrix deposition. *Biomaterials* **20,** 2281–2286 (1999).

153. Horton, E. R., Vallmajo-martin, Q., Martin, I., Snedeker, J. G., Ehrbar, M. & Blache, U. Extracellular matrix production by mesenchymal stromal cells in hydrogels facilitates cell spreading and is inhibited by FGF-2. *Adv. Healthc. Mater.* **1901669,** 1–10 (2020).

154. Loebel, C., Mauck, R. L. & Burdick, J. A. Local nascent protein deposition and remodelling guide mesenchymal stromal cell mechanosensing and fate in three-dimensional hydrogels. *Nat. Mater.* **18,** 883–891 (2019).

155. Caldeira, J., Sousa, A., Sousa, D. M. & Barros, D. in *Pept. Proteins as Biomater. Tissue Regen. Repair* 29–72 (Elsevier Ltd., 2018).

156. Mwenifumbo, S. & Stevens, M. M. in *Biomed. nanostructures* (eds E.Gonsalves, K., R. Halberstadt, C., T.Laurencin, C. & Nair, L. S.) 225–253 (John Wiley & Sons, 2008).

157. Mark, K. V. D., Park, J. & Bauer, S. Nanoscale engineering of biomimetic surfaces : cues from the extracellular matrix. *Cell Tissue Res.,* 131–153 (2010).

158. Ayad, S., Boot-Handford, R., J.Humphries, M., E.Kadler, K. & Shuttleworth, A. in *Extracell. Matrix Factsb.* 11–20 (1998).

159. Yue, B. Biology of the extracellular matrix: an overview. *J. Glaucoma* **23,** 1–7 (2014).

160. Theocharis, A. D., Skandalis, S. S., Gialeli, C. & Karamanos, N. K. Extracellular matrix structure. *Adv. Drug Deliv. Rev.* **97,** 4–27 (2015).

161. Karp, G., Iwasa, J. & Marshall, W. *Cell and Molecular Biology* (Wiley, 2020).

162. Muncie, J. M. & Weaver, V. M. *The physical and biochemical properties of the extracellular matrix regulate cell fate* 1st ed., 1–37 (Elsevier Inc., 2018).

163. Carré, A. & Lacarrière, V. How substrate properties control cell adhesion. A physical-chemical approach. *J. Adhes. Sci. Technol.* **24,** 815–830 (2010).

164. Anselme, K., Ploux, L. & Ponche, A. Cell / material interfaces : influence of surface chemistry and surface topography on cell adhesion. *J. Adhes. Sci. Technol.* **24,** 37–41 (2016).

165. Hlady, V. & Buijs, J. Protein adsorption on solid surfaces. *Curr. Opin. Biotechnol.* **7,** 72–77 (1996).

166. Leal-egaña, A., Díaz-cuenca, A. & Boccaccini, A. R. Tuning of cell – biomaterial anchorage for tissue regeneration. *Adv. Mater.* **25,** 4049–4057 (2013).

167. Kaivosoja, E., Barreto, G., Levon, K., Virtanen, S., Ainola, M. & Konttinen, Y. Chemical and physical properties of regenerative medicine materials controlling stem cell fate. *Ann. Med.* **44,** 635–650 (2012).

168. Shelton, R. M., Davies, J. E. & Rad, B. Protein adsorption at the interface between charged polymer substrata and migrating osteoblasts. *Biomaterials* **9,** 24–29 (1988).

169. Schneider, G. B., English, A., Abraham, M., Zaharias, R., Stanford, C. & Keller, J. The effect of hydrogel charge density on cell attachment. *Biomaterials* **25,** 3023–3028 (2004).

170. Harbers, G. M. & Grainger, D. W. in *An Introduction to Biomaterials* 15–45 (CRC Press, 2006).

171. Sun, Y., Chen, C. S. & Fu, J. Forcing stem cells to behave : A biophysical perspective of the cellular microenvironment. *Annu. Rev. Biophys.* **41,** 519–542 (2012).

172. Vazquez, C. P., Boudou, T., Dulong, V., Nicolas, C., Picart, C. & Glinel, K. Variation of polyelectrolyte film stiffness by photo-Cross-linking : A new way to control cell adhesion. *Langmuir* **25,** 3556–3563 (2009).

173. Picart, C. Polyelectrolyte multilayer films: from physico-chemical properties to the control of cellular processes. *Curr. Med. Chem.* **15,** 685–697 (2008).

174. Pelham, R. J. & Wang, Y.-l. Cell locomotion and focal adhesions are regulated by substrate flexibility. *Proc. Natl. Acad. Sci. U. S. A.* **94,** 13661–13665 (1997).

175. Gray, D. S., Tien, J. & Chen, C. S. Repositioning of cells by mechanotaxis on surfaces with micropatterned Young ' s modulus. *J. Biomed. Mater. Res.* **66,** 605–614 (2002).

176. Wong, J. Y., Velasco, A., Rajagopalan, P. & Pham, Q. Directed movement of vascular smooth muscle cells on gradient-compliant hydrogels. *Langmuir,* 1908–1913 (2003).

177. Lo, C.-M., Wang, H.-B., Dembo, M. & Wang, Y.-L. Cell movement is guided by the rigidity of the substrate. *Biophys. J.* **79,** 144–152 (2000).

178. Engler, A. J., Sen, S., Sweeney, H. L. & Discher, D. E. Matrix elasticity directs stem cell lineage specification. *Cell* **126,** 677–689 (2006).

179. Huebsch, N., Arany, P. R., Mao, A. S., Shvartsman, D., Ali, O. A., Bencherif, S. A., Rivera-feliciano, J. & Mooney, D. J. Cell/matrix interface to control stem-cell fate. *Nat. Mater.* **9,** 518–526 (2010).

180. Pek, Y. S., Wan, A. C. A. & Ying, J. Y. The effect of matrix stiffness on mesenchymal stem cell differentiation in a 3D thixotropic gel. *Biomaterials* **31,** 385–391 (2010).

181. Chaudhuri, O., Gu, L., Darnell, M., Klumpers, D., Bencherif, S. A., Weaver, J. C., Huebsch, N. & Mooney, D. J. Substrate stress relaxation regulates cell spreading. *Nat. Commun.* **6,** 1–7 (2015).

182. Chaudhuri, O., Gu, L., Klumpers, D., Darnell, M., Sidi, A., Weaver, J. C., Huebsch, N., Lee, H.-p., Lippens, E., Duda, G. N. & Mooney, D. J. Hydrogels with tunable stress relaxation regulate stem cell fate and activity. *Nat. Mater.* **15,** 326–334 (2016).

183. Chaudhuri, O. Viscoelastic hydrogels for 3D cell culture. *Biomater. Sci.* **5,** 1480–1490 (2017).

184. Cameron, A. R., Frith, J. E. & Cooper-White, J. J. The influence of substrate creep on mesenchymal stem cell behaviour and phenotype. *Biomaterials* **32,** 5979–5993 (2011).

185. Lou, J., Stowers, R., Nam, S., Xia, Y. & Chaudhuri, O. Stress relaxing hyaluronic acid-collagen hydrogels promote cell spreading, fiber remodeling, and focal adhesion formation in 3D cell culture. *Biomaterials* **154,** 213–222 (2018).

186. Lagunas, A., Caballero, D. & Samitier, J. in *Adv. Surfaces Stem Cell Res.* 87–141 (2016).

187. Anselme, K., Ponche, A. & Ploux, L. in *Compr. Biomater. II* 364–386 (Elsevier Ltd., 2017).

188. Gentile, F., Tirinato, L., Battista, E., Causa, F., Liberale, C., Enzo, M. & Decuzzi, P. Cells preferentially grow on rough substrates. *Biomaterials* **31,** 7205–7212 (2010).

189. Hou, Y., Xie, W., Yu, L., Camacho, L. C., Nie, C., Zhang, M., Haag, R. & Wei, Q. Surface Roughness Gradients Reveal Topography-Specific Mechanosensitive Responses in Human Mesenchymal Stem Cells. *Small* **1905422** (2020).

190. Vagaská, B., Bačáková, L., Filová, E. & Balík, K. Osteogenic cells on bio-inspired materials for bone tissue engineering. *Physiol. Res.* **59,** 309–322 (2009).

191. Boyan, B. D., Bonewald, L. F., Paschalis, E. P., Lohmann, C. H., Rosser, J., Cochran, D. L., Dean, D. D., Schwartz, Z. & Boskey, A. L. Osteoblast-mediated mineral deposition in culture is dependent on surface microtopography. *Calcif. Tissue Int.* **71,** 519–529 (2002).

192. Kim, H. J. *et al.* Varying Ti-6Al-4V surface roughness induces different early morphologic and molecular responses in MG63 osteoblast-like cells. *J. Biomed. Mater. Res.* **74,** 366–373 (2005).

193. Lossdörfer, S., Schwartz, Z., Wang, L., Lohmann, C. H., Turner, J. D., Wieland, M., Cochran, D. L. & Boyan, B. D. Microrough implant surface topographies increase osteogenesis by reducing osteoclast formation and activity. *J. Biomed. Mater. Res. Part A* **70,** 4–6 (2004).

194. Zhao, G., Zinger, O., Schwartz, Z., Wieland, M., Landolt, D. & Boyan, B. D. Osteoblast-like cells are sensitive to submicron-scale surface structure. *Clin. Oral Implants Res.* **17,** 258–264 (2006).

195. Schneider, G. B., Perinpanayagam, H., Clegg, M., Zaharias, R., Seabold, D., Keller, J. & Stanford, C. Implant surface roughness affects osteoblast gene expression. *J. Dent. Res.* **82,** 372–376 (2003).

196. Faia-torres, A. B., Guimond-lischer, S., Rottmar, M., Charnley, M., Goren, T., Maniura-weber, K., Spencer, N. D., Reis, R. L., Textor, M. & Neves, N. M. Differential regulation of osteogenic differentiation of stem cells on surface roughness gradients. *Biomaterials* **35,** 9023–9032 (2014).

197. Webster, T. J. & Ejiofor, J. U. Increased osteoblast adhesion on nanophase metals : Ti, Ti6A14V, and CoCrMo. *Biomaterials* **25,** 4731–4739 (2004).

198. Werner, M., Blanquer, S. B., Haimi, S. P., Korus, G., Dunlop, J. W., Duda, G. N., Grijpma, D. W. & Petersen, A. Surface Curvature Differentially Regulates Stem Cell Migration and Differentiation via Altered Attachment Morphology and Nuclear Deformation. *Adv. Sci.* **4,** 1–11 (2017).

199. Pieuchot, L. *et al.* Curvotaxis directs cell migration through cell-scale curvature landscapes. *Nat. Commun.* **9,** 3995 (2018).

200. Callens, S. J., Uyttendaele, R. J., Fratila-Apachitei, L. E. & Zadpoor, A. A. Substrate curvature as a cue to guide spatiotemporal cell and tissue organization. *Biomaterials* **232,** 119739 (2020).

201. Werner, M., Petersen, A., Kurniawan, N. A. & Bouten, C. V. Cell-Perceived Substrate Curvature Dynamically Coordinates the Direction, Speed, and Persistence of Stromal Cell Migration. *Adv. Biosyst.* **3** (2019).

202. Parisi, L., Toffoli, A., Ghezzi, B., Mozzoni, B., Lumetti, S. & Macaluso, G. M. A glance on the role of fibronectin in controlling cell response at biomaterial interface. *Jpn. Dent. Sci. Rev.* **56,** 50–55 (2020).

203. Lebaron, R. G. & Athanasiou, K. A. Extracellular matrix cell adhesion peptides: Functional applications in orthopedic materials. *Tissue Eng.* **6,** 85–103 (2000).

204. Mark, K. V. D. & Park, J. Engineering biocompatible implant surfaces Part II : Cellular recognition of biomaterial surfaces : Lessons from cell – matrix interactions. *Prog. Mater. Sci.* **58,** 327–381 (2013).

205. Toffoli, A., Parisi, L., Bianchi, M. G., Lumetti, S. & Macaluso, G. M. Thermal treatment to increase titanium wettability induces selective proteins adsorption from blood serum thus affecting osteoblasts adhesion. *Mater. Sci. Eng. C,* 110250 (2019).

206. Custódio, C. A., Alves, C. M., Reis, R. L. & Mano, J. F. Immobilization of fibronectin in chitosan substrates improves cell adhesion and proliferation. *J. Tissue Eng. Regen. Med.* **4,** 316–323 (2010).

207. Preissner, K. T. Structure and biological role of Vitronectin. *Annu. Rev. Cell Biol.* **7,** 275–310 (1991).

208. Lam, A. T.-L., Li, J., Chen, A. K.-L., Reuveny, S., Oh, S. K.-W. & Birch, W. R. Cationic surface charge combined with either vitronectin or laminin dictates the evolution of human embryonic stem cells/microcarrier aggregates and cell growth in agitated cultures. *Stem Cells Dev.* **23,** 1688–1703 (2014).

209. Rivera-Chacon, D. M., Alvarado-Velez, M., Acevedo-Morantes, C. Y., Singh, S. P., Gultepe, E., Nagesha, D., Sridhar, S. & Ramirez-Vick, J. E. Fibronectin and vitronectin promote human fetal osteoblast cell attachment and proliferation on nanoporous titanium surfaces. *J. Biomed. Nanotechnol.* **9,** 1092–1097 (2013).

210. Rodin, S., Domogatskaya, A., Ström, S., Hansson, E. M., Chien, K. R., Inzunza, J., Hovatta, O. & Tryggvason, K. Long-term self-renewal of human pluripotent stem cells on human recombinant laminin-511. *Nat. Biotechnol.* **28,** 611–615 (2010).

211. Chen, A. K. L., Chen, X., Choo, A. B. H., Reuveny, S. & Oh, S. K. W. Critical microcarrier properties affecting the expansion of undifferentiated human embryonic stem cells. *Stem Cell Res.* **7,** 97–111 (2011).

212. Ricard-blum, S. The Collagen Family. *Cold Spring Harb Perspect Biol* **3,** 1–19 (2011).

213. Fratzl, P. in *Collagen Struct. Mech.* 1–13 (2008).

214. Rest, M. V. D. & Garrone, R. Collagen family of proteins. *FASEB J.* **273,** 2814–2823 (1991).

215. Glowacki, J. & Mizuno, S. Collagen scaffolds for tissue engineering collagen scaffolds for tissue engineering. *Biopolymers* **89,** 338–344 (2007).

216. Rammelt, S., Schulze, E., Bernhardt, R., Hanisch, U., Scharnweber, D., Worch, H., Zwipp, H. & Biewener, A. Coating of titanium implants with type-I collagen. *J. Orthop. Reserch* **22,** 1025–1034 (2004).

217. Hum, J. & Boccaccini, A. R. Collagen as coating material for 45S5 bioactive glass-based scaffolds for bone tissue engineering. *Int. J. Mol. Sci.* **19,** 1807 (2018).

218. Yan, R., Chen, Y., Gu, Y., Tang, C., Huang, J., Hu, Y. & Ouyang, H. A Collagen-coated sponge silk scaffold for functional meniscus regeneration. *J. Tissue Eng. Regen. Med.* **13,** 156–173 (2019).

219. Floss, D. M., Schallau, K., Rose-john, S. & Conrad, U. Elastin-like polypeptides revolutionize recombinant protein expression and their biomedical application. *Trends Biotechnol.* **28,** 37–45 (2009).

220. Yeo, G. C., Mithieux, S. M. & Weiss, A. S. The elastin matrix in tissue engineering and regeneration. *Curr. Opin. Biomed. Eng.* **6,** 27–32 (2018).

221. Wen, Q., Mithieux, S. M. & Weiss, A. S. Elastin biomaterials in dermal repair. *Trends Biotechnol.* **38,** 280–291 (2020).

222. Barenghi, R., Beke, S., Romano, I., Gavazzo, P., Farkas, B., Vassalli, M., Brandi, F. & Scaglione, S. Elastin-coated biodegradable photopolymer scaffolds for tissue engineering applications. *Biomed. Res. Int.* **2014,** 1–9 (2014).

223. Foraida, Z. I., Kamaldinov, T., Nelson, D. A., Larsen, M. & Castracane, J. Elastin-PLGA hybrid electrospun nanofiber scaffolds for salivary epithelial cell self-organization and polarization. *Acta Biomater.* **62,** 116–127 (2017).

224. Wondimu, Z., Gorfu, G., Kawataki, T., Smirnov, S., Yurchenco, P., Tryggvason, K. & Patarroyo, M. Characterization of commercial laminin preparations from human placenta in comparison to recombinant laminins 2 ($\alpha 2\beta 1\gamma 1$), 8 ($\alpha 4\beta 1\gamma 1$), 10 ($\alpha 5\beta 1\gamma 1$). *Matrix Biol.* **25,** 89–93 (2006).

225. Lin, C.-y. & Liu, J. C. Modular protein domains : an engineering approach toward functional biomaterials. *Curr. Opin. Biotechnol.* **40,** 56–63 (2016).

226. Demain, A. L. & Vaishnav, P. Production of recombinant proteins by microbes and higher organisms. *Biotechnol. Adv.* **27,** 297–306 (2009).

227. Braam, S. R., Zeinstra, L., Litjens, S., Oostwaard, D. W.-V., den Brink, S. V., Laake, L. V., Lebrin, F., Kats, P., Hochstenbach, R., Passier, R., Sonnenberg, A. & Mummery, C. L. Recombinant vitronectin is a functionally defined substrate that supports human embryonic stem cell self-renewal via αV β5 integrin. *Stem Cells* **26,** 2257–2265 (2008).

228. Cutler, S. M. & Garcia, A. J. Engineering cell adhesive surfaces that direct integrin $\alpha 5\beta 1$ binding using a recombinant fragment of fibronectin. *Biomaterials* **24,** 1759–1770 (2003).

229. Punet, X., Mauchau, R., Giannotti, M. I., Rodr, J. C., Sanz, F., Engel, E., Mateos-timoneda, M. A. & Planell, J. A. Enhanced cell-material interactions through the biofunctionalization of polymeric surfaces with engineered peptides. *Biomacromolecules* **14,** 2690–2702 (2013).

230. Somamoto, S. & Tabata, Y. Effect of ProNectin F derivatives on cell attachment and proliferation. *Acta Biomater.* **9,** 5194–5200 (2013).

231. Ishii-Watabe, A., Kanayasu-Toyoda, T., Suzuki, T., Kobayashi, T., Yamaguchi, T. & Kawanishi, T. Influences of the recombinant artificial cell adhesive proteins on the behavior of human umbilical vein endothelial cells in serum-free culture. *Biologicals* **35,** 247–257 (2007).

232. Heslot, H. Artificial fibrous proteins: A review. *Biochimie* **80,** 19–31 (1998).

233. Werten, M. W., Eggink, G., Cohen Stuart, M. A. & de Wolf, F. A. Production of protein-based polymers in Pichia pastoris. *Biotechnol. Adv.* **37,** 642–666 (2019).

234. Confalonieri, D., Marca, M. L., van Dongen, E. M. W. M., Walles, H. & Ehlicke, F. A novel injectable recombinant collagen I peptide – based macroporous microcarrier allows superior expansion of C2C12 and human bone marrow - derived mesenchymal stromal cells and supports deposition of mineralized matrix. *Tissue Eng. - Part A* **23,** 1–32 (2016).

235. Pierschbacher, M. D. & Ruoslahti, E. Cell attachment activity of fibronectin can be duplicated by small synthetic fragments of the molecule. *Nature* **309,** 30–33 (1984).

236. Bellis, S. L. Advantages of RGD peptides for directing cell association with biomaterials. *Biomaterials* **32,** 4205–4210 (2011).

237. Siemion, I. Z., Kluczyk, A. & Cebrat, M. *RGD Peptides* 705–713 (Elsevier Inc., 2013).

238. Aota, S.-i., Nomizu, M. & Yamada, K. M. The Short amino acid sequence Pro-His-Ser-Arg-Asn in human fibronectin enhances cell-adhesive function. *J. Biol. Chem.* **269,** 24756–24761 (1994).

239. Ruoslahti, E. RGD and other recognition sequences for integrins. *Annu. Rev. Cell Dev. Biol.* **12,** 697–715 (1996).

240. Chua, P. H., Neoh, K. G., Kang, E. T. & Wang, W. Surface functionalization of titanium with hyaluronic acid/chitosan polyelectrolyte multilayers and RGD for promoting osteoblast functions and inhibiting bacterial adhesion. *Biomaterials* **29,** 1412–1421 (2008).

241. Shi, Z., Neoh, K. G., Kang, E. T., Poh, C. & Wang, W. Bacterial adhesion and osteoblast function on titanium with surface-grafted chitosan and immobilized RGD peptide. *J. Biomed. Mater. Res. - Part A* **86,** 865–872 (2008).

242. Heller, M., Kumar, V. V., Pabst, A., Brieger, J., K, P. W., Al-Nawas, B. & Kämmerer, P. W. Osseous response on linear and cyclic RGD-peptides immobilized on titanium surfaces in vitro and in vivo. *J. Biomed. Mater. Res. - Part A* **106,** 419–427 (2018).

243. Tatrai, P., Sagi, B., Szigeti, A., Szepesi, A., Szabo, I., Bosze, S., Kristof, Z., Marko, K., Szakacs, G., Urban, I., Gabor, M., Uher, F. & Német, K. A novel cyclic RGD-containing peptide polymer improves serum-free adhesion of adipose tissue-derived mesenchymal stem cells to bone implant surfaces. *J. Mater. Sci. Mater. Med.* **24,** 479–488 (2013).

244. Rowley, J. A., Madlambayan, G. & Mooney, D. J. Alginate hydrogels as synthetic extracellular matrix materials. *Biomaterials* **20,** 45–53 (1999).

245. Salinas, C. N. & Anseth, K. S. The influence of the RGD peptide motif and its contextual presentation in PEG gels on human mesenchymal stem cell viability. *J. Tissue Eng. Regen. Med.* **2,** 296–304 (2008).

246. Dhillon, J., Young, S. A., Sherman, S. E., Bell, G. I., Amsden, B. G., Hess, D. A. & Flynn, L. E. Peptide-modified methacrylated glycol chitosan hydrogels as a cell-viability supporting pro-angiogenic cell delivery platform for human adipose-derived stem/stromal cells. *J. Biomed. Mater. Res. - Part A* **107,** 571–585 (2019).

247. Sawyer, A. A., Hennessy, K. M. & Bellis, S. L. Regulation of mesenchymal stem cell attachment and spreading on hydroxyapatite by RGD peptides and adsorbed serum proteins. *Biomaterials* **26,** 1467–1475 (2005).

248. Durrieu, M. C., Pallu, S., Guillemot, F., Bareille, R., Amédée, J., Baquey, C., Labrugre, C. & Dard, M. Grafting RGD containing peptides onto hydroxyapatite to promote osteoblastic cells adhesion. *J. Mater. Sci. Mater. Med.* **15,** 779–786 (2004).

249. Gutiérrez-Sánchez, M., Escobar-Barrios, V. A., Pozos-guillén, A. & Escobar-García, D. M. RGD-functionalization of PLA/starch scaffolds obtained by electrospinning and evaluated in vitro for potential bone regeneration. *Mater. Sci. Eng. C* **96,** 798–806 (2019).

250. Duque-sanchez, L., Brack, N., Postma, A., Meagher, L. & Pigram, P. J. Engineering the biointerface of electrospun 3D scaffolds with functionalized polymer brushes for enhanced cell binding. *Biomacromolecules* **20,** 813–825 (2018).

251. Dias, A. D., Elicson, J. M. & Murphy, W. L. Microcarriers with synthetic hydrogel surfaces for stem cell expansion. *Adv. Healthc. Mater.* **6,** 1–9 (2017).

252. Kim, M. R., Jeong, J. H. & Park, T. G. Swelling induced detachment of chondrocytes using RGD-modified Poly(N-isopropylacrylamide) hydrogel beads. *Biotechnol. Prog.* **18,** 495–500 (2002).

253. Rahmany, M. B. & Dyke, M. V. Biomimetic approaches to modulate cellular adhesion in biomaterials : A review. *Acta Biomater.* **9,** 5431–5437 (2013).

254. Huettner, N., Dargaville, T. R. & Forget, A. Discovering cell-adhesion peptides in tissue engineering: beyond RGD. *Trends Biotechnol.* **36,** 372–383 (2018).

255. Shin, H., Jo, S. & Mikos, A. G. Biomimetic materials for tissue engineering. *Biomaterials* **24,** 4353–4364 (2003).

256. Rusmini, F., Zhong, Z. & Feijen, J. Protein immobilization strategies for protein biochips. *Biomacromolecules* **8,** 1775–1789 (2007).

257. Kim, D. & Herr, A. E. Protein immobilization techniques for microfluidic assays. *Biomicrofluidics* **7,** 041501 (2013).

258. Rao, S. V., Anderson, K. W. & Bachas, L. G. Oriented immobilization of proteins. *Mikrochim. Acta* **128,** 127–143 (1998).

259. Tallawi, M., Rosellini, E., Barbani, N., Grazia Cascone, M., Rai, R., Saint-Pierre, G. & Boccaccini, A. R. Strategies for the chemical and biological functionalization of scaffolds for cardiac tissue engineering: A review. *J. R. Soc. Interface* **12** (2015).

260. Garcia, A. J. in *Princ. Regen. Med.* (eds Atala, A., Nerem, R., Tony, L. & Robert, M.) 663–673 (Elsevier Inc., 2011).

261. Hirano, B. Y. & Mooney, D. J. Peptide and protein presenting materials for tissue engineering. *Adv. Mater.* **16,** 17–25 (2004).

262. Seitz, T. L., Noonan, K. D., Hench, L. L. & Noonan, N. E. Effect of fibronectin on the adhesion of an established cell line to a surface reactive biomaterial. *Journal of Biomedical Materials Research* **16,** 195–207 (1982).

263. Jonkheijm, P., Weinrich, D., Schröder, H., Niemeyer, C. M. & Waldmann, H. Chemical strategies for generating protein biochips. *Angew. Chemie Int. Ed.* **47,** 9618–9647 (2008).

264. Liu, Y. & Yu, J. Oriented immobilization of proteins on solid supports for use in biosensors and biochips: a review. *Microchim. Acta* **183,** 1–19 (2016).

265. Masri, M. S. & Friedman, M. Protein reactions with methyl and ethyl vinyl sulfones. *J. Protein Chem.* **7,** 49–54 (1988).

266. Amani, H., Arzaghi, H., Bayandori, M., Dezfuli, A. S., Pazoki-Toroudi, H., Shafiee, A. & Moradi, L. Controlling Cell Behavior through the Design of Biomaterial Surfaces: A Focus on Surface Modification Techniques. *Adv. Mater. Interfaces* **6,** 1–30 (2019).

267. Goddard, J. M. & Hotchkiss, J. H. Ã. Polymer surface modification for the attachment of bioactive compounds. **32,** 698–725 (2007).

268. Igwe, J. C., Mikael, P. E. & Nukavarapu, S. P. Design , fabrication and in vitro evaluation of a novel polymer-hydrogel hybrid scaffold for bone tissue engineering. *J. Tissue Eng. Regen. Med.* **8,** 131–142 (2012).

269. Gorbahn, M. & Klein, M. O. Promotion of osteogenic cell response using quasicovalent immobilized fibronectin on titanium surfaces : introduction of a novel biomimetic. *J. Oral Maxillofac. Surg.* **70,** 1827–1834 (2012).

270. Fabbri, P. & Messori, M. in *Modif. Polym. Prop.* (eds Jasso-Gastinel, C. F. & Kenny, J. M.) 109–130 (Elsevier Inc., 2017).

271. Ulman, A. Formation and structure of self-assembled monolayers. *Chem. Rev.* **96,** 1533–1554 (1996).

272. Schreiber, F. Structure and growth of self-assembling monolayers. *Prog. Surf. Sci.* **65,** 151–256 (2000).

273. Ratner, B. D. & Hoffman, A. S. in *Biomater. Sci. An Introd. to Mater. Med.* (eds Ratner, B. D., Hoffman, A. S., Schoen, F. J. & Lemons, J. E.) 1, 259–276 (Elsevier, 2013).

274. Raynor, J. E., Capadona, J. R., Collard, D. M., Petrie, T. A. & García, A. J. Polymer brushes and self-assembled monolayers : Versatile platforms to control cell adhesion to biomaterials. *Biointerphases* **4,** FA3–16 (2009).

275. Nicosia, C. & Huskens, J. Reactive self-assembled monolayers : from surface functionalization to gradient formation. *Mater. Horizons* **1,** 32–45 (2014).

276. Smith, R. K., Lewis, P. A. & Weiss, P. S. Patterning self-assembled monolayers. *Prog. Surf. Sci.* **75,** 1–68 (2004).

277. Kind, M. & Wöll, C. Organic surfaces exposed by self-assembled organothiol monolayers : Preparation, characterization, and application. *Prog. Surf. Sci.* **84,** 230–278 (2009).

278. Faucheux, N., Schweiss, R., Lutzow, K., Werner, C. & Groth, T. Self-assembled monolayers with different terminating groups as model substrates for cell adhesion studies. *Biomaterials* **25,** 2721–2730 (2004).

279. Gallant, N. D., Capadona, J. R., Frazier, A. B., Collard, D. M. & Garcia, A. J. Micropatterned surfaces to engineer focal adhesions for analysis of cell adhesion strengthening. *Langmuir* **18,** 5579–5584 (2002).

280. Brittain, W. J. & Minko, S. A structural definition of polymer brushes. *J. Polym. Sci. Part A* **45,** 3505–3512 (2007).

281. Zhao, B. & Brittain, W. J. Polymer brushes : surface-immobilized macromolecules. *Prog. Mater. Sci.* **25,** 677–710 (2000).

282. Glinel, K., Jonas, A. M., Jouenne, T. & Huck, W. T. S. Antibacterial and antifouling polymer brushes incorporating antimicrobial peptide. *Bioconjug. Chem.* **20,** 71–77 (2009).

283. Minko, S. Responsive polymer brushes. *J. Macromol. Sci.* **46,** 397–420 (2006).

284. Welch, M. E. & Ober, C. K. Responsive and patterned polymer brushes. *J. Polym. Sci.* **51,** 1457–1472 (2013).

285. Krishnamoorthy, M., Hakobyan, S., Ramstedt, M. & Gautrot, J. E. Surface-initiated polymer brushes in the biomedical field : applications in membrane science, biosensing, cell culture, regenerative medicine and antibacterial coatings. *Chem. Rev.* **114,** 10976–11026 (2014).

286. Edmondson, S., Osborne, V. L. & Huck, W. T. S. Polymer brushes via surface-initiated polymerizations. *Chem. Soc. Rev.* **33,** 14–22 (2004).

287. Matyjaszewski, K. & Xia, J. Atom transfer radical polymerization. *Chem. Rev.* **101,** 2921–2990 (2001).

288. Li, D., Zheng, Q., Wang, Y. & Chen, H. Combining surface topography with polymer chemistry: exploring new interfacial biological phenomena. *Polym. Chem.* **5,** 14–24 (2013).

289. Chen, R., Li, L., Feng, L., Luo, Y., Xu, M. & Leong, K. W. Biomaterials assisted scalable cell production for cell therapy. *Biomaterials* **230,** 119627 (2020).

290. Decher, G., Hong, J. D. & Schmitt, J. Buildup of ultrathin multilayer films by a self-assembly process : III . Consecutively alternating adsorption of anionic and cationic polyelectrolytes on charged surfaces. *Thin Solid Films* **210-211,** 831–835 (1992).

291. Decher, G. in *Multilayer Thin Film. Seq. Assem. Nanocomposite Mater.* (eds Decher, G. & Schlenoff, J. B.) 1–22 (Wiley, 2012).

292. Hammond, P. T. Recent explorations in electrostatic multilayer thin film assembly. *Curr. Opin. Colloid Interface Sci.* **4,** 430–442 (2000).

293. Borges, J. & Mano, J. F. Molecular interactions driving the Layer-by-Layer assembly of multilayers. *Chem. Rev.* **114,** 8883–8942 (2014).

294. Decher, G. in *Multilayer thin Film.* (eds Decher, G. & Schlenoff, J. B.) 1–39 (Wiley, 2002).

295. Richardson, J. J., Björnmalm, M. & Caruso, F. Technology-driven layer-by-layer assembly of nanofilms. *Science (80-.).* **348,** 411 (2015).

296. Chiarelli, B. P. A., Johal, M. S., Casson, J. L., Roberts, J. B., Robinson, J. M. & Wang, H.-l. Controlled fabrication of polyelectrolyte multilayer thin films using spin-assembly. *Adv. Mater.* **13,** 1167–1171 (2001).

297. Cho, J., Char, K., Hong, J.-d. & Lee, K.-b. Fabrication of highly ordered multilayer films using a spin self-assembly method. *Adv. Mater.* **13,** 1076–1078 (2001).

298. Lee, S.-s., Hong, J.-d., Kim, C. H., Kim, K., Koo, J. P. & Lee, K.-b. Layer-by-Layer deposited multilayer assemblies of ionene-type polyelectrolytes based on the spin-coating method. *Macromolecules* **34,** 5358–5360 (2001).

299. Schlenoff, J. B., Dubas, S. T. & Farhat, T. Sprayed polyelectrolyte multilayers. *Langmuir* **16,** 9968–9969 (2000).

300. Burke, S. E. & Barrett, C. J. Controlling the physicochemical properties of weak polyelectrolyte multilayer films through acid/base equilibria. *Pure Appl. Chem.* **76,** 1387–1398 (2004).

301. Volodkin, D. & Von Klitzing, R. Competing mechanisms in polyelectrolyte multilayer formation and swelling: Polycation-polyanion pairing vs. polyelectrolyte-ion pairing. *Curr. Opin. Colloid Interface Sci.* **19,** 25–31 (2014).

302. Picart, C., Mutterer, J., Richert, L., Luo, Y., Prestwich, G. D., Schaaf, P., Voegel, J. C. & Lavalle, P. Molecular basis for the explanation of the exponential growth of polyelectrolyte multilayers. *Proc. Natl. Acad. Sci.* **99,** 12531–12535 (2002).

303. Elbert, D. L., Herbert, C. B. & Hubbell, J. A. Thin polymer layers formed by polyelectrolyte multilayer techniques on biological surfaces. *Langmuir* **15,** 5355–5362 (1999).

304. Picart, C., Lavalle, P., Hubert, P., Cuisinier, F. J., Decher, G., Schaaf, P. & Voegel, J. C. Buildup mechanism for poly(L-lysine)/hyaluronic acid films onto a solid surface. *Langmuir* **17,** 7414–7424 (2001).

305. Hervy, M. Modulation of cell structure and function in response to subtrate stiffness and external forces. *J. Adhes. Sci. Technol.* **24,** 963–973 (2010).

306. Boudou, T., Crouzier, T., Ren, K., Blin, G. & Picart, C. Multiple functionalities of polyelectrolyte multilayer films: New biomedical applications. *Adv. Mater.* **22,** 441–467 (2010).

307. Dai, J., Jensen, A. W., Mohanty, D. K., Erndt, J. & Bruening, M. L. Controlling the Permeability of Multilayered Polyelectrolyte Films through Derivatization , Cross-Linking , and Hydrolysis. *Langmuir* **17,** 931–937 (2001).

308. Richert, L., Boulmedais, F., Lavalle, P., Mutterer, J., Ferreux, E., Decher, G., Schaaf, P., Voegel, J. C. & Picart, C. Improvement of stability and cell adhesion properties of polyelectrolyte multilayer films by chemical cross-linking. *Biomacromolecules* **5,** 284–294 (2004).

309. Schuetz, P. & Caruso, F. Copper-assisted weak polyelectrolyte multilayer formation on microspheres and subsequent film crosslinking. *Advanced Functional Materials* **13,** 929–937 (2003).

310. Gribova, V., Auzely-Velty, R., Picart, C. & Fourier, J. Polyelectrolyte Multilayer Assemblies on Materials Surfaces: From Cell Adhesion to Tissue Engineering Europe PMC Funders Group. *Chem Mater* **24,** 854–869 (2012).

311. Picart, C., Elkaim, R., Richert, L., Audoin, F., Arntz, Y., Cardoso, M. D. S., Schaaf, P., Voegel, J. C. & Frisch, B. Primary cell adhesion on RGD-functionalized and covalently crosslinked thin polyelectrolyte multilayer films. *Adv. Funct. Mater.* **15,** 83–94 (2005).

312. Gribova, V., Gauthier-Rouvière, C., Albigès-Rizo, C., Auzely-Velty, R. & Picart, C. Effect of RGD functionalization and stiffness modulation of polyelectrolyte multilayer films on muscle cell differentiation. *Acta Biomater.* **9,** 6468–6480 (2013).

313. Gentile, P., Carmagnola, I., Nardo, T. & Chiono, V. Layer-by-layer assembly for biomedical applications in the last decade. *Nanotechnology* **26,** 422001 (2015).

314. Hartmann, H. & Rumen Krastev. Biofunctionalization of surfaces using polyelectrolyte multilayers. *BioNanoMaterials* **18,** 20160015 (2017).

315. Schneider, A., Francius, G., Obeid, R., Schwinté, P., Hemmerlé, J., Frisch, B., Schaaf, P., Voegel, J. C., Senger, B. & Picart, C. Polyelectrolyte multilayers with a tunable young's modulus: Influence of film stiffness on cell adhesion. *Langmuir* **22,** 1193–1200 (2006).

316. Ren, K., Crouzier, T., Roy, C. & Picart, C. Polyelectrolyte multilayer films of controlled stiffness modulate myoblast cells differentiation. *Adv. Funct. Mater.* **18,** 1378–1389 (2008).

317. Semenov, O. V., Malek, A., Bittermann, A. G., Vörös, J. & Zisch, A. H. Engineered polyelectrolyte multilayer substrates for adhesion, proliferation, and differentiation of human mesenchymal stem cells. *Tissue Eng. Part A* **15,** 2977–2990 (2009).

318. Silva, J. M., García, J. R., Reis, R. L., García, A. J. & Mano, J. F. Tuning cell adhesive properties via layer-by-layer assembly of chitosan and alginate. *Acta Biomater.* **51,** 279–293 (2017).

319. Gaudiere, F., Morin-grognet, S., Bidault, L., Lembre, P., Pauthe, E., Vannier, J.-p., Atmani, H. & Ladam, G. Genipin-crosslinked Layer-by-Layer assemblies : biocompatible microenvironments to direct bone cell fate. *Biomacromolecules* **15,** 1602–1611 (2014).

320. Garlotta, D. A literature review of poly(lactic acid). *J. Polym. Environ.* **9,** 63–64 (2002).

321. Rasal, R. M., Janorkar, A. V. & Hirt, D. E. Poly(lactic acid) modifications. *Prog. Polym. Sci.* **35,** 338–356 (2010).

322. Middleton, J. C. & Tipton, A. J. Synthetic biodegradable polymers as orthopedic devices. *Biomaterials* **21,** 2335–2346 (2000).

323. Ulery, B. D., Nair, L. S. & Laurencin, C. T. Biomedical applications of biodegradable polymers. *J. Polym. Sci. Part B Polym. Phys.* **49,** 832–864 (2011).

324. Lasprilla, A. J., Martinez, G. A., Lunelli, B. H., Jardini, A. L. & Filho, R. M. Poly-lactic acid synthesis for application in biomedical devices - A review. *Biotechnol. Adv.* **30,** 321–328 (2012).

325. Working, P. K., Newman, M. S., Johnson, J. & Cornacoff, J. B. in *Poly(ethylene glycol)* (eds Harris, J. M. & Zalipsky, S.) 45–57 (American Chemical Society, 1997).

326. Garay, R. P., El-gewely, R., Armstrong, J. K., Garratty, G. & Richette, P. Antibodies against polyethylene glycol in healthy subjects and in patients treated with PEG- conjugated agents. *Expert Opin. Drug Deliv.* **9,** 1319–1323 (2012).

327. Knop, K., Hoogenboom, R., Fischer, D. & Schubert, U. S. Poly(ethylene glycol) in drug delivery : pros and cons as well as potential alternatives. *Angew. Chemie Int. Ed.* **49,** 6288–6308 (2010).

328. Armstrong, J. K., Hempel, G., Koling, S., Chan, L. S., Fisher, T., Meiselman, H. J. & Garratty, G. Antibody against poly(ethylene glycol) adversely affects PEG-asparaginase therapy in acute lymphoblastic leukemia patients. *Cancer* **110,** 103–111 (2007).

329. Richter A. W. and Akerblom E. Polyethylene glycol reactive antibodies in man: titer distribution in allergic patients treated with monomethoxy polyethylene glycol modified allergens or placebo, and in healthy blood donors. *Int Arch Allergy Appl Immunol.* **74,** 36–39 (1984).

330. Garay, R. P. & Labaune, J. P. Immunogenicity of polyethylene glycol (PEG). *Open Conf. Proc. J.* **2,** 104–107 (2011).

331. Zhang, P., Sun, F., Liu, S. & Jiang, S. Anti-PEG antibodies in the clinic: current issues and beyond PEGylation. *J. Control. Release* **244,** 184–193 (2017).

332. Schellekens, H., Hennink, W. E. & Brinks, V. The immunogenicity of polyethylene glycol: Facts and fiction. *Pharm. Res.* **30,** 1729–1734 (2013).

333. Enriquez-navas, P. M. & Garcia-martin, M. L. in *Met. Nanoparticles Nanoalloys* (eds Johnston, R. & Wilcoxon, J.) 233–245 (Elsevier LTD., 2012).

334. Rescignano, N., González-Alfaro, Y., Fantechi, E., Mannini, M., Innocenti, C., Ruiz-Hitzky, E., Kenny, J. M. & Armentano, I. Design, development and characterization of a nanomagnetic system based on iron oxide nanoparticles encapsulated in PLLA-nanospheres. *Eur. Polym. J.* **62,** 145–154 (2015).

335. Laurent, S., Forge, D., Port, M., Roch, A., Robic, C., Elst, L. V. & Muller, R. N. Magnetic iron oxide nanoparticles : synthesis, stabilization, vectorization, physicochemical characterizations, and biological applications. *Chem. Rev.* **108,** 2064–2110 (2008).

336. Markides, H., Rotherham, M. & El Haj, A. J. Biocompatibility and toxicity of magnetic nanoparticles in regenerative medicine. *J. Nanomater.* **2012,** 13–15 (2012).

337. Keith, H. D. & Padden, F. J. A phenomenological theory of spherulitic crystallization. *J. Appl. Phys.* **34,** 2409–2421 (1963).

338. Yasuniwa, M., Iura, K. & Dan, Y. Melting behavior of poly(l-lactic acid): Effects of crystallization temperature and time. *Polymer (Guildf).* **48,** 5398–5407 (2007).

339. Younes, H. & Cohn, D. Phase separation in poly(ethylene glycol)/poly(lactic acid) blends. *Eur. Polym. J.* **24,** 765–773 (1988).

340. Nakafuku, C. & Sakoda, M. Melting and crystallization of poly(l-lactic acid) and poly(ethylene oxide) binary mixture. *Polym. J.* **25,** 909–917 (1993).

341. Nakafuku, C. Effects of molecular weight on the melting and crystallization of poly(L-lactic acid) in a mixture with poly(ethylene oxide). *Polym. J.* **28,** 568–575 (1996).

342. Sungsanit, K., Kao, N. & Bhattacharya, S. N. Properties of linear poly(lactic acid)/polyethylene glycol blends. *Polym. Eng. Sci.* **52,** 108 (2012).

343. Li, F. J., Tan, L. C., Zhang, S. D. & Zhu, B. Compatibility, steady and dynamic rheological behaviors of polylactide/poly(ethylene glycol) blends. *J. Appl. Polym. Sci.* **133,** 1–10 (2016).

344. Gokduman, K., Bestepe, F., Li, L., Yarmush, M. L. & Usta, O. B. Dose-, treatment- and time-dependent toxicity of superparamagnetic iron oxide nanoparticles on primary rat hepatocytes. *Nanomedicine* **13,** 1267–1284 (2018).

345. Jarockyte, G., Daugelaite, E., Stasys, M., Statkute, U., Poderys, V., Tseng, T.-c., Hsu, S.-h., Karabanovas, V. & Rotomskis, R. Accumulation and toxicity of superparamagnetic iron oxide nanoparticles in cells and experimental animals. *Int. J. Mol. Sci.* **17,** 1193 (2016).

346. Farah, S., Anderson, D. G. & Langer, R. Physical and mechanical properties of PLA, and their functions in widespread applications — A comprehensive review. *Adv. Drug Deliv. Rev.* **107,** 367–392 (2016).

347. *Cytoline 1 and Cytoline 2 Macroporous microcarriers* Amersham Biosciences (2009).

348. Gritsch, L., Conoscenti, G., La Carrubba, V., Nooeaid, P. & Boccaccini, A. R. Polylactide-based materials science strategies to improve tissue-material interface without the use of growth factors or other biological molecules. *Mater. Sci. Eng. C* **94,** 1083–1101 (2019).

349. Bacakova, M., Musilkova, J., Riedel, T., Brynda, E., Zaloudkova, M. & Bacakova, L. The potential applications of fibrin-coated electrospun polylactide nanofibers in skin tissue engineering. *Int. J. Nanomedicine* **11,** 771–789 (2016).

350. Guo, S., Zhu, X. & Loh, X. J. Controlling cell adhesion using layer-by-layer approaches for biomedical applications. *Mater. Sci. Eng. C* **70,** 1163–1175 (2017).

351. Francius, G., Hemmerlé, J., Ohayon, J., Schaaf, P., Voegel, J. C., Picart, C. & Senger, B. Effect of crosslinking on the elasticity of polyelectrolyte multilayer films measured by colloidal probe AFM. *Microsc. Res. Tech.* **69,** 84–92 (2006).

352. Boudou, T., Ren, K., Crouzier, T. & Picart, C. in *Multilayer Thin Film. Seq. Assem. Nanocomposite Mater. Second Ed.* (eds Decher, G. & Schlenoff, J. B.) 659–690 (Wiley, 2012).

353. Laurent, T. C., Laurent, U. B. & Fraser, J. R. E. The structure and function of hyaluronan: An overview. *Immunol. Cell Biol.* **74,** A1–A7 (1996).

354. Volpi, N., Schiller, J., Stern, R. & Soltes, L. Role, Metabolism, Chemical Modifications and Applications of Hyaluronan. *Curr. Med. Chem.* **16,** 1718–1745 (2009).

355. Leach, J. B. & Schmidt, C. E. in *Encycl. Biomater. Biomed. Eng.* 1421–1431 (Taylor and Francis: New York, 2014).

356. Morra, M. Engineering of biomaterials surfaces by hyaluronan. *Biomacromolecules* **6,** 1205–1223 (2005).

357. Necas, J., Bartosikova, L., Brauner, P. & Kolar, J. Hyaluronic acid (hyaluronan): A review. *Vet. Med. (Praha).* **53,** 397–411 (2008).

358. Kogan, G., Šoltés, L., Stern, R. & Gemeiner, P. Hyaluronic acid: A natural biopolymer with a broad range of biomedical and industrial applications. *Biotechnol. Lett.* **29,** 17–25 (2007).

359. Darrabie, M. D., Kendall, W. F. & Opara, E. C. Characteristics of Poly-L-Ornithine-coated alginate microcapsules. *Biomaterials* **26,** 6846–6852 (2005).

360. Tam, S. K., Bilodeau, S., Dusseault, J., Langlois, G., Hallé, J. & Yahia, L. H. Biocompatibility and physicochemical characteristics of alginate – polycation microcapsules. *Acta Biomater.* **7,** 1683–1692 (2011).

361. Tian, L., Prabhakaran, M. P., Hu, J., Chen, M., Besenbacher, F. & Ramakrishna, S. Synergistic effect of topography, surface chemistry and conductivity of the electrospun nanofibrous scaffold on cellular response of PC12 cells. *Colloids Surfaces B Biointerfaces* **145,** 420–429 (2016).

362. Jung, M.-s., Jang, H. B., Lee, S.-e., Park, J.-h. & Hwang, Y.-s. In vitro micro-mineralized tissue formation by the combinatory condition of adipose-derived stem cells, macroporous PLGA microspheres and a bioreactor. *Macromol. Res.* **22,** 47–57 (2014).

363. Richert, L., Lavalle, P., Payan, E., Shu, X. Z., Prestwich, G. D., Stoltz, J. F., Schaaf, P., Voegel, J. C. & Picart, C. Layer by Layer buildup of polysaccharide films: physical chemistry and cellular adhesion aspects. *Langmuir* **20,** 448–458 (2004).

364. Toole, B. P. Hyaluronan in morphogenesis. *Cell Dev. Biol.* **12,** 79–87 (2001).

365. Lin, T.-m., Tsai, J.-l., Lin, S.-d. & Lai, C.-s. Accelerated growth and prolonged lifespan of adipose tissue-derived human mesenchymal stem cells in a medium using reduced calcium and antioxidants. *Stem Cells Dev.* **102,** 92–102 (2005).

366. Baer, P. C., Griesche, N., Luttmann, W., Schubert, R., Luttmann, A. & Geiger, H. Human adipose-derived mesenchymal stem cells in vitro : evaluation of an optimal expansion medium preserving stemness. *Cytotherapy* **12,** 96–106 (2010).

367. Koellensperger, E. V. A., Bollinger, N., Dexheimer, V., Gramley, F., Germann, G. & Leimer, U. W. E. Choosing the right type of serum for different applications of human adipose tissue e derived stem cells : influence on proliferation and differentiation abilities. *J. Cytotherapy* **16,** 789–799 (2014).

368. Fossett, E. & Khan, W. S. Optimising human mesenchymal stem cell numbers for clinical application : a literature review. *Stem Cells Int.* **2012,** 1–5 (2012).

369. Young, D. A., Choi, Y. S., Engler, A. J. & Christman, K. L. Stimulation of adipogenesis of adult adipose-derived stem cells using substrates that mimic the stiffness of adipose tissue. *Biomaterials* **34,** 8581–8588 (2013).

370. Liu, X., Feng, Q., Bachhuka, A. & Vasilev, K. Surface chemical functionalities affect the behavior of human adipose-derived stem cells in vitro. *Appl. Surf. Sci.* **270,** 473–479 (2013).

371. Dong, Y., Cui, M., Qu, J., Wang, X., Hyung, S., Barrera, J., Elvassore, N. & Gurtner, G. C. Conformable hyaluronic acid hydrogel delivers adipose-derived stem cells and promotes regeneration of burn injury. *Acta Biomater.* **108,** 56–66 (2020).

372. Tatrai, P., Sagi, B., Szigeti, A., Szepesi, A., Ildiko, S., Bosze, S., Kristof, Z., Marko, K., Szakcs, G., Urban, I., Mezo, G., Uher, F. & Nemet, K. A novel cyclic RGD-containing peptide polymer improves serum-free adhesion of adipose tissue-derived mesenchymal stem cells to bone implant surfaces. *J. Mater. Sci. Mater. Med.* **24,** 479–488 (2013).

373. Estes, B. T., Diekman, B. O., Gimble, J. M. & Guilak, F. Isolation of adipose derived stem cells and their induction to a chondrogenic phenotype. *Nat. Protoc.* **5,** 1294–1311 (2010).

374. Derakhti, S., Hamid, S. & Amoabediny, G. Attachment and detachment strategies in microcarrier-based cell culture technology : A comprehensive review. *Mater. Sci. Eng. C* **103,** 109782 (2019).

375. Hu, W. S., Meier, J. & Wang, D. I. A mechanistic analysis of the inoculum requirement for the cultivation of mammalian cells on microcarriers. *Biotechnol. Bioeng.* **95,** 306–316 (1985).

376. Wang, C., Gong, Y., Lin, Y., Shen, J. & Wang, D. A. A novel gellan gel-based microcarrier for anchorage-dependent cell delivery. *Acta Biomater.* **4,** 1226–1234 (2008).

377. Frauenschuh, S., Reichmann, E., Ibold, Y., Goetz, P. M., Sittinger, M. & Ringe, J. A microcarrier-based cultivation system for expansion of primary mesenchymal stem cells. *Biotechnol. Prog.* **23,** 187–193 (2007).

378. Chui, C. Y., Odeleye, A., Nguyen, L., Kasoju, N., Soliman, E. & Ye, H. Electrosprayed genipin cross-linked alginate–chitosan microcarriers for ex vivo expansion of mesenchymal stem cells. *J. Biomed. Mater. Res. - Part A* **00,** 1–12 (2018).

379. Shekaran, A., Sim, E., Tan, K. Y., Kok, J., Chan, Y., Choolani, M., Reuveny, S. & Oh, S. Enhanced in vitro osteogenic differentiation of human fetal MSCs attached to 3D microcarriers versus harvested from 2D monolayers. *BMC Biotechnol.* **15,** 1–13 (2015).

380. Rafiq, Q. A., Ruck, S., Hanga, M. P., Heathman, T. R., Coopman, K., Nienow, A. W., Williams, D. J. & Hewitt, C. J. Qualitative and quantitative demonstration of bead-to-bead transfer with bone marrow-derived human mesenchymal stem cells on microcarriers: utilising the phenomenon to improve culture performance. *Biochem. Eng. J.* **135,** 11–21 (2017).

381. Leber, J., Barekzai, J., Blumenstock, M., Pospisil, B., Salzig, D. & Czermak, P. Microcarrier choice and bead-to-bead transfer for human mesenchymal stem cells in serum-containing and chemically defined media. *Process Biochem.* **59,** 255–265 (2017).

382. Wang, Y. & Ouyang, F. Bead-to-bead transfer of Vero cells in microcarrier culture. *Bioprocess Eng.* **21,** 211–213 (1999).

383. Luo, F., Sun, H., Geng, T. & Qi, N. Application of Taguchi's method in the optimization of bridging efficiency between confluent and fresh microcarriers in bead-to-bead transfer of Vero cells. *Biotechnol. Lett.* **30,** 645–649 (2008).

384. Dürrschmid, M., Landauer, K., Simic, G., Blüml, G. & Doblhoff-Dier, O. Scalable inoculation strategies for microcarrier-based animal cell bioprocesses. *Biotechnol. Bioeng.* **83,** 681–686 (2003).

385. Eibes, G., dos Santos, F., Andrade, P. Z., Boura, J. S., Abecasis, M. M., da Silva, C. L. & Cabral, J. M. Maximizing the ex vivo expansion of human mesenchymal stem cells using a microcarrier-based stirred culture system. *J. Biotechnol.* **146,** 194–197 (2010).

386. Croughan, M. S. & Wang, D. C. Effects of microcarrier concentration in animal cell culture. *Biotechnol. Bioeng.* **32,** 975–982 (1987).

387. Jorgenson, K. D., Hart, D. A., Krawetz, R. & Sen, A. Production of Adult Human Synovial Fluid-Derived Mesenchymal Stem Cells in Stirred-Suspension Culture. *Stem Cells Int.* **2018,** 1–16 (2018).

388. Huang, H.-l., Hsing, H.-w., Lai, T.-c., Chen, Y.-w., Lee, T.-r., Chan, H.-t., Lyu, C., Wu, C.-l., Lu, Y.-c., Lin, S.-t., Lin, C.-w., Lai, C.-h., Chang, H.-t., Chou, C. & Chan, H.-l. Trypsin-induced proteome alteration during cell subculture in mammalian cells. *J. Biomed. Sci.* **17,** 36 (2010).

389. Yu, J., Shi, J., Zhang, Y., Zhang, Y., Huang, Y., Chen, Z. & Yang, J. The replicative senescent mesenchymal stem / stromal cells defect in DNA damage response and anti-oxidative capacity. *Int. J. Med. Sci.* **15,** 771 (2018).

390. Kapiszewskat, M., Reddy, N. M. S. & Lange, C. S. Trypsin-induced changes in cell shape and chromatin structure result in radiosensitization of monolayer Chinese hamster V79. *Int. J. Radiat. Biol.* **60,** 635–646 (1991).

391. Nie, Y., Bergendahl, V., Hei, D. J., Jones, J. M. & Palecek, S. P. Scalable culture and cryopreservation of human embryonic stem cells on microcarriers. *Biotechnol. Prog.* **25,** 20–31 (2009).

392. Leong, W. & Wang, D.-a. Cell-laden polymeric microspheres for biomedical applications. *Trends Biotechnol.* **33,** 653–666 (2015).

393. Declercq, H. A., Caluwé, T. D., Krysko, O., Bachert, C. & Cornelissen, M. J. Bone grafts engineered from human adipose-derived stem cells in dynamic 3D-environments. *Biomaterials* **34,** 1004–1017 (2013).

394. Yan, S., Xia, P., Xu, S., Zhang, K., Li, G., Cui, L. & Yin, J. Nanocomposite porous microcarriers based on strontium-substituted HA-g-poly (γ-benzyl-L-glutamate) for bone tissueeEngineering. *ACS Appl. Mater. Interfaces* **10,** 16270–16281 (2018).

395. Maitz, M. Applications of synthetic polymers in clinical medicine. *Biosurface and Biotribology* **1,** 161–176 (2015).

396. Park, J. S., Yang, H. N., Woo, D. G., Jeon, S. Y. & Park, K.-h. Biomaterials SOX9 gene plus heparinized TGF- b 3 coated dexamethasone loaded PLGA microspheres for inducement of chondrogenesis of hMSCs. *Biomaterials* **33,** 7151–7163 (2012).

397. Niu, X., Liu, Z., Hu, J., Rambhia, K. J., Fan, Y. & Ma, P. X. Microspheres assembled from chitosan-Graft-poly(lactic acid) micelle-like core-shell nanospheres for distinctly controlled release of hydrophobic and hydrophilic biomolecules. *Macromol. Biosci.* **16,** 1039 (2016).

398. Naito, Y., Terukina, T., Galli, S., Kozai, Y., Vandeweghe, S., Tagami, T., Ozeki, T., Ichikawa, T., Coelho, P. G. & Jimbo, R. The effect of simvastatin-loaded polymeric microspheres in a critical size bone defect in the rabbit calvaria. *Int. J. Pharm.* **461,** 157–162 (2014).

399. Alenezi, A., Naito, Y., Terukina, T., Prananingrum, W., Jinno, Y., Tagami, T., Ozeki, T., Galli, S. & Jimbo, R. Controlled release of clarithromycin from PLGA microspheres enhances bone regeneration in rabbit calvaria defects. *J. Biomed. Mater. Res. - Part B Appl. Biomater.* **106,** 201–208 (2018).

400. Swed, A., Cordonnier, T., Dénarnaud, A., Boyer, C., Guicheux, J., Weiss, P. & Boury, F. Sustained release of TGF-β1 from biodegradable microparticles prepared by a new green process in CO2 medium. *Int. J. Pharm.* **493,** 357–365 (2015).

401. Pouponneau, P., Bringout, G. & Martel, S. Therapeutic magnetic microcarriers guided by magnetic resonance navigation for enhanced liver chemoembilization : a design review. *Ann. Biomed. Eng.* **42,** 929–939 (2014).

402. Pouponneau, P., Leroux, J.-c., Soulez, G., Gaboury, L. & Martel, S. Co-encapsulation of magnetic nanoparticles and doxorubicin into biodegradable microcarriers for deep tissue targeting by vascular MRI navigation. *Biomaterials* **32,** 3481–3486 (2011).

403. Monge, C., Almodóvar, J., Boudou, T. & Picart, C. Spatio-temporal control of LbL films for biomedical applications: From 2D to 3D. *Adv. Healthc. Mater.* **4,** 811–830 (2015).

404. Zelikin, A. N. Drug releasing polymer thin films : new era of surface-mediated drug delivery. *ACS Nano* **4,** 2494–2509 (2010).

405. Martin, Y., Eldardiri, M., Lawrence-watt, D. J. & Sharpe, J. R. Microcarriers and their potential in tissue regeneration. *Tissue Eng. Part B* **17,** 71–80 (2011).

406. Levato, R., Visser, J., Planell, J. A., Engel, E., Malda, J. & Mateos-Timoneda, M. A. Biofabrication of tissue constructs by 3D bioprinting of cell-laden microcarriers. *Biofabrication* **6,** 1–12 (2014).

407. Davis, H. E., Binder, B. Y. K., Schaecher, P., Yakoobinsky, D. D. & Leach, J. K. Enhancing osteoconductivity of fibrin gels with apatite-coated polymer microspheres. *Tissue Eng. - Part A* **19,** 1773–1782 (2013).

408. Zhang, Q., Tan, K., Ye, Z., Zhang, Y., Tan, W. & Lang, M. Preparation of open porous polycaprolactone microspheres and their applications as effective cell carriers in hydrogel system. *Mater. Sci. Eng. C* **32,** 2589–2595 (2012).

409. Kim, B. S., Choi, J. S., Kim, J. D., Yeo, T. Y. & Cho, Y. W. Improvement of stem cell viability in hyaluronic acid hydrogels using dextran microspheres. *J. Biomater. Sci. Polym. Ed.* **21,** 1701–1711 (2012).

410. Hong, Y., Gong, Y., Gao, C. & Shen, J. Collagen-coated polylactide microcarriers/chitosan hydrogel composite : injectable scaffold for cartilage regeneration. *J. Biomed. Mater. Res. - Part A* **85,** 628–637 (2007).

411. Mikael, P. E., Golebiowska, A. A., Xin, X., Rowe, D. W. & Nukavarapu, S. P. Evaluation of an engineered hybrid matrix for bone regeneration via endochondral ossification. *Ann. Biomed. Eng.* **48,** 992–1005 (2020).

412. Kandalam, S., Sindji, L., Delcroix, G. J., Violet, F., Garric, X., André, E. M., Schiller, P. C., des Rieux, A., Guicheux, J. & Montero-menei, C. N. Pharmacologically active microcarriers delivering BDNF within a hydrogel: novel strategy for human bone marrow-derived stem cells neural/neuronal differentiation guidance and therapeutic secretome enhancement. *Acta Biomater.* **49,** 167–180 (2016).

413. Kandalam, S., Berdt, P. D., Ucakar, B., Vanvarenberg, K., Bouzin, C., Gratpain, V., Diogenes, A., Montero-Menei, C. N. & des Rieux, A. Human dental stem cells of the apical papilla associated to BDNF-loaded pharmacologically active microcarriers (PAMs) enhance locomotor function after spinal cord injury. *Int. J. Pharm.* **587,** 119685 (2020).

A

Appendix

A.1 Accepted paper: Green and Tunable Animal Protein-Free Microcarriers for Cell Expansion.

The author contributed to the following paper, accepted in ACS Applied Materials & Interfaces.

Green and Tunable Animal Protein-Free Microcarriers for Cell Expansion

Eleana Somville,[1] Anitha Ajith Kumar,[1] Jérôme Guicheux,[2,3] Boris Halgand,[2,3] Sophie Demoustier-Champagne,[1] Anne des Rieux,[1,4,] Alain M. Jonas,[1] and Karine Glinel[1,]**

(1) Institute of Condensed Matter and Nanosciences, Bio and Soft Matter, Université catholique de Louvain, Croix du Sud 1, box L7.04.02, 1348 Louvain-la-Neuve, Belgium.

(2) Inserm, UMR 1229, RMeS, Regenerative Medicine and Skeleton, Université de Nantes, ONIRIS, 44042 Nantes, France.

(3) Centre Hospitalier Universitaire de Nantes, PHU4 OTONN, 44093 Nantes, France.

(4) Louvain Drug Research Institute, Advanced Drug Delivery and Biomaterials, Université catholique de Louvain, Av. E. Mounier 73, box B1.73.12, 1200 Brussels, Belgium.

KEYWORDS. poly(L-lactide); human adipose stromal cell; dynamic culture; spherulite; cell proliferation.

ABSTRACT. Cell culture on microcarriers emerges as an alternative of two-dimensional culture to produce large cell doses which are required for cell-based therapies. Herein, we report a versatile and easy solvent-free greener fabrication process to prepare microcarriers based on a biosourced and compostable polymer. The preparation of the microcarrier core, which is based on poly(l-lactide) crystallization from a polymer blend, allows to easily tune the density, porosity and size

of the microparticles. A bioadhesive coating based on biopolymers, devoid of animal protein and optimized to improve cell adhesion, is then successfully deposited on the surface of the microcarriers. The ability of these new microcarriers to expand human adipose-derived stromal cells with a good yield, in semistatic and dynamic conditions, is demonstrated. Finally, bead-to-bead cell transfer is shown to increase the yield of cell production without having to stop the culture. These microcarriers are therefore a promising and efficient green alternative to currently existing systems.

1. Introduction

Live cell-based therapies are by now well established in modern medicine and the therapeutic potential of a wide variety of cell types (i.e., fibroblasts, lymphocytes, endothelial cells, pancreatic islets, stem cells) has been successfully demonstrated.[1] However, regardless of the specific application, one major challenge that still impedes the industrial development of cell-based therapies is the large number of cells required to treat a single patient.[2] For example, in the case of human mesenchymal stromal cells (hMSCs), which are considered as especially promising candidates for cell therapy, doses ranging from 100 to 150 million cells per patient are usually required.[3] This highlights the critical need for efficient cell expansion technologies to ensure the full development of cell-based therapies.

The expansion of anchorage-dependent cells usually involves the culture of cells as a monolayer in plastic flasks in static conditions.[4–7] When large number of cells are not required, this two-dimensional (2D) culture technique offers the advantages of simplicity and easy handling. However, it shows also a series of drawbacks such as the limited possibility to monitor cell growth during the culture and the static nature of the culture which leads to gradients of pH, dissolved oxygen, nutrient and metabolite concentrations.[5,6] Moreover, the scalability of this 2D approach to

produce a larger number of cells is considerably limited, and would generate considerable amounts of nonrecycled waste.

To overcome these limitations of 2D culture, microcarrier (MC) technology was introduced by Van Wezel in 1967. It relies on cell growth on the surface of small solid particles suspended in the growth medium under slow agitation.[8] The main asset of cell culture on MCs is to provide a large solid surface for cell proliferation in a limited volume of the medium, while keeping relatively homogeneous and controlled environmental culture conditions.[9] However, dynamic culture using MCs is a complex and multiparameter approach that requires a careful selection of the appropriate MC depending on the type of vessel, stirring regime and cell type.[10] In this context, a wide variety of MCs with various characteristics have been commercially developed.[11] However, they have been designed with the aim of propagating anchorage-dependent cell lines used in the production of vaccines and biopharmaceuticals and are usually not optimized for cells directly used as therapeutic agents, notably stem cells, which need to be gently harvested after culture. Moreover, they are frequently coated with animal proteins to ensure cell adhesion which might restrict their application for therapeutic applications due to safety concerns.[12]

Additionally, techniques often used to fabricate MCs usually generate a lot of waste and do not to take into account the requirements of a truly circular economy. For instance, a very popular approach is based on an emulsion solvent evaporation process. Although this technique allows controlling the porosity of the microparticles via the use of effervescent or porogenic additives and, to a lesser extent, to vary their size,[13–15] it is not biocompatible and environmentally-friendly since it relies on toxic organic solvents. To overcome this drawback, nonsolvent-based techniques such as jet milling based on a grinding process,[16] and jet break-up solvent displacement,[17] have

been developed. However, these methods allowed controlling MC size but not their morphology, which limits their application in cell culture.

Recently, we developed in our group an organic solvent-free process to produce microcarriers of tunable size and porosity.[18] This process relies on the spherulitic crystallization of poly(l-lactide) (PLLA), an FDA-approved, biosourced and industrially compostable polymer, in its miscible blend with poly(ethylene glycol) (PEG). At the end of the process, PEG is dissolved in water to retrieve individual PLLA spherulites (**Figure 1A**).[18]

Herein, we show that the processing parameters used to fabricate such PLLA spherulites can be adapted to the production of MC cores with constant core composition but tunable porosity, size and density for both semistatic and dynamic cell cultures. Moreover, to improve cell adhesion, the MC surface is subsequently modified with a bioadhesive coating devoid of animal proteins and toxic chemicals. For this, a layer-by-layer (LbL) film composed of biocompatible hyaluronic acid (HA) and poly(l-ornithine) (PLO) is deposited from aqueous solutions on the MC surface and then chemically cross-linked and grafted with an RGD peptide (**Figure 1B)**. Therefore, the whole fabrication process developed to produce MCs for cell culture is fully green and free from toxic chemicals, since it requires only biocompatible materials and water. The performance of these surface-functionalized MCs is then demonstrated in both semistatic and dynamic culture conditions (spinner flasks) using human adipose-derived stromal cells (hASCs).

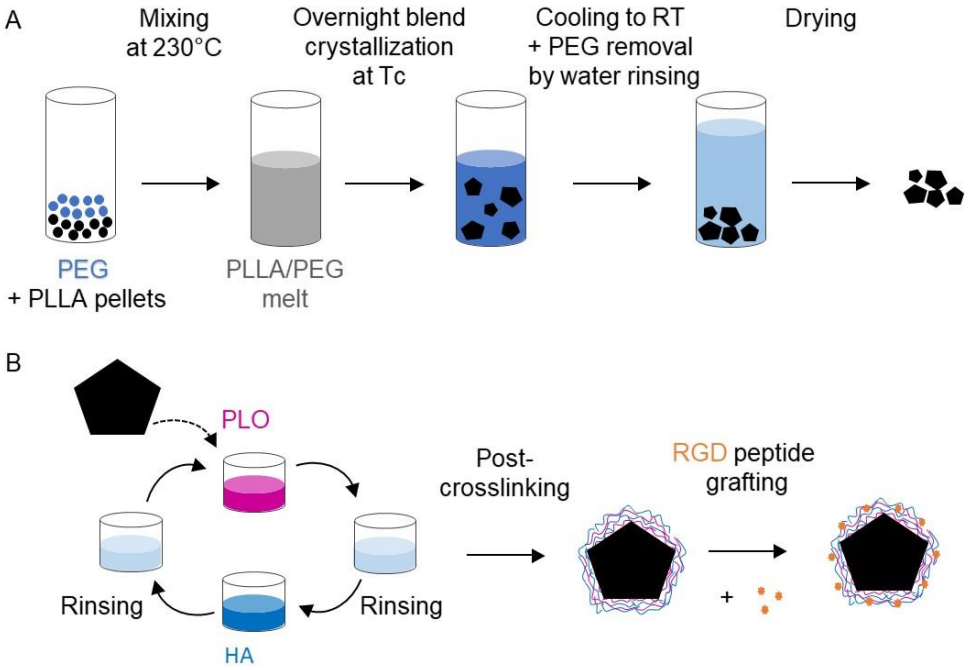

Figure 1: Description of the fabrication process of porous microcarriers via spherulitic crystallization of PLLA (A) and subsequent surface biofunctionalization by layer-by-layer assembly of poly(l-ornithine) (PLO) and hyaluronic acid (HA) followed by post-cross-linking and grafting of a bioadhesive RGD peptide (B).

2. Results and Discussion

2.1. Fabrication, Characterization and Optimization of Microcarrier Cores

MCs need to meet three stringent specifications to be used as microcarriers for dynamic cell expansion: an optimal size for cell growth and maximization of available surface area, an appropriate sedimentation rate to avoid accumulation at the bottom of the reactor under reasonable stirring rates (i.e., 25 – 50 rpm),[19] and sufficient mechanical resistance to withstand stirring. For

microporous MCs, diameters of 100 – 230 µm are reported to be the optimal size.[9] This size range results from a compromise between the maximization of the total surface area, the stability of the suspension (both in favor of a smaller size) and a minimal surface area per microcarrier. For dynamic cell expansion, MCs also need to be well suspended in the medium to optimize nutrient and waste-product transfers between cells and the surrounding medium as well as to avoid microcarrier aggregation which can compromise cell viability.[20] Commercial microporous MCs typically show sedimentation rates between 12 and 19 cm min^{-1}.[21] Finally, MCs need to be able to withstand the mechanical stress induced by the agitation in dynamic conditions as breakage products would be detrimental to the final cell product.[5]

To produce MC cores showing optimal characteristics for dynamic culture, we used a fabrication process based on the PLLA crystallization in a PLLA/PEG blend (**Figure 1A**) which allows us to tune easily the characteristics of MCs by varying the processing parameters.[18] Briefly, PLLA and PEG pellets are mixed in a given ratio and heated at 230 °C to obtain an homogeneous blend. The resulting melt is subsequently cooled to the crystallization temperature (between 103 and 130 °C) to allow PLLA crystallization. The blend is then cooled to room temperature and individual spherulites are retrieved following the dissolution of PEG in water. The effects of blend composition, crystallization temperature and PLLA molar mass on PLLA spherulite characteristics were systematically investigated to provide PLLA core MCs well adapted for dynamic cell expansion in spinner flasks.

2.1.1. Influence of the PLLA/PEG Blend Composition

Younes et al. characterized PLLA/PEG blends made from 10:90 to 90:10 mass ratios. According to their findings, if one component represents more than 20% of the blend, it crystallizes leading to two partially segregated crystalline phases dispersed in an amorphous matrix. For more dilute

compositions, crystallization is possible only for the dominant component, resulting in a noncrystalline matrix composed of the minor component and the noncrystallized fraction of the semicrystalline dominant component.[22] Several authors also reported that a PEG content lower than 10% does not result in a crystallization-induced phase separation.[23–25] Based on these observations, theoretical PLLA/PEG blend compositions leading to crystallization-induced phase separation can range from 10:90 to 80:20. The influence of blend composition on spherulite morphology for PLLA/PEG ratios ranging from 10:90 to 30:70 was described by Kuterbekov et al.[18] They reported that a higher PLLA content led to denser spherulites with smaller pores. However, they did not investigate the properties of these MCs in aqueous solutions.

Scanning electron microscopy (SEM) images of spherulites prepared at a crystallization temperature of 110° C from different PLLA/PEG ratios (using a PLLA of a lower molar mass 20 000 g mol^{-1}, hereafter called PLLA20), including much higher PLLA concentrations than reported by Kuterbekov et al., are shown in **Figure 2**. As expected, a higher PLLA content leads to denser MCs showing a reduced pore size, but also to MCs presenting a better-defined shape with an increasing number of facets as the PLLA content increases. This polyhedral shape results from the impingement of adjacent spherulites due to the competing spherulitic growth inside the blend.[26] By changing the blend composition, it is thus possible to obtain a variety of morphologies ranging from irregularly shaped and highly porous spherulites to denser and well-faceted spherulites. While less dense spherulites could have an appropriate sedimentation rate for dynamic culture applications, they may lack the mechanical resistance required to withstand the agitation necessary to dynamic cell culture.

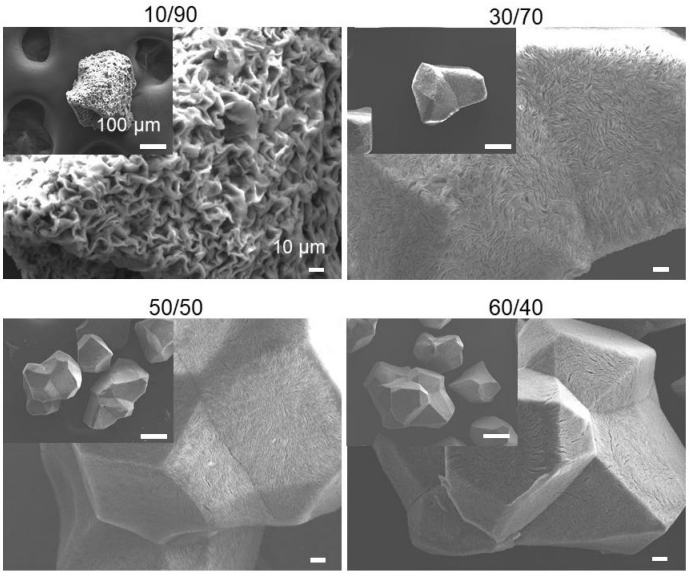

Figure 2: SEM images illustrating the influence of the PLLA20/PEG ratio on MC morphology. The microcarriers were obtained at a crystallisation temperature of 110° C. The scale bars are identical in the four panels.

2.1.2. Influence of the Crystallization Temperature

It is well known that crystallization temperature influences the spherulite size due to the strong temperature dependence of the spherulite nucleation process, with lower temperatures leading to smaller spherulites[18] and higher temperatures corresponding to less numerous nucleation seeds and therefore larger spherulites.[18] The inspection of SEM images of spherulites prepared from a 20:80 PLLA20/PEG ratio, using different crystallization temperatures of 103, 110, 120 and 130 °C (as well as a boxplot with quantitative measurements of the spherulite size) indeed showed that the higher the crystallization temperature, the larger the size of the MCs, as expected (**Figure 3**). Notably, by selecting the crystallization temperature in a range narrower than 30 °C, the average spherulite size can be varied by a factor as large as four, showing the considerable versatility of

the fabrication process. We noticed also that the MC morphology remained very similar for the different tested crystallization temperatures, demonstrating that this parameter does not affect the MC microstructure.

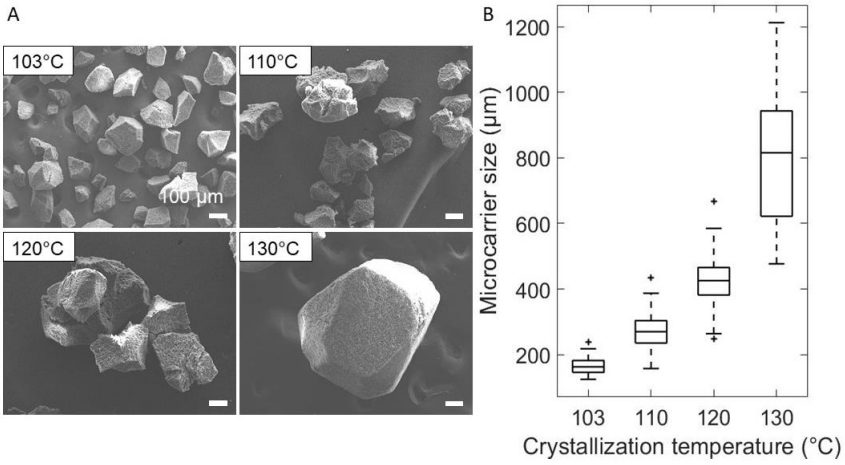

Figure 3: (A) SEM images of PLLA20 MCs prepared with a PLLA20/PEG ratio of 20:80 at different crystallization temperatures. The scale bars are identical in all panels. (B) Boxplot showing the variation of the PLLA20 MC size versus crystallization temperature.

2.1.3. Influence of the PLLA Molar Mass

The influence of the PLLA molar mass on spherulite morphology was also investigated using two PLLA samples of 20 000 (PLLA20) and 40 000-70 000 g mol^{-1} (PLLA40), respectively, whereas the PEG molar mass, the composition of the PLLA/PEG blend (50:50) and the crystallization temperature (110 °C) were kept constant at their finally selected values (see below). The morphology of MCs observed by SEM was very similar whatever the PLLA molar mass, showing multiple faceted particles of similar porosity (**Figure 4A**). Moreover, an increase of PLLA molar mass led to a slight decrease of MC size (**Figure 4B**).

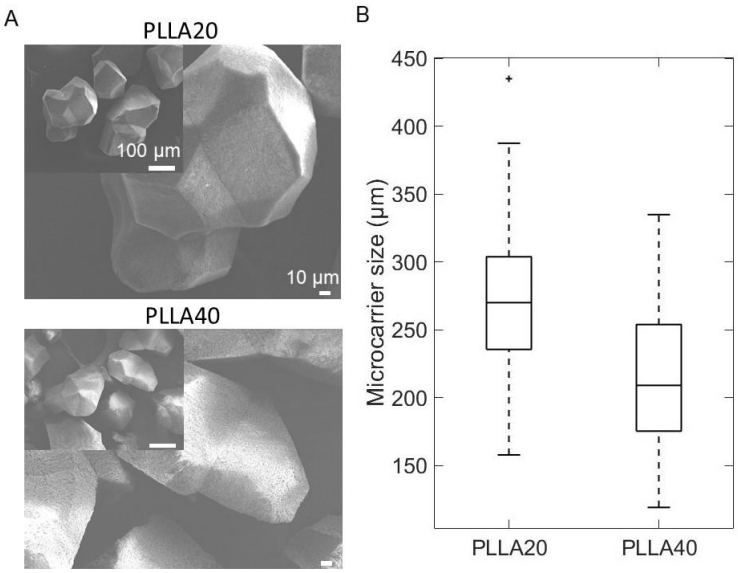

Figure 4: SEM images (A) and size (B) of MCs prepared at a crystallization temperature of 110°C, using the same PLLA/PEG ratio (50:50) but different PLLA molar masses (i.e., PLLA20 and PLLA40). The scale bars are identical in all panels.

2.1.4. Microcarrier Optimization for Dynamic Culture

The sedimentation rate depends not only on the medium density and viscosity but also on the MC density, size, shape and porosity. As the density of PLLA is reported to be 1.24 g cm^{-3} [27] and the MC shape is defined by the crystallization process, the only parameters that can be modified to tune the sedimentation rate are the MC porosity and size. The MC porosity can be modulated by changing the PLLA/PEG ratio and the MC size depends on the crystallization temperature and, to a much lesser extent, on PLLA molar mass, as described above.

Suspension and mechanical resistance under agitation (40 rpm) of PLLA20 MCs produced at different crystallization temperatures (from 110 to 130 °C) and with blends of different

PLLA20/PEG ratios (20:80, 30:70, 50:50 and 70:30) were first tested in spinner flasks to select the optimal MC cores for dynamic cell culture. Some of these PLLA20 MCs suspended well in an aqueous solution under slow agitation (40 rpm). However, their mechanical resistance was limited as they broke after only 2 days of agitation (**Figure 5A**). To overcome this problem, PLLA40 cores prepared with a PLLA sample of a higher molar mass were investigated. Indeed, higher molar masses are expected to result in an increased proportion of tie molecules bridging different lamellar crystals within the spherulites, which should contribute to reinforcing their mechanical resistance. The sedimentation rates of such MCs prepared from different PLLA40/PEG ratios (30:70, 50:50 and 70:30) and at different crystallization temperatures (103, 110, 120 and 130 °C) were first measured in an aqueous solution (**Figure 5D**). Commercial microporous MCs typically show sedimentation rates between 12 and 19 cm min^{-1}.[21] The values obtained here varied between 15 and 85 cm min^{-1} (**Figure 5D**), with the MCs obtained either from a 30:70 ratio crystallized at 110 °C, or from a 50:50 ratio crystallized at 110 or 103 °C, being close to this requirement. Other MCs had a higher sedimentation rate due to their larger size or smaller porosity. Crucially, MCs prepared from a 50:50 ratio at 110 and 103 °C (Figure 5C) were significantly more mechanically resistant than the ones prepared from a 30:70 ratio (Figure 5B), as they did not break even after 7 days of stirring in the aqueous solution. Diameter measurements performed by optical microscopy on 50:50 MCs prepared at 110 °C provided values of 220 ± 56 and 217 ± 45 µm before and after 7 day stirring at 40 rpm, respectively, confirming that microcarriers are not broken under stirring. Therefore, PLLA40 prepared with a 50:50 ratio and crystallization temperatures of 103 and 110 °C were selected for the cell culture assays. The average sizes of these MCs were 132 ± 23 and 220 ± 56 µm, respectively (**Figure S1**).

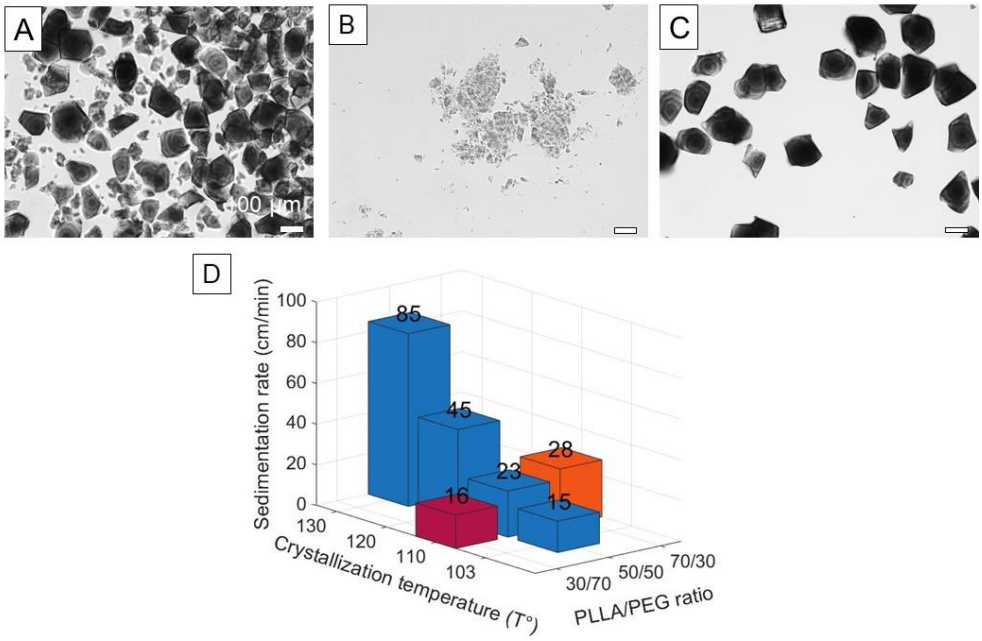

Figure 5: (Top) optical microscopy images of MCs prepared from (A) a 50:50 PLLA20/PEG blend crystallized at 110 °C and stirred for 2 days, (B) a 30:70 PLLA40/PEG blend crystallized at 110 °C and stirred for 4 days and (C) a 50:50 PLLA40/PEG blend crystallized at 110 °C and stirred for 7 days; the stirring was performed in a spinner flask at 40 rpm. The scale bars are identical in all images. (Bottom) Variation of the sedimentation rate of PLLA40 MCs measured in water as a function of the processing parameters used for their fabrication, i.e., crystallization temperature and PLLA40/PEG ratio.

2.2. Bioadhesive Coating Fabrication and Characterization

A (PLO/HA) LbL coating was deposited on the MC surface in order to promote cell adhesion. Coatings based on these polymers showed good results for a variety of cell culture applications[28–31] and this specific polyelectrolyte association was previously successfully deposited on

microparticles used as a scaffold for bone regeneration.[32] This (PLO/HA) film was subsequently cross-linked using a biocompatible cross-linking reaction based on carbodiimide chemistry to improve the stability and the mechanical properties of the coating toward stem cells.[33–35] Then a bioadhesive RGD peptide was grafted on the cross-linked LbL to increase cell adhesion, challenged by the shear stress occurring in dynamic culture conditions.[20] The overall strategy is illustrated in **Figure 1B**.

The variation of the thickness of dry (PLO/HA) film as a function of the number of deposited (PLO/HA) bilayers was investigated on planar model surfaces (**Figure S2A**). It was previously demonstrated that eight bilayers were sufficient to obtain a homogeneous film in a similar system.[36] MCs coated with eight (PLO/HA) bilayers were thus dipped in a rhodamine solution to visualize the film distribution on MCs. This allowed confirming that MCs were uniformly covered by the LbL film (**Figure S2B**). Therefore, such a coating with $(PLO/HA)_8$ was used to modify the MC surface. This LbL coating was subsequently grafted with an RGD peptide and two RGD concentrations (1 and 0.1 mM) were tested to optimize cell adhesion and proliferation on MCs. Indeed, as of now, no consensus has been reached on the optimal RGD concentration. While a higher RGD surface density is usually related to cell spreading, survival and proliferation,[37] it has also been reported that a large adhesion strength tends to reduce cell migration/proliferation and to induce cell differentiation instead.[38]

The grafting of RGD peptide on $(PLO/HA)_8$ films deposited on planar surfaces was first investigated by using a fluorescent RGD-FITC peptide at two concentrations following an N-hydroxysulfosuccinimide (Sulfo-NHS)/N-(3-dimethylaminopropyl)-N'-ethylcarbodiimide hydrochloride (EDC) activation step. A control sample prepared without activation step was also produced. Imaging by epifluorescence microscopy of the samples grafted using 1 and 0.1 mM

RGD (**Figure 6A** and **6B**, respectively) revealed the successful grafting of the peptide. As seen from the difference of fluorescence intensity between those two images, the higher the peptide concentration used for the grafting, the higher the fluorescence intensity on the film, which means a higher degree of peptide grafting (qualitative evaluation). Moreover, the chemical grafting of the peptide on the $(PLO/HA)_8$ films required the activation of the carboxylic groups present on HA chains. Indeed, when the activation step was omitted (**Figure 6C**), the peptide was simply slightly adsorbed on the film and rinsed away in subsequent steps, as evidenced by the much lower fluorescence intensity. Similar experiments were performed to evaluate the grafting of the peptide on $(PLO/HA)_8$-modified MCs (**Figure 6D, E, F**) confirming that the activation step is required to chemically graft the peptide on the film and that a higher peptide concentration led to a larger amount of peptide grafted on the film.

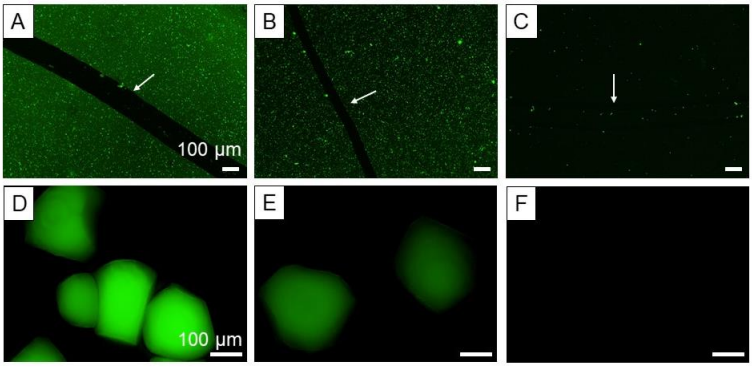

Figure 6: Fluorescence microscopy images of $(PLO/HA)_8$ bilayer films deposited on flat model surfaces activated by sulfo-NHS/EDC and incubated in (A) 1 mM or (B) 0.1 mM RGD-FITC solution and (C) control without any prior activation incubated in 0.1 mM RGD-FITC solution.

Deliberate scratches (see white arrows) were made on the films to visualize the fluorescence background. Fluorescence microscopy images of MCs coated with eight (PLO/HA) bilayer films activated and incubated in (D) 1 mM or (E) 0.1 mM RGD-FITC peptide solution and (F) control without any prior activation then incubated in 0.1 mM RGD-FITC solution. The scale bars are identical in each line.

2.3. Cell Culture on Microcarriers

2.3.1. Culture in Semistatic Conditions

hASCs were selected to assess the MC performance for cell expansion as they are replacing bone-derived MSCs as the gold standard for MSC-based therapy.[39,40] As the MCs presented here are novel, no information on how they would interact with cells is available. Thus, their ability to support hASC adhesion and proliferation was first evaluated in semistatic conditions. The objective was also to select the most efficient surface modification and then test the same parameters in dynamic conditions.

To perform assays in semistatic conditions, intermittent agitation was only carried out during the adhesion step and then the rest of the culture was done in static conditions. PLLA cores prepared from a PLLA40/PEG ratio of 50:50 crystallized at 110 °C were used for these studies. These PLLA cores were coated with a film of cross-linked LbL grafted with RGD (0.1 and 1 mM, referred to as MC-RGD 0.1 and MC-RGD 1, respectively). Bare MCs and MCs coated with cross-linked LbL (referred to as MC-LbL) were used as controls. Cell proliferation was followed over time (up to 5 days).

The initial cell adhesion was quantified 4 h after seeding on MCs in semistatic conditions (intermittent agitation) by measuring their metabolic activity. hASCs were able to attach and grow on MCs whatever the surface treatment but adhesion and proliferation were higher when the MCs

were grafted with RGD (**Figure 7A**). Coating the surface of MCs with cross-linked LbL increased cell proliferation but not initial cell adhesion. Only MC-RGD 1 allowed a higher cell attachment than the bare MCs. Overtime, hASC proliferation was higher on RGD-coated MCs, but no significant difference was observed between the two concentrations of RGD. This observation was confirmed by a live/dead assay (**Figure 7B**). Cells reached confluency on MC-RGD 1 after 5 days when almost no cells were visible on the bare MCs. The absence of PI (red) staining indicated the lack of major cytotoxicity of the MCs, whatever their surface treatment.

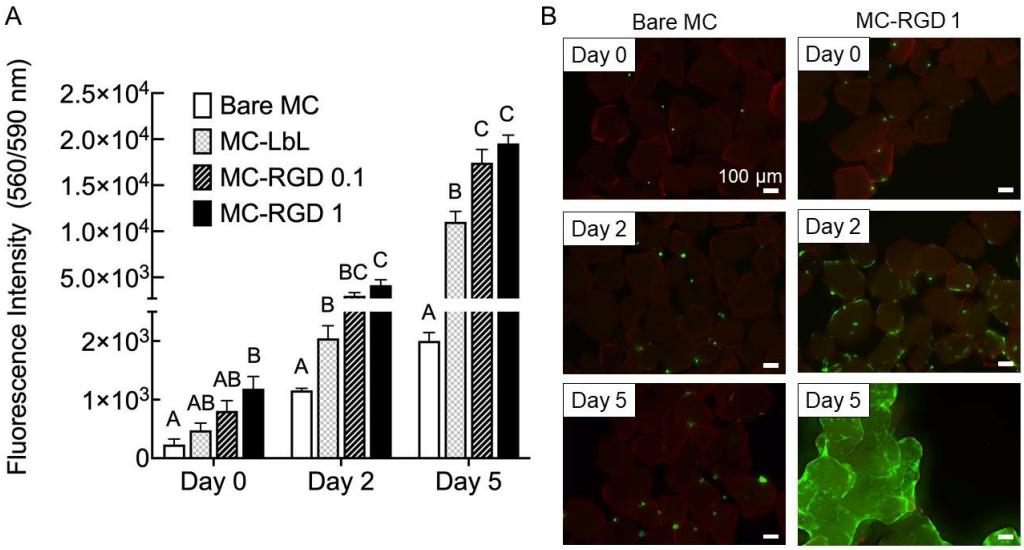

Figure 7: hASC proliferation performed in semistatic conditions on different MCs: (A) Metabolic activity evolution (PrestoBlue™) of cells grown on bare MCs, MC coated with cross-linked LbL (MC-LbL), MCs coated with cross-linked LbL grafted with 0.1 mM (MC-RGD 0.1) and 1 mM RGD (MC-RGD 1), over 5 days ($N = 2$, $n = 3$). Bars topped with different letters indicate a significant difference ($p < 0.05$). (B) Live/dead images of bare MCs and MC-RGD 1 on days 0, 2 and 5. The scale bars are identical in all panels.

DNA content quantification was also performed to measure cell proliferation. However, the kit reagents interacted with MCs whatever the experimental settings, precluding any accurate quantification (data not shown).

Cell adhesion and viability on MC-RGD-1 with different core morphologies (obtained from MCs prepared from 30:70, 50:50 and 70:30 PLLA40/PEG blends) was also investigated (**Figure S3**). No difference could be observed between MCs prepared from 30:70 and 50:50 PLLA40/PEG ratios, while a lower cell adhesion was found on MCs prepared from a 70:30 PLLA40/PEG ratio, indicating that cell adhesion is influenced by the MC surface morphology underneath the coating.

2.3.2. Culture in Dynamic Conditions

For the dynamic culture, PLLA cores prepared with a 50:50 PLLA40/PEG ratio crystallized at 103°C were used. These PLLA cores showed the same morphology and porosity as the ones used for semi-static studies (**Figure S4**) but could be suspended better under gentle agitation, thanks to their lower average size (**Figure S1**). Similarly to the MCs used for semi-static culture, these PLLA cores were coated with LbL and grafted using 1 mM peptide (MC-RGD 1). Indeed, preliminary assays performed on bare MCs and MCs coated with LbL only, confirming that cell adhesion was not high enough on these MCs to perform cell culture in dynamic conditions (**Figure S5**). An agitation speed of 45 rpm was selected as the best compromise between maintaining the MCs in suspension in the spinner flask and keeping cells on the MCs (data not shown).

Very little to no toxicity was observed when hASCs were grown on MC-RGD 1, even after 7 days of culture (**Figure 8A-C**). Cells were metabolically active and continued to proliferate over time

(**Figure 8D)**. The number of cells on MCs increased by a 7.42 ± 0.97-fold between day 1 and day 4 and up to a 13.27 ± 2.27-fold between day 1 and day 7 to reach confluency.

Slight MC aggregation was observed by day 7 due to cell-cell adhesion between MCs (**Figure 8C**). MC aggregate formation was also reported for culture performed on commercial Cytodex® MCs, which caused mass-transfer limitations forming stagnant cores and leading to cell necrosis.[41–43] However, in our study the MC aggregates were small-sized (250-400 μm) and did not cause cell death.

To compare the performance of PLLA MCs with commercial ones, dynamic culture assays were also performed using Cytodex® 3 microcarriers (**Figure S6**). The final fold increase obtained with these MCs was 22 ± 1.49 by day 7 of culture, which is comparable to the one measured for PLLA MCs, albeit slightly higher.

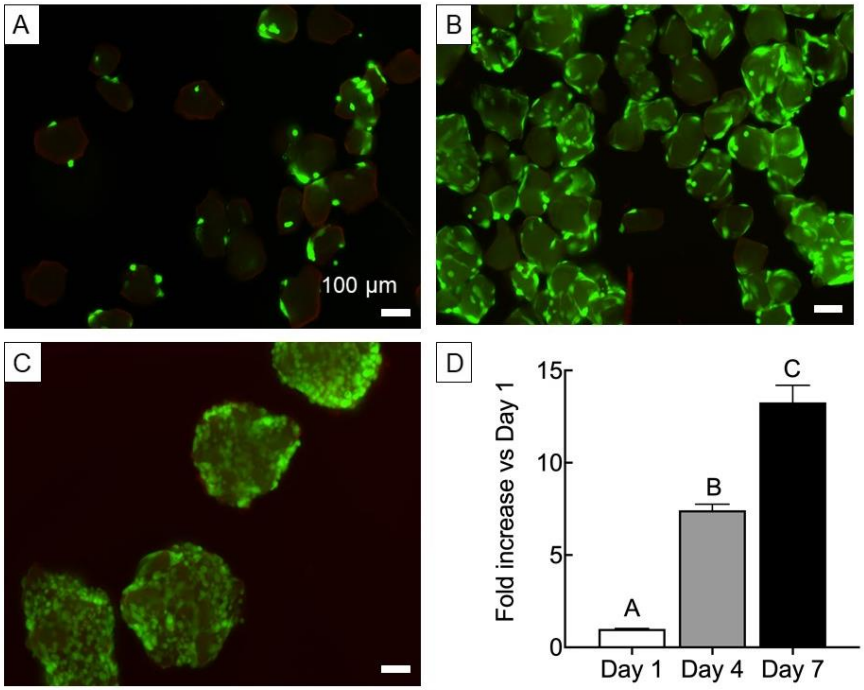

Figure 8: Viability and proliferation of hASCs grown on MC-RGD 1 in dynamic conditions: analysis of hASC viability by live/dead staining on (A) day 1, (B) day 4 and (C) day 7. The scale bars are identical in all panels. (D) Quantification of cellular metabolic activity (measured with PrestoBlue™). Bars topped with different letters indicate a significant difference ($p < 0.05$) ($N = 3$, $n = 3$).

The morphology and cytoskeletal organization of hASCs grown on the MC-RGD 1 surface were studied by staining of the cell cytoskeleton at different time points. The cell nucleus was simultaneously counterstained with (4′,4′,6-diamidine-2′- phenylindole dihydrochloride (DAPI) (**Figure 9A**). Layer-by-layer Z stacking and 3D reconstruction from the confocal laser scanning microscopy (CLSM) images showed that cells exhibited prominent actin fibers on the MC surface

as early as on day 1 after seeding. By day 4, the cells spread on the MC surface with well-defined actin filaments which progressively increased with culture duration and covered the entire surface of the microcarriers by day 7.

Additionally, SEM analysis was conducted at the same time points to characterize cell morphology on MCs. On day 1, the cells appeared rounded on the carriers (**Figure 9B**). However, on day 4 after seeding, cells flattened and appeared well spread on the MC surface. On day 7, the cells underwent active proliferation and formed several cell bridges with the adjacent MCs to form aggregates (**Figure 9B**).

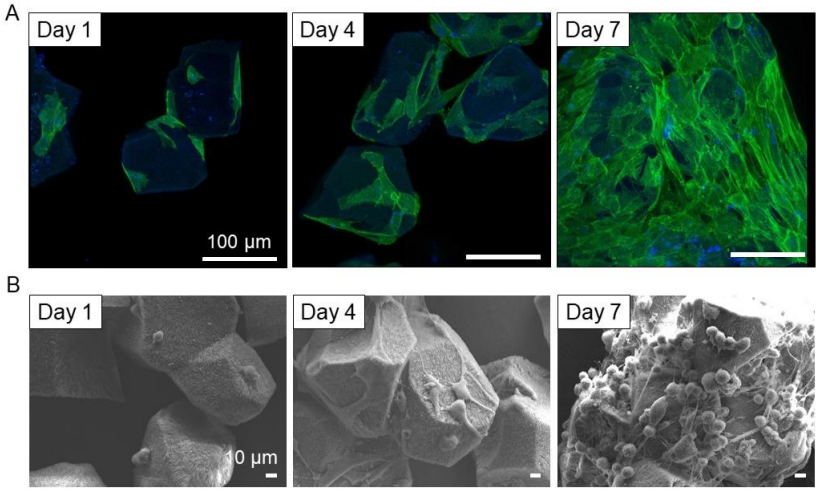

Figure 9: Cytoskeletal organization and spreading of hASCs grown on MC-RGD 1 surface: (A) CLSM micrographs of F-actin stained hASCs. Phalloidin stains actin filaments (green) and DAPI stains cell nuclei (blue). The blue color observed on the MC surface at day 1 and day 4 results from the interaction between DAPI and the bioadhesive coating deposited on the MC surface. (B) SEM images of hASCs grown on MC-RGD 1.

Several studies describing mesenchymal stromal cell expansion on various commercial microcarriers are available in the literature. Eibes et al. cultured MSCs on Cultispher®-S microcarriers in a spinner flask and obtained an 8.4-fold increase in the cell number on day 8.[44] A fourfold increase in the growth rate of hMSCs was reported on Cytodex®1 microcarriers on day 7 of spinner flask culture by Schop et al.[45] Similarly, a 13.6-fold expansion on Cytodex® 3 microcarriers was reported on day 11.[46] Even though a direct comparison with these earlier reports may not be accurate due to variations in cell type, cell source, methodology for cell characterization, culture medium and culture duration, it can be stated that the MCs developed in our study allowed a significantly high cell proliferation rates in dynamic culture over a short duration of 7 days.

2.3.3. Cell Proliferation by Bead-to-Bead transfer

One advantage of dynamic culture on MCs is the possibility to increase the yield of cells at the end of the production period by the addition of fresh MCs during the proliferation phase to perform what is called "bead-to-bead transfer". This offers new surfaces to the cells to attach and proliferate.

New MC-RGD 1 was introduced into the spinner flasks at a ratio of 0.5:1 (new MCs/initial MCs), 5 days after initial seeding. To discriminate the fresh MCs from the initial ones, the coating of fresh MCs was labeled with polyallylamine-rhodamine (**Figure 10A**). The culture was maintained at an intermittent mode of agitation for 12 h (i.e., agitated for 2 min and then kept static for 28 min). Maintaining an intermittent agitation[47] allowed the MCs to be in close proximity with one another, which enabled the transfer of cells from initial MCs to the new MCs.[48] It was observed that cell transfer started as early as 1 h after the addition of fresh MCs.

The transfer of cells from the initial microcarriers to the new ones added during the culture can be explained by two possible mechanisms. The first one is related to the attachment of free-floating cells in the medium. Indeed, cells can detach from the confluent microcarriers and then colonize the new MCs. Verbruggen et al. attributed the high increase in the cell number after the addition of fresh beads in the medium to this mechanism, rather than to increased proliferation rates.[49] According to the second mechanism, cells attached to initial MCs migrate on the new ones thanks to the formation of cellular bridges between both MCs during the intermittent agitation performed just after the addition of the new MCs in the medium.[50] According to the microscopy images recorded just after the intermittent agitation step (**Figure 10A**) and the fact that we observed only a very few free-floating cells in our cultures, we assume that the second mechanism of cell transfer was achieved during our bead-to-bead cell transfer assays.

Quantification of cell proliferation by evaluation of cell metabolic activity was performed during the culture (**Figure 10B**). Values of 16.89 ± 1.8 and 21.87 ± 0.6-fold increase were measured on day 7 and day 9, respectively, proving the advantage of bead-to-bead cell transfer to improve the cell yield.

After the MCs reach confluency, a portion can be extracted from the culture system and fresh empty MC can be added instead to provide the additional surface area for cells to attach and continue the proliferation.[51] Routine and extensive subculturing of cells has shown to induce cells into replicative senescence, a state of growth arrest.[52] Bead-to-bead methodology of cell transfer does not require intermediate passaging of cells, and therefore provides opportunities for cell expansion with minimum manipulation. In this study, we give a direct evidence that hASCs display

bead-to-bead transfer on the PLLA MCs. Therefore, this methodology offers a cost-effective alternative to scale up the commercial production of stem cells.

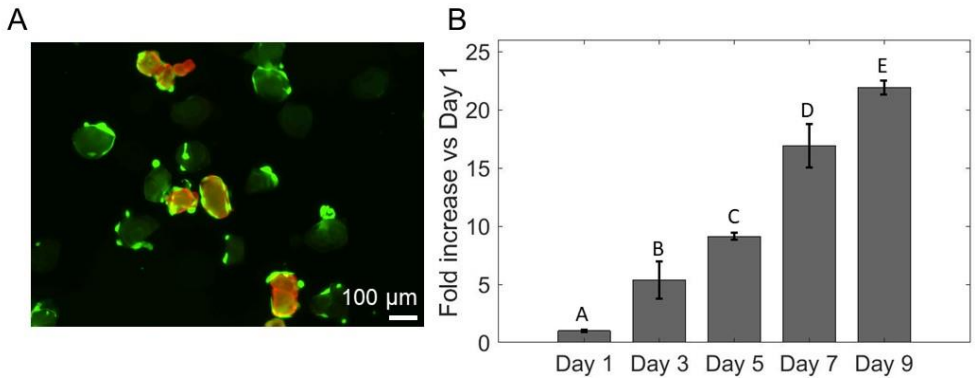

Figure 10: Bead-to-bead cell-transfer assay performed with hASC cultured on MC-RGD 1. In total, 50% of fresh MC-RGD 1 (stained in red with poly(allylamine)-rhodamine) were added to the existing culture after 5 days of cell expansion. (A) Live/dead images after 12 h of intermittent agitation. Cells were stained with calcein-AM. (B) Quantification of cellular metabolic activity (PrestoBlue™). ($N = 1$, $n = 3$). Bars topped with different letters indicate a significant difference ($p < 0.05$).

2.4. Magnetic Microcarriers

After the expansion step on MCs, the cells usually need to be detached and separated from MCs.[6] As of now, the separation step has received little attention and usually involves the use of filtration or centrifugation.[53] Alternatively, MCs displaying magnetic properties could facilitate MC handling during MC-cell separation by allowing to immobilize MCs using a magnet. This feature could also ease MC handling during culture such as for medium replenishment. To test the fabrication of magnetic PLLA MCs, magnetic nanoparticles (MNPs) were incorporated into the

PEG powder used for the preparation of PLLA/PEG (**Figure 1A**). The obtained MCs displayed a superparamagnetic behaviour (**Figure S7A**) and could simply be attracted in a solution using a 1.4 T magnet (**Figure S7B**). The release of iron in solution was measured after a storage time of several weeks and was found negligible (data not shown) evidencing the stability of these MCs. Additionally, these magnetic MCs supported cell adhesion and proliferation to the same extent as nonmagnetic MCs (results not shown). These experiments contribute to demonstrate the versatility of our fabrication process to produce MCs with a large range of characteristics.

3. Conclusions

We have disclosed the preparation of biodegradable MCs composed of a biosourced and nonexpensive polymer, easy to produce with a scalable solvent-free process, which could even be industrially composted after use for optimal circularity. Their preparation process is extremely versatile, and the MC size, porosity and mechanical resistance can easily be optimized by tweaking trivial processing parameters such as crystallization temperature and PEG content, without impacting the global process. Additionally, the MC surface can be easily functionalized with an animal protein-free bioadhesive polysaccharide/polypeptide coating, which constitutes a supplementary asset with respect to current regulations; this coating is subsequently grafted with an RGD peptide for optimal cell adhesion.

The PLLA MCs support growth and proliferation of stem cells in semi-static conditions and, most importantly, in dynamic conditions too. hASCs can be easily expanded (more than by 12-fold over 1 week) and the cell production yield can be increased by successful bead-to-bead cell transfer. Cell retrieval and separation from the MCs can even be facilitated by providing them with magnetic properties. Alternatively, as they are composed of biocompatible FDA-approved components and are animal- and organic-solvent-free, directly implanting the cell-MC complexes

may be considered in the future, provided that in vivo studies demonstrate no toxicity. Therefore, our new MCs are a promising animal protein-free greener alternative to commercial MCs used for stem cell expansion and tissue engineering alike.

4. Experimental Section

Materials

PLLA20 (20 000 g mol^{-1}, Đ 1.1), PEG (3 500 g/mol) were obtained from Sigma-Aldrich. PLLA40 (Mn 40 000-70 000 g mol^{-1}) was obtained from Polysciences. Dextran-coated iron oxide magnetic nanoparticles (MNPs) were purchased from Ocean Nanotech. Sodium hyaluronate (HA) (360 000 g mol^{-1}) was obtained from Lifecore Biomedical. Poly-l-ornithine hydrobromide (PLO) (78 000 g mol^{-1}) was purchased from Alamanda Polymers. Rhodamine-labeled poly(allylamine) (Mw 15 000 g mol^{-1}) was purchased from Surflay Nanotec GmbH. Poly(ethyleneimine) (PEI) (Mn 60 000 g mol^{-1}), N-hydroxysulfosuccinimide sodium salt (Sulfo-NHS) (98 %), N-(3-dimethylaminopropyl)-N'-ethylcarbodiimide hydrochloride (EDC) (98 %), 4-(2-hydroxyethyl)piperazine-1-ethanesulfonic acid (HEPES) (99.5 %), sodium chloride (NaCl) (99.5 %), dimethylsulfoxide (DMSO), hexamethyldisilazane (HMDS) (99 %) were bought from Sigma-Aldrich. 2-(N-morpholino)ethanesulfonic acid (MES) (99 %) and absolute ethanol (95 %) were obtained from Acros. GRGDS peptide (RGD peptide) (98 %) and fluorescent RGDK-FITC (95 %) were provided by Genecust. Milli-Q grade water (resistivity of $18.2.10^6$ Ω.m) was produced by a Milli-Q™Reference system of Merck Millipore. Mesenchymal stem cell growth medium 2 (basal medium supplemented with supplement mix) was purchased from Promocell. Dulbecco's phosphate buffered saline devoid of calcium and magnesium (DPBS)), StemPro™ Accutase Cell Dissociation Reagent, Alexa Fluor 488 phalloidine, calcein-AM, and PrestoBlue™ Cell Viability reagent were provided by ThermoFisher Scientific. Penicillin/streptomycin (PEST) was obtained

from Life Technologies. Triton TM X-100, bovine serum albumin (96 %) (BSA), glutaraldehyde aqueous solution (25 %) and 4',4',6- diamidine-2'-phenylindole dihydrochloride (DAPI) (98 %) were purchased from Sigma-Aldrich. Corning® Costar® Ultra-Low Attachment Multiple Well Plates were purchased from VWR. Cellstar® 24-well cell culture plates were purchased from Greiner Bio-one. Spinner flasks of 125 mL capacity equipped with a magnetic ball impellor (Magna-Flex™, Wheaton) were used to perform cell culture in dynamic conditions. Single-side-polished (100) silicon wafers were purchased from TOPSIL. Cytodex® 3 microcarriers were obtained from GE Healthcare. Ethidium bromide was purchased from Biotium. Human adipose-derived stromal cells (hASCs) were collected from lipoaspirates harvested from one adult donor who had provided their informed consent.

Fabrication of Microcarriers

PLLA microcarriers were prepared via isothermal spherulitic crystallization of PLLA/PEG blends as described in **Figure 1A**. PLLA of two different molar masses (PLLA20 and PLLA40) were used. PLLA and PEG in the form of dry powders were first combined with the desired PLLA/PEG ratio (ranging from 10:90 to 70:30) and melt-mixed at 230 °C for 5 min under dry argon, followed by vortexing to obtain a homogeneous melt. The melt was then isothermally crystallized overnight under inert atmosphere in a glass tube fitted with a rubber septum at a given temperature (comprised between 103 ± 0.1°C and 130 ± 0.1°C) fixed by a heated oil bath. After crystallization, the blend was cooled down to room temperature and then repeatedly washed with Milli-Q water to remove PEG and collect the insoluble PLLA microcarriers.

Surface Biofunctionalization of Microcarriers

The (PLO/HA) films were deposited onto the MC surface by the LbL deposition technique.[54] An anchoring PEI layer was deposited as a first layer. PLO and HA dissolved in 0.15 M NaCl (pH 7.4)

at concentrations of 0.5 and 1 mg mL^{-1}, respectively, were adsorbed alternately on MCs by immersing the sample for 5 min in the polyelectrolyte solutions. Then, three washing steps were performed in 0.15 M NaCl (pH 7.4), consisting, respectively, of 1 s dipping for ten times, 5 s dipping for five times and 10 s dipping for one time. The resulting films are denoted $(PLO/HA)_n$, where *n* is the number of PLO/HA deposited bilayers. The (PLO/HA) films were also built onto silicon wafers used as model surfaces. For this, silicon wafers were first cleaned by immersion in a freshly prepared piranha mixture [H_2O_2 (35 %)/H_2SO_4 (98 %) (1:1 v/v)] for 20 min, rinsed extensively with Milli-Q water and dried under an argon stream. The LbL films were deposited on the samples using an automated dipping machine (Riegler and Kirstein GmbH). For LbL deposition on MCs, wet MCs were placed in porous cell culture inserts (Corning Netwell, 74-µm mesh size) that were fixed on the arm of the dipping robot. After LbL deposition, (PLO/HA) films were cross-linked through an overnight incubation at 4°C in a freshly prepared cross-linking solution containing 70 mg mL^{-1} of EDC and 11 mg mL^{-1} of sulfo-NHS in 0.15 M NaCl (pH 5.5).[33] Then the samples were rinsed five times for 20 min in HEPES (20 mM in NaCl 0.15 M, pH 7.4) buffer.

The bioadhesive GRGDS peptide was grafted on the cross-linked (PLO/HA) films using the same EDC/sulfo-NHS chemistry as for the cross-linking step. Briefly, MCs or silicon wafers covered by a cross-linked (PLO/HA) film were incubated for 15 min at 4°C in a freshly prepared 0.1 M MES solution (pH 6.5) containing 0 mg mL^{-1} EDC and 11 mg mL^{-1} sulfo-NHS. Samples were then rinsed thoroughly with the MES solution before being incubated overnight at 4°C in the peptide solution at a concentration of 0.1 mM or 1 mM in the MES buffer. Following the grafting, flat samples were rinsed eight times for 20 min in HEPES (20 mM in NaCl 0.15 M, pH 7.4) buffer, thrice for 20 min in ethanol/Milli-Q (50:50 v:v) solution and twice for 20 min in Milli-Q water to

completely remove the non-grafted peptide. For MCs, an additional overnight wash in HEPES was performed before the ethanol/Milli-Q washing step to ensure complete removal of the nongrafted peptide. The same conditions were used to graft fluorescent RGDK-FITC peptide on crosslinked (PLO/HA) films. Control samples were also prepared by omitting the EDC/sulfo-NHS activation step prior to incubation in the peptide solution. MCs grafted with 0.1 mM and 1 mM peptide concentrations are denoted MC-RGD 0.1 and MC-RGD 1, respectively. The fluorescent MCs were fabricated in a similar manner except that PAH-rhodamine was deposited as the first layer during the LbL process.

Morphology and Structure of Microcarriers

MCs dried overnight at room temperature and then sputter-coated with a 8 nm-thick layer of chromium under high vacuum, were observed by scanning electron microscopy (SEM) using a JEOL 7600F scanning electron microscope operated at an acceleration voltage of 15 kV.

Measurement of the Microcarrier Size

MCs suspended in water were imaged by bright-field microscopy using an Olympus epifluorescence IX71 microscope. The MC average size was obtained as the geometric average between the longest and shortest dimension of 50 randomly selected MCs, as measured using the microscope software (CellSensDimension).

Sedimentation Rate Estimation

Wet MCs prepared at different crystallization temperatures and PLLA40/PEG ratios were deposited on the top surface of a water column. The time needed for them to sink over 20 cm was recorded five times, with t_0 and t_f being the times for the first and last MCs, respectively, to cover

a fixed distance of 20 cm. For each condition, the sedimentation rate was estimated as the median of t_0 and t_f.

Qualitative Observation of Microcarrier Mechanical Resistance under Stirring

To qualitatively assess the resistance of MCs prepared using different processing parameters to dynamic culture conditions, 50 mL of MC suspension (1 mg mL^{-1}) was placed in a spinner flask under agitation at 40 rpm for up to seven days. MCs were then observed by bright-field microscopy.

Determination of the LbL Coating Thickness

The thickness of $(PLO/HA)_n$ with *n* varying from 2 to 10 deposited on flat silicon wafers then cross-linked and dried, was measured by ellipsometry using an Accurion EP4 single-wavelength ellipsometer. The wavelength of the laser was 658 nm and the incidence angle ranged from 60° to 80° (2° increment). The film thickness was determined by fitting a one-layer model with built-in software. The refractive index of the (PLO/HA) films was fixed at 1.5 and that of the silicon substrate to the value tabulated by the manufacturer.

Visualization of the LbL Coating onto Microcarriers

MCs coated with a (PLO/HA) film were dipped in a rhodamine aqueous solution and then imaged with a Zeiss LSM 700 confocal laser scanning microscope to visualize the coverage of the microcarrier surface by the polyelectrolyte coating.

Evidence for the Peptide Grafting on LbL Coatings by Epifluorescence Microscopy

The grafting of the RGDK-FITC peptide on both flat model films and surface-modified MCs was evidenced by imaging the samples with an Olympus epifluorescence IX71 microscope equipped with a blue filter U-MNUA2 (excitation 360-370 nm and emission 420-460 nm), a green filter U-

MWIBA3 (excitation 460-495 nm and emission 510-550 nm) and a red filter U-MNIGA3 (excitation 540-550 nm and emission 575-625 nm). The UV light was provided by an X-Cite module, series 120PCQ from Lumen Dynamics. On flat surfaces, a deliberate scratch was made to evaluate the background fluorescence. The fluorescence intensity of the samples was estimated by comparing the fluorescence intensity measured on the scratch and on the rest of the sample surface.

MC Preparation for Cell Culture Assays

MCs were first rinsed in ethanol 70% then transferred in sterile DPBS. They were subsequently sterilized by exposure to UV light for 30 min either in well plates or Petri dishes depending on the treated quantity. Following sterilization, the MCs were transferred in the appropriate culture vessels (well plate or spinner flask), the supernatant was removed, replaced by cell culture medium and conditioned in an incubator for 30 min.

Routine Culture of hASCs

hASC cells were routinely cultured in cell culture flasks in reconstituted Mesenchymal Stem Cell Growth Medium 2 from PromoCell supplemented with 1% (v/v) PEST in an incubator (Binder CB170 E7) at 37 °C and 5% CO_2. The supplemented culture medium was renewed three times per week and confluent cells were subcultured using Accutase. Cells were used from passage 4 to passage 8.

Cell culture in Semistatic Conditions

On day 0 of the experiments, four types of MC samples prepared from a PLLA40/PEG ratio of 50:50, were placed in wells of ultralow attachment 24-well plates: uncoated MCs (referred to as bare MCs), MCs coated with $(PLO/HA)_8$ (referred to as MC-LbL), and MCs coated with $(PLO/HA)_8$ grafted using 0.1 mM RGD peptide (referred to as MC-RGD 0.1) or 1 mM RGD

peptide (referred to as MC-RGD 1). Then, 300 µL of supplemented medium was added in each well and the plates were placed in the incubator for 30 min for conditioning. During this time, hASCs cultured in cell culture flasks were detached from the flask using Accutase and counted using a Burker cell counting chamber. The supernatant was removed from each well and 300 µL of cell suspension was added, resulting in a final concentration of 3 500 cells/well. Well plates were placed in the incubator and manually agitated for 2 min every 28 min for 4 h. Then, each well was rinsed two times with 500 µL of PBS to remove nonadhered cells. The supplemented medium (300 µL) was added to each well and the plates were incubated for 5 days. The medium was replaced by 500 µL of fresh supplemented medium on day 2. Moreover, on days 0, 2 and 5 of the experiment, metabolic assays were performed in triplicate by incubating the samples for 3 h in 250 µL of reactive medium containing PrestoBlue™ Cell Viability Reagent (10 %). One hundred microliters of supernatant was transferred to a flat-bottom black well plate and the fluorescence intensity was measured using a TECAN Infinite M1000 microplate reader (560 nm/590 nm excitation/emission). Finally, MCs were retrieved, rinsed twice with 500 µL of PBS and then stained for cell characterization. For any experiment, the number of independent repetitions of the experiment and the number of replicates used for each repetition are referred to as N and n, respectively.

Cell Culture in Dynamic Conditions

Cell culture in dynamic conditions was performed using 125 mL spinner flask equipped with a magnetic ball impellor. To prevent cell and microcarrier adhesion on the inner surface of the spinner flask, it was siliconized with Sigmacote® agent (Sigma-Aldrich). After treatment, the spinner flask was thoroughly washed with Milli-Q water to remove the nongrafted product. The

surface-modified spinner flask was autoclaved prior to use. Experiments have been performed in triplicate.

MC-RGD 1 prepared from a 50:50 PLLA40/PEG ratio and sieved to obtain a size ranging from 100 to150 µm was selected for dynamic culture assays. Indeed, such MCs allowed getting stable dispersions in the spinner flask. Sixty milligrams of freshly sterilized MC-RGD 1 was conditioned in 30 mL of fresh medium in a spinner flask for 30 min. Then, the medium was removed and fresh culture medium was added to obtain a final MC concentration of 1 mg mL^{-1}. Cells were seeded at a density of 8 365 cells mg^{-1} of MC or 3.5 cells per MC[1]. To ensure cell adhesion, spinner flask agitation was kept intermittent overnight, with a 2 min agitation at 45 rpm, followed by 28 min rest. The following day, the medium with unattached cells was removed and the fresh medium was added. The agitation was then continued at 45 rpm throughout the culture period. The medium was completely replaced every 3 days.

During the cultures in the spinner flask, a tiny fraction of MCs was collected at designated times points for analysis. To maintain consistency, the flask content was mixed by a gentle manual agitation and a representative sample was collected from the center of the culture content. One milliliter of the medium containing about 1 mg of MCs was transferred to individual wells of an ultralow adhesion well plate. After MC settling, the supernatant was removed and MCs were rinsed with PBS for further analyses.

The metabolic activity of the cells grown on MCs was also quantified during the culture by the PrestoBlue™ Cell Viability assay, as described above. For any experiment, the number of

[1] One milligram of MC prepared from a 50:50 PLLA/PEG ratio at 103°C, contains approximately 2 390 ± 157 individual microcarriers according to microscopy analysis. Therefore, an initial seeding density of 8 365 cells mg^{-1} of MC means roughly 3.5 cells per microcarrier.

independent repetitions of the experiment and the number of replicates used for each repetition are referred to as *N* and *n*, respectively.

Bead-to-Bead Cell Transfer Assays

When the first batch of cells cultured on MC-RGD 1 in the spinner flask was close to 50% confluency (at day 4), fresh MCs were added in the spinner flask at a 50% concentration of the initial MC concentration to perform bead-to-bead transfer. The LbL coating of these fresh MCs was labeled with PAH-rhodamine (deposited as the first layer during the LbL deposition process) to discriminate them from MCs initially present in the flask. Just after the addition of fresh MCs, an intermittent agitation was applied (2 min agitation at 45 rpm, followed by 28 min rest) for 12 h to encourage the transfer of cells from the initial MCs to the new MCs. The agitation was then changed to the continuous mode at 45 rpm for the remaining duration of the culture.

Cell Viability

Live/dead staining was performed by incubating the sample in a combined solution of calcein-AM (2 µL mL^{-1} in PBS) and ethidium bromide (1 µL mL^{-1} in PBS) for 30 min at room temperature. Stained cells were then imaged by epifluorescence microscopy.

Nucleus and Cytoskeleton Staining

Cells grown on MCs were fixed in glutaraldehyde aqueous solution (1 %) overnight then permeabilized in 0.1 % Triton X-100 and blocked by incubation in PBS containing 5 % BSA for 45 min. Staining of actin filaments by Alexa fluor 488 Phalloidine (10 µL mL^{-1} in PBS supplemented with 1% BSA) was performed for 30 min. Then, the samples were rinsed with PBS supplemented with 1% BSA two times for 5 min followed by nucleus staining using DAPI

(0.1 µL mL^{-1} in PBS supplemented with 1% BSA) for 10 min. Samples were rinsed again with PBS two times for 5 min before being imaged by CLSM.

Cell Morphology

Cell grown on MC samples were fixed in 1 % (w/w) glutaraldehyde aqueous solution and then serially dehydrated in 20, 40, 60, 80 and 100 % (v/v) ethanol/water solutions (5 min each) followed by 10 min immersion in hexamethyldisilazane (HMDS) and overnight drying in a fumehood. The dried samples were sputter-coated with a 10 nm thick layer of gold and imaged by SEM.

ASSOCIATED CONTENT

Supporting Information. The following files are available free of charge. SEM images and average sizes of PLLA40 MCs prepared from a 50:50 PLLA40/PEG ratio at different crystallization temperatures; growth curve of (PLO/HA) films on flat and MCs coated with $(PLO/HA)_8$ labeled with rhodamine; characterization of initial adhesion and viability of h-ASCs on MC-RGD-1 with three different cores; live/dead images of hASCs grown on bare MC, MC-LbL and MC-RGD-1 in dynamic conditions, on days 1 and day 3; characterization of cell viability and proliferation on Cytodex® 3 in dynamic conditions; magnetic moment of magnetic MCs and images showing MC attraction using a magnet (PDF).

AUTHOR INFORMATION

Corresponding Author

Karine Glinel : karine.glinel@uclouvain.be; Anne des Rieux : anne.desrieux@uclouvain.be

Author Contributions

E.S. and A.A.K. contributed equally to this work. The manuscript was written through the contributions of all authors. All authors have given approval to the final version of the manuscript. K.G., A.d.R., A.M.J. and S.D.-C. designed and supervised the study. E.S. and A.A.K. carried out the experiments. J.G. and B.H. contributed to cell culture experiments.

Funding Sources

This research was financially supported by the European Regional Development Fund (ERDF) and Wallonia in the framework of the operational program "Wallonia-2020.EU".

Notes

The authors declare no conflict of interest.

ACKNOWLEDGMENT

The authors thank A. Mwema and V. Gratpain for help with cell culture, D. Magnin and W. Xu for their help with SEM and CLSM images, respectively, Tristan da Câmara Santa Clara Gomes for the measurement of magnetic properties of the MCs and M. Kuterbekov for the fruitful discussions. K.G. and A.d.R. are Senior Research Associates of F.R.S.-FNRS.

ABBREVIATIONS

hASCs, human adipose-derived stromal cells; hMSCs, human mesenchymal stromal cells, MC, microcarrier; PLLA, poly(l-lactide); PEG, poly(ethylene glycol); LbL layer-by-layer; HA, hyaluronic acid; PLO, poly(l-ornithine); SEM, scanning electron microscopy; sulfo-NHS, N-hydroxysulfosuccinimide; EDC, N-(3-dimethylaminopropyl)-N'-ethylcarbodiimide hydrochloride; CLSM, confocal laser scanning microscopy; MNPs, magnetic nanoparticles.

REFERENCES

(1) Heathman, T. R. J.; Nienow, W.; Mccall, M. J.; Coopman, K.; Kara, B.; Hewitt, C. J. The Translation of Cell-Based Therapies : Clinical Landscape and Manufacturing Challenges. *Regener. Med.* **2015**, *10*, 49–64.

(2) dos Santos, F.; Andrade, P. Z.; Abecasis, M. M.; Gimble, J. M.; Chase, L. G.; Campbell, A. M.; Boucher, S.; Vemuri, M. C.; da Silva, C. L.; Cabral, J. M. S. Toward a Clinical-Grade Expansion of Mesenchymal Stem Cells from Human Sources: A Microcarrier-Based Culture System under Xeno-Free Conditions. *Tissue Eng. Part C* **2011**, *17*, 1201–1210.

(3) Kabat, M.; Bobkov, I.; Kumar, S.; Grumet, M. Trends in Mesenchymal Stem Cell Clinical Trials 2004-2018 : Is Efficacy Optimal in a Narrow Dose Range ? *Stem Cells Transl. Med.* **2020**, *9*, 17–27.

(4) Heathman, T. R. J.; Rafiq, Q. A.; Coopman, K.; Nienow, A. W.; Hewitt, C. J. The Scale-up of Human Mesenchymal Stem Cell Expansion and Recovery. In *Bioprocessing for Cell Based Therapies*; Wiley-Blackwell, 2016; pp 91–125.

(5) Merten, O.-W. Advances in Cell Culture: Anchorage Dependence. *Philos. Trans. R. Soc. B. Biol. Sci.* **2015**, *370*, 20140040.

(6) Schnitzler, A. C.; Verma, A.; Kehoe, D. E.; Jing, D.; Murrell, J. R.; Der, K. A.; Aysola, M.; Rapiejko, P. J.; Punreddy, S.; Rook, M. S. Bioprocessing of Human Mesenchymal Stem/Stromal Cells for Therapeutic Use: Current Technologies and Challenges. *Biochem. Eng. J.* **2016**, *108*, 3–13.

(7) Spier, M. R.; Porto, L.; Vandenberghe, D. S.; Bianchi, A.; Medeiros, P.; Soccol, C. R.

Application of Different Types of Bioreactors in Bioprocesses. In *Bioreactors: Design, Properties and Applications*; Antolli, P. G., Liu, Z., Eds.; Nova Science Publishers, Inc., 2011; pp 55–90.

(8) van Wezel, A. L. Growth of Cell-Strains and Primary Cells on Micro-Carriers in Homogeneous Culture. *Nature* **1967**, *216*, 64-65.

(9) Markicheva, E.; Grandfils, C. Microcarriers for Animal Cell Culture. In *Biomaterials for Cell Immobilization*; 2004; pp 734–763.

(10) Rafiq, Q. A.; Coopman, K.; Nienow, A. W.; Hewitt, C. J. Systematic Microcarrier Screening and Agitated Culture Conditions Improve Human Mesenchymal Stem Cell Yield in Bioreactors. *Biotechnol. J.* **2016**, *11*, 473–486.

(11) Jossen, V.; van den Bos, C.; Eibl, R.; Eibl, D. Manufacturing Human Mesenchymal Stem Cells at Clinical Scale: Process and Regulatory Challenges. *Appl. Microbiol. Biotechnol.* **2018**, *102*, 3981–3994.

(12) Tavassoli, H.; Alhosseini, S. N.; Tay, A.; Chan, P. P. Y.; Oh, S. K. W.; Warkiani, M. E. Large-Scale Production of Stem Cells Utilizing Microcarriers: A Biomaterials Engineering Perspective from Academic Research to Commercialized Products. *Biomaterials* **2018**, *181*, 333–346.

(13) Kim, T. K.; Yoon, J. J.; Lee, D. S.; Park, T. G. Gas Foamed Open Porous Biodegradable Polymeric Microspheres. *Biomaterials* **2006**, *27*, 152–159.

(14) Zhou, A.; Ye, Z.; Zhou, Y.; Tan, W. S. Bioactive Poly(ε-Caprolactone) Microspheres with Tunable Open Pores as Microcarriers for Tissue Regeneration. *J. Biomater. Appl.* **2019**, *33*,

1242–1251.

(15) Kankala, R. K.; Zhao, J.; Liu, C. G.; Song, X. J.; Yang, D. Y.; Zhu, K.; Wang, S. Bin; Zhang, Y. S.; Chen, A. Z. Highly Porous Microcarriers for Minimally Invasive In Situ Skeletal Muscle Cell Delivery. *Small* **2019**, *15*, 1901397.

(16) Nykamp, G.; Carstensen, U.; Muller, B. W. Jet Milling — a New Technique for Microparticle Preparation. *Int. J. Pharm.* **2002**, *242*, 79–86.

(17) Levato, R.; Mateos-timoneda, M. A.; Planell, J. A. Preparation of Biodegradable Polylactide Microparticles via a Biocompatible Procedure. *Macromol. Biosci.* **2012**, *12*, 557–566.

(18) Kuterbekov, M.; Machillot, P.; Lhuissier, P.; Picart, C.; Jonas, A. M.; Glinel, K. Solvent-Free Preparation of Porous Poly(L-Lactide) Microcarriers for Cell Culture. *Acta Biomater.* **2018**, *75*, 300–311.

(19) De Soure, A. M.; Fernandes-platzgummer, A.; Silva, C. L.; Cabral, J. M. S. Scalable Microcarrier-Based Manufacturing of Mesenchymal Stem/Stromal Cells. *J. Biotechnol.* **2016**, *236*, 88–109.

(20) Berry, J. D.; Liovic, P.; Šutalo, I. D.; Stewart, R. L.; Glattauer, V.; Meagher, L. Characterisation of Stresses on Microcarriers in a Stirred Bioreactor. *Appl. Math. Model.* **2016**, *40*, 6787–6804.

(21) Amersham Biosciences. *Microcarrier Cell Culture: Principles and Methods,* 2005.

(22) Younes, H.; Cohn, D. Phase Separation in Poly(Ethylene Glycol)/Poly(Lactic Acid) Blends. *Eur. Polym. J.* **1988**, *24*, 765–773.

(23) Sungsanit, K.; Kao, N.; Bhattacharya, S. N. Properties of Linear Poly(Lactic Acid)/Polyethylene Glycol Blends. *Polym. Eng. Sci.* **2012**, *52*, 108-116.

(24) Li, F. J.; Zhang, S. D.; Liang, J. Z.; Wang, J. Z. Effect of Polyethylene Glycol on the Crystallization and Impact Properties of Polylactide-Based Blends. *Polym. Adv. Technol.* **2015**, *26*, 465–475.

(25) Li, F. J.; Tan, L. C.; Zhang, S. D.; Zhu, B. Compatibility, Steady and Dynamic Rheological Behaviors of Polylactide/Poly(Ethylene Glycol) Blends. *J. Appl. Polym. Sci.* **2016**, *133*, 42919.

(26) Keith, H. D.; Padden, F. J. A Phenomenological Theory of Spherulitic Crystallization. *J. Appl. Phys.* **1963**, *34*, 2409–2421.

(27) Farah, S.; Anderson, D. G.; Langer, R. Physical and Mechanical Properties of PLA, and Their Functions in Widespread Applications — A Comprehensive Review. *Adv. Drug Delivery. Rev.* **2016**, *107*, 367–392.

(28) Tam, S. K.; Bilodeau, S.; Dusseault, J.; Langlois, G.; Hallé, J.; Yahia, L. H. Biocompatibility and Physicochemical Characteristics of Alginate – Polycation Microcapsules. *Acta Biomater.* **2011**, *7*, 1683–1692.

(29) Darrabie, M. D.; Kendall, W. F.; Opara, E. C. Characteristics of Poly-L-Ornithine-Coated Alginate Microcapsules. *Biomaterials* **2005**, *26*, 6846–6852.

(30) Tian, L.; Prabhakaran, M. P.; Hu, J.; Chen, M.; Besenbacher, F.; Ramakrishna, S. Synergistic Effect of Topography, Surface Chemistry and Conductivity of the Electrospun Nanofibrous Scaffold on Cellular Response of PC12 Cells. *Colloids Surf. B* **2016**, *145*, 420–

429.

(31) Jung, S.; Panchalingam, K. M.; Wuerth, R. D.; Rosenberg, L.; Behie, L. A. Large-Scale Production of Human Mesenchymal Stem Cells for Clinical Applications. *Biotechnol. Appl. Biochem.* **2012**, *59*, 106–120.

(32) Kuterbekov, M. Surface Biofunctionalization of 3D Porous Scaffolds for Bone Tissue Engineering, PhD thesis, Université catholique de Louvain, May 2019.

(33) Richert, L.; Boulmedais, F.; Lavalle, P.; Mutterer, J.; Ferreux, E.; Decher, G.; Schaaf, P.; Voegel, J. C.; Picart, C. Improvement of Stability and Cell Adhesion Properties of Polyelectrolyte Multilayer Films by Chemical Cross-Linking. *Biomacromolecules* **2004**, *5*, 284–294.

(34) Vazquez, C. P.; Boudou, T.; Dulong, V.; Nicolas, C.; Picart, C.; Glinel, K. Variation of Polyelectrolyte Film Stiffness by Photo-Cross-Linking : A New Way to Control Cell Adhesion. *Langmuir* **2009**, *25*, 3556–3563.

(35) Schneider, A.; Francius, G.; Obeid, R.; Schwinté, P.; Hemmerlé, J.; Frisch, B.; Schaaf, P.; Voegel, J. C.; Senger, B.; Picart, C. Polyelectrolyte Multilayers with a Tunable Young's Modulus: Influence of Film Stiffness on Cell Adhesion. *Langmuir* **2006**, *22*, 1193–1200.

(36) Picart, C.; Lavalle, P.; Hubert, P.; Cuisinier, F. J. G.; Decher, G.; Schaaf, P.; Voegel, J. C. Buildup Mechanism for Poly(L-Lysine)/Hyaluronic Acid Films onto a Solid Surface. *Langmuir* **2001**, *17*, 7414–7424.

(37) Hersel, U.; Dahmen, C.; Kessler, H. RGD Modified Polymers: Biomaterials for Stimulated Cell Adhesion and Beyond. *Biomaterials* **2003**, *24*, 4385–4415.

(38) Bacakova, L.; Filova, E.; Rypacek, F.; Svorcik, V.; Stary, V. Cell Adhesion on Artificial Materials for Tissue Engineering. *Physiol. Res.* **2004**, *53*, 35–45.

(39) Bajek, A.; Gurtowska, N.; Olkowska, J.; Kazmierski, L.; Maj, M.; Drewa, T. Adipose-Derived Stem Cells as a Tool in Cell-Based Therapies. *Arch. Immunol. Ther. Exp.* **2016**, *64*, 443–454.

(40) Nagata, T.; Mitsumori, T.; Iwaguro, H. Adipose Tissue-Derived Stem and Regenerative Cells for Tissue Regeneration. *J. Oral Biosci.* **2013**, *55*, 127–131.

(41) Jossen, V.; Schirmer, C.; Mostafa Sindi, D.; Eibl, R.; Kraume, M.; Pörtner, R.; Eibl, D. Theoretical and Practical Issues That Are Relevant When Scaling up HMSC Microcarrier Production Processes. *Stem Cells Int.* **2016**, *2016*, 4760414.

(42) Ferrari, C.; Balandras, F.; Guedon, E.; Olmos, E.; Chevalot, I.; Marc, A. Limiting Cell Aggregation during Mesenchymal Stem Cell Expansion on Microcarriers. *Biotechnol. Prog.* **2012**, *28*, 780–787.

(43) Lembong, J.; Kirian, R.; Takacs, J.; Olsen, T.; Lock, L. T.; Rowley, J.; Ahsan, T. Bioreactor Parameters for Microcarrier-Based Human MSC Expansion under Xeno-Free Conditions in a Vertical-Wheel System. *Bioengineering* **2020**, *7*, 73.

(44) Eibes, G.; dos Santos, F.; Andrade, P. Z.; Boura, J. S.; Abecasis, M. M. A.; da Silva, C. L.; Cabral, J. M. S. Maximizing the Ex Vivo Expansion of Human Mesenchymal Stem Cells Using a Microcarrier-Based Stirred Culture System. *J. Biotechnol.* **2010**, *146*, 194–197.

(45) Schop, D.; van Dijkhuizen-Radersma, R.; Borgart, E.; Janssen, F. W.; Rozemuller, H.; Prins, H.-J.; De Bruijn, J. D. Expansion of Human Mesenchymal Stromal Cells on

Microcarriers: Growth and Metabolism. *J. Tissue Eng. Regen. Med.* **2010**, *4*, 131–140.

(46) Goh, T. K.-P.; Zhang, Z.-Y.; Chen, A. K.-L.; Reuveny, S.; Choolani, M.; Chan, J. K. Y.; Oh, S. K.-W. Microcarrier Culture for Efficient Expansion and Osteogenic Differentiation of Human Fetal Mesenchymal Stem Cells. *Biores. Open Access* **2013**, *2*, 84–97.

(47) Jorgenson, K. D.; Hart, D. A.; Krawetz, R.; Sen, A. Production of Adult Human Synovial Fluid-Derived Mesenchymal Stem Cells in Stirred-Suspension Culture. *Stem Cells Int.* **2018**, *2018*, 8431053.

(48) Wang, Y.; Ouyang, F. Bead-to-Bead Transfer of Vero Cells in Microcarrier Culture. *Bioprocess Eng.* **1999**, *21*, 211–213.

(49) Verbruggen, S.; Luining, D.; van Essen, A.; Post, M. J. Bovine Myoblast Cell Production in a Microcarriers-Based System. *Cytotechnology* **2018**, *70*, 503–512.

(50) Luo, F.; Sun, H.; Geng, T.; Qi, N. Application of Taguchi's Method in the Optimization of Bridging Efficiency between Confluent and Fresh Microcarriers in Bead-to-Bead Transfer of Vero Cells. *Biotechnol. Lett.* **2008**, *30*, 645–649.

(51) Abeille, F.; Mittler, F.; Obeid, P.; Huet, M.; Kermarrec, F.; Dolega, M. E.; Navarro, F.; Pouteau, P.; Icard, B.; Gidrol, X.; Agache, V.; Picollet-D'hahan, N. Continuous Microcarrier-Based Cell Culture in a Benchtop Microfluidic Bioreactor. *Lab Chip* **2014**, *14*, 3510-3518.

(52) Yu, J.; Shi, J.; Zhang, Y.; Zhang, Y.; Huang, Y.; Chen, Z.; Yang, J. The Replicative Senescent Mesenchymal Stem / Stromal Cells Defect in DNA Damage Response and Anti-Oxidative Capacity. *Int. J. Med. Sci.* **2018**, *15*, 771-781.

(53) Chen, A. K.-L.; Reuveny, S.; Oh, S. K. W. Application of Human Mesenchymal and Pluripotent Stem Cell Microcarrier Cultures in Cellular Therapy: Achievements and Future Direction. *Biotechnol. Adv.* **2013**, *31*, 1032–1046.

(54) Decher, G.; Eckle, M.; Schmitt, J.; Struth, B. Layer-by-Layer Assembled Multicomposite Films. *Curr. Opin. Colloid Interface Sci.* **1998**, *3*, 32–39.

TOC

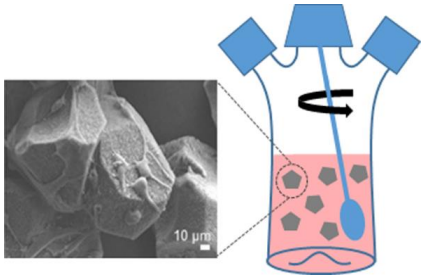

Supporting Information

Green and Tunable Animal Protein-Free Microcarriers for Cell Expansion

Eleana Somville,[1] Anitha Ajith Kumar,[1] Jérôme Guicheux,[2] Boris Halgand,[2,3] Sophie Demoustier-Champagne,[1] Anne des Rieux,[1,4,] Alain M. Jonas,[1] and Karine Glinel[1,*]*

(1) Institute of Condensed Matter and Nanosciences, Bio and Soft Matter, Université catholique de Louvain, Croix du Sud 1, box L7.04.02, 1348 Louvain-la-Neuve, Belgium.

(2) Inserm, UMR 1229, RMeS, Regenerative Medicine and Skeleton, Université de Nantes, ONIRIS, 44042 Nantes, France.

(3) Centre Hospitalier Universitaire de Nantes, PHU4 OTONN, 44093 Nantes, France.

(4) Louvain Drug Research Institute, Advanced Drug Delivery and Biomaterials, Université catholique de Louvain, Av. E. Mounier 73, box B1.73.12, 1200 Brussels, Belgium.

Authors for correspondence: karine.glinel@uclouvain.be; anne.desrieux@uclouvain.be

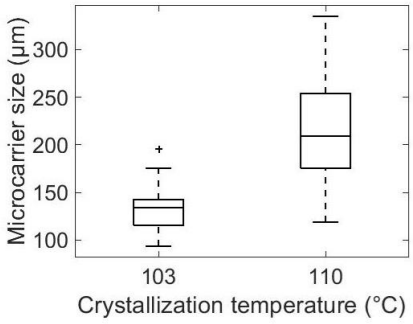

Figure S1: Size distribution of PLLA40 MCs prepared from a PLLA40/PEG ratio of 50:50 and different crystallization temperatures.

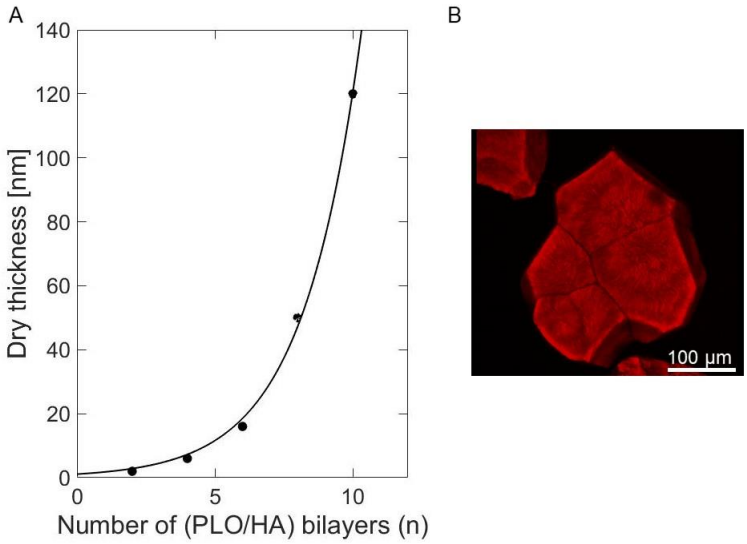

Figure S2: (A) Variation of the dry thickness of $(PLO/HA)_n$ films grown on silicon substrate, as a function of the number of deposited bilayers (n) as measured by ellipsometry. (B) CLSM image of $(PLO/HA)_8$-coated microcarriers dipped in rhodamine solution.

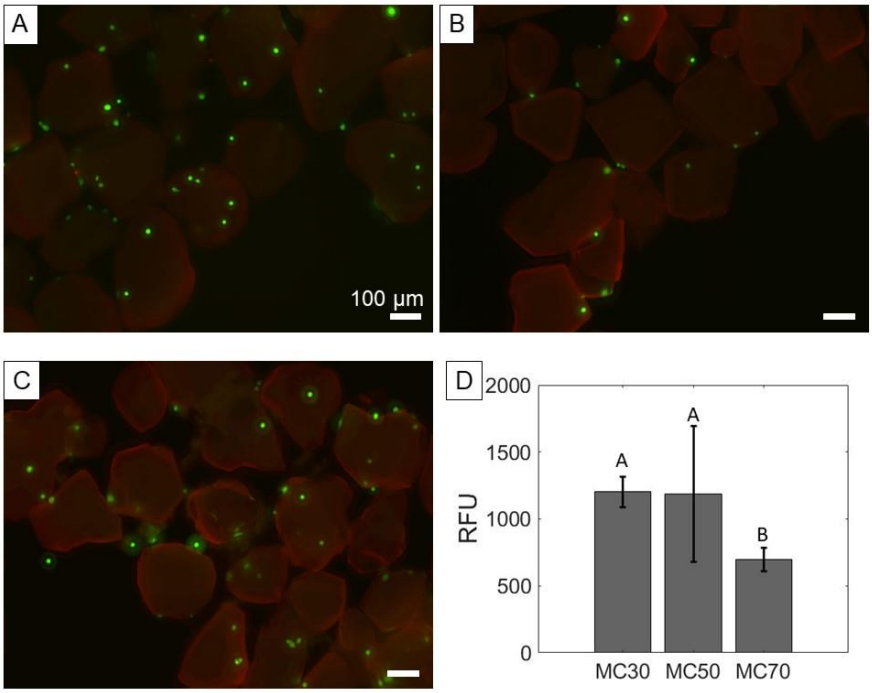

Figure S3: Live/dead images of hASCs grown on MC-RGD-1 in semi-static conditions on day 0 for three different cores: (A) MCs prepared from a 30:70 PLLA40/PEG blend (MC30), (B) MCs prepared from a 50:50 PLLA40/PEG blend (MC50) and (C) MCs prepared from a 70:30 PLLA40/PEG blend (MC70). Scale bars are identical in all panels. (D) Metabolic activity quantification of cells adhered on the three types of MC-RGD-1 (N = 2, n = 3), showing a reduced adhesion on MC70 compared to the two other types of MC cores. Bars topped with different letters indicate a significant difference ($p < 0.05$).

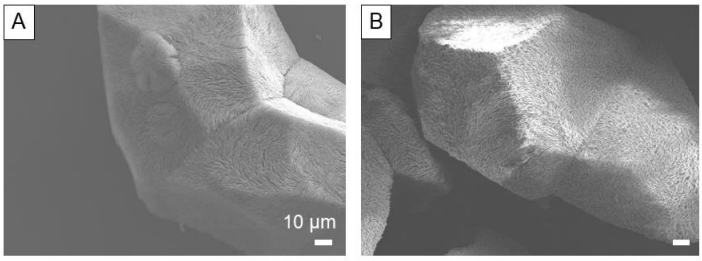

Figure S4: SEM images of PLLA40 MCs prepared from a 50:50 PLLA40/PEG ratio at a crystallization temperature of 103 (A) and 110 °C (B). Scale bares are identical in both panels.

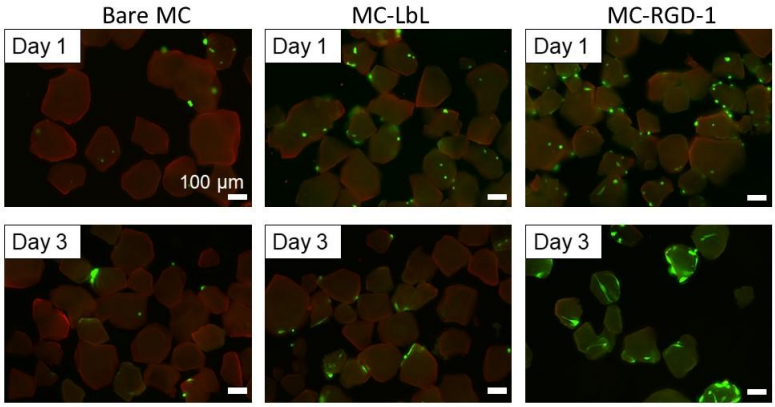

Figure S5: Live/dead images of hASCs grown in dynamic conditions on bare MCs, MC-LbL and MC-RGD-1 prepared from a 50:50 PLLA40/PEG. Images were recorded on (top) day 1 and (bottom) day 3. A large portion of empty MCs is observed on bare MCs and MC-LbL by day 3; in contrast, MC-RGD-1 are largely covered by cells by day 3. Scale bars are identical in all panels.

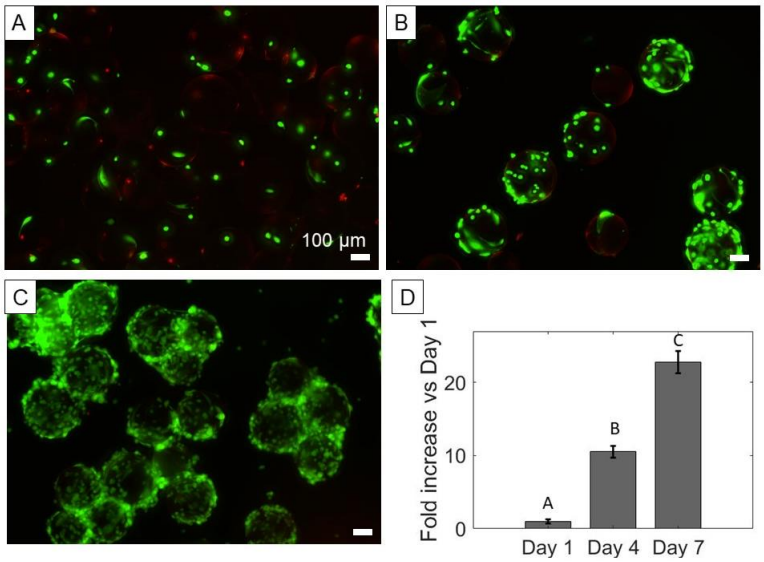

Figure S6: Viability and proliferation of hASCs grown on Cytodex® 3 in dynamic conditions. Live/dead images recorded on (A) day 1, (B) day 4 and (C) day 7. The scale bars are identical in all panels. (D) Quantification of cellular metabolic activity (N = 1, n = 3). Bars topped with different letters indicate a significant difference ($p < 0.05$).

Magnetic microcarriers

Production of magnetic microcarriers

Magnetic MCs were obtained following the protocol described in Experimental section except that a PEG powder containing MNPs was used instead of the regular PEG. This powder was obtained following the incorporation of MNPs in a PEG aqueous solution and a subsequent freeze-drying step. The concentration of MNPs was set to obtain a final concentration of 3 mg of iron per g of PLLA in the blend.

Characterization of magnetic properties

The magnetic properties of magnetic MCs were assessed using a MicroMag 2900 Alternating Gradient Magnetometer (AGM).

Characterization of magnetic nanoparticle incorporation in PLLA core and release

MNP incorporation and release was quantified using ICP-AES (ICAP 6500, Thermo Scientific).

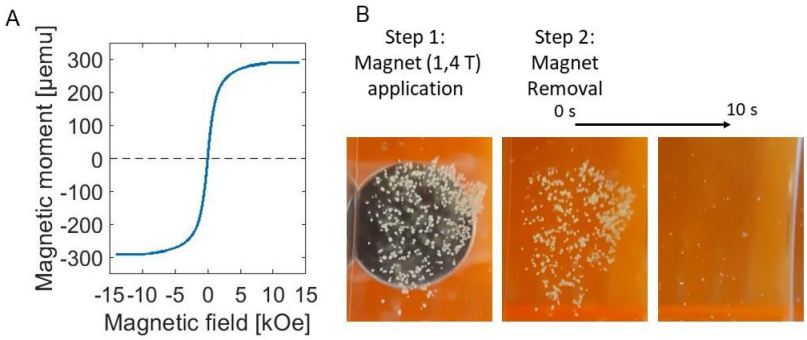

Figure S7: (A) Hysteresis curve of magnetic MCs showing their superparamagnetic behavior. (B) Magnetic MCs can be immobilized in solution by using a magnet and quickly released after magnet removal.